

STRESS-STRAIN BEHAVIOR OF LOW GRAMMAGE
AND/OR
LIGHTLY BONDED PAPERS BY DOT MATRIX TECHNIQUE

by


Rubens Chaves de Oliveira

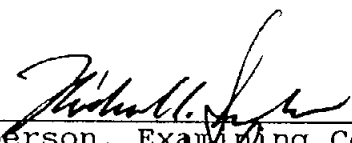
A thesis
submitted in partial fulfillment
of the requirement for the
Doctor of Philosophy Degree

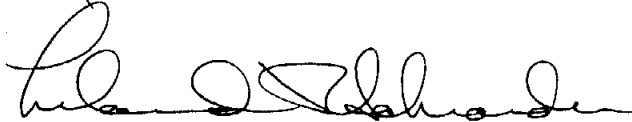
State University of New York
College of Environmental Science
and Forestry
Syracuse, New York

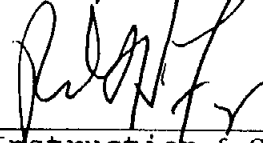
December 1993

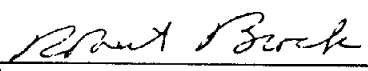
Approved:
Faculty of Paper Science and Engineering


Major Professor


Chairperson, Examining Committee


Faculty Chairperson


Dean, Instruction & Graduate Studies


Director



To my wife Doris, and
our children Igor and Thiago

"Love of learning is seldom unrequited."

Arnold H. Clasow

ACKNOWLEDGEMENTS

I acknowledge and thank my major professor, Dr. Richard Edward Mark, for his valuable advice and encouragement in the development and completion of this thesis. In addition, I thank him for his academic guidance throughout the duration of my graduate studies program.

My sincere thanks to Dr. Richard W. Perkins Jr. for his assistance and valuable suggestions during the course of this work.

Thanks to the other members of my advisory committee, Dr. Robert B. Hanna, Dr. Richard W. Heimborg, Mr. Thomas B. Reagan and Mr. James L. Thorpe for the suggestions and other forms of assistance they gave.

Special appreciation is extended to Clay Crosby for his reading and suggestions in organizing this dissertation, and to Amin Eusufzai who also substantially contributed to my training program.

My thanks to all other members of the Paper Physics Research group, especially Noel Lazo, Fuushern Wu and Luiz H. Donega for their participation and friendship. Thanks to the former members of the group, Dr. Yung B. Seo, Dr. Bernard Castagnede and Dr. M.K. Ramasubramanian. Thanks also to Richard C. Mark for the airbrush demonstration that inspired the development of the dot matrix technique. Thanks to Edward J. Mulligan and Donald P. Haggart for their efficiency in building the needed experimental equipment.

Thanks to Procter & Gamble for providing the materials used in the study.

Thanks to CNPq and Universidade Federal de Vicosa - Brazil for the scholarship which made my studies possible. I also thank ESPRI/PSE for financial support at the end of my research program.

Thanks to my wife Doris for typing this dissertation and, together with our children, for providing the total support I needed. Also thanks to our parents who are always waiting for us to come back home.

We thank our friend Dr. Jose Livio Gomide for motivating us to come to the United States.

Finally, I thank to all ESPRI/PSE students, faculty and staff for their friendship during my time at this fine institution.

TABLE OF CONTENTS

ACKNOWLEDGEMENTS	iii
LIST OF TABLES	viii
LIST OF FIGURES	x
ABSTRACT	xxi
 CHAPTER 1. SOME METHODS AND INSTRUMENTS USED FOR STRAIN DETERMINATION IN PAPER	 1
 CHAPTER 2. THE TENSION BUCKLING PHENOMENON: A SPECIMEN DESIGN PROBLEM IN TENSILE TESTING OF LOW GRAMMAGE AND/OR LIGHTLY BONDED PAPERS	 10
2.1. Introduction	11
2.2. Effects of End Constraint During the Tensile Test	12
2.3. Effect of Specimen Configuration on the Tension Buckling Phenomenon	14
2.3.1. Experimental Approach for Wrinkling Determination	15
2.3.2. Determination of Amplitudes of the Wrinkle Waves	17
2.3.3. Wrinkling Behavior of Rectangular Specimens	18

2.3.4. The Structural Behavior of Necked- Down Specimens	22
2.4. Conclusion	27
2.5. Literature	28
CHAPTER 3. THE DOT MATRIX: A TECHNIQUE FOR STRAIN MEASUREMENT OF LOW GRAMMAGE AND/OR LIGHTLY BONDED PAPERS	
3.1. Introduction	48
3.2. Design of the Grid Pattern	49
3.3. Recording Procedure for the Dot Matrix System	50
3.4. Data Acquisition for Stress Computations	53
3.5. Data Acquisition for Displacement Measurements	56
3.6. Data Processing for Strain Calculations	59
3.7. Results of the Stress-Strain Relationships	62
3.8. Results of Strain Field Characterization	66
3.9. Conclusion	69
3.10. Literature	84
3.11. Appendix A	87
3.12. Appendix B	146
CHAPTER 4. EXPERIMENTAL MEASUREMENTS: PRECISION AND ACCURACY OF THE DOT MATRIX TECHNIQUE	
4.1. Introduction	162
4.2. Errors in the Determination of Applied Load	163
	165

4.3. Errors in the Determination of Cross-sectional Area of the Specimens	165
4.3.1. Errors in Width Determination	166
4.3.2. Errors in Thickness Determination	166
4.4. Errors in Strain Computations	167
4.4.1. Errors in the Determination of Modulus of Elasticity due to Strain Computations	169
4.4.2. Errors in the Determination of the Axial Strain Field	171
4.4.3. Errors in the Determination of Lateral Contraction Ratios	173
4.5. Effect of Moisture Content of the Exposed Photograph Films on Data Processing	175
4.6. Final Remarks	178
4.7. Literature	179
 CHAPTER 5. THE APPLICATION OF DOT MATRIX TECHNIQUE TO EVALUATE THE EFFECTS OF STRUCTURE ON THE MECHANICAL PROPERTIES OF PAPER	 190
5.1. Introduction	191
5.2. Relationship Between Grammage and Film Absorbance	192
5.3. Experimental Approach for Mass Distribution Characterization	196
5.4. Characterization of Two-dimensional Strain Field Distribution	200

	vii
5.5. Relationship Between Grammage and Strain	202
5.6. Conclusion	215
5.7. Literature	216
5.8. Appendix A	249
5.9. Appendix B	250
5.10. Appendix C	251
5.11. Appendix D	252
5.12. Appendix E	255
5.13. Appendix F	265
5.14. Appendix G	269
VITA	271

LIST OF TABLES

CHAPTER 3:

Table 1. Regression equations used to estimate the strain at failure.	90
Table 2. Results from stress-strain and load-strain relationships for machine-made papers and handsheets.	91

CHAPTER 4:

Table 1. Moduli of elasticity obtained for different digitizing procedures and their characteristic distributions.	170
Table 2. Characteristic of distribution of the axial strain field.	172
Table 3. Characteristic of distribution of lateral contraction ratios.	174
Table 4. Effect of immersion in water of the exposed photographs on the characteristic distribution of lateral contraction ratios (L.C.R.).	177

CHAPTER 5:

Table 1. Array dimensions for correlation analysis.	204
--	-----

Table 2. Correlation matrices generated per test specimen in 1mm squares basis.	219
Table 3. Correlation matrices generated from the average of three test specimens in 1,2, 3 and 4mm squares basis.	220
Table 4. Correlation matrices generated from the average of three test specimens in 1mm squares basis for two different locations within the test area.	221

LIST OF FIGURES

CHAPTER 2:

- Fig.1. Force distributions in the vicinity of the grips. 31
- Fig.2. Strain distribution in a rectangular isotropic specimen in the vicinity of a clamp. 31
- Fig.3. Perspective view of the photographic approach. 32
- Fig.4. Side view of the photographic approach. 33
- Fig.5. Projected photographic image of the wrinkled surface (baseline) of the tensile test specimen. 34
- Fig.6. Wrinkle at zero displacement level for rectangular tensile specimen (MD). 35
- Fig.7. Wrinkle at 2% of crosshead displacement for rectangular tensile specimen (MD). 35
- Fig.8. Wrinkle at failure (7.73% crosshead displacement) for rectangular tensile specimen (MD). 35
- Fig.9. Wrinkle at zero displacement level for rectangular tensile specimen (CD). 36
- Fig.10. Wrinkle at 2% of crosshead displacement

- for rectangular tensile specimen (CD). 36
- Fig.11. Wrinkle at failure (11% crosshead displacement for rectangular tensile specimen (CD). 36
- Fig.12. Wrinkle at zero displacement level for rectangular tensile specimen (handsheet) 37
- Fig.13. Wrinkle at 1% crosshead displacement for rectangular tensile specimen (handsheet) 37
- Fig.14. Pattern of lateral compressive stress for handsheet paper. 38
- Fig.15. Pattern of lateral compressive stress for machine-made paper. 39
- Fig.16. Rectangular tensile CD specimen photographed at 3% of crosshead displacement. Wrinkling occurs along the entire length. Length: 240mm. Width: 20mm. Aspect ratio (L/W) = 12. 40
- Fig.17. Rectangular tensile CD specimen photographed at 3% of crosshead displacement. Wrinkling occurs along the entire length. Length: 240mm. Width: 50mm. Aspect ratio (L/W) = 4.8. 40
- Fig.18. The finite element models used to demonstrate lateral stress fields in necked-down specimens. 41

Fig.19. Models of necked-down specimens used for tension test trials. Transition ratios (W/w) = 5, 3.75 and 3	42
Fig.20. Models of necked-down specimens used for tension test trials. Transition ratios (W/w) = 3.33, 2.5 and 2.	43
Fig.21. Necked-down tensile CD specimen. Photographed at 6.5% of crosshead displacement (close to total failure)	44
Fig.22. Wrinkle at zero displacement level for necked-down tensile specimen (MD).	45
Fig.23. Wrinkle at 6.4% of crosshead displacement for necked-down tensile specimen (MD).	45
Fig.24. Wrinkle at zero displacement level for necked-down tensile specimen (CD).	46
Fig.25. Wrinkle at 10.35% of crosshead displacement for necked-down tensile specimen (CD).	46
Fig.26. Wrinkle at failure level for necked-down tensile specimen (CD).	46
Fig.27. Wrinkle at zero displacement level for necked-down tensile specimen (handsheet)	47
Fig.28. Wrinkle at 1% of crosshead displacement for necked-down tensile specimen (handsheet).	47
Fig.29. Wrinkle at failure displacement level for necked-down tensile specimen (handsheet).	47

CHAPTER 3:

Fig.1.	The airbrush.	92
Fig.2.	Partial sectional view of dot formation.	93
Fig.3.	Top view of the photographic approach.	94
Fig.4.	Output response (spikes) from the photoelectric cell corresponding to each photographic flash illumination.	95
Fig.5.	Load-time relationship.	95
Fig.6.	Test specimen and sampling procedure for thickness measurements.	96
Fig.7.	Projected image of a typical grid pattern	97
Fig.8.	The grid pattern for digitizing.	98
Fig.9.	Typical grid pattern in the undeformed (unstrained) and deformed (strained) stages.	99
Fig.10.	Geometry of the specimen in uniaxial tensile testing.	100
Fig.11.	Basic unit of displacement.	101
Fig.12.	Displacement vectors components for one basic unit.	101
Fig.13.	Geometry and design for different basic units of processing in a uniaxial tensile specimen.	102
Fig.14.	Array dimensions for strain calculations.	103
Fig.15.	Typical strain vs time relationship.	104

Fig.16. Typical relationships from the tensile test for the machine-made paper type A.	105
Fig.17. Typical relationships from the tensile test for the machine-made paper type B.	106
Fig.18. Typical relationships from the tensile test for handsheets.	107
Fig.19. Typical axial strain distribution for MD specimens, paper type A.	108
Fig.20. Typical lateral strain distribution for MD specimens, paper type A.	110
Fig.21. Typical shear strain distribution for MD specimens, paper type A.	112
Fig.22. Typical axial strain distribution for CD specimens, paper type A.	114
Fig.23. Typical lateral strain distribution for CD specimens, paper type A.	116
Fig.24. Typical shear strain distribution for CD specimens, paper type A.	118
Fig.25. Typical axial strain distribution for MD specimens, paper type B.	120
Fig.26. Typical lateral strain distribution for MD specimens, paper type B.	122
Fig.27. Typical shear strain distribution for MD specimens, paper type B.	124
Fig.28. Typical axial strain distribution for CD specimens, paper type B.	126

Fig.29. Typical lateral strain distribution for CD specimens, paper type B.	128
Fig.30. Typical shear strain distribution for CD specimens, paper type B.	130
Fig.31. Typical axial strain distribution for handsheets.	132
Fig.32. Typical lateral strain distribution for handsheets.	134
Fig.33. Typical shear strain distribution for handsheets.	136
Fig.34. Axial strain vs lateral strain, MD specimens, paper type A.	138
Fig.35. Axial strain vs lateral strain, CD specimens, paper type A.	139
Fig.36. Axial strain vs lateral strain, MD specimens, paper type B.	140
Fig.37. Axial strain vs lateral strain, CD specimens, paper type B.	141
Fig.38. Axial strain vs lateral strain, handsheet specimens.	142
Fig.39. Axial strain vs lateral strains. Average for paper type A, paper type B and handsheet.	143
Fig.40. Typical axial strain-lateral contraction ratio relationship.	144
Fig.41. Axial strain-lateral contraction ratio relationship. Average for paper type A, paper type B and handsheet.	145

CHAPTER 4:

- Fig.1. Precision and accuracy of four digitizing procedures for the determination of modulus of elasticity. 180
- Fig.2. Precision and accuracy in the determination of modulus of elasticity using digitizing procedure # 1. 181
- Fig.3. Precision and accuracy in the determination of modulus of elasticity using digitizing procedure # 3. 181
- Fig.4. Precision and accuracy in the determination of modulus of elasticity using digitizing procedure # 5. 182
- Fig.5. Precision and accuracy in the determination of modulus of elasticity using digitizing procedure # 10. 182
- Fig.6. Precision and accuracy of four digitizing procedures for the determination of axial strain field. 183
- Fig.7. Precision and accuracy in the determination of axial strain field using digitizing procedure # 1. 184
- Fig.8. Precision and accuracy in the determination of axial strain field using digitizing procedure # 3. 184

Fig.9. Precision and accuracy in the determination of axial strain field using digitizing procedure # 5.	185
Fig.10. Precision and accuracy in the determination of axial strain field using digitizing procedure # 10.	185
Fig.11. Precision and accuracy of four digitizing procedures for the determination of lateral contraction ratios.	186
Fig.12. Precision and accuracy in the determination of lateral contraction ratios using digitizing procedure # 1.	187
Fig.13. Precision and accuracy in the determination of lateral contraction ratios using digitizing procedure # 3.	187
Fig.14. Precision and accuracy in the determination of lateral contraction ratios using digitizing procedure # 5.	188
Fig.15. Precision and accuracy in the determination of lateral contraction ratios using digitizing procedure # 10.	188
Fig.16. Effect of moisture content of the exposed photographs on the precision and accuracy of the determination of lateral contraction ratios.	189

CHAPTER 5:

Fig.1.	Schematics of the beta-radiography chamber.	222
Fig.2.	Preparation of the necked-down specimen for beta-radiography and for the tensile test.	223
Fig.3.	Array dimensions for strain calculations.	224
Fig.4.	Influence of the spatial average parameters on the correlation between grammage and strains.	225
Fig.5.	Typical 3-dimensional view of the grammage distribution on 1mm square basis for machine made paper and handsheet.	226
Fig.6.	Typical 3-dimensional view of the axial strain distribution on 1mm square basis for machine made paper and handsheet.	227
Fig.7.	Typical 3-dimensional view of the lateral strain distribution on 1mm square basis for machine made paper and handsheet.	228
Fig.8.	Typical 3-dimensional view of the shear strain distribution on 1mm squares basis for machine made paper and handsheet.	229
Fig.9.	Relationship between grammage and axial strain for MD specimens on 1mm square basis.	230

- Fig.10. Relationship between grammage and axial strain for CD specimens on 1mm square basis. 231
- Fig.11. Relationship between grammage and axial strain for handsheet specimens on 1mm square basis. 232
- Fig.12. Relationship between grammage and axial strain for MD specimens on 1,2,3 and 4mm squares basis. 233
- Fig.13. Relationship between grammage and axial strain for CD specimens on 1,2,3 and 4mm squares basis. 234
- Fig.14. Relationship between grammage and axial strain for handsheet specimens on 1,2,3 and 4mm squares basis. 235
- Fig.15. Relationship between grammage and lateral strain for MD specimens on 1mm square basis. 236
- Fig.16. Relationship between grammage and lateral strain for CD specimens on 1mm square basis. 237
- Fig.17. Relationship between grammage and lateral strain for handsheet specimens on 1mm square basis. 238
- Fig.18. Relationship between grammage and lateral

strain for MD specimens on 1,2,3 and 4mm
squares basis. 239

Fig.19. Relationship between grammage and lateral
strain for CD specimens on 1,2,3 and 4mm
squares basis. 240

Fig.20. Relationship between grammage and lateral
strain for handsheet specimens on 1,2,3
and 4mm squares basis. 241

Fig.21. Relationship between grammage and shear
strain for MD specimens on 1mm square
square basis. 242

Fig.22. Relationship between grammage and shear
strain for CD specimens on 1mm square
basis. 243

Fig.23. Relationship between grammage and shear
strain for Handsheet specimens on 1mm
square basis. 244

Fig.24. Relationship between grammage and shear
strain for MD specimens on 1,2,3 and 4mm
squares basis. 245

Fig.25. Relationship between grammage and shear
strain for CD specimens on 1,2,3 and 4mm
squares basis. 246

Fig.26. Relationship between grammage and shear
strain for handsheet specimens on 1,2,3
and 4mm squares basis. 247

OLIVEIRA, RUBENS C.

Stress-Strain Behavior of Low Grammage and/or Lightly Bonded Papers by Dot Matrix Technique.

Typed and bound thesis, xxi + 271 pages, 10 tables, 112 figures, appendices, 1990.

This study develops a suitable method for strain field determination in lightweight and/or lightly bonded paper material like tissue, and apply it to problems such as the evaluation of local or global structure effects on mechanical properties. Any description of the elastic stress-strain behavior of materials includes the stipulations that plane sections remain plane and that deformations are recoverable upon release of stress. Until now it has been difficult to characterize lightweight papers in a way that meets these requirements because of their tendencies to quickly wrinkle when conventional testing is done.

With experimental evidence and finite element analysis, we have examined the phenomena and mechanisms responsible for tension buckling. We have taken into consideration specimen geometry, anisotropy, and actual boundary conditions, as they influence tension buckling, which has important implications for the proper measurement of mechanical properties of tissue. A solution is obtained by selecting an appropriate specimen configuration.

We describe the development of a photographic grid technique, called dot matrix, that can be utilized conveniently in conjunction with a previously described necked-down specimen design, to measure in-plane deformations on specimens. This present work includes the design of the grid pattern, data acquisition, recording and processing procedures, and presentation of results for handsheets and two types of lightly-creped machine-made tissues.

In order to appraise both the dot matrix and beta-radiography approaches, we describe procedures to apply these techniques to obtain in a pointwise basis the relationship between grammage and strain. Included in such applications are (a) specimen preparation for beta-radiography and tensile test, (b) instructions for a computerized beta-radiography scanning procedure to obtain local spatial variation in mass distribution, (c) average stepwise procedures needed to match strain data with local position in the specimen, and (d) results of correlation between grammage and strains.

Author's name in full: Rubens Chaves de Oliveira

Candidate for the degree of Ph.D. Date: January, 1990

Major Professor: Dr. Richard E. Mark

Environmental and Resource Engineering Program

State University of New York College of Environmental Science and Forestry, Syracuse, New York

Signature of Major Professor:

CHAPTER 1

SOME METHODS AND INSTRUMENTS USED FOR STRAIN DETERMINATION IN PAPER

This chapter presents, in a general fashion, some information about present and future developments in instrumentation and methods used for strain determination in paper.

For many years it is well known that reliable displacement measurement in paper can not be obtained by the crosshead movement [1-5]. Nonetheless it is the commonly used method for tensile properties determination in the paper field [6]. In this method, the distance between the clamps is usually considered the gage length for determination of deformation. Thus the dimensional change and the resultant strain calculation represent an average value over the free span which includes parts of the specimen that are not free to deform due to grip effects. Other problems are slippage of the specimen in the grips and lack of accuracy in the determination of the gage length [7]. The need for instruments

that accurately measure displacement independent of the loading mechanism is evident.

Basic features of different methods (mechanical, acoustical and optical) for determination of in-plane and out-of-plane elastic constants of paper are well discussed in reference [8].

The existing methods for measuring displacements include various mechanical devices, which generate electrical, acoustical, or light signals. The most common one is the electrical resistance strain gage, whose principle was discovered by Lord Kelvin, who observed that the resistance of a wire changes when it is deformed by mechanical force. However, no use was made of this principle for strain measurement until the 1930's when it was rapidly developed into one of the most useful tools in experimental strain analysis [9]. However, there are some limitations to the use of such devices to measure strain in paper. They are usually mounted on a small flexible metal beam that is typically attached to the paper specimen at two points by means of pins, pointed screws or knife edges that rotate or translate as the specimen changes dimensionally during the straining process. The friction of the contact point on the specimen influences the mechanical-electrical output. Usually, space on the specimen does not permit the attachment of more than two such devices, so point-to-point variations in strains can not be obtained. A strain-gage device weighing even a few grams may

impose bending or other loads on the specimen. This problem is especially severe in the case of lightweight papers, where almost anything that contacts the specimen may influence its behavior.

Elastic constants can be determined by acoustical techniques, which eliminate the need for displacement measurement. Craver and Taylor [10, 11] were the first to use sonic velocity measurements in paper materials. Later, other researchers have used this method to obtain the entire set of in-plane elastic constants [12]. This method presents several advantages: It is non-destructive, fast and usable for routine mechanical testing. However, the applicable acoustical theory requires that the material be homogeneous and of uniform thickness [13, 14], a condition not often satisfied by paper; this makes its use not recommended for lightweight papers such as tissue.

The use of laser speckle interferometry (LSI) permits detailed two-dimensional strain information in the plane of an object surface to be obtained by recording double-exposure photographs of the specimen in the speckle-illuminated state. This technique has been useful in materials science, principally to measure small magnitudes of displacement which can pose difficult problems in experimental mechanics [15, 16]. Laser speckle seems to be well-suited for problems involving fragile specimens, surface phenomena and difficult specimen environments [17]. It has been successfully

used in the paper field to obtain a two-dimensional strain distribution by mapping point-to-point strain variations in paper [18]. It has been used in combination with an extensometer and a modified off-axis tensile test to determine in-plane elastic constants of paper, such as Young's modulus, poisson ratio, and shear modulus [19].

However, there are limitations to the application of this method to displacement measurements in paper. A decorrelation of the speckle pattern [18], which may occur during the straining is sensitive to the characteristics of specimen alignment and curvature, the material surface, the ability of light to penetrate into the structure, and to the range of incremental strain (between two photographic film exposures), which is limited to a small range [20]. To eliminate or minimize the characteristics of penetration of light to the interior layers and roughness (severe local variation in thickness), which can be problems for materials such as paper, the surface is usually coated with a very thin layer of reflective paint [21]. The paint coating renders LSI inappropriate for lightweight paper because the coating can change the mechanical properties of the material being tested. Another problem is that the small incremental strains between the double exposures (typically about 0.05%, [21]) are difficult to monitor without the help of an extensometer attached to the specimen. The problems raised by attaching such a device to lightweight materials have already been

discussed.

An interesting method has been recently reported in the literature [22, 23], involving an automatic data acquisition and data analysis system for the study of surface deformation in paper through image analysis. The specimen is usually illuminated with a standard white light source, and the illuminated surface is imaged by a video camera and stored digitally in the computer disk. Although the test specimen could not be loaded continuously, probably because of the time for the image acquisition and transfer to the computer disk (about 12 min for five images), the advantages of the method are: it has the capability to acquire local variations in strain distribution; it is noncontacting and may be applied on a microscale. Progress in developing faster electronic image systems will make this method more useful for paper strain determination.

Other methods have found special applications. For example, a photographic technique that has proven useful in the measurement of tensile elongations of lightweight papers (2.5 to 6.4 g/m²) involved exposures of a square grid pattern of one hundred squares, each of side 0.5cm traced onto the specimen using a ruler and a sharp 6B pencil. The changes in distances between the lines in the longitudinal and lateral directions as a result of the straining process were recorded using a traveling microscope; thus the spacing between the lines in the undeformed stage provides the gage length and

subsequent changes in spacing can provide axial and lateral displacement information if the specimen remains flat [24].

The displacement of xerographic particles fused to the surface of the sheet has been used to obtain strain information in paper. The method requires a scanning electron microscope (SEM) for observation and measurement of displacements at the sheet and fiber levels. Photographs of paper specimens were taken in the SEM at various strain levels. Photogrammetric technique employing stereoscopic superposition of the photographs and a device such as optical comparator was used for displacement measurements [25].

From this discussion it can be seen that it is not simple to obtain strain information from lightweight papers. In the following chapters we discuss other aspects of this problem and propose procedures for strain determination in lightweight materials such as tissue.

LITERATURE

1. JEWETT, Douglas M. An electrical strain gage for the tensile testing of paper. Madison, Wis., Forest Products Research Laboratory, 1963. 3p. (U.S. Forest Service Research Note FPL-03)
2. SETTERHOLM, Vance C. & KUENZI, Edward W. "Method for determining tensile properties of paper." Tappi, 40(6): 197A-204A, June 1957.

3. VAN DEN AKKER, J.A. & HARDACKER, K.W. "Instrumentation studies. LXXXI. The automatic recording of the load elongation characteristic of paper. III. The table model INSTRON (Universal Testing Instrument)." *Tappi*, 41(8): 224A-231A, Aug. 1958.
4. WINK, W.A.; HARDACKER, K.W.; VAN EPEREN, R.H.; VAN DEN AKKER, J.A. "The effect of initial span on the measured tensile properties of paper." *Tappi*, 47(1): 47-54, Jan. 1964.
5. SETTERHOLM, Vance C. & GUNDERSON, Dennis E. "Observations on load-deformation testing." In: MARK, Richard E. (ed.). *Handbook of physical and mechanical testing of paper and paperboard*. New York, M. Dekker, 1983. chapter 4, pp. 115-143.
6. T494 Om-81. Tensile breaking properties of paper and paperboard (using constant rate of elongation apparatus), Official Test Method, *Tappi*, 1982.
7. WINK, W.A.; HARDACKER, K.W.; VAN EPEREN, R.H. "The IPC line-type specimen clamp." *Tappi*, 47(1):13-15, Jan. 1964.
8. CASTAGNEDE, B.; MARK, R.E.; SEO, Y.B. "New concepts and experimental implications in the description of the 3-D elasticity of paper. Part I: General considerations." *Journal of Pulp and Paper Science*, 15(5): J178-J182, Sept. 1989.
9. HENDRY, A.W. "The electrical resistance strain gauge." In: *Elements of experimental stress analysis*. SI edition. Oxford, Pergamon Press, 1977. chapter 4, pp. 32-47.
10. CRAVER, J.K. & TAYLOR, D.L. "Nondestructive sonic measurement of paper elasticity." *Tappi*, 48(3): 142-147, Mar. 1965.
11. TAYLOR, D.L. & CRAVER, J.K. "Anisotropic elasticity of paper from sonic velocity measurements." In: BOLAM, Francis (ed.). *Consolidation of the paper web; Transactions of the Symposium held at Cambridge, Sept. 1965*. London, Technical Section of the British Paper and Board Makers' Association, 1966. v.2, pp. 852-874.
12. MANN, R.W.; BAUM, G.A.; HABEGGER, C.C. "Determination of all nine orthotropic elastic constants for machine-made paper." *Tappi*, 63(2): 163-166, Feb. 1980.

13. MANN, R.W.; BAUM, G.A.; HABEGER, C.C. "Elastic wave propagation in paper." *Tappi*, 62(8): 115-118, Aug. 1979.
14. MOSELEY JR., W.W. "The measurement of molecular orientation in fibers by acoustic methods." *Journal of Applied Polymer Science*, 3(9): 266-276, 1960.
15. KHETAN, R.P. & CHIANG, F.P. "Strain analysis by one-beam laser speckle interferometry. 1. Single aperture method." *Applied Optics*, 15(9): 2205-2215, Sept. 1976.
16. ARCHBOLD, E.; BURCH, J.M.; ENNOS, A.E. "Recording of in-plane surface displacement by double-exposure speckle photography." *Optica Acta*, 17(12): 883-898, 1970.
17. FRANCON, M. *Laser speckle and applications in optics*. New York, Academic Press, 1979. 161p.
18. CASTAGNEDE, B. & MARK, R.E. "Etude d'un champ de deformation inhomogene dans un materiau translucide par Photographie Laser du champ de granularite." *C. R. Acad. Sci. Paris*, t.305, Serie II, pp. 221-224, 1987.
19. SEO, Yung B. "Determination of in-plane elastic constants" In: *Application of laser speckle interferometry (LSI) to the determination of in-plane elastic constants of paper*. Syracuse, State University of New York, College of Environmental Science and Forestry, 1988. (Ph.D. Thesis) chapter VII, pp. 149-174.
20. ARCHBOLD, E. & ENNOS, A.E. "Displacement measurement from double-exposure laser photographs." *Optica Acta*, 19(4): 253-271, 1972.
21. SEO, Yung B. "Experimental procedure for the application of LSI." In: *Application of laser speckle interferometry (LSI) to the determination of in-plane elastic constants of paper*. Syracuse, State University of New York, College of Environmental Science and Forestry, 1988. (Ph.D. Thesis) chapter VI, pp. 121-148.
22. SUTTON, Michael A. & CHAO, Yuh J. "Measurement of strains in a paper tensile specimen using computer vision and digital image correlation. Part 1. Data acquisition and image analysis system." *Tappi Journal*, 71: 173, Mar. 1988.

23. CHAO, Yuh J. & SUTTON, Michael A. "Measurement of strains in a paper tensile specimen using computer vision and digital image correlation. Part 2. Tensile specimen test." Tappi Journal, 71: 153-156, April 1988.
24. DODSON, C.T.J. A contribution to the development of a statistical rheology of bonded fibrous network. London, Brunel University, Department of Physics, 1968. (Ph.D. Thesis) 171p.
25. KYANKA, George Harry. An experimental investigation of the micromechanics of the paper web. Syracuse, N.Y., Syracuse University, Mechanical and Aerospace Engineering, 1976. (Ph.D. Thesis) 124p.

CHAPTER 2

THE TENSION BUCKLING PHENOMENON: A SPECIMEN DESIGN PROBLEM IN TENSILE TESTING OF LOW GRAMMAGE AND/OR LIGHTLY BONDED PAPERS

2.1. Introduction

2.2. Effects of End Constraint During the Tensile Test

2.3. Effect of Specimen Configuration on the Tension Buckling Phenomenon

2.3.1. Experimental Approach for Wrinkling Determination

2.3.2. Determination of Amplitudes of the Wrinkle Waves

2.3.3. Wrinkling Behavior of Rectangular Specimens

2.3.4. The Structural Behavior of Necked-Down Specimens

2.4. Conclusion

2.5. Literature

2.1. INTRODUCTION

The principal objective of this study was to find a specimen configuration appropriate to the uniaxial tensile test. Any experimental determination of specimen geometry must consider the complex structure of the material and the effects of the boundary conditions on the load transfer mechanism, and consequently on the properties to be evaluated. Therefore, no claim is made that the specimen geometry found in this approach is ideal for every grade of paper. However, it gives an indication of how to find the correct geometry in order to avoid undesirable phenomena that could compromise the test method.

In a recent study, Seo [1] used a finite element method to describe the strain distribution in a clamped rectangular tensile test specimen. His subsequent studies [2] on the effects of tension wrinkles on the measurement of elastic constants have emphatically demonstrated the necessity of determining the correct specimen configuration, especially for low grammage and/or lightly bonded papers.

Specimen design represents a compromise between theoretical and practical considerations; both have been incorporated in the development of the dot matrix technique. Therefore, in the following discussion, considerable attention

will be given to the phenomena and mechanisms responsible for unsatisfactory performance of a paper sample under tension loading, and to methods of avoiding these.

2.2. EFFECTS OF END CONSTRAINT DURING THE TENSILE TEST

To perform a uniaxial tensile test, the specimen should be in a pure state of tension. However, it is not easy to achieve this condition, especially in the case of lightweight heterogeneous materials. The conventional test method uses an Instron or similar test machine. The specimen is clamped in the thickness (Z) direction and the load is applied by a continuous motion of the crosshead transmitted through one clamp. The load or force is transferred from the clamp to the specimen through the paper/clamp boundary. The boundary forces are transmitted from fiber to fiber in a shear mode via the interfiber bonds. Although the principal resultant force acting on the specimen is tensile in nature, a complex and anomalous state of stress and strain [3, 4] develops near the grips (Figs. 1 and 2).

The application of constant end displacement induces shearing forces, in-plane lateral restraint of the normal Poisson effect, and bending couples at the edges of the

grips. These factors all contribute to non-uniform deformation across the specimen. At center-span of a long specimen, however, a state of uniform tensile stress and strain exists across the width, according to St. Venant's principle [5].

Analytical and experimental evidence of the tension buckling phenomenon during paper testing has been found by our research group [2]. Our experiments show that the buckling phenomenon, which is caused by the action of conventional clamping devices in a tensile test, is especially severe for lightweight papers. Tension buckling appears in the form of a physical wrinkling of the surface. The wrinkling phenomenon has been studied extensively in the fabrics field [6-9] and is commonly associated with the deformation of a thin membrane. Analysis of such deformations is part of what is generally referred to as tension field theory. However, in the paper field, the theory has not received the attention that it deserves. In this chapter we will discuss the tension buckling phenomenon, its implications and effects on the measurement of paper properties, and the selection of an appropriate specimen configuration to overcome the problem.

2.3. EFFECT OF SPECIMEN CONFIGURATION ON THE TENSION BUCKLING PHENOMENON

Many studies have described the effects of specimen configuration on the mechanical properties of papers and other solid materials [10-14]. Two commonly-cited effects are stress concentration and material inhomogeneity. Recently, considerable attention has also been given to the tension buckling phenomenon [2]. We now realize that even though this effect is localized, it manifests itself in lightweight papers in such a way as to compromise the reliability of the tensile test. It is far superior to avoid the phenomenon, rather than try to account for it in the determination of material mechanical properties. But before one can minimize or eliminate its occurrence, the phenomenon requires quantification. To accomplish this measurement, a non-contact technique was devised. It is discussed in the following sections.

2.3.1. EXPERIMENTAL APPROACH FOR WRINKLING DETERMINATION

It was determined that a quantitative measurement of the wrinkling of a specimen during tensile testing in the Instron was needed. We found that the technique used by Seo [2] for measuring the wrinkles of medium and high basis weight papers was inappropriate for low grammage and/or lightly bonded papers.

Since the wrinkling phenomenon is an out-of-plane displacement of the specimen, we should be able to photograph it from a low angle to the cross section of the specimen. To do this, a very fine horizontal line was drawn on the surface across the width at the center of the free-span of the specimens. Using airbrush¹ techniques [15, 16] and drawing² ink with quick drying properties we were able to draw such a line without any damage and without applying any significant pressure to the surface of the specimen. This reference line was used as a baseline to be photographed in an undeformed shape (unstrained) and later in an out-of-plane deformed shape (strained), if such deformation in fact took place.

After the test specimen was conditioned [17] it was

1 - See Chapter 3, Figure 1, for complete description.
2 - Higgins - Noon waterproof drawing ink. Black 4425. For extra-fine lines. For use with airbrush. Faber-Castell Corporation, Lewisburg, TN 37091, USA

loaded in tension up to the point of failure. A constant crosshead speed of 2mm/min. was used. A sequential set of photographs was taken at various strain levels from the unstrained condition up to the level at which the wrinkles of the baseline on the specimen were pronounced. The environmentally pre-conditioned films were developed and reconditioned back to the same environmental condition [17] used to perform the tensile tests and to take the photographs. The negatives were placed between two optical glass plates, and enlarged onto an electronic digitizing table¹. The projected baseline image, representing a profile of the wrinkled surface of the specimen, was then digitized; the computerized data were stored for later analysis. The wrinkles were represented in graphic form by the difference of amplitudes of the baseline waves, from the unstrained to the strained condition. Figs. 3 and 4 are schematics of the experimental approach for the photographic procedure.

The paper material used was a lightweight tissue paper of 25g/m² basis weight. It was supplied in three forms: highly oriented machine made paper, moderately oriented machine made paper, and handsheets. Specimens of rectangular and necked-down shapes with different geometric configurations were tested.

1 - Altek Digitizer AC90C, Altek Corp., 2150 Industrial Parkway, Silver Spring, MD 20904, USA.

2.3.2. DETERMINATION OF AMPLITUDES OF THE WRINKLE WAVES

The amplitudes of the wrinkle waves were obtained by the following procedure: The amplitude at any position across the width of the specimen was calculated as the vertical difference between it and the corresponding point on a linear regression line fitted on it. The regression line was used as a baseline rather than the same point unstrained because of the complex state of in-plane and out-of-plane displacement in the wrinkled specimen, which did not allow alignment of the digitized data of the unstrained baseline in an x-y coordinate system.

Ideally the amplitudes should be determined in a plane parallel to the cross sectional area of the test specimen, but this was not possible due to the tilted angle (parallax angle) at which the photographs were taken. It was necessary to rotate the amplitude data into this plane (through angle \angle_P in Fig. 5). To do so, we used the equation [2.1] shown in Fig. 5, with the help of an IBM Personal Computer. The results are shown in graphic form in Figs. 6 through 13 for rectangular tensile specimens and in Figs. 22 through 29 for necked-down tensile specimens.

The necessity of rotating the amplitude data illustrates the ability of the system to detect the amplitude of the wrinkling (A in Fig. 5), in which a minimum parallax

angle (α) is desirable. Referring again to Fig. 5: In order to satisfy the condition $A = A_1$ in equation [2.1], (i.e., no rotation of the data is needed), we must have $\cos \alpha_p = 1$. However, this occurs only at $\alpha_p = 0$, when photographs are taken in a plane perfectly parallel to the cross section of the tensile test specimen (no parallax). Therefore, the ability of the system to detect wrinkling is reduced as the parallax angle α_p becomes greater than zero degrees. Using the mirror technique and photographing the virtual image of the baseline rather than the baseline on the test specimen, we minimize the parallax effect about 50%, as a result of reducing the parallax angle by the same amount. A parallax angle of 27 degrees was the smallest that could be achieved under the experimental conditions.

2.3.3. WRINKLING BEHAVIOR OF RECTANGULAR SPECIMENS

Although a necked-down tensile test specimen is used for most composite materials [12, 18], the most common, practical and recommended shape for paper has been rectangular [19]. Analytical solutions to the problem of buckling under tension of rectangular membranes with anisotropic and nonlinear elastic properties have been reported in the

literature [6, 8, 9]. The tension buckling phenomenon is demonstrably the cause of wrinkling in rectangular tensile paper specimens [2]. However, our objective is to develop a wrinkle-free tensile specimen for stress-strain analysis, rather than to show a mathematical solution for the problem.

There is a relationship between the geometrical properties of the specimen and the influence on the end constraint in testing anisotropic materials [20, 21]. These factors are important components of equations that describe for flat plates [22], the critical stress condition at which wrinkling begins. An experiment in which we used rectangular tensile test specimens of different sizes was set up. Lengths of 100, 150 and 240mm, and widths of 15, 20, 25 and 50mm were used, which generated a factorial combination of twelve different aspect (length to width) ratios. Specimens with aspect ratios ranging from 2 to 16 were tested. Consequently, four different thickness to width ratios (t/W) were also tested. These tests were performed both for the papers with fiber orientation and for the handsheets.

Unfortunately, all attempts to achieve a wrinkle-free rectangular tensile test specimen failed. The results of tests on specimens with an aspect ratio of 12, shown in Figs. 6 through 13, are typical of every rectangular specimen tested. Aspect ratio *per se* is not a controlling factor. The tests demonstrated that for a tensile test specimen of finite length, there is a grip effect (restraint of lateral

shape of the cross-sections of the MD, CD and handsheet specimens at high strain levels (close to the point of failure). From these figures, it can be seen that no significant changes in the shape of the cross-sections in the width direction are observable (cf. equivalent shapes in the unstrained state, Figs. 22, 24 and 27 respectively).

An interesting phenomenon was observed for CD and handsheet specimens: The total failure (rupture) was not as abrupt as in the MD specimens, and at the moment of rupture, the buckle-preventing action of the lateral tension field was interrupted, the structure became unstable, tension buckling took place and a pronounced out-of-plane displacement occurred (Figs. 26 and 29). At this point, the specimen was unable to carry the load, it became wrinkled and an abrupt load decrease was observed on the load-time curve. We have taken advantage of this phenomenon to identify the imminent point of rupture of these specimens during the test.

2.4. CONCLUSION

For low grammage and lightly bonded papers under any state of uniaxial tensile loading, the rectangular specimens should be avoided. In this experiment the necked-

down specimen was successfully used to prevent tension buckling and thus to provide wrinkle-free specimen performance during the entire tensile test. Other advantages of such a specimen design have been reported in the literature [9]. Specimen design ideally should be derived by a combination of experimental investigation and finite element analysis. Our experimental model E, which was the model chosen to be used for strain measurements by the dot matrix technique, might not be the best one for other grades of paper. The appropriate specimen configuration should be determined individually for the grade to be tested.

The approach developed in this chapter is not restricted to paper science. The mechanism of wrinkle prevention by means of developing a lateral tensile stress field, as occurs in necked-down specimens, may be applied to other sheet or foil materials as well. In these cases, specimen design should be done for each specific material.

2.5. LITERATURE

1. SEO, Yung B. Application of laser speckle interferometry (LSI) to the determination of in-plane elastic constants of paper. Syracuse, N.Y., State University of New York, College of Environmental Science and Forestry, 1988. (Ph.D. Thesis), Chapter IV, pp. 52-82.

2. SEO, Yung. B. *ibid.*, Chapter V, pp. 83-120.
3. JOHNSON, Jay A.; BENNETT, Keith A.; MONTREY, Henry M. "Failure phenomena." In: MARK, Richard E. (ed.) *Handbook of physical and mechanical testing of paper and paperboard*. New York, M. Dekker, 1983. v.1, chapter 5, pp. 145-253.
4. KIMURA, M. & NAKAO, T. "Stress and strain analysis of a rectangular specimen in an enforced-equal-displacement condition." *Tappi* 68(8): 114-115, Aug. 1985.
5. BEER, F. P. & JOHNSTON, E.R. "Stress and strain - axial loading." In: *Mechanics of materials*. New York, McGraw-Hill, 1981, Chapter 2.
6. MANSFIELD, E. H. "Analysis of wrinkled membranes with anisotropic and nonlinear elastic properties." *Proc. Roy. Soc. Lond. A.* 353: 475-498, 1977.
7. MANSFIELD, E. H. "Load transfer via a wrinkled membrane." *Proc. Roy. Soc. Lond. A.* 316: 269-289, 1970.
8. STEIN, Manuel & HEDGEPEETH, John M. "Analysis of partly wrinkled membranes." *National Aeronautics and Space Administration. Technical Note D-813*, July 1961.
9. WU, Chien H. & CANFIELD, Thomas R. "Wrinkling in finite plane-stress theory." *Quarterly of Applied Mathematics* 39(2): 179-197, July 1981.
10. BODIG, Jozsef & FRANCE, Raymond C. "A necked-down tensile test specimen for paper." *Tappi* 57(11): 125-128, Nov. 1974.
11. FINDLEY, W.N. & REED, R.M. "Effect of specimen shape and cyclic loading on tension tests of two epoxy resins." *Journal of Testing and Evaluation* 9(1): 24-27, Jan. 1981.
12. MARKWARDT, L. J. & YOUNGQUIST, W. G. *Tension test methods for wood, wood-base materials, and sandwich constructions*. Madison, Wis., U. S. Department of Agriculture, Forest Service, Forest Products Laboratory, 1956. (Report no. 2055).
13. SETTERHOLM, Vance & KUENZI, E. W. "Method for determining tensile properties of paper." *Tappi* 40(6): 197A-204A, June 1957.

14. UESAKA, Tetsu. "Specimen design for mechanical testing of paper and paperboard." In: MARK, Richard E. (ed.) Handbook of physical and mechanical testing of paper and paperboard. New York, M. Dekker, 1983. v.1., Chapter 3, pp. 77-113.
15. PAASCHE AIRBRUSH COMPANY. 22 airbrush lessons for beginners. Harwood Heights, Il. 11p.
16. OWEN, Peter & SUTCLIFFE, John. The manual of airbrushing. London, Thames & Hudson, 1985. 159p.
17. TAPPI T 402. Standard conditioning and testing atmospheres for paper, board, pulp handsheets and related products, TAPPI, 1982.
18. ASTM D805-72. Standard methods of testing veneer, plywood, and other glued veneer construction. 1973 Annual Book of ASTM Standards, pp. 213-225.
19. TAPPI T 494 om-81. Tensile breaking properties of paper and paperboard (using constant rate of elongation apparatus), TAPPI, April 1983. 5p.
20. PAGANO, N.J. & HALPIN, J.C. "Influence of end constraint in the testing of anisotropic bodies." J. Composite Materials 2(1): 18-31, Jan. 1968.
21. RIZZO, R.R. "More on the influence of end constraints on off-axis tensile tests." J. Composite Materials 3(4): 202-219, April 1969.
22. SEELY, F.B. & SMITH, J.O. "Buckling of cylindrical tubes under uniform external pressure." In: Advanced mechanics of materials. 2nd. ed. New York, J. Wiley, 1952. chapter 21, pp. 607-625.
23. HOLLMARK, H. "Mechanical properties of tissue." In: MARK, Richard E. (ed.) Handbook of physical and mechanical testing of paper and paperboard. New York, M. Dekker, 1983. v.1, chapter 11, pp. 497-521.
24. SEO, Yung B. FEM stress distribution. unpublished note.

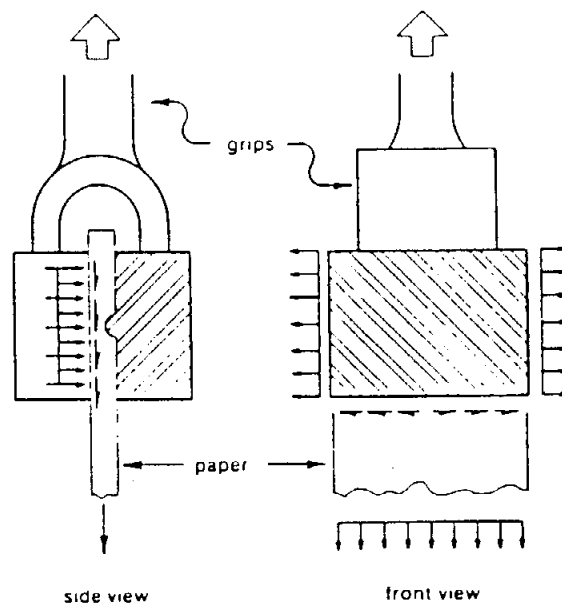


Fig. 1. Force distributions in the vicinity of the grips.
[from Ref. 3].

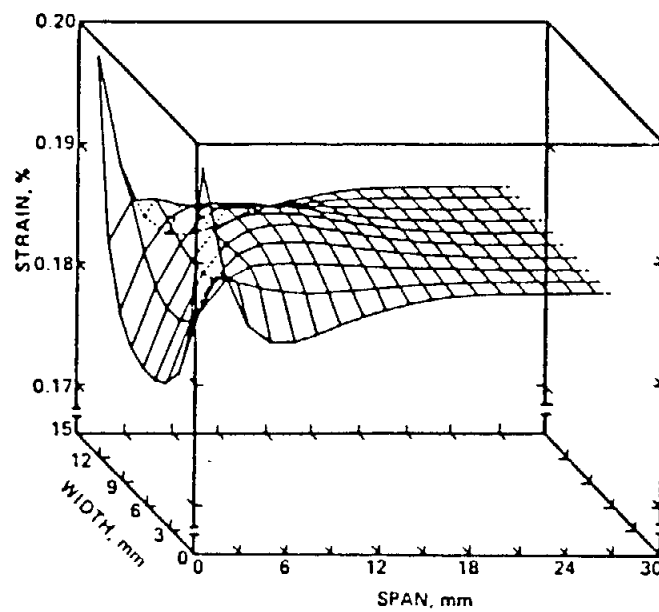
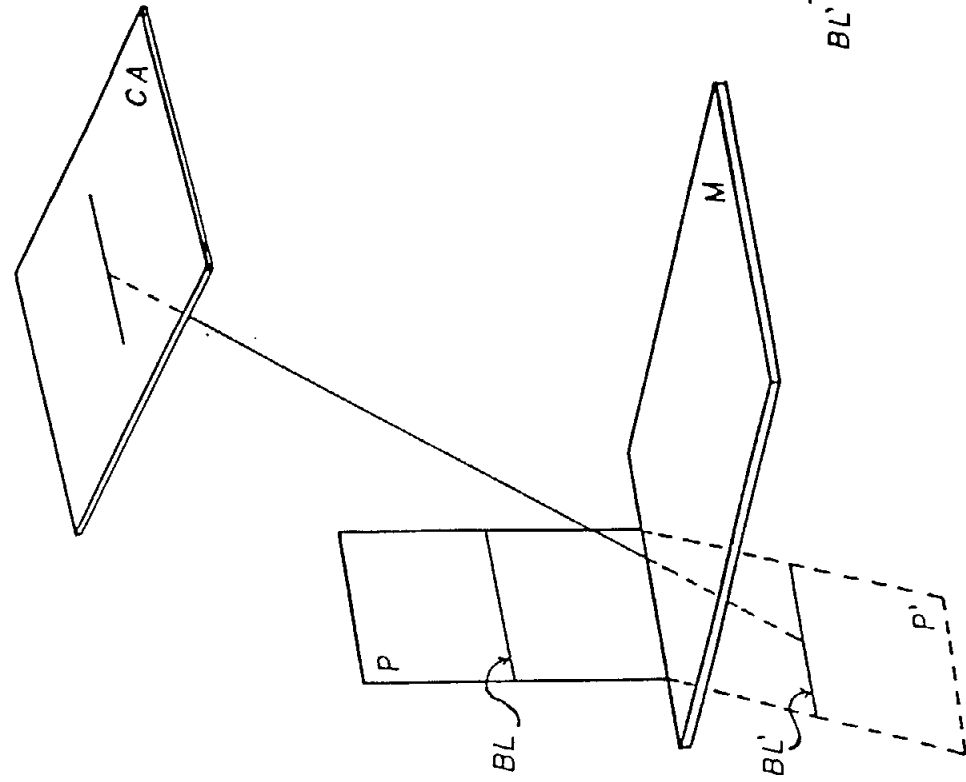


Fig. 2. Strain distribution in a rectangular isotropic specimen in
the vicinity of a clamp [from Ref. 4].

Fig. 3. Perspective view of the photographic approach.

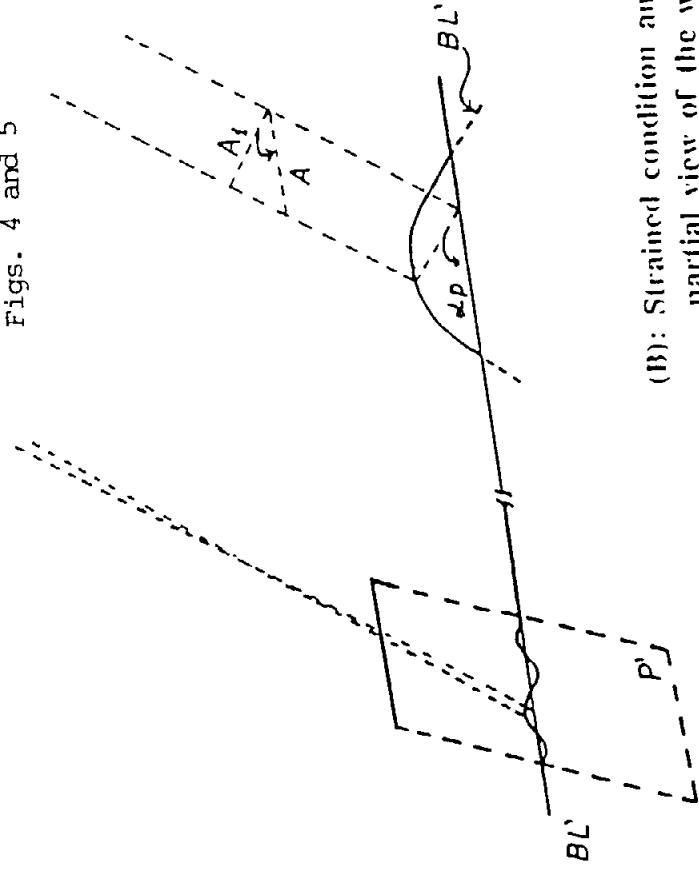


(A): Unstrained condition

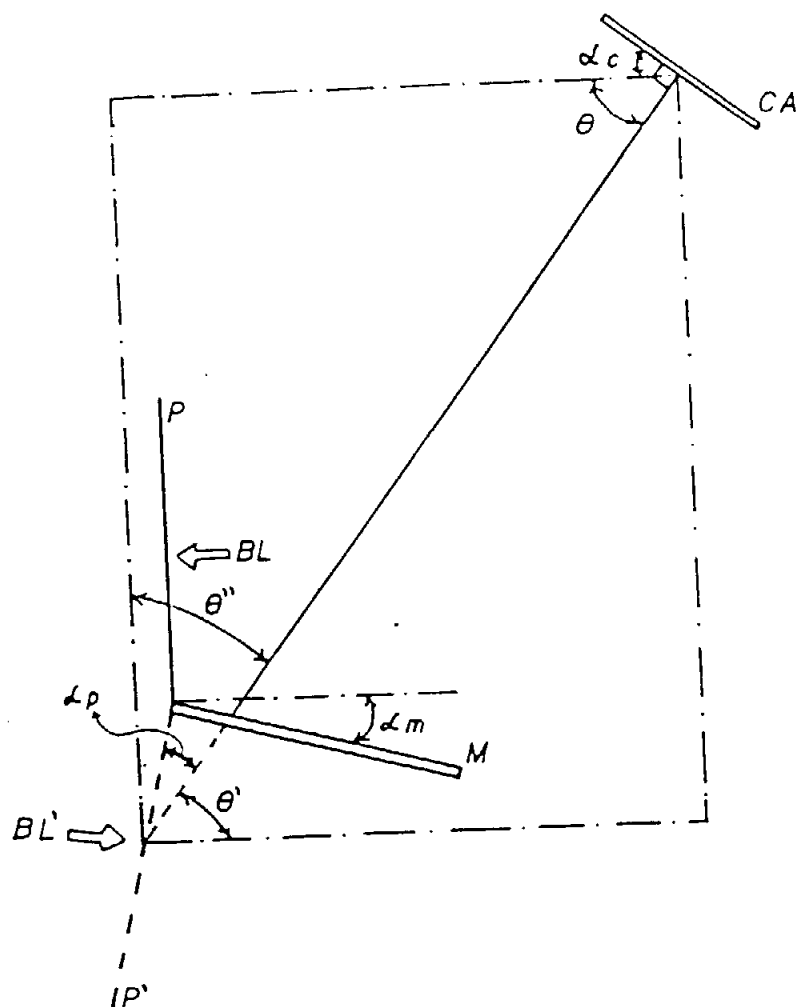
LEGEND:

- CA : View camera (photographic plate)
 - P : Tensile test specimen
 - BL : Baseline on the Tensile test specimen
 - M : First surface mirror
 - BL': Virtual image of the baseline (To be photographed)
 - P': Virtual image of the Tensile test specimen
 - Δ_1 : Digitized amplitude
 - A : Rotated amplitude due to the parallax angle (αp)
 - αp : Parallax angle (photographic angle)
- This angle is the same as αp in

Figs. 4 and 5



(B): Strained condition and enlarged partial view of the wrinkled baseline.



NOTE:

$$\theta = 90^\circ - \alpha_c$$

$$\theta = \theta'$$

$$\theta'' = 90^\circ - \theta'$$

$$\alpha_p = \theta'' - \alpha_m$$

MEASURED EXPERIMENTALLY:

$$\alpha_m = 10^\circ$$

$$\alpha_c = 37^\circ$$

Fig. 4. Side view of the photographic approach.

LEGEND:

CA : View camera (Photographic plate)

M : First surface mirror

P : Tensile test specimen

α_c : Angle between the camera (photographic plate) and the horizontal

P' : Virtual image of the tensile test specimen

α_m : Angle between the mirror and the horizontal

α_p : Parallax angle (photographic angle) from a parallel plane of the virtual image of the cross sectional area of the tensile test specimen. at the baseline

BL : Position of the baseline on the test specimen

BL' : Position of the baseline on the virtual image of the test specimen

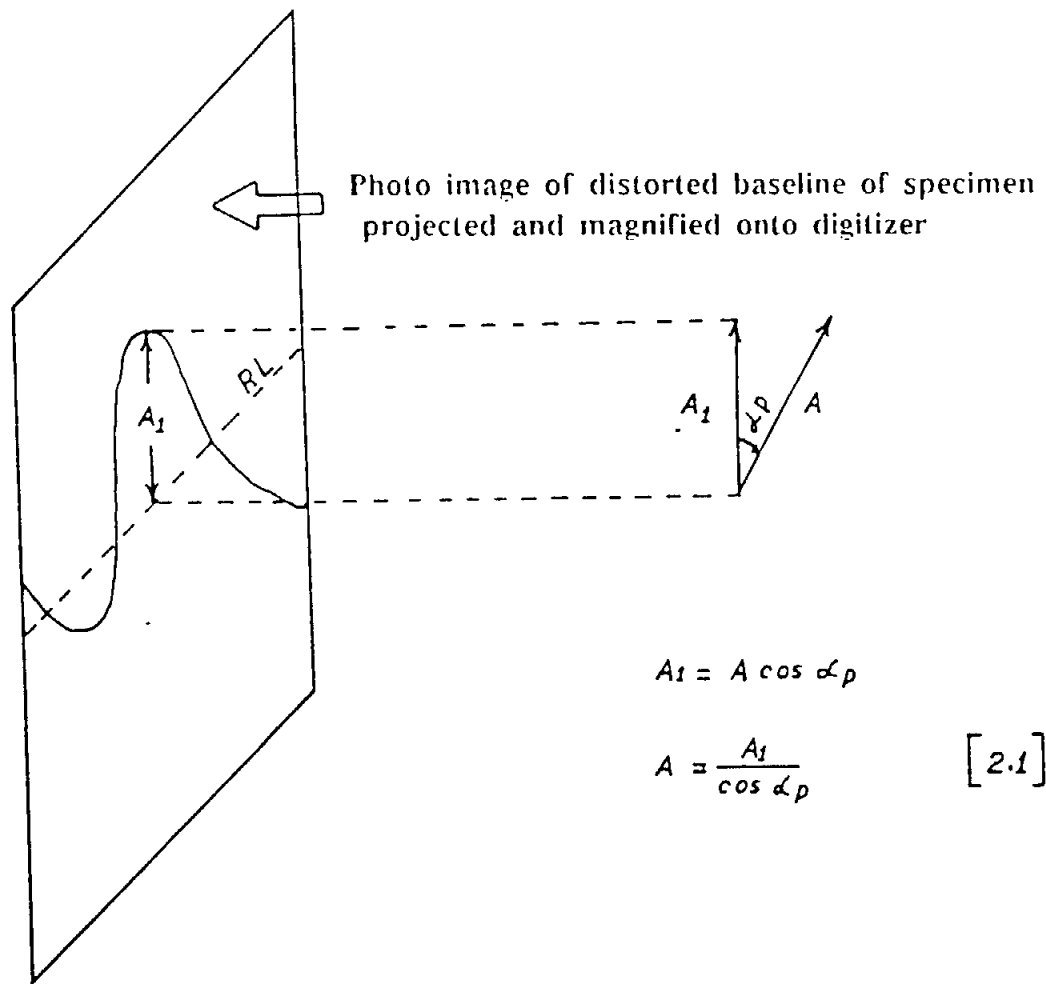


Fig. 5. Projected photographic image of the wrinkled surface (baseline) of the tensile test specimen.

LEGEND:

A_1 : Digitized amplitude of the wrinkle waves

A : Rotated amplitude through the parallax angle α_p

RL : Fitted regression line

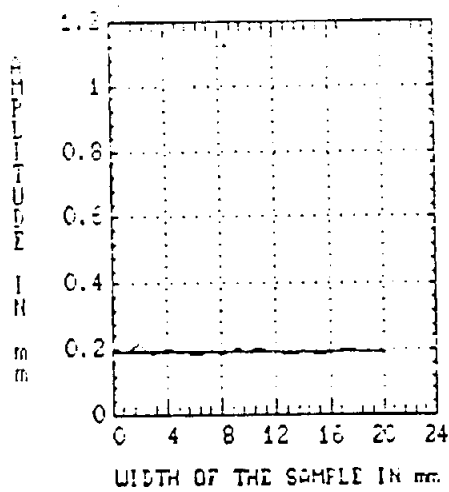


Fig. 6. Wrinkle at zero displacement level for rectangular tensile specimen (MD). Aspect ratio (L/W)=12

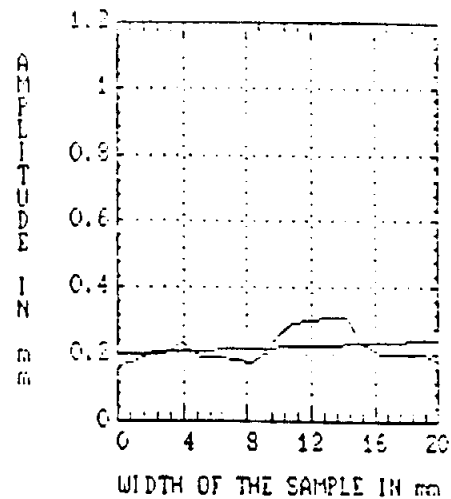


Fig. 7. Wrinkle at 2% of crosshead displacement for rectangular tensile specimen (MD). Aspect ratio (L/W)=12

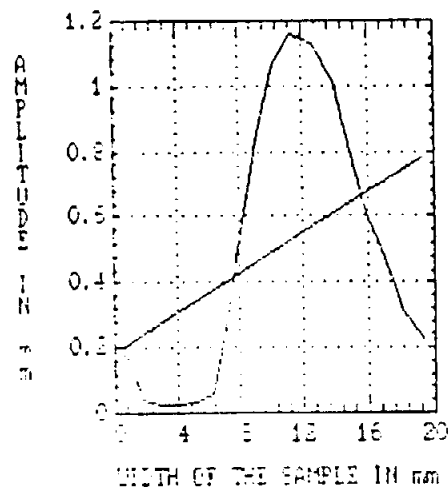


Fig. 8. Wrinkle at Failure (7.73% crosshead displacement) for rectangular tensile specimen (MD). Aspect ratio (L/W)=12

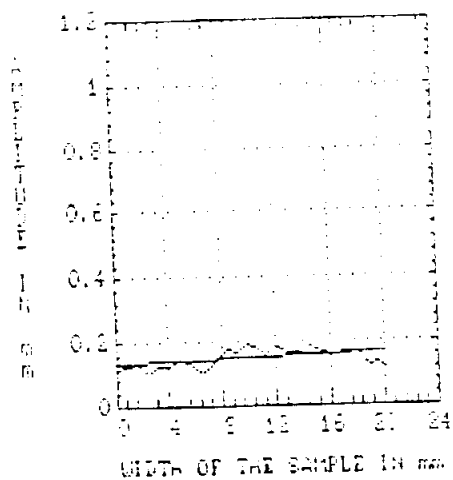


Fig. 9. Wrinkle at zero displacement level for rectangular tensile specimen (CD). Aspect ratio (L/W)=12

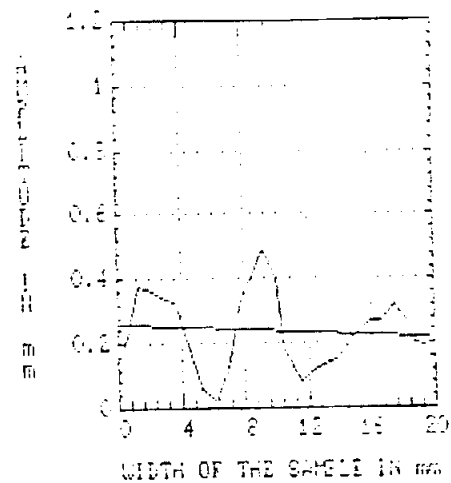


Fig. 10. Wrinkle at 2% of crosshead displacement for rectangular tensile specimen (CD). Aspect ratio (L/W)= 12

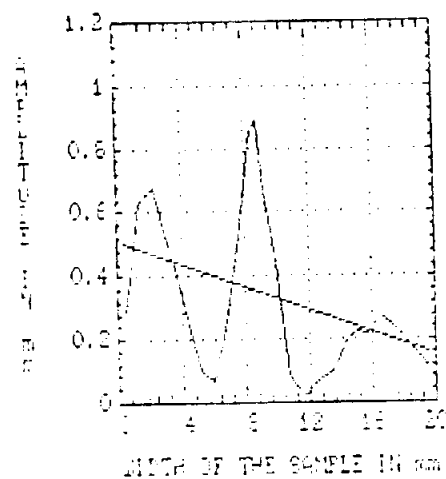


Fig. 11. Wrinkle at failure (11% crosshead displacement) for rectangular tensile specimen (CD). Aspect ratio (L/W)=12

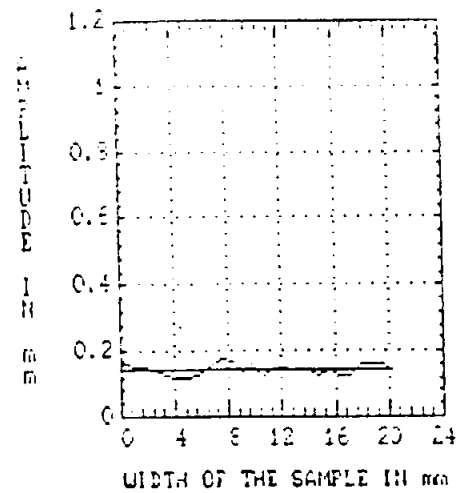


Fig. 12. Wrinkle at zero displacement level
for rectangular tensile specimen (handsheet).
Aspect ratio (L/W)=12

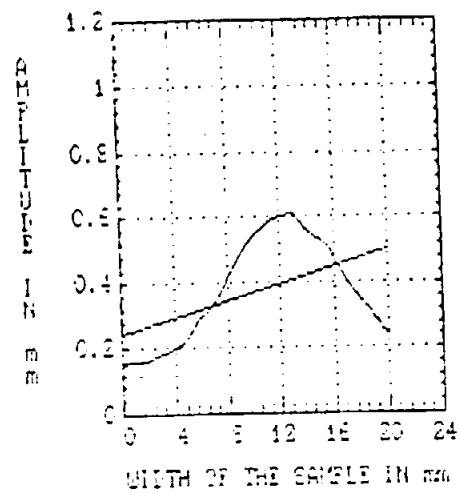


Fig. 13. Wrinkle at 1% crosshead displacement
for rectangular tensile specimen (handsheet).
Aspect ratio (L/W)=12

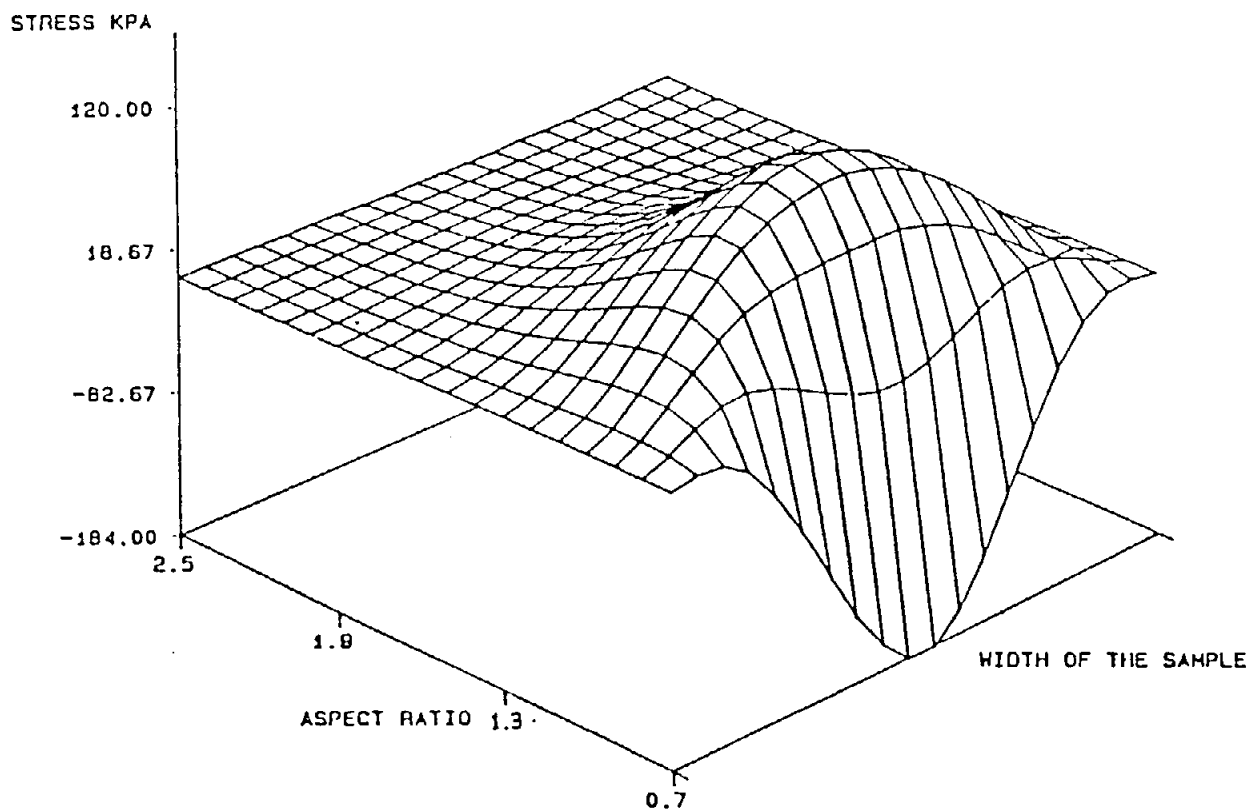


Fig. 14. Pattern of lateral compressive stress for handsheet paper. Compressive stress is denoted as positive. [from Ref. 1].

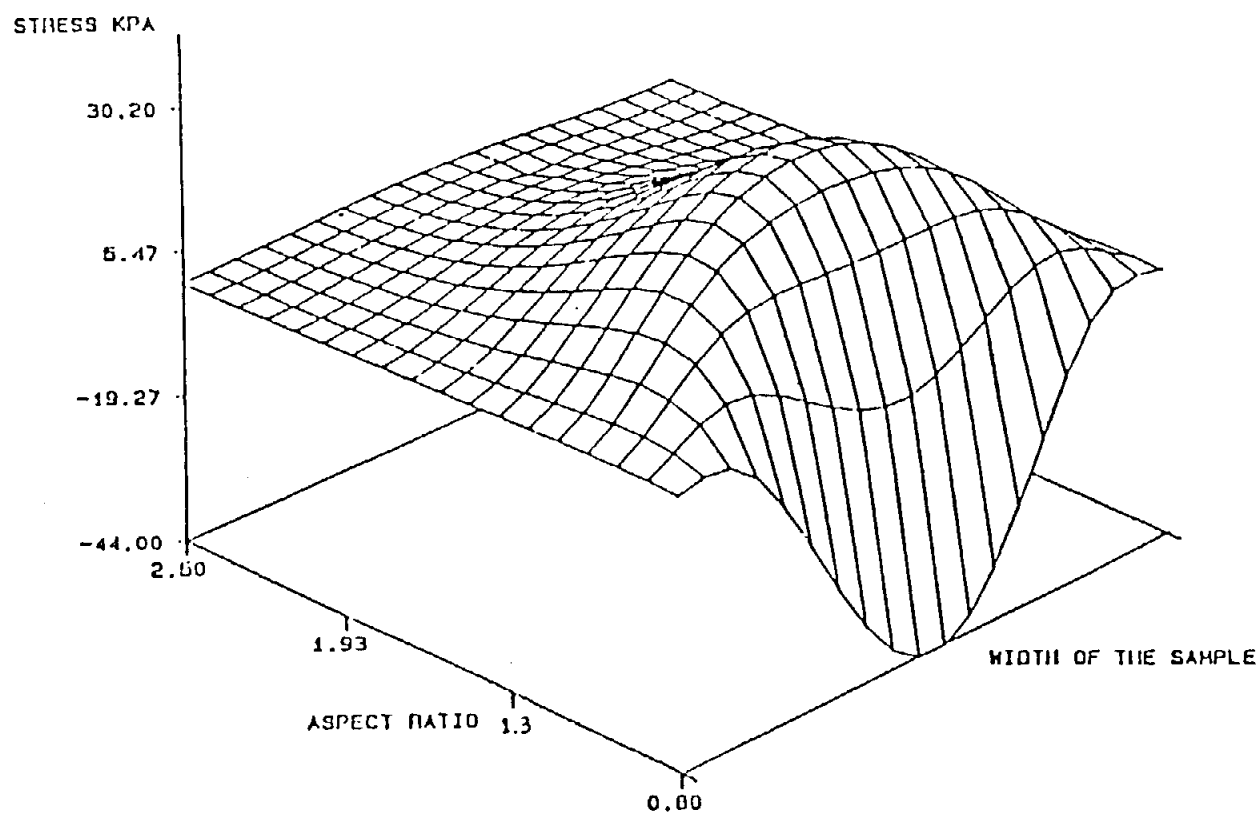


Fig. 15. Pattern of lateral compressive stress for machine-made paper. Compressive stress is denoted as positive. [from Ref. 1].

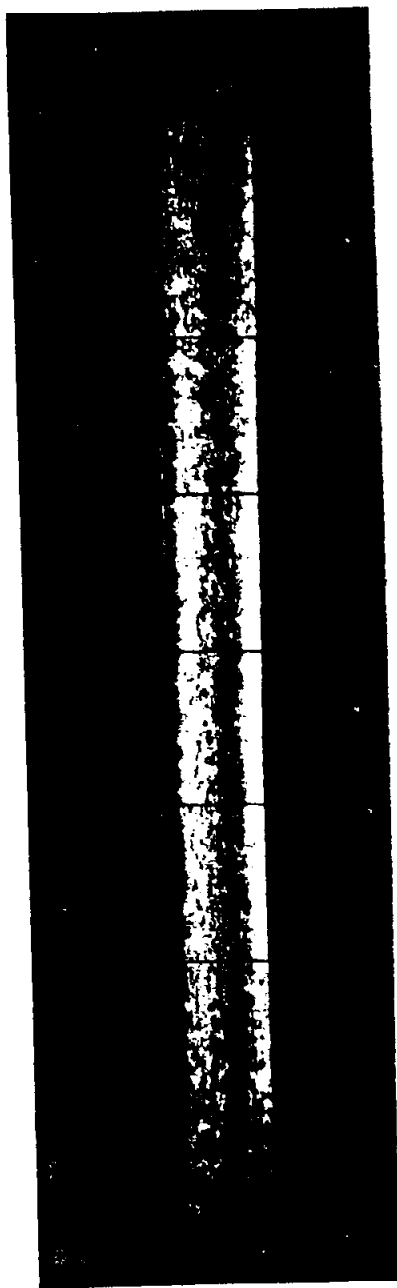


Fig. 16. Rectangular tensile CD specimen photographed at 3% of crosshead displacement. Wrinkling occurs along the entire length.
Length : 240mm
Width : 20mm
Aspect ratio (L/W) = 12



Fig. 17. Rectangular tensile CD specimen photographed at 3% of crosshead displacement. Wrinkling occurs along the entire length.
Length : 240mm
Width : 50mm
Aspect ratio (L/W) = 4.8

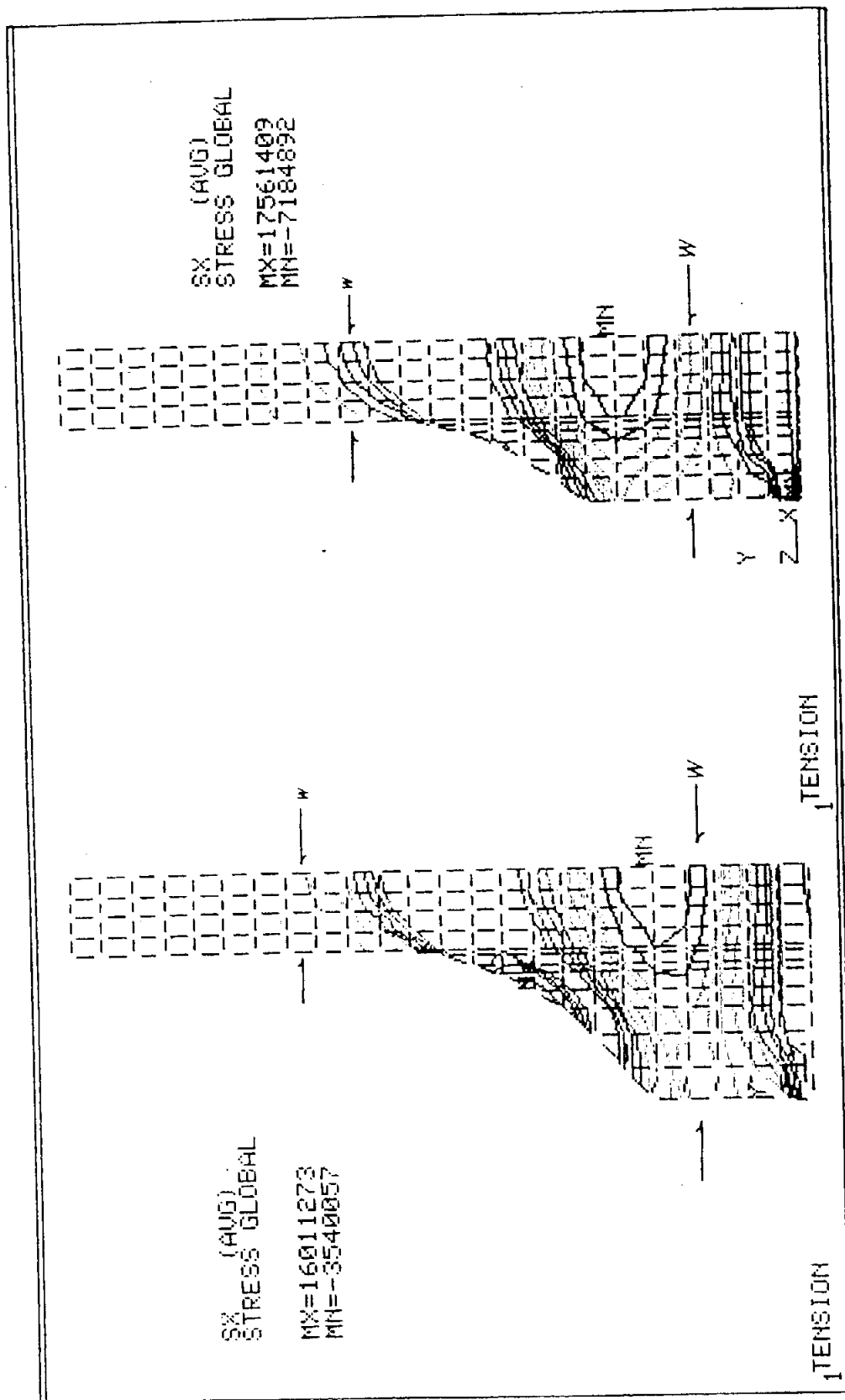


Fig. 18. The finite element models used to demonstrate lateral stress fields in necked-down specimens (figure shows 1/4 of the specimen). From Seo[24].
 left: transition ratio $(W'/w)=4.7$ right: transition ratio $(W/w)=3.3$
 Distribution of the lateral stress field:
 red(maximum-tension)) yellow) green) light blue) dark blue(minimum-compression)

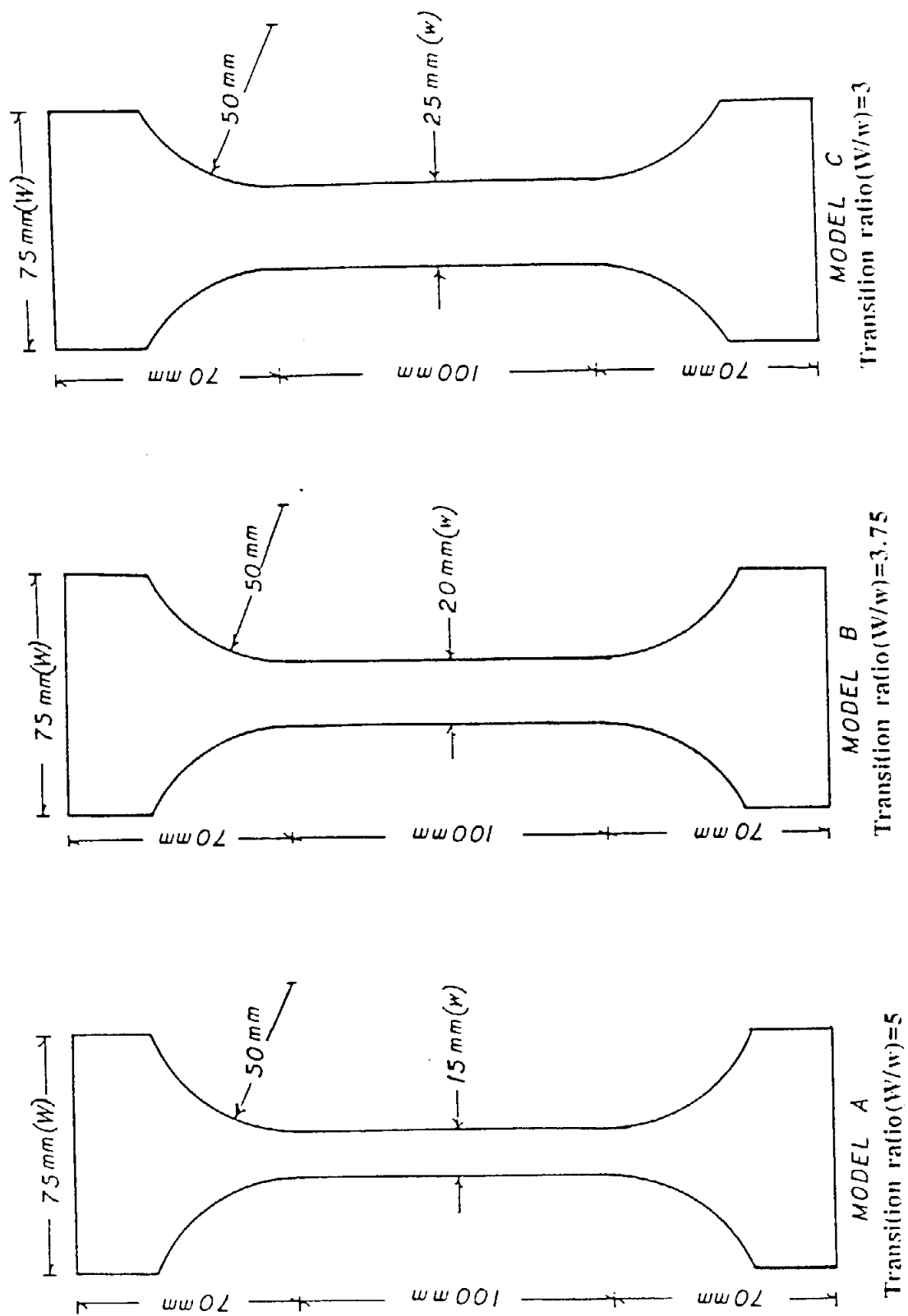


Fig. 19. Models of necked-down specimens used for tension test trials.

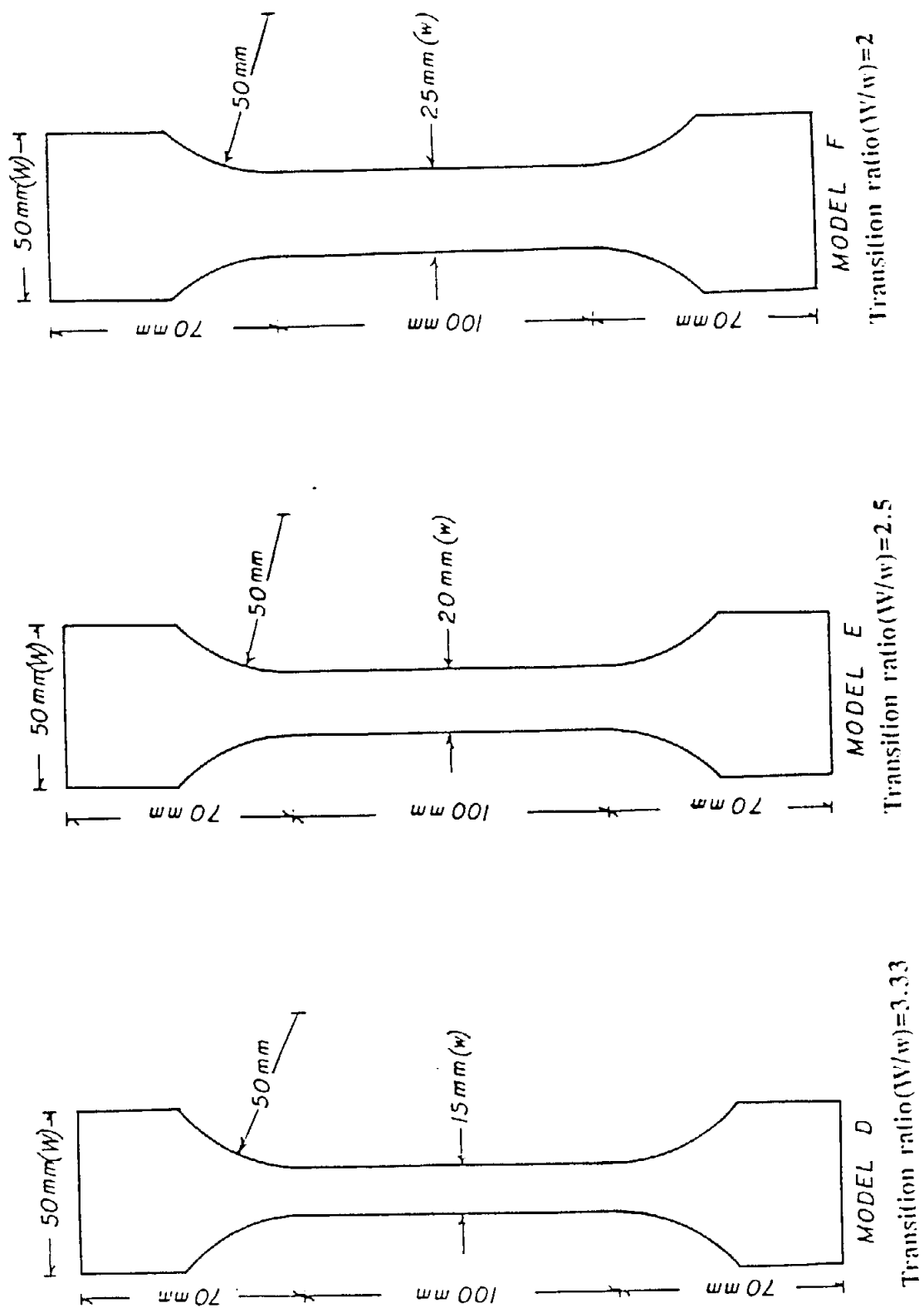


Fig. 20. Models of necked-down specimens used for tension test trials.

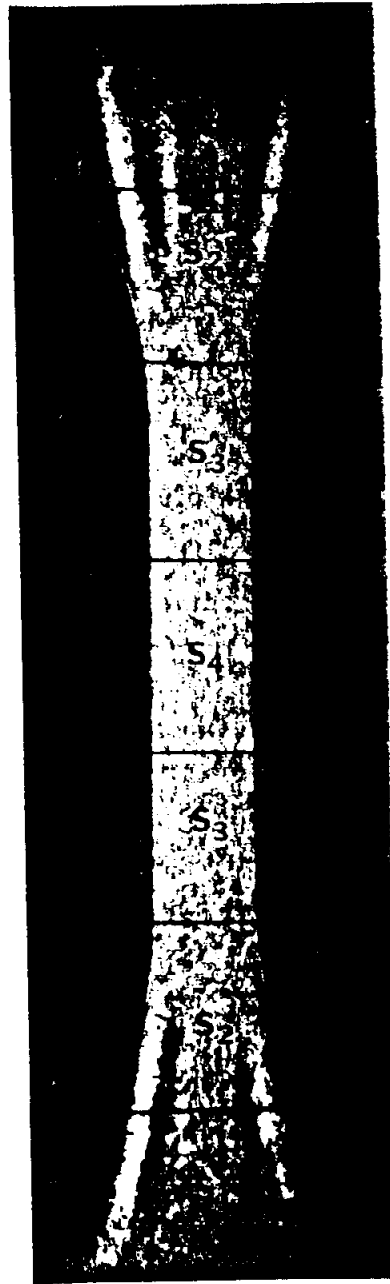


Fig. 21. Necked-down tensile CD specimen (Model E in Fig. 20). Photographed at 6.5% of crosshead displacement (close to total failure). The central section(S_4) is wrinkle free.

S_1 : Wide rectangular sections (near the grips)

S_2 : Transition sections

S_3, S_4 : Narrow rectangular sections

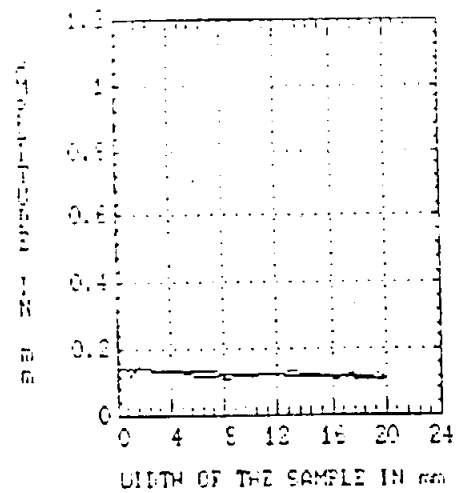


Fig. 22. Wrinkle at zero displacement level for necked-down tensile specimen (MD).
Transition ratio (W/w)=2.5

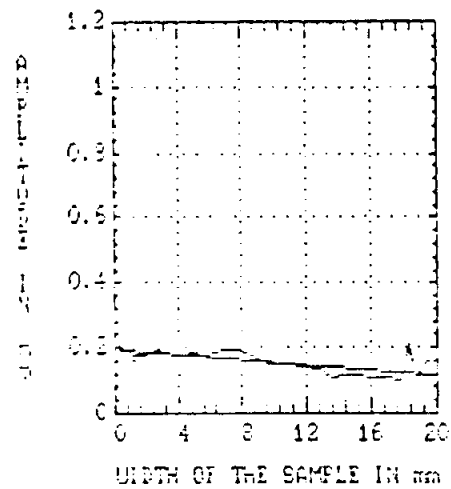


Fig. 23. Wrinkle at 6.4% of crosshead displacement for necked-down tensile specimen (MD).
Transition ratio (W/w)=2.5

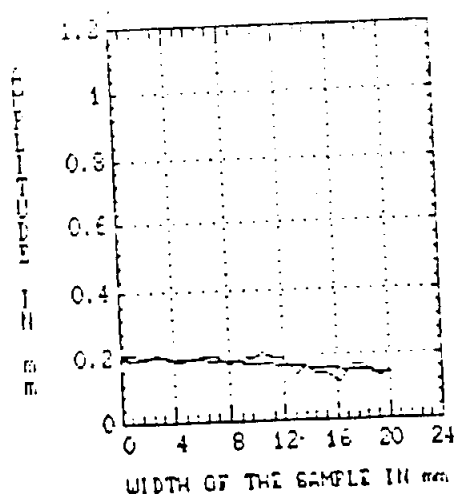


Fig. 24. Wrinkle at zero displacement level for necked-down tensile specimen (CD).
Transition ratio (W/w)=2.5

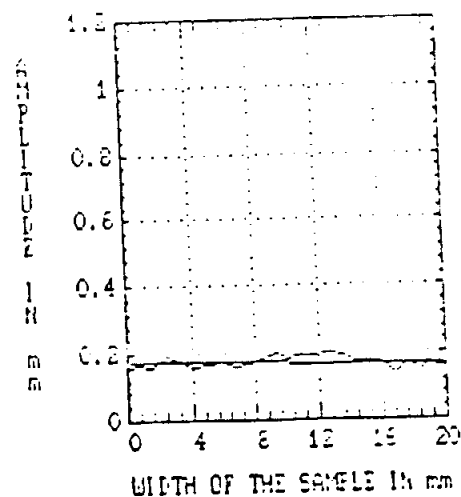


Fig. 25. Wrinkle at 10.35% of crosshead displacement for necked-down tensile specimen (CD).
Transition ratio (W/w)=2.5

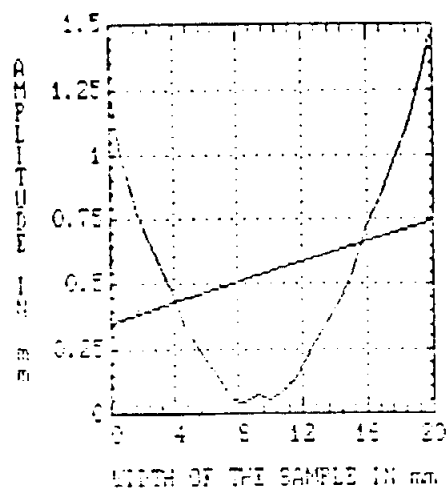


Fig. 26. Wrinkle at failure level for necked-down tensile specimen (CD).
This phenomenon occurs only instantaneously as rupture commences.
Transition ratio (W/w)=2.5

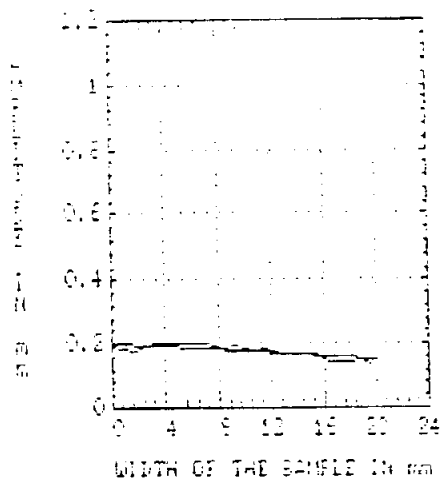


Fig. 27. Wrinkle at zero displacement level for necked-down tensile specimen (handsheet).
transition ratio $(W/w)=2.5$

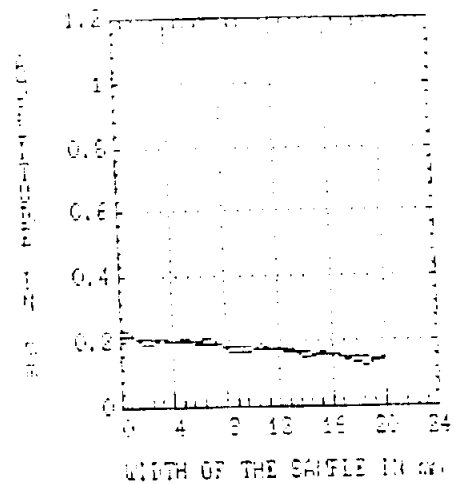


Fig. 28. Wrinkle at 1% of crosshead displacement for necked-down tensile specimen (handsheet).
Transition ratio $(W/w)=2.5$

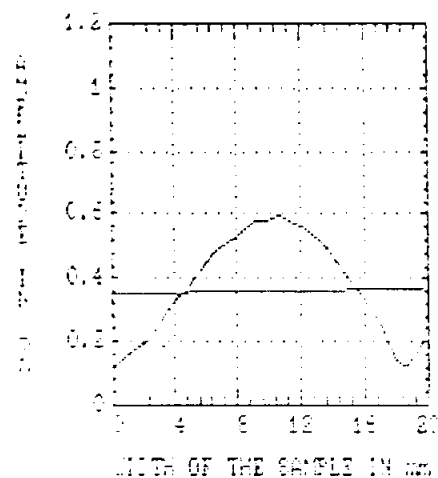


Fig. 29. Wrinkle at failure displacement level for necked-down tensile specimen (handsheet). Transition ratio $(W/w)=2.5$
This phenomenon occurs only instantaneously as rupture commences.

CHAPTER 3

THE DOT MATRIX: A TECHNIQUE FOR STRAIN MEASUREMENT OF LOW GRAMMAGE AND/OR LIGHTLY BONDED PAPERS

- 3.1. Introduction
- 3.2. Design of the Grid Pattern
- 3.3. Recording procedure for the dot matrix system
- 3.4. Data Acquisition for Stress Computations
- 3.5. Data Acquisition for Displacement Measurements
- 3.6. Data Processing for Strain Calculations
- 3.7. Results of the Stress-strain Relationships
- 3.8. Results of Strain Field Characterization
- 3.9. Conclusion
- 3.10. Literature
- 3.11. Appendix A
- 3.12. Appendix B

3.1. INTRODUCTION

In this chapter, we report on the development of the Dot Matrix Technique, a system that essentially involves a combination of airbrush and photographic techniques for non-contacting displacement measurements. We believe that this technique offers many new possibilities for deformation and strain determination in thin sheet materials such as paper; it has special utility for lightweight papers. A prime example is tissue, which characteristically has low grammage and density, high bulk and softness, large voids and a lightly bonded network. These characteristics make the use of conventional mechanical, optical and acoustical systems difficult or impossible. As a metrological tool, the Dot Matrix method is simple and allows modification during data acquisition or processing to adapt to the particular needs of the researcher. Better methods for measuring displacements are always needed, and we believe this technique will find wide application as it is further automated and improved.

The Dot Matrix system is based on the geometric interpretation of displacement vectors computed from two sets of data obtained from a grid pattern (matrix of dots) in the undeformed and deformed states. By knowing the distance and direction between dots and their corresponding displacements, normal and shear strains at different points in the specimen

within the grid can be determined. The matrix of dots is applied on the surface of the paper using an airbrush technique. A camera records the image of the matrix from its undeformed and deformed states through the entire range of a test. These constitute the fundamentals of the method. The concepts and applications of the method will be presented and discussed in the following sections.

3.2. DESIGN OF THE GRID PATTERN

The airbrush is a painting instrument that can produce effects ranging from pencillike lines to smooth, uniform areas of different tonal gradations that may be controlled from the lightest discernible tint to complete opaque coverage [1]. The exact date of the invention of the airbrush is not certain; it was probably shortly before 1893, at which time Charles L. Burdick, an American, patented the device in England and later brought it to the United States [2]. It is a versatile tool with many applications in the design, engineering and commercial art fields. For example, it has been used extensively in architectural and technical illustration and in rendering production drawings for textiles, plastics, ceramics and other industrial products.

In our case, the airbrush (Fig. 1) was used to produce a grid pattern (a matrix of dots) on the surface of the paper specimen with the use of a masking (template) technique.

The template material was MYLAR film type D300-gauge [3], a lightweight, strong, tough, transparent plastic film made from polyethylene terephthalate. Suitable physical, chemical, thermal, and optical properties [4] enabled it to be used in our application.

For convenience, easy handling, and cleaning during routine use, a rectangular plate of the film with dimensions of 100 x 70 x 0.119mm was used. To make the template, this plate was mounted on an X-Y translation stage. A sharp-pointed steel needle of uniform diameter ($100 \pm 5 \mu\text{m}$) was positioned in a Z-translation stage to punch the plastic plate, thus producing a perforated template of 25 rows and 17 columns of holes (25 x 17 matrix with a total of 425 holes) located $1 \pm 0.005\text{mm}$ apart, center to center. Two extra columns of holes were made parallel and very close to the edges of the test specimen. The separation distance of these columns was 20mm. These columns (columns of alignment) were used to align the template parallel to the edges of the test specimen. The test specimen (model E shown in Fig. 20 of chapter 2 and also shown in Fig. 6 of this chapter) was fixed on a flat piece of cardboard with adhesive tape at the ends. The alignment was done under a stereo microscope by superpositioning the

template on the center of the test specimen in a manner such that the holes that constituted the columns of alignment for the template coincided with the edges of the test specimen. To avoid any subsequent misalignment of the template over the test specimen, the template was also fixed on the cardboard with adhesive tape. This set-up facilitated the handling of the test specimen during the airbrush procedure.

The airbrush sprays a cone of fluid (Fig. 2) in a constant quantity per unit time, given stable air pressure and lever position. No matter how far the target (template and test specimen) is from the nozzle, it receives the same amount of colorant. It follows, then, that if the same amount of colorant is distributed over a small area versus a large area, the density of the color in the two areas will differ. The colorant will be more concentrated in the small area, and more diffuse in the larger area. The distance of the airbrush from the target therefore affects both the intensity of the color and the area it covers.

In our spraying procedure, the airbrush was held free-hand at a distance of 5 ± 2 cm from the template. The air pressure was kept constant at 30psi. During the spraying, the flow of colorant was momentarily interrupted for about 2 seconds to allow each layer to dry, then released again by moving the airbrush horizontally, maintaining the same rhythm until the entire template was covered. Since our goal was to obtain dots on the surface of the test specimen that are

almost identical in circular geometric shape and in color intensity, some practice in operating the airbrush [1,2,5] was required before speed and accuracy were attained.

Fig. 2 illustrates the spraying procedure. It is fast and accurate, taking less than 60 seconds to spray onto a specimen the entire matrix of dots with the characteristics of the template. A rectangular grid is created, having 25 rows of dots in 17 columns with reasonably circular shapes. The dots have diameters ranging from 80 to 100 μm ; the distances between them will be $1 \pm 0.005\text{mm}$. Although dots of almost identical size and circular shape could be applied on a uniform flat surface, this will not always be the result on the surface of low grammage and lightly bonded papers owing to the heterogeneity of these materials. The colorant used was Higgins non-waterproof drawing ink -- Black 4425, for extra-fine lines, -- with fast drying properties that allowed us to remove the template from the test specimen immediately after the spraying.

3.3. RECORDING PROCEDURE FOR THE DOT MATRIX SYSTEM

After the rectangular grid of dots was prepared, as described in the previous section, the specimen was tested

using the Instron test machine. To do that, a special metal clamp was designed to fit the test specimen. To prevent slippage of the specimen during the tensile test, the inner surface of one grip of the clamp was lined, with very hard rubber material [6]. The other grip was lined with a very fine (360 grit) waterproof silicon carbide sandpaper. The clamps were fitted to regular Instron grips which provided the pressure (60 psi air pressure) to clamp the test specimen. To mark the free span on the specimen and to serve as guidelines to align it in correct plane with the grips (and therefore with the direction of load), two fine lines were drawn across the width of the specimen using the airbrush [5]. These lines represent a cross sectional plane perpendicular to the longitudinal axis of the specimen. Alignment was achieved by matching these lines with the parallel edges of the upper and lower clamps. The width of the specimen at these lines was the same as the width of the clamps; thus the longitudinal axis at the center of the specimen coincided with the center of the clamps. Initially, a lower air pressure (15-20psi) was used in the grips, and a small load was applied to allow the same to self-align along the loading axis by in-plane rotation of the clamps about its own pin. The pressure was then increased to 60psi to prevent further in-plane rotation. The grips were fixed to the load cell to avoid in-plane and out-of-plane movement.

For the photographing procedure a 4 x 5 inch

conventional "view camera" and Agfa-Gevaert 10E75 Holographic film with a spatial resolution of 2700 lines/mm were used. The test specimen was illuminated by two adjacent fluorescent lamps, and by an electronic flash synchronized with the camera shutter (see Fig. 3). The camera was firmly attached to a heavy metal-wood table with the lens and backfocal plate in plane with the test specimen. This was achieved by positioning the camera so that the entire narrow rectangular section of the necked-down specimen with the grid of dots on its center was in correct focus. The focus was enhanced by using a light-blue background color to obtain a better contrast between the matrix of black dots and the white paper specimen.

The scale of reproduction of image formation was determined using the Gaussian lens formula and its corresponding equation for magnification [7-9].

$$1/DO + 1/DI = 1/f \quad [1]$$

$$M = DI/DO = I/O \quad [2]$$

where

DO = object distance from the lens; DI = image distance from the lens; f = focal length of camera lens; M = image scale of reproduction (magnification); I = image size; O = object size.

In our study, a lens of focal length of 135mm was used and the specimen distance (DO in the equation [1]) was kept at 272mm. From the equations [1] and [2] the image size was calculated to be 0.985x the size of the object. A

diaphragm opening of $f/4.7$ and an exposure time of 50 msec were used.

Before use, the films were conditioned to the same temperature and relative humidity conditions used to test the specimen [10]. Then, a set of photographs was taken, for each specimen, sequentially along the load-displacement curve almost to failure, without stopping the Instron crosshead (speed of 2 mm/min was used in this study). After developing, the negatives were again conditioned in the same conditions of temperature and relative humidity used to test the specimen.

3.4. DATA ACQUISITION FOR STRESS COMPUTATIONS

The major problem with load-displacement acquisition systems that acquire the displacement independently from the load is to synchronize the displacement level to the corresponding applied load. In our study this problem was solved by setting a photoelectric cell near the test specimen (Fig. 3). During the test, the electric output from the load cell¹ and from the photoelectric cell² was read

-
1. Instron tensile load cell B; max. capacity of 2000g.
 2. Photodiode having an electric output that varies in response to light.

by the Keithley-DAS, a data acquisition interface system controlled by an IBM personal computer. The electric signals were time-interfaced synchronized; that is, the output from the photoelectric cell was acquired at the same time as that acquired from the load cell. This approach allowed us to identify the load carried by the specimen at the moment of the photograph. A sudden variation in the illumination of the specimen (triggering of the electronic flash) causes an equivalent output response from the photoelectric cell. A typical response of the photoelectric cell to variations of light intensity is illustrated in Fig. 4. In this figure, each spike corresponds to the moment when a photograph was taken. Obviously, the number of spikes corresponds to the number of photographs taken per specimen along the test. Fig. 5 shows the load-time curve. In this figure the time axis is the same as that used to collect the output from the photoelectric cell.

Figs. 4 and 5 are included only as a graphic representation of this approach. Appendix A shows the computer program used for data acquisition control and a part of the data acquired by the system. In this Appendix, one can observe that the data output is in the form of a matrix of N rows by 2 columns, where N represents the number of data points for light intensity (1st column) and for load (2nd column). Therefore, the sudden increase in the value of the light intensity data (1st column) was used to identify for each

individual photograph the corresponding signal for load (2nd column). This is indicated by the arrows in both columns at a given row number. The values for load calculations corresponding to the sequential number of the photograph taken along the test were easily identified by scrolling down through the matrix of data on the computer monitor. Each row of data points was acquired in a 50 millisecond time interval. Although a large value of data points was acquired per specimen, only a few data points (equal to the number of photographs taken per specimen) were necessary for load and stress calculations.

The rectangular cross sectional area of the narrow section of the necked-down specimen (Fig. 6) was used for stress calculations. The width of this section was constant at 20mm. However, due to the softness characteristics of the tissue paper and the susceptibility of its surface to damage, it was not possible to use this section of the specimen for thickness measurement. Therefore, the following procedure was established: After cutting the specimen, the trimmed piece (part A in Fig. 6) was saved for thickness measurement. This part was divided in smaller parts, coded by A₁, A₂ and A₃. Briefly, it was frozen in liquid nitrogen and, using a very sharp knife, each of these parts was again divided equally into 5 smaller parts, with the cutting direction perpendicular to the MD symmetry direction. These parts were then used for thickness measurements. This procedure avoided crushing the

fibers during the cutting and permitted a direct measurement of the edge-thickness using a light microscope. A total of 100 points per specimen were measured and the mean value was used as the thickness of the specimen.

The thickness of specimens measured by this method was compared with the thickness measured in thin cross sections obtained by an embedding [11] and microtoming technique. No statistical difference at the level of 5% of significance was found between them.

3.5. DATA ACQUISITION FOR DISPLACEMENT MEASUREMENTS

As was described in the previous section, the grid pattern (matrix of dots) printed on the surface of the test specimen was photographed at intervals from the unstrained state up to near failure. The displacement field and the respective displacement angles for each photograph corresponding to each level of applied load was obtained by applying trigonometric relations (equations 3 and 4 inserted in Fig. 8) to the differences in x-y coordinates between the undeformed (unstrained) and the deformed (strained) grid. This was achieved by placing the negatives between two optical glass plates and then projecting the enlarged image onto an

electronic digitizing table¹ in plane with the glass plates (negatives). The projected image of the grid pattern, representing the surface of the test specimen, was digitized two-dimensionally over the entire grid and the data were acquired by an IBM personal computer (software is shown in Appendix B) and were stored for later strain calculations. Figs. 7 and 8 illustrate this procedure. Fig. 9 shows a typical grid pattern in the undeformed (unstrained) and deformed (strained) stages.

In order to be sure that the projected image of the grid pattern was registered in the correct two-dimensional plane, the x-y coordinate data of every individual dot over the entire grid was rotated and translated to an x-y reference axis which we know is in the correct plane with the electronic digitizing table. To do this, it was necessary, before starting the test, to have an orientation dot-line near the grid pattern and parallel to the edges of the specimen. This dot-line consisted of 15 dots at 1mm intervals having the same shape as the dots of the grid pattern. It was printed on the surface of a small piece (2 x 2 cm) of self-adhesive paper using the same airbrush technique used to spray the grid on the surface of the test specimen. However, in this case, this self-adhesive paper, which also served to stick the specimen

1 - Altek Digitizer AC90C, Altek Corp., 2150 Industrial Parkway, Silver Spring, MD 20904, USA

label, was fixed to a thin metal piece attached to the mobile grip of the Instron machine. This dot-line, which appears on each photograph, was digitized. A linear regression line was fitted to its x-y coordinates, and the slope of this fitted dot-line was used to calculate the rotation angle (THETA_L in the APL function ALIGN3 shown in the appendix B) of the x-y coordinate data of each individual dot of the grid pattern. The registry was achieved by calculating for each dot the polar coordinates (r, θ) using the trigonometric relations [equations 5 and 6] and the rotated rectangular (x, y) coordinates by using the interrelated parametric equations [equations 7 and 8]. Then these (x, y) coordinates were translated to the reference axis arbitrarily chosen in the plane of the digitizing table.

$$\begin{array}{ll}
 r^2 = x^2 + y^2 & [5] \\
 \tan \theta = y/x ; \theta_D = \theta \pm \theta_L & [6] \\
 X = r \cos \theta_D & [7] \\
 Y = r \sin \theta_D & [8]
 \end{array}$$

Where:

r = radial distance of each dot from the origin of the x-y digitizing table.

x,y = digitized coordinates of each dot.

θ = polar angle of each dot with x-axis of the digitizing table.

θ_D = rotated angle.

θ_L = rotation angle (slope of the orientation dot-line).

X,Y = rotated coordinates.

The data alignment was automatically done by the software shown in Appendix B.

3.6. DATA PROCESSING FOR STRAIN CALCULATIONS

At this stage of our discussion we are able to demonstrate how to map a two-dimensional displacement field over the grid pattern.

The in-plane displacement to which each individual dot is subjected, is represented by the displacement vectors indicated by the arrows shown on the geometric center region of the tensile test specimen in Fig. 10. Using the data previously obtained, the displacement vector components are obtained for the entire grid. Then, the strain field is obtained by finite difference relations from the displacement vector components over the entire grid. The different strain components are calculated as demonstrated for the basic unit of displacement shown in Figs. 11 and 12 using the following finite difference algorithm:

$$(\epsilon_{xx})_{i,j+\alpha} = 1/\Delta L_{i,j+\alpha} \{ d_{i,j+\alpha} \cdot \cos \theta_{i,j+\alpha} - d_{i,j} \cdot \cos \theta_{i,j} \} \quad [9]$$

$$(\epsilon_{yy})_{i,i+\beta}^j = 1/\Delta L_{r,i+\beta}^j \{ d_{i+\beta}^j \cdot \sin \theta_{i+\beta}^j - d_i^j \cdot \sin \theta_i^j \} \quad [10]$$

$$(\epsilon_{xy})_{i,i+\beta}^{j,j+\alpha} = 1/2 \left\{ \left[(d_{i+\beta}^{j+\alpha} \cdot \sin \theta_{i+\beta}^{j+\alpha} - d_i^j \cdot \sin \theta_i^j) / \Delta L_{r,i+\beta}^{j,j+\alpha} \right] + \right. \\ \left. + \left[(d_{i+\beta}^j \cdot \cos \theta_{i+\beta}^j - d_i^j \cdot \cos \theta_i^j) / \Delta L_{r,i+\beta}^j \right] \right\} \quad [11]$$

where, $\alpha = \text{STEPX}$ and $\beta = \text{STEPLY}$

for $1 \leq i \leq \text{LENY} - \beta$
 $1 \leq j \leq \text{LENX} - \alpha$

Referring again to Figs. 10, 11 and 12 we must clearly distinguish between the two following quantities:

- a - The two dimensional gage length $\Delta L_{r,i+1}^j$ and $\Delta L_{r,i}^{j+1}$ correspond to the spacing between dots within a row (y-direction) and within a column (x-direction), respectively for the dots on the corner of the basic unit selected. These quantities are calculated by processing the data obtained from the entire unstrained grid.
- b - STEPX and STEPLY are average parameters within a column (x-direction) and within a row (y-direction). They can be chosen independently. These are positive non-zero integers such as:
 $\text{STEPX} \leq \text{LENX} - 1$; $\text{STEPLY} \leq \text{LENY} - 1$
- c - LENX, LENY = Number of rows and columns over the entire grid. In this study, 7 x 5.

With the methods and algorithms previously

described we were able to perform a strain analysis on the data from each photograph. After the axial, lateral and shear strains are calculated, the Mohr's circle [13] is used for the transformation of plane strain and consequently to calculate the principal axes of strain and the principal strain components, determined by:

$$\theta_p = 1/2 \arctan [\epsilon_{xy} / (\epsilon_{xx} - \epsilon_{yy})] \quad [12]$$

$$\begin{matrix} \epsilon_{xx'} \\ \epsilon_{yy'} \end{matrix} = 1/2(\epsilon_{xx} + \epsilon_{yy}) \pm \{ 1/4[(\epsilon_{xx} - \epsilon_{yy})^2 + \epsilon_{xy}^2] \}^{0.5} \quad [13]$$

where each quantity is expressed for each basic unit of data processing over the entire grid taking into account the average step parameters. That is, the basic unit [i, i+ STEPX; j, j + STEPY]. Then, the in-plane lateral contraction ratio (LCR), which is simply the ratio of principal strain components determined for each basic unit, over the entire grid, is calculated by:

$$LCR = - \epsilon_{yy'} / \epsilon_{xx'} \quad [14]$$

where $\epsilon_{xx'}$ and $\epsilon_{yy'}$ represent the principal axial strain and the principal lateral component, respectively.

Although we produced a grid pattern (matrix of dots) with dimensions of 27 x 17 dots with 1 ± 0.005 mm apart, in this part of our study a matrix of 7 x 5 dots was processed

(the intermediate dots were ignored). In this case, the spacing between dots to be processed over the grid was increased from 1mm to 4mm. This procedure reduces the number of data points to be collected, but it covers the same specimen area for strain measurements. Since this part of our study does not involve evaluation of the effects of paper structure on the mechanical properties, the size of the grid of 7 x 5 dots proved more than adequate and convenient for our purpose.

Based on our previous experience and results of other authors [12] we know that the strain field in paper material is inhomogeneous. Since the description of the quantities ϵ_{xx} , ϵ_{yy} and ϵ_{xy} are described in finite difference form, we can average these quantities in order to stabilize the data at each given position over the entire grid. To achieve this, we followed procedures already developed by our research group [12] for mapping the strain field in high basis weight paper by laser speckle interferometry. However, some modifications to those procedures were necessary to adapt it to the dot matrix technique.

Using the basic algorithms for a two-dimensional inhomogeneous displacement field, the mapping procedure for strain information can be applied using any size of basic unit of data processing illustrated in Fig. 13 or any other suitable size within the grid dimension.

The array dimensions for strain calculations are

illustrated in Fig. 14.

3.7. RESULTS OF THE STRESS-STRAIN RELATIONSHIPS

The mechanical behavior of a solid material is usually described by the relationship between the stress and the resultant strain [14]. The axial tensile strains used to build the stress-strain diagrams of the papers used in this study were obtained by processing the displacement data for two extreme dots located in the center column of the 7x5 grid, which corresponds to the axial geometric center of the test specimen. The displacements associated with the rigid body motion was removed by using the finite difference algorithm, equation [9] described in item 3.6, which generates axial strains $(\epsilon_{xx})_{i,j,j+\alpha}$ in absolute values over the gage length $\Delta L_{i,j,j+\alpha}$, where: $\alpha = \text{LENX}-1$; $i = [(\text{LENY}-1) \div 2] + 1$; $j = 1$; for $\text{LENX} = 7$ and $\text{LENY} = 5$.

Since it was difficult to photograph the specimen at the exact moment of rupture, the strain at failure was estimated using the following procedure: The strain values obtained during the test, up to near failure, were plotted against time. A regression line was fitted to these data, and the strain at failure was estimated by extrapolation (using

the time corresponding to the failure load). The regression equations used to estimate the strain at failure are given in Table 1. Fig. 15 shows a typical strain vs time relationship.

The three kinds of papers used in this study were:

- (a) Type A: a machine made creped tissue with a relatively high degree of fiber orientation having a K value for von Mises distribution of fiber segment orientation [20] of 0.508,
- (b) Type B: a machine made creped tissue with a moderate degree of fiber orientation having $K = 0.270$, and
- (c) an uncreped handmade tissue with $K = 0.115$. The K values were obtained from measurements on approximately 700 dyed fibers in each type of paper (a typical fiber had 7 or 8 segments).

Typical stress-strain and load (per unit of width)-strain diagrams for those papers are shown in Figs. 16 through 18. Those relationships represent the average of data obtained from five specimens tested for each type of paper. The shapes of the curves for those relationships depend to a great extent on the crepe effect. The difference in appearance of the curves for the specimens tested in machine direction (Figs. 16.1, 16.2, 17.1 and 17.2) can be contrasted with those obtained from the specimens tested in cross-machine direction (Figs. 16.3, 16.4, 17.3 and 17.4). A possible explanation is that for a machine-made paper the mechanism of crepe formation occurs in the MD [15], which imparts extensibility and reduces the ability for the material to absorb load in earlier stages of the test. For CD specimens the crepe effect is not

pronounced as in MD, and it may occur only at the beginning of the test. This may be shown by the lag phase of the curve in Figs. 16.3, 16.4, 17.3 and 17.4, which is typical for all CD specimens tested for both types of machine-made papers used in this study. As expected, such behavior is not observed in handsheets, since it had not been creped (Fig. 18). A typical large linear range is observed, which is more characteristic of handsheets and CD specimens.

Table 2 shows some results obtained from the stress-strain and load-strain relationships for the papers used in this study. For machine-made papers, the initial apparent modulus E_1 corresponding to the slope of the initial stage of the stress-strain curve (lag phase of the curve), which may express the tensile behavior of the paper under crepe effect, is higher for MD than CD specimens. The difference between MD and CD is larger for the paper Type A than type B. However, a comparison between the two papers shows E_1 higher for the paper type A only for the specimens tested in MD direction. Similar trend of results were obtained for E_2 , which we define as apparent modulus of elasticity, corresponding the slope of the linear part of the stress-strain curve without crepe effect (apparent modulus of uncreped sheet). The results are also expressed in grams per unit of width.

The strain (LPH) corresponding to the lag phase of the stress-strain curve, the stress and the load at failure

are higher for MD specimens than CD.

For the paper type B the strains at failure for MD specimens are about twice as high as those for CD specimens. In this case we might attribute this unusual behavior to the lower degree of fiber orientation, along with the crepe effect, which enhances extensibility in the machine direction.

We attribute the difference in results between the two machine-made papers due to the difference in fiber orientation distribution between the two papers. Paper type A has a higher degree of fiber orientation, as described earlier.

Referring again to Table 2 one can see that there is a large difference in modulus of elasticity between handsheets and machine-made papers; the handsheets being stiffer. A possible explanation for this is that the handsheets were not creped; tissue papers normally are [15]. Therefore, the handsheets may be of limited use in predicting the behavior of machine-made papers.

3.8. RESULTS OF STRAIN FIELD CHARACTERIZATION

In the previous section the application of the Dot Matrix Technique to obtain stress-strain relationships was

described. In this item, the results obtained show that this method is capable of quantifying a 2-D displacement field. The 2-D strain field, local (point-to-point) strain variations, and lateral contraction ratio could be obtained along the tensile test.

The natural characteristic of inhomogeneity in the paper network is well documented in the literature [16-20]. Variations in mass distribution, thickness, free fiber length, fiber orientation, floc size, floc orientation, and degree of fiber bond are consequences of formation and drying processes. Those characteristics are postulate to be responsible for non-homogeneity of the strain field in a test specimen under load. Typical distributions of axial, lateral, and shear strains that result when the samples were stressed are shown in Figs. 19 - 24 for machine-made paper type A, Figs. 25 - 30 for type B, and Figs. 31 - 33 for handsheets. These values were calculated according to the scheme in Fig. 14, discussed in section 3.6. The axial, lateral, and shear strain distributions, expressed as non-dimensional value are shown at different nominal strain levels along the tensile test, with the x-direction representing the direction of the load applied to the specimen. Based on my observations of all tests, these graphs typify the results obtained.

Changes in distribution patterns of axial, lateral, and shear strains occurred during tensile straining for all papers tested. This can be noted by comparing the data of

strain distributions in earlier stages of the test with those obtained in a more advanced stage. This is presented more clearly in the three-dimensional plots. In other words, the strain fluctuations may randomly change their course in the specimen during straining. A possible explanation is that when the load transferred via shear mode through the inter-fiber bonds increases, each specific location or region in the specimen will respond and will transfer that load according to its own structural network characteristic. Therefore, a specific location with a large strain at the beginning may not necessarily undergo the largest strain in advanced stages of the test. This can be noted by comparison of Figs. 19.1 - 19.6 (machine made paper type A, tested on MD direction) where a local band of relatively high strain (1E, 2E, 3E, 4E, 5E) could be observed across the entire width of this specimen by the time the nominal axial strain level of 1.291% had been achieved (Fig. 19.1); the rest of the dot matrix area was strained rather uniformly. This pattern changed at an overall higher level of strain (Figs. 19.2 and 19.3) and the strain started to increase everywhere at the center area of the specimen. The three small negative strains (1F, 3F, 5F) at 2.129% of nominal strain level became all positive. Again, the pattern was accentuated at an overall higher level of strain (Figs. 19.4, 19.5, 19.6), where the weak band (1D, 2D, 3D, 4D, 5D) started to strain far more than the rest of the center area of the specimen even though there were increases

everywhere.

Figs. 20.1 - 20.6 demonstrate the smaller and generally more uniform 7x4 pattern of lateral strains observed on the same specimen and at the same levels of nominal axial strain along the tensile test. Considering that the sign convention is positive for tensile and negative for compressive strains, almost all signs were negative, as would be expected for specimens subjected to high levels of axial extension. However, positive strains appeared across the width (4B, 3D, 4F, 4G in Fig. 20.1), even though a nominal axial strain of 1.291% was applied. The transverse strain pattern on z-axis of the 3-dimensional plots (note scale change in Figs. 20.1 - 20.6) reinforces our previous discussion on the reduction of lateral strain values along the tensile test, since, as it would be expected, the lateral strains are essentially negative strains.

Shear strain distribution along the tensile test is demonstrated in Figs. 21.1 - 21.6. For homogeneous and uniform materials it would be expected a symmetrical distribution of positive and negative signs of shear strain across the width of the test area. This was not found and the positive and negative strains occurred rather randomly for the paper material under study. The compensation effect of positive and negative strains over the grid makes the overall average of shear strains very small.

Thus, the dot matrix system picks up local strain

patterns and it is capable of tracking these at any point on the stress-strain curve. Local variability, which could be the result of crepe effects in machine-made tissue or one or more of the factors mentioned earlier in this item, is quantitatively identified.

Figs. 22 - 24 show typical test results for highly-oriented tissue (paper type A). However, these illustrations are for tests in which the specimen is loaded in cross machine (CD) direction. Figs. 22.1 - 22.6 show axial strain distribution. Although there is a difference in stress-strain behavior between MD and CD specimens, as discussed in the previous item, it is not clear from the results obtained that fluctuations in strain distribution are affected by the symmetry direction of the test specimen. In similar fashion, the graphs of axial strain distribution, for MD specimen, demonstrated the existence of relatively extensible bands (1E, 2E, 3E, 4E, 5E) in earlier stages of the tensile test (Figs. 22.1 and 22.2). At nominal axial strain level of 2.50%, the distribution pattern started to change (Fig. 22.3), where after that, the strain started to increase everywhere. The presence of local bands (Figs. 22.4 and 22.5) of relatively stiff (position E and F across the width) and relatively extensible area (1D, 2D, 3D, 4D, 5D) extended across the entire width and started to dissipate at higher nominal strain level of 7.940% (Fig. 22.6). It seems that, in general, the distribution of strain occurs randomly over the deformed grid

contraction) that causes a lateral compressive stress to build up in the area near the grip, in accordance with theory [2]. The lateral compressive stress in turn leads to local tension buckling, which may propagate as the specimen is stretched. In cases where the thickness to width ratio (t/W) is important, the parameter thickness (t) must be critical since it is constant for a given material; the ratio t/W can be varied only by changing W , and W cannot be made unrealistically small. That is, we cannot increase t/W by reducing the width of the test specimen below a certain value at which the sample would not be representative of the material under test.

For the specimen material we used (tissue paper - ²25g/m) it became evident that CD specimens are more susceptible than those of MD orientation to the wrinkling phenomenon; this can be observed by comparing Fig. 7 with Fig. 10. At the same applied strain, both the amplitude and number of wrinkles are greater for CD specimens than for MD. A possible explanation is that when a machine-made paper is creped, the stiffness in the width direction of CD specimens is reduced. In addition, the wire marks which are pronounced in tissue papers produce a kind of crepe pattern almost in phase with the direction of the creping procedure, which enhances the conditions for wrinkling to take place [see creping mechanisms in Ref. 23].

In summary, the wrinkling behavior of rectangular tensile test specimens may be described by the following

mechanism: When a lightweight paper structure undergoes a uniaxial tensile test, lateral contraction in the vicinity of the grips is restrained and an in-plane lateral tensile stress is developed. In response to that restraint and to the dominant uniaxial tensile force, bending couples [21] at the end of the grips build up a lateral compressive stress pattern which arises across the width from the lateral edges toward the center of the specimen (Figs. 14 and 15). The compressive stress may attain such a magnitude that in these regions the structure becomes unstable and buckles. The stress distribution in the remaining (unbuckled) portion of the specimen will certainly change, especially near the voids and thin spots, giving rise to stress concentrations. As the end displacement continues, the wrinkling propagates along the axis in the direction toward the center of the specimen. Wrinkling does not necessarily cause failure, but from the point of wrinkle initiation on, the load transfer mechanism will be via a wrinkled structure (Figs. 16 and 17).

2.3.4. THE STRUCTURAL BEHAVIOR OF NECKED-DOWN SPECIMENS

From the experimental results described in the previous section, it was concluded that the geometry of the specimen had no significant effect on controlling the wrinkling of the rectangular tensile test specimens. However, for most of the rectangular specimens tested, we could experimentally observe that the wrinkles start at a certain distance from the grips and then propagate toward the center of the specimen. If the principal mechanism responsible for buckling the structure is lateral compressive stress, we should be able to prevent such buckling by generating a lateral tensile stress pattern to nullify the compressive stress field. This lateral tensile stress pattern must be larger or at least of the same magnitude as the compressive stress field. It should occur over the region of the specimen located beyond the critical distance from the grips (the distance at which the wrinkles begin) in order to prevent propagation toward the center of the specimen. This exact critical distance is quite impossible to detect experimentally. However, the maximum lateral compressive stress has been reported [1] to occur in a rectangular tensile test specimen in the region where the ratio of the distance from the grip edges along the longitudinal axis to width of the specimen is about 1.5 (aspect ratio of 1.5 in Figs. 14 and

15).

Following our experience with rectangular tensile specimens, we set up a preliminary experiment using necked-down tensile specimens. From this experiment we observed that the necked-down specimens might provide a wrinkle-free tensile test if an appropriate specimen configuration could be found. During this experiment a finite element analysis (FEM) was conducted by Seo [24]. His approach was to investigate the distribution of the lateral tensile and compressive stress fields for different models of necked-down shapes, two of which are shown in Fig. 18. For all models, the transition regions of the specimens were able to generate a pattern of lateral tensile stresses that exceeded the lateral compressive stress field imposed by the grip action. Their practical potential encouraged us to do some more precise experimentation in order to derive the most appropriate geometry.

Several geometric properties were taken into consideration as basic elements of specimen design: First, the wide rectangular end sections of the necked-down specimen should have an aspect ratio of less than 1.0 in order to minimize the total length of the specimen. Second, the center of the transition section (curvature section) should be where the ratio of the distance from the grip edges along the longitudinal axis to width of the narrow rectangular section is equal or larger than 1.5. Third, the narrow rectangular

section should have an aspect ratio of at least 4 in order to provide enough test area of homogeneous strain field [1] at the center of the specimen. Finally, the rectangular test section of the necked-down specimen should be, before testing, free of wrinkles in order to provide reliable results. This was achieved by conditioning the machine-made sheets in the environmental room [17] before cutting the test specimens. The phenomenon of self-wrinkle was observed only if CD specimens were cut in conditions of temperature and relative humidity quite different from the environmental condition used for testing.

The experimental procedure employed six different models of necked-down specimens, corresponding to six different transition ratios (that is, the ratio of the width of the wide rectangular section to that of the narrow rectangular section, W/w), viz. 3.3, 3.75, and 5 in Fig. 19, and 2, 2.5 and 3 in Fig. 20. The length of the narrow section was kept constant at 100mm. The transition radius (radius of curvature) of the necked section was also kept constant at 50mm, following the recommendation of Setterholm & Kuenzi [13]. Finally, the total free span was kept at 240mm in all cases. Tests were performed on machine-made paper in both MD and CD, as well as for handsheets. The Instron tensile tester was set at the same crosshead speed (2mm/min.) used for rectangular specimens.

From our experiments we observed that all the

models shown in Figs. 19 and 20 had wrinkle-inhibiting properties, but only models A and B in Fig. 19 and D and E in Fig. 20 were capable of providing a wrinkle-free specimen performance from the beginning of the test through failure. Seo [24] has shown by finite element analysis that the higher the transition ratio of the specimen, the higher will be the lateral tensile stress field generated in the necked-down region. This analysis is consistent with our results in that models C (Fig. 19) and F (Fig. 20) were not able to prevent wrinkling at the lateral edges during the more advanced stages of the load-elongation test. However, we believe that the thickness to width ratio in this section of the specimen must also play an important role. We may have used an inappropriately large width for such a lightweight paper, which may have contributed to the unsatisfactory performance of these two models.

In order to provide a large enough test area for strain measurements, and also for easier handling and preparation of test specimens, model E (Fig. 20) was chosen to be used with our strain field measurement procedure (the dot matrix technique). A photograph of a sample of configuration E under test is shown in Fig. 21. This photo was taken with the specimen at a high level of applied strain (6.5% by crosshead displacement); it failed at 6.66% strain. For convenience, the test specimen was divided into sections by printing lines on it using an airbrush technique [15, 16]. The wrinkles are

easily observable on both end sections of the specimen (sections S_1). In the transition sections (S_2) wrinkling is prevented from propagating to the rectangular sections (sections S_3 and S_4) which are wrinkle-free and therefore are appropriate sites for reliable strain measurements. Section S_4 at the center of the specimen was actually used for this purpose. The region of interruption of the wrinkling propagation in the transition areas (sections S_2) coincides with the region of the largest lateral tension fields in the finite element models, demonstrated by the region in yellow in Fig. 18. The region in blue represents lateral compressive stress, which occurs at certain distances from the grip edges anterior to the large tension field that prevents the wrinkle from propagating toward the center of the specimen.

We propose that the mechanism of wrinkle prevention of the lateral tensile stress field is the following: As load transfer via the shear mode increases, so does the magnitude of the lateral tensile stress, which resists the out-of-plane displacement engendered by the buckling action of the compressive stress; these opposing actions result in a more stable cross sectional area across the width of the narrow rectangular section of the necked-down specimen (sections S_3 and S_4).

The behavior of necked-down model E is shown in Figs. 22 through 26 for machine made paper, and in Figs. 27 through 29 for handsheets. Figs. 23, 25 and 28 represent the

at locals of relatively stiff points (like 1D, 3D, 2E) and relatively extensible areas (like 2D, 4D, 5D, 1E, 3E) appear everywhere.

Figs. 23.1 - 23.6 show the lateral strain distribution of highly-oriented tissue (paper type A) tested in cross machine direction (CD). The pattern of lateral strain, in general, presented a more uniform distribution in earlier stages of the test (Figs. 23.1 - 23.3). However, the resulting strain patterns in advanced stages (Figs. 23.3 - 23.6) along the tensile test, were not definitive and considerable variation appeared over the grid. In this experiment, the positive strains that appeared in some local points over the lateral strain pattern (4E, 3G in Fig. 23.1) occurred along the tensile test (4C, 4E, 4F, 3G, 4G in Fig. 23.4 for example). Although a reduction of the number of positive strains over the grid was noted along the test (4E, 3G, 4G in Fig. 23.5), it still occurred in a more advanced stage of the test (4E in fig. 23.6).

Figs. 24.1 - 24.3 show a more uniform pattern of shear strain distribution in the earlier stages of the stress-strain curve, where nominal strain levels of 1.633%, 2.008% and 2.5% were applied on the test specimen. As the applied nominal strain was increased (Fig. 24.4 - 24.6), a progressively larger perturbation appeared across the width. In these Figures, it can be noted points of local positive strains (2C, 4F, as example) and negative strains (3B, 1C, 1D,

as example) until the end of the test.

Typical axial strain distributions for moderately-oriented tissue (paper type B) representing the specimen loaded in the machine direction (MD) are showed in Figs. 25.1-25.6. These Figures are, to some degree, analogous to Figs. 19.1 - 19.6. However, it is apparent that the lower degree of fiber orientation allows greater extensions before failure. The nominal axial strain data presented in the captions of Figs. 25.1 - 25.6 demonstrate that the tensile strains observed in these specimens just before failure were greater than the comparable strains in highly-oriented tissue. Here again, the presence of extensible bands (1D, 2D, 3D, 4D, 5D in Fig. 25.1) changed positions across the width along the tensile test. This can be noted by comparing Figs. 25.1 - 25.6, where the extensible band in Fig. 25.2 and 25.3 appeared in the positions 1E, 2E, 3E, 4E, 5E, respectively. In a more advanced stage of the test, the extensible bands appeared in positions 1C, 2C, 3C, 4C, 5C in Figs. 25.4 and 25.5, respectively, just before failure (positions 1D, 2D, 3D, 4D, 5D in Fig. 25.6). As it has been previously noted, for highly-oriented tissue (paper type A, MD specimens) some negative strains appeared across the width of the specimen. However, this was observed only at the beginning of the test (positions 1F, 2F, 3F, 4F, 5F in Fig. 25.1).

The results of lateral strain distribution for moderately-oriented tissue (paper type B, MD specimen) are

showed in Figs. 26.1 - 26.6. The 3-dimensional graphical representations of lateral strain contours at different positions on the specimen indicate that, in general, the distribution of strain occurs randomly over the deformed grid. In some cases, localized stress concentration may develop in some particular region and may cause a lateral strain reversal in others. This strain reversal (positive lateral strain) appeared across the width until a nominal axial strain level of 4.35% was applied (3F, 2G in Fig. 26.4). After that, all strains were negative.

The shear strain pattern showed in Figs. 27.1 - 27.6 for moderately-oriented tissue (paper type B) tested on machine direction (MD) indicates random distribution along the tensile test rather than systematic. It is important to note that a specific location with a positive or negative strain at the beginning may not necessarily undergo the same sign of strain along the test. Typical perturbations of this type can be observed by following the positions 3A, 3B in Figs. 27.1 - 27.6. This reinforces the previous discussion, that is, the strain fluctuations may randomly change their course in the specimen during the straining process.

The axial strain distribution for moderately-oriented tissue (paper type B) tested in cross machine direction is showed in Figs. 28.1 - 28.6. The 3-dimensional graphical representations of axial strain contours at different positions demonstrated the existence of local bands

of relatively extensible areas (1D, 2D, 3D, 4D, 5D in Figs. 28.1 and 28.2), and strain reversal at positions 4E, 1F, 3F, 5F in Fig. 28.1 and across the specimen width at positions 1F, 2F, 3F, 4F, 5F in Fig. 28.2. However, as the tensile test continued, the strain started to increase at the center area of the specimen. It caused an attenuation effect on the relatively extensible band, at nominal axial strain level of 2.382% and 2.812% (Figs. 28.3 and 28.4). Those bands appeared again in a more advanced stage of the test, in the same position across the width (1D, 2D, 3D, 4D, 5D in Figs. 28.5 and 28.6) as it had been noted at the beginning of the test.

The pattern of lateral and shear strain distributions for moderately-oriented tissue (paper type B, CD specimen) in Figs. 29 and 30 demonstrated a behavior analogous to previous specimens, independently if it was tested in MD or CD orientation. That is, the distribution of strain occurs randomly over the deformed grid rather than in definitive bands of strain across the width along the tensile test. The lateral strain patterns showed in Figs. 29.1 - 29.6 indicate lateral strain reversal (positive strain) only in earlier stages of the test, at positions 4C, 4F, 4G in Fig. 29.1 and at positions 2A, 4E, 4F in Fig. 29.2.

Axial, lateral, and shear strain contours for handsheet specimens are showed in Figs. 31 - 33. As it has been previously noted, handsheets show substantially less extensibility, sustain greater tensile stresses and

demonstrate higher moduli of elasticity than the machine-made tissues. These differences are undoubtedly the result of the crepe that is imparted to the machine tissues. Figs. 31.1 - 31.6 show axial strain field data. In these Figures the existence of local band of relatively extensible areas in the specimen (positions 1E, 2E, 3E, 4E, 5E) was evident and appeared at the same position along all the test. Strain reversal across the width was noted since the beginning (positions 1A, 5C, 1D, 2D, 4D, 5D, 1F, 5F in Fig. 31.1) and continued until the end of the test (positions 4D, 4F, 5F in Fig. 31.6). Nevertheless, it is evident that some structural factors other than creping are at least partly responsible for the presence of relatively stiff and relatively extensible zones in the material. From the results, it is evident that the presence of extensible zones is a typical characteristic tissue paper, independently if it was machine-made or handsheets. Lateral strain (Figs. 32.1 - 32.6) presented smaller and generally more uniform patterns. However, some local peaks of high strain along the test (position 2F) was noted.

It is also important to note that, at the beginning of the test (Fig. 32.1) where a small nominal axial strain level of 0.303% was applied over the specimen, the overall average of lateral strain estimated for this specific grid presented positive value (AVG = 0.00116). At the present time, no obvious explanation for this anomalous behavior is

apparent. However, a possible explanation may lie on the adjustment of the necked-down specimen in the grips at the beginning of the loading process. As it has been discussed in Chapter 2 of this dissertation, the transition regions (necked-down regions) of the specimens are able to generate a pattern of lateral tensile stress that exceed the lateral compressive stress imposed by the grip action. This phenomenon is responsible for the wrinkle-inhibiting properties of necked-down specimens during a tensile test. In this experiment, the rectangular test section of the necked-down specimen should be, before testing, free of wrinkles. This was achieved after locating the specimen in the grips and a small load was applied to allow the same to self-align along the loading axis. This prevents the specimen from a possible initial self-wrinkle effect and it makes the rectangular section of the specimen entirely flat. The flatness was certified by watching out for any small curvature in the rectangular section of the specimen. However, in this specific case of handsheet specimen, the small load (pre-load) might not have been enough to stretch out some very small wrinkle (very small curvature undetectable by the eyes). Therefore, the small nominal axial strain (0.303%) applied over the specimen probably caused most of local areas in the grid to elongate rather than to contract. This data is shown intentionally (Fig. 32.1) to demonstrate such anomalous behavior since it occurred for almost all handsheet specimens.

Other possibility to explain such results is that, for small displacement differences, the method lacks accuracy. The digitizing table used to register the data may not have had enough resolution to detect small displacement differences. Certainly, potential future applications of the dot matrix system points out, in many situations, to data acquisition by automatic image analysis. Data processing at our laboratory is computerized nowadays and automatic acquisition is a logical next step.

The shear strain field for handsheet specimen showed in Figs. 33.1 - 33.6 demonstrated analogous behavior to machine-made tissues. That is, the distribution of strain occurred randomly over the deformed grid rather than in definitive bands of strain across the width. In the same specimen, the positive and negative shear strains occurred randomly rather than symmetrically over the grid and presented a relatively more uniform pattern along all tensile test.

Although the lateral and axial strain components along the tensile test can be calculated using different average step parameters, as defined in section 3.6, here, in this case, the displacement data were taken from the most extreme dots in the deformed grid and those values were averaged out. This is a recommendable procedure since it has the advantage to cover a larger deformed area in the specimen and the lateral contraction ratio can be calculated later on.

Trends in lateral-axial strain relationships along

the tensile test for each specimen are demonstrated by 2-dimensional graphs in Figs. 34 - 38 for all machine made tissue and handsheet specimens. It should be noted that as the nominal axial strain level is raised, lateral strains are reduced. This was noted for all specimens, independently if they were machine made tissue or handsheet specimens. This is reinforced by the slope of the fitted line in the Figures. Those slopes indicate the rate of changes along the straining process. That is, if the slope was 45 degrees, the change in axial strain was followed by a proportional change in lateral strain and, in this case, no variation of lateral contraction ratio would be expected.

Comparing the correlation coefficients obtained from the relationship between axial and lateral strain (Figs. 34 - 38) it can be seen that handsheets presented smaller values than machine made tissues. The smaller correlation values found for handsheet may indicate that small displacement differences lack accuracy. Again, these results could be related to the instruments used for displacement data collection, rather than to the dot matrix technique itself. The digitizing table used had a resolution of 25.4 microns and the accuracy of data collection for small displacement could be significantly reduced.

In order to compare trends and better characterize the papers under study, overall averages of axial and lateral strains were calculated using data obtained from all specimens

tested for each type of paper. The results plotted at the same scale are presented in Fig. 39. Paper type A (Fig. 39.1), tested in machine direction (MD specimens), showed the greatest amount of change. This can be certified by comparing the slope of the fitted line in the Figures. Again, a possible explanation lies in the crepe effect. That is, the process of crepe formation occurs in MD direction [15], which imparts extensibility and reduces the ability of the material to absorb load during the straining process. However, for paper type B (Figs. 39.3 and 39.4) differences between MD and CD specimens were the opposite of what was observed for paper type A. Fiber orientation distribution may have had an important role. However, such behavior may be more related to the big influence of the crepe on the more oriented paper (Type A), which may not be so great on Type B.

The trend of lateral-axial strain relationship for handsheets is shown in Fig. 39.5. In this Figure, it is demonstrated that the handsheet specimen presented lesser extensibility than machine made tissue. This can be demonstrated by comparing the data range of axial and lateral strains, showed in Fig. 39.5, with the data range obtained for machine made tissues (Figs. 39.1 - 39.4). These graphs show that changes in lateral strain, as the axial strain increases, are more accentuated for machine made tissue.

Finally, in this section some plots are included to show the trend of lateral contraction ratio (LCR) along the

straining process. Fig. 40 shows LCR for typical specimens. Fig. 41 shows the average values from five specimens. Based on my observations of all the tests, these graphs typify the results obtained.

Contrary to what might be expected, the lateral contraction ratios presented significant changes during the test. These changes were related to the type of paper (paper type A, paper type B and handsheet), and to the plane symmetry direction of the specimens (MD and CD specimens).

Based on the fitted line shown in Figs. 40.1 - 40.5, highly oriented tissue (paper type A) showed an initial decline in LCR followed by a leveling off, and then a rising. Type B tissue tested in MD orientation showed similar behavior to type A, but only a very modest rise in LCR with axial strain was noted. Type B tissue in CD orientation presented a tendency to have a more constant LCR accompanied by a much smaller axial strain than the others. Handsheets showed steady increases in LCR followed by leveling off, then a decline.

Differences in behavior observed for those papers were probably caused by the creping effect which seems to have a more pronounced effect on type A than on type B paper. However, initial LCR values when sheet strains are small may have no meaning because two extremely small strains are being divided and, therefore, inaccuracy is great and large fluctuations in LCR will occur. This has also been observed

when other methods have been used to measure lateral contraction ratio [25]. Those initial points are emphasised by arrows inserted in Figs. 40.1, 40.2, 40.3 and 40.5. If one would not take them in consideration, certainly trends of the new fitted lines would be different and closer to those found for type B tissue of CD orientation (Fig. 40.4).

When the average values of five specimens for each type of paper (Figs. 41.1 - 41.5) are plotted, it can be seen that the less oriented Type B tissue tends to show a more constant lateral contraction ratio with only a slight increase as axial strain increases.

3.9. CONCLUSION

In this chapter, we discussed the theory and application of the Dot Matrix Technique for measuring strains in paper. We believe that the data clearly demonstrate the method's versatility as a metrological tool. It is not simple to obtain from a single experimental method stress-strain relationships, 2-D strain analysis and lateral contraction ratio along the entire tensile test, as has been accomplished by this method. However, as with any novel experimental method, there are limitations, principally to the degree of

accuracy that can be achieved. In chapter 4 the major problems in analysing the data are discussed.

The manual system (digitizer table) used to process the data for strain computations was slow, tedious, and contains the potential for inaccuracies. The steps of processing the photographic films also contribute to time delay between the test and the final results. However, for practical reasons, we kept in mind the importance of the spatial resolution of the photograph films. The method described requires an automatic, digital image programmable system in order to be up-to-date. The progress made in manufacturing electronic image sensors [21-23] has been phenomenal. Higher resolution and faster processing speed of electronic imaging systems may soon bring electronic imaging closer to the quality of photographic films. We are awaiting this as the next step to improve the data acquisition system of the Dot Matrix Technique.

The main advantages of the method are:

1. It is a non-contact technique.
2. Its application is not restricted to paper science; it may also be used for thin laminates, films and other foil materials.
3. For a single specimen, detailed strain information can be recorded all along the stress-strain curve.
4. There is no severe restriction for the size of the grid for displacement measurements. The system is flexible

and permits use of different gage lengths (spacing between dots in the 2-D plane) and different sizes of the basic unit of displacement (some examples are shown in Fig. 13) which permit different combinations of average parameters to process different regions on the specimen.

5. The method permits the size of specimen to be large enough to be easily handled and tested at the Instron which is the test machine routinely used in material test laboratories.

6. The potential, versatility and simple handling of the data acquisition and strain analysis software (available from our paper physics research group at PS&E-SUNY) permit it to be used by technicians with little or no computer literacy.

The limitations of the present system are:

1. The semi-automatic processing of large amounts of displacement data may involve human judgement and fatigue if precautions are not taken.

2. The method is restricted to the study of two-dimensional strain field.

3. It is necessary to avoid, or at least minimize, rotation and vibration during the recording procedure.

In the future, the method could be applied to a wide range of problems: - Strain measurements for a biaxial test configuration; strain measurements in wet paper and/or at different moisture contents; determination of shear moduli for

lightweight papers by the combination of this method with modified off-axis tensile testing [24]; study of the parameters responsible for the strain fluctuations shown in this chapter (mass distribution, local fiber orientation, thickness variations, etc.).

3.10. LITERATURE

1. MISSTEAR, Cecil & SCOTT-HARMAN, Helen. The Advanced airbrush book. New York, Van Nostrand Reinhold, 1984. 160p.
2. TOMBSCURTIS, Seng-Gye & HUNT, Christopher. The airbrush book: art, history, and technique. New York, Van Nostrand Reinhold, 1980. 160p.
3. MYLAR product information: Type D 300-700 gauge - on a roll with quality. Wilmington, DE, Du Pont Company. (E-99491, 3/88)
4. MYLAR safe handling: Safety in handling and use. Wilmington, DE, DuPont Company, Polymer Products Dept., Industrial Films Division. (E-36496, 9/80)
5. PAASCHE AIRBRUSH COMPANY. 22 Airbrush lessons for beginners. Harwood Heights, Il. 11p.
6. "Flange and gasketing material." In: A. W. CHESTERTON CO. Chesterton Sealing Devices. Stoneham, Mass., 1982. pp.79.
7. JENKINS, Francis A. & WHITE, Harvey E. "Thin lenses." In: Fundamentals of Optics. 2nd.ed. New York, McGraw-Hill, 1950. Chapter 3, pp. 36-50.
8. FRANKE, Georg. "A perfect image formation." In: Physical Optics in Photography. London, The Focal Press, 1966. pp. 11-63.

9. HECHT, Eugene & ZAJAC, Alfred. "Geometrical optics -- paraxial theory." In: Optics. Reading, Mass., Addison-Wesley, 1976. pp. 99-166.
10. TAPPI T 402. Standard conditioning and testing atmospheres for paper, board, pulp handsheets and related products, TAPPI, 1982.
11. EM-bed-812. Fort Washington, PA, Electron Microscopy Sciences (E.M.S.) 2p.
12. CASTAGNEDE, Bernard & MARK, Richard E. "Etude d'un champ de deformation inhomogene dans un materiau translucide par Photographie Laser du Champ de granularite." C. R. Acad. Sci. Paris, t.305, Serie II, pp. 221-224, 1987.
13. BEER, F.P. & JOHNSTON, E.R. "Transformations of stress and strain." In: Mechanics of Materials. New York, McGraw-Hill, 1981. chapter 6.
14. PERKINS, R.W. "Models for describing the elastic, visco-elastic and inelastic mechanical behavior of paper and board." In: MARK, Richard E. (ed.) Handbook of physical and mechanical testing of paper and paperboard. New York, M. Dekker, 1983. v.1, chapter 2, pp. 23-75.
15. HOLLMARK, H. "Mechanical properties of tissue." In: MARK, Richard E. (ed.) Handbook of physical and mechanical testing of paper and paperboard. New York, M. Dekker, 1983. v.1, chapter 11, pp. 497-521.
16. NORMAN, Bo. "Overview of the physics of forming." [Paper presented at the] Fundamentals of papermaking; Ninth Fundamental Research Symposium, Cambridge, Engl., 17-22 Sept. 1989. 70p.
17. HAGLUND, Lennart; NORMAN, Bo; WAHREN, Douglas. "Mass distribution in random sheets - theoretical evaluation and comparison with real sheets." Svensk papperstidning 77(10): 362-70, 1974.
18. BRISTOW, J. Anthony & KOLSETH, Petter (eds.). Paper structure and properties. New York, M. Dekker, 1986. 390p. (International Science and Technology Series, 8)
19. RANCE, H.F. (ed.). The structure and physical properties of paper. Amsterdam, Elsevier, 1982. vol.2, 288p.
20. MARK, R.E. "Structure and structural anisotropy." In: MARK, Richard E. (ed.) Handbook of physical and mechanical testing of paper and paperboard. New York, M. Dekker, 1983. v.2, chapter 24, pp. 283-377.

21. INONE, Shinya. "Video imaging devices, cameras, and monitors." In: *Video microscopy*. New York, Plenum Press, 1987. chapter 7, pp. 191-262.
22. PRINCETON SCIENTIFIC INSTRUMENTS. Model V CCD camera/data acquisition system. Kingston, N.Y. 2p.
23. "Computer ready photography." *Computer Graphics Today*, 5 (12): 5, Dec. 1988.
24. SEO, Yung B. "Determination of in-plane elastic constants." In: *Application of laser speckle interferometry (LSI) to the determination of in-plane elastic constants of paper*. Syracuse, State University of New York, College of Environmental Science and Forestry, 1988. (Ph.D. Thesis), chapter VII, pp. 149-174.
25. SCHAFF, J.R. "Compression and tension testing of 240 g/m² paper." Unpublished REU report, Syracuse University, Dept. of Mech. Aero. Engineering, August 1990.

Table 1. Regression Equations Used to Estimate the Strain at Failure.

	Test Number	Intercept (a)	Slope (b)	Correlation Coefficient
Paper Type A (MD)	1	0.36574	0.01220	0.97965
	2	-0.16145	0.01675	0.99914
	3	-0.17366	0.01775	0.99913
	4	0.26392	0.01436	0.99647
	5	0.29261	0.01580	0.99645
Paper Type A (CD)	1	-0.26289	0.01949	0.99137
	2	-0.29544	0.03187	0.99745
	3	-0.10736	0.06389	0.99535
	4	-0.25069	0.01834	0.99135
	5	-0.36176	0.02013	0.99601
Paper Type B (MD)	1	-0.30810	0.01987	0.99523
	2	-0.75227	0.01340	0.98482
	3	-0.46997	0.01462	0.99359
	4	-0.4216	0.01305	0.99358
	5	-0.43989	0.01485	0.99576
Paper Type B (CD)	1	-0.01311	0.01576	0.99596
	2	0.04972	0.01560	0.99194
	3	-0.24054	0.02193	0.99148
	4	-0.07709	0.01880	0.99772
	5	0.25141	0.01394	0.99714
Handsheets	1	-0.06249	0.01294	0.98975
	2	-0.01530	8.4049E-3	0.99267
	3	-0.04776	0.015447	0.99575
	4	-0.10372	0.011015	0.99439
	5	-0.15707	0.01253	0.98744

NOTE: The regression equations are of form: $y = a + bx$, where
 y = strain in %; x = time in seconds

Table 2. Results from Stress-Strain and Load-Strain Relationships for Machine-Made Papers and Handsheets.

Test P Number	MD					CD										
	E1		E2		LFB (%)	E1		E2		LFB (%)						
	(MPa)		(g/cm)			(MPa)		(g/cm)								
	(g/cm)	(g/cm)	(MPa)	(g/cm)		(MPa)	(g/cm)									
	STS	LOAD	STS	LOAD	STR	STS	LOAD	STS	LOAD	STR						
	(MPa)	(g/cm)	(MPa)	(g/cm)	(%)	(MPa)	(g/cm)	(MPa)	(g/cm)	(%)						
1	20.451	2091.97	40.765	4169.90	0.765	1.503	153.181	4.61	2.354	220.41	8.320	779.07	0.856	0.283	26.524	7.94
2	20.145	1816.68	36.742	3321.85	1.083	1.735	156.918	6.09	2.133	187.58	1.701	677.32	0.665	0.245	21.509	7.17
3	18.325	1917.20	38.228	3896.51	0.796	1.617	172.464	6.45	1.313	128.89	8.271	812.49	0.888	0.309	30.318	9.70
4	16.282	1585.20	37.569	3462.89	1.113	1.521	148.072	5.43	2.209	220.43	8.938	891.81	0.958	0.251	25.022	7.49
5	17.235	1533.07	40.625	3784.11	1.610	1.718	162.952	5.97	2.002	219.18	8.054	882.30	0.825	0.237	25.935	7.49
6	18.608	1800.82	38.786	3727.45	1.080	1.631	158.413	5.71	2.002	189.34	8.258	808.62	0.838	0.265	25.874	7.96

P Number	MD					CD										
	E1		E2		LFB (%)	E1		E2		LFB (%)						
	(MPa)		(g/cm)			(MPa)		(g/cm)								
	(g/cm)	(g/cm)	(MPa)	(g/cm)		(MPa)	(g/cm)									
	STS	LOAD	STS	LOAD	STR	STS	LOAD	STS	LOAD	STR						
	(MPa)	(g/cm)	(MPa)	(g/cm)	(%)	(MPa)	(g/cm)	(MPa)	(g/cm)	(%)						
1	8.500	913.99	18.757	1821.47	2.495	0.945	89.214	9.72	6.070	459.65	17.115	1620.9	0.357	0.387	36.551	3.19
2	9.278	901.02	23.017	2235.18	0.694	0.860	83.546	6.01	5.148	459.80	18.754	1674.66	0.398	0.422	39.438	3.21
3	13.452	1119.87	26.772	2228.76	2.249	1.134	144.328	7.01	6.283	369.80	16.183	1397.09	0.427	0.438	37.805	3.60
4	12.577	1269.19	24.460	2468.35	1.013	1.277	128.864	6.22	5.515	566.15	17.624	1809.09	0.288	0.451	45.315	3.46
5	10.959	1089.08	24.097	2394.68	2.239	1.112	119.547	7.04	5.248	551.22	18.072	1899.15	0.245	0.359	37.805	2.71
6	10.953	1058.63	23.421	2229.69	1.098	1.186	111.300	7.20	5.813	481.32	17.562	1680.02	0.343	0.415	39.583	3.23

P Number	MD					CD				
	E1		E2		LFB (%)	E1		E2		LFB (%)
	(MPa)		(g/cm)			(MPa)		(g/cm)		
	(g/cm)	(g/cm)	(MPa)	(g/cm)		(MPa)	(g/cm)			
	STS	LOAD	STS	LOAD	STR	STS	LOAD	STS	LOAD	STR
	(MPa)	(g/cm)	(MPa)	(g/cm)	(%)	(MPa)	(g/cm)	(MPa)	(g/cm)	(%)
1	210.94	19733.8	2.113	197.662	1.59					
2	217.37	18101.5	1.733	144.323	1.11					
3	214.95	17321.9	2.998	185.881	2.09					
4	212.95	18492.2	2.182	189.521	1.36					
5	210.44	20801.1	2.153	212.836	1.48					
6	213.33	18890.1	2.235	186.045	1.53					

MD = Machine direction; CD = Cross machine direction; E1 = Initial apparent modulus; E2 = Apparent modulus of elasticity;
LFB = Strain of the lag phase of the stress-strain curve; STS = Stress at failure; LOAD = Load per unit of width at failure; STR = Strain at failure.

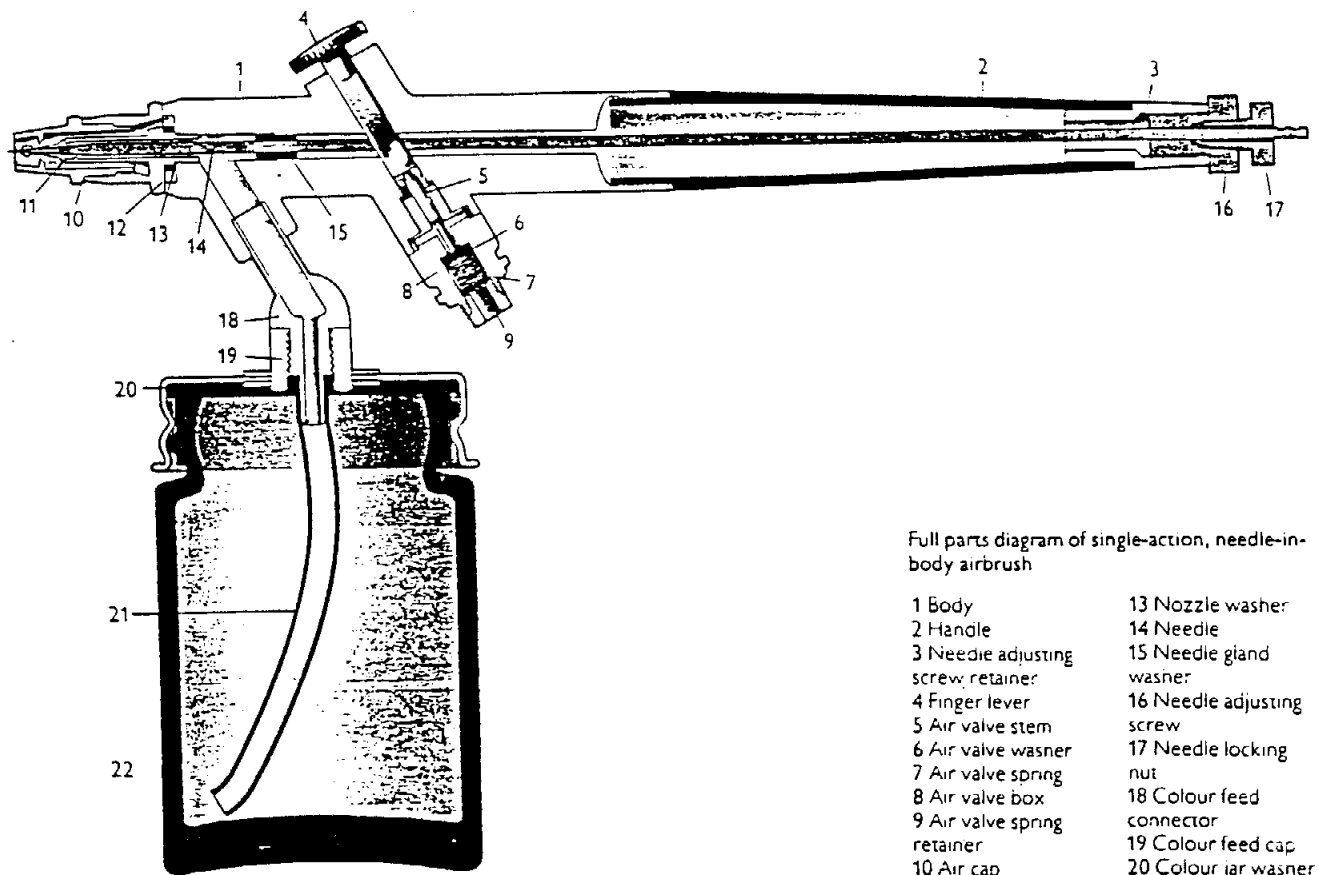


Fig. 1. The airbrush. [from Ref. 2].

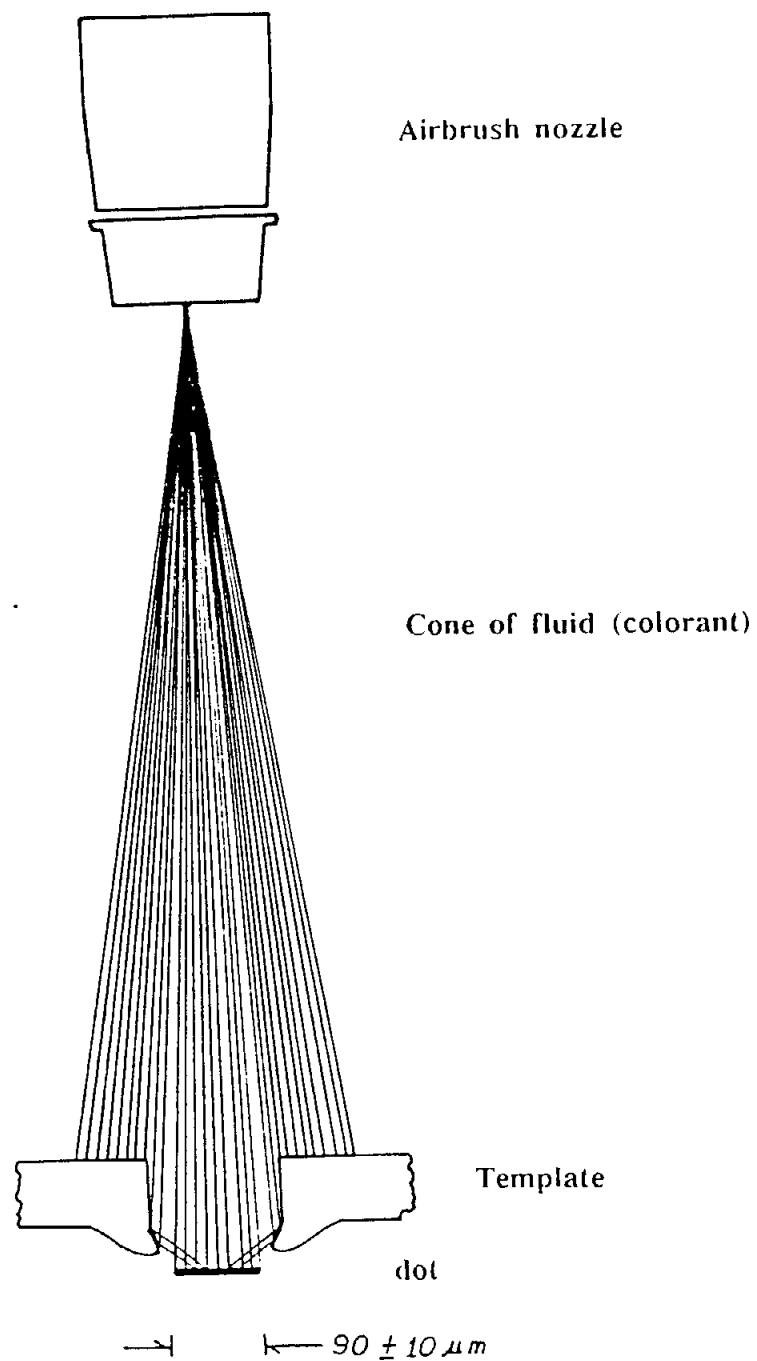


Fig. 2. Partial sectional view of dot formation (the figure shows the formation of one dot).

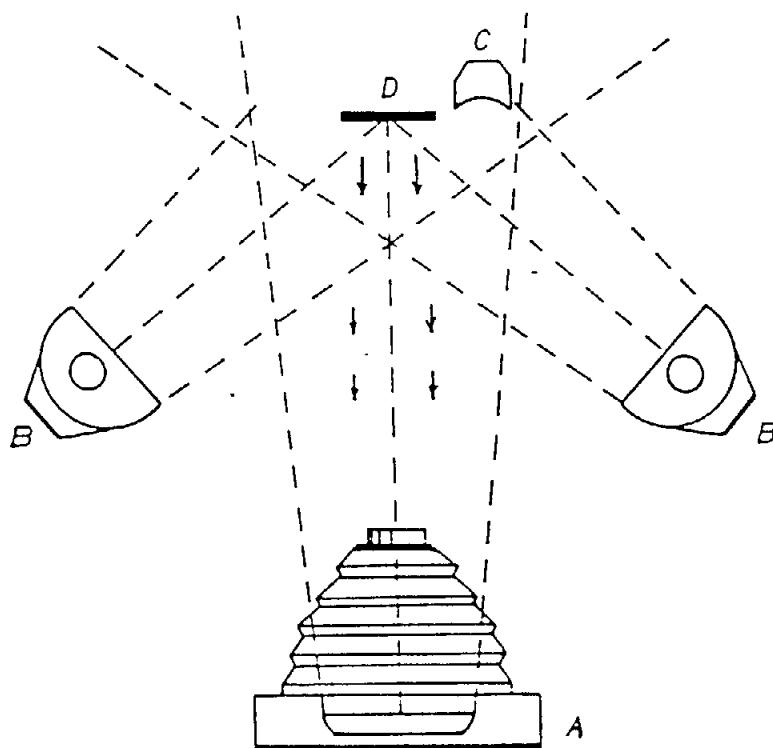


Fig. 3. Top view of the photographic approach.

A: Conventional photographic camera equipped with electronic flash.

B: Fluorescence lamps.

C: Photoelectric cell.

D: Test specimen.

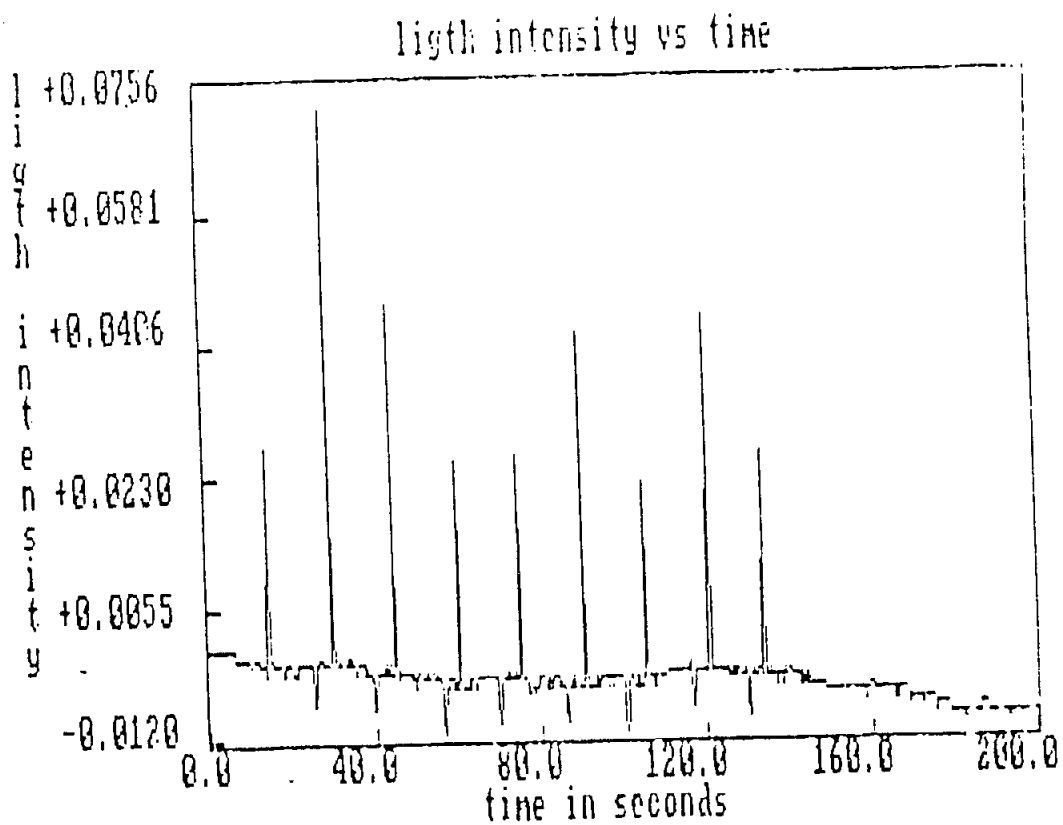


Fig. 4. Output response (spikes) from the photoelectric cell corresponding to each photographic flash illumination.

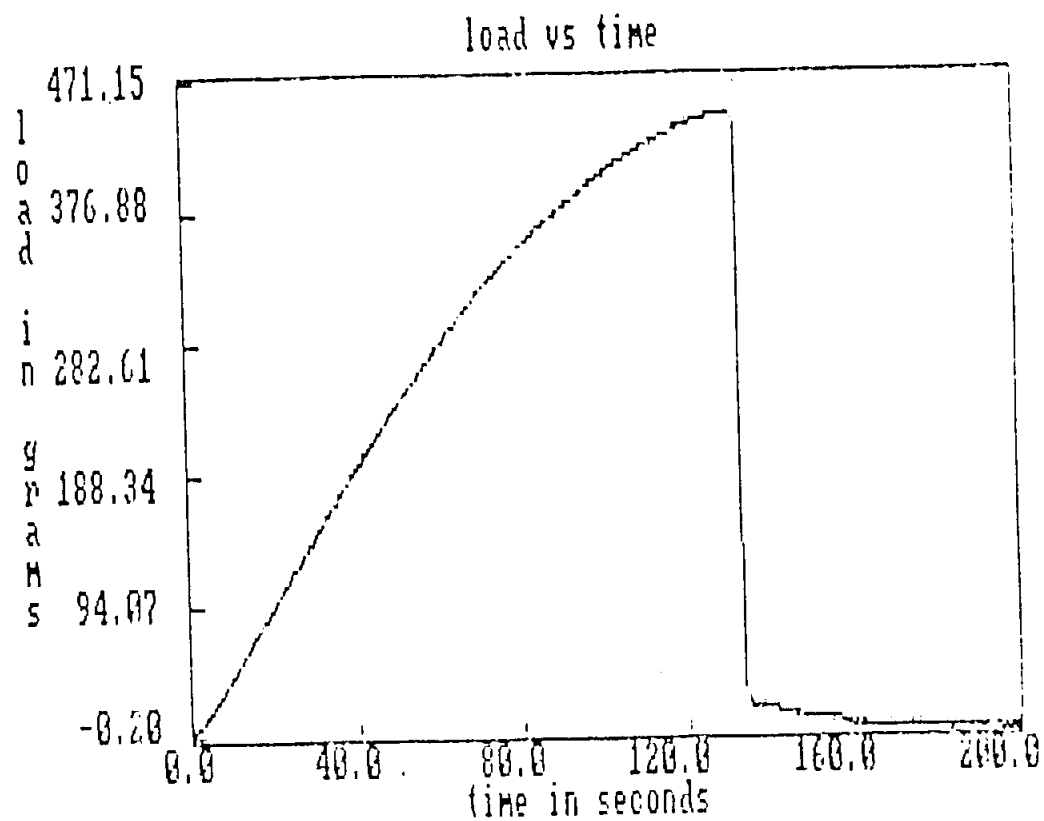


Fig. 5. Load-time relationship.

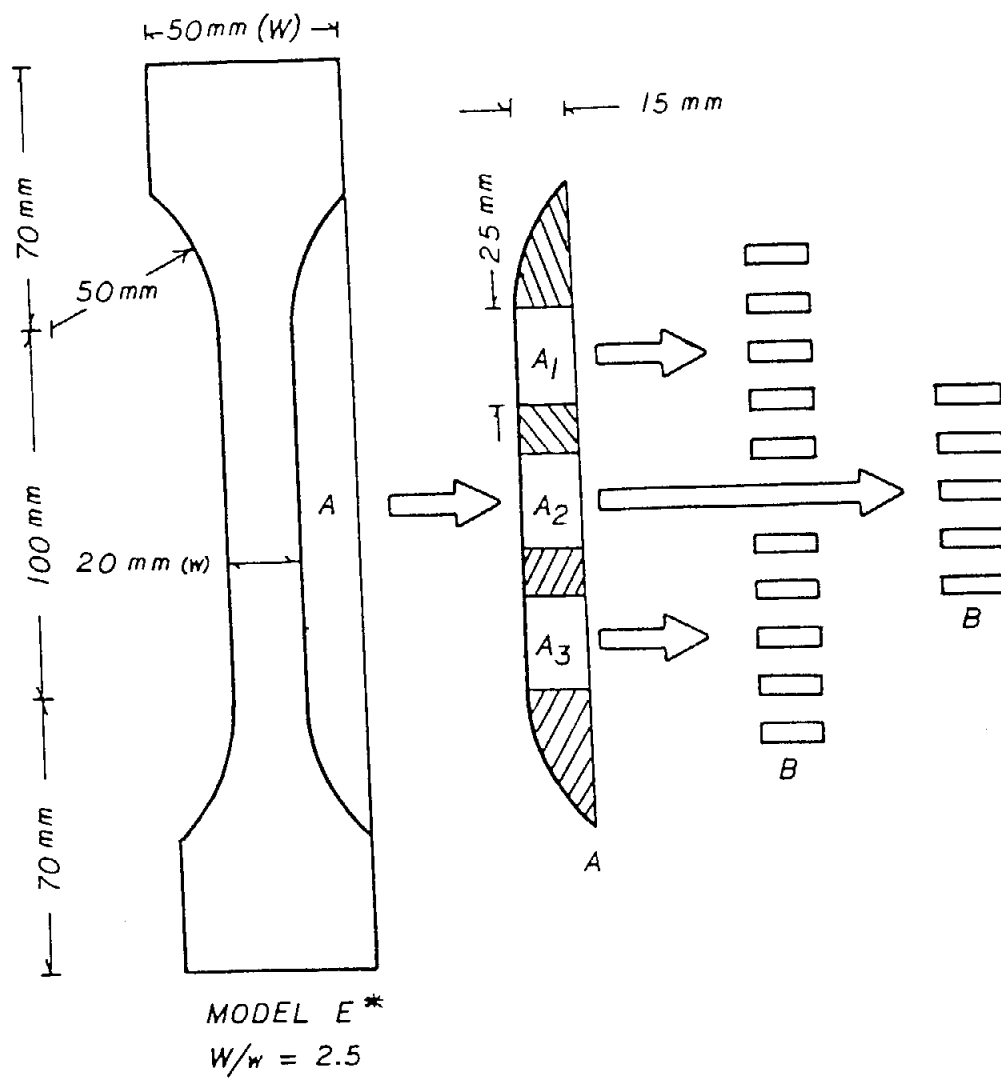


Fig. 6. Test specimen and sampling procedure for thickness measurements.

* It is also showed in Fig. 20 on Chapter 2.

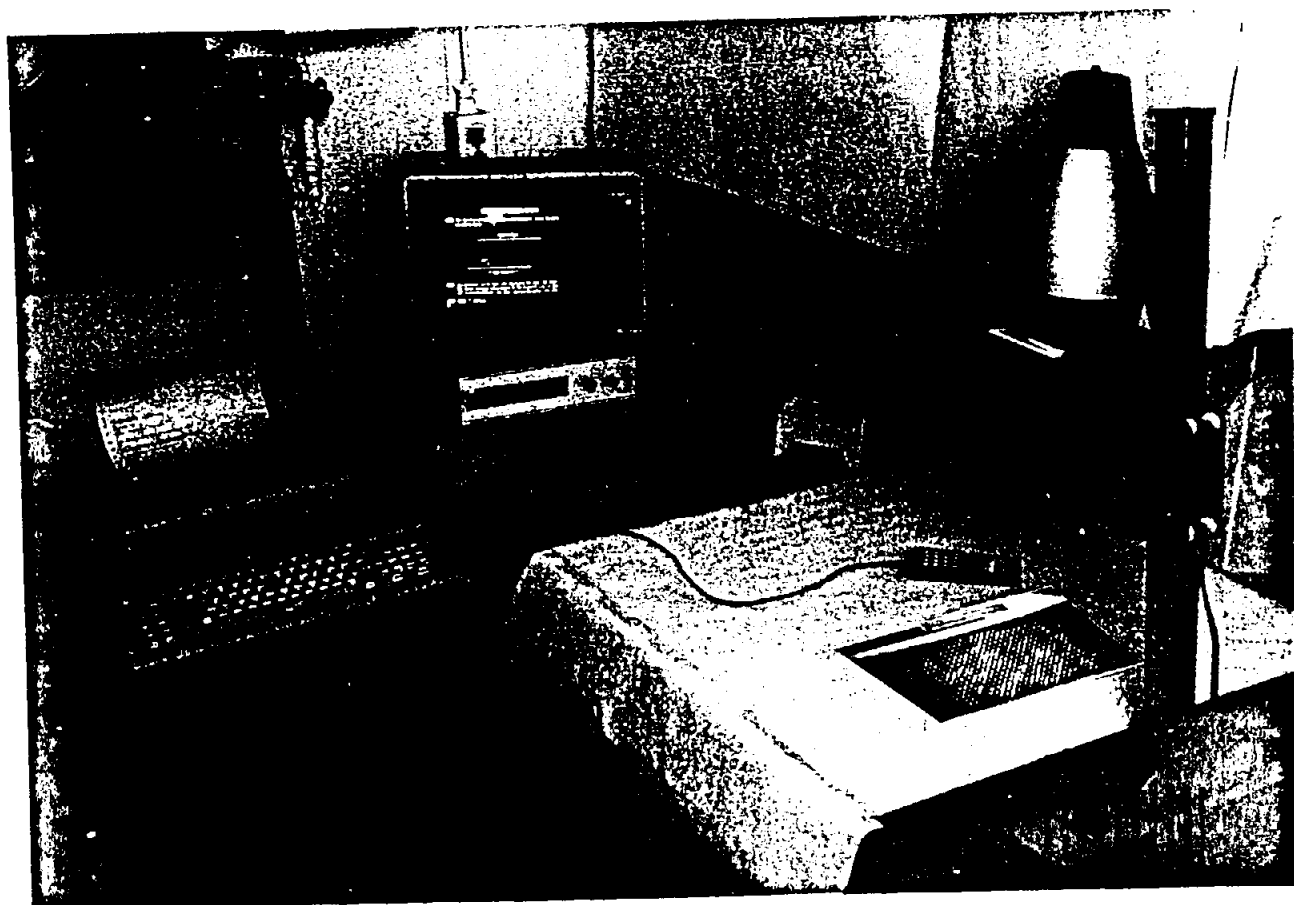
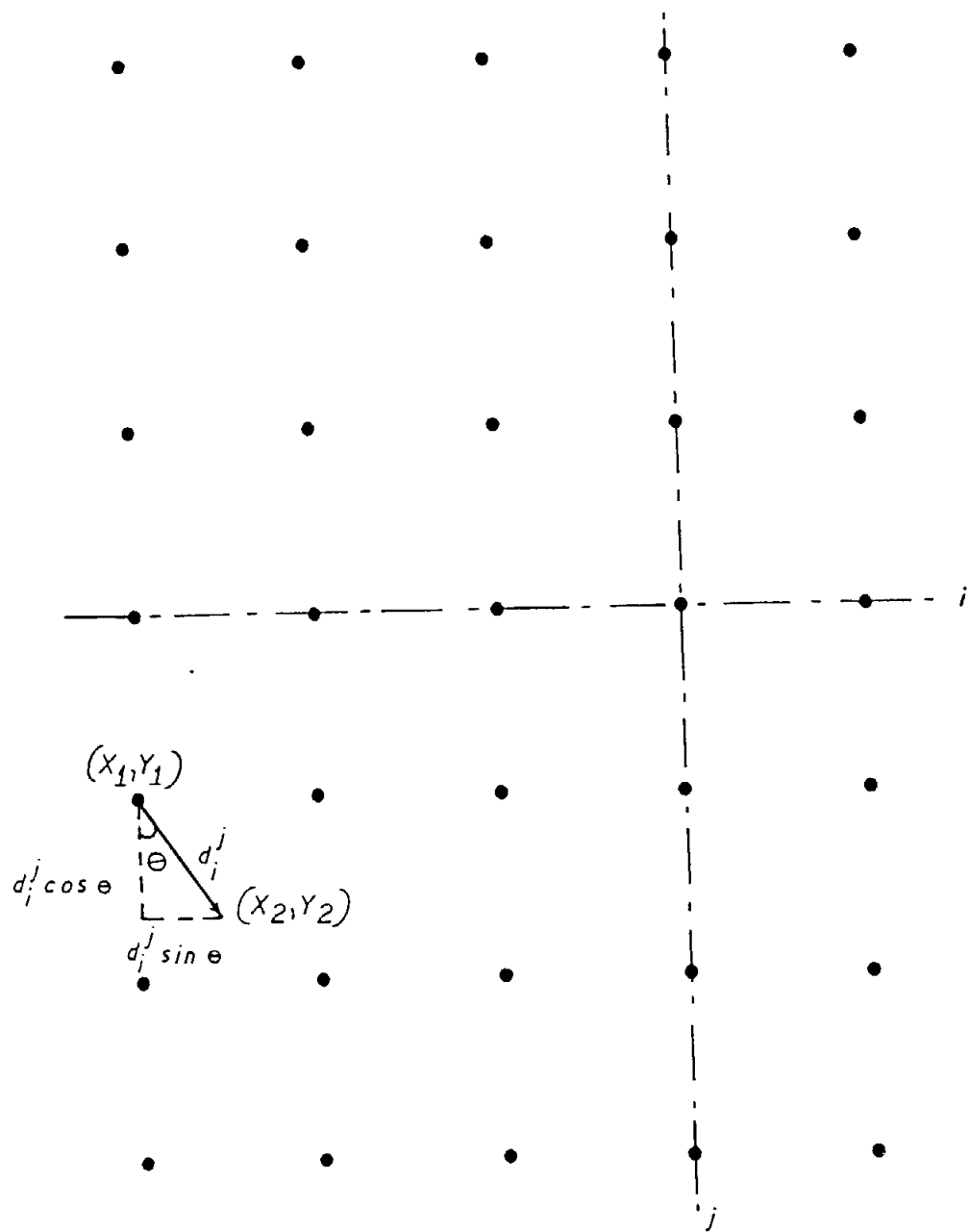


Fig. 7. Projected image of a typical grid pattern



$$d_i^j = \sqrt{(X_2 - X_1)^2 + (Y_2 - Y_1)^2} \quad [3]$$

$$\Theta = \arctan \left(\frac{Y_2 - Y_1}{X_2 - X_1} \right) \quad [4]$$

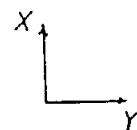


Fig. 8. The grid pattern for digitizing.

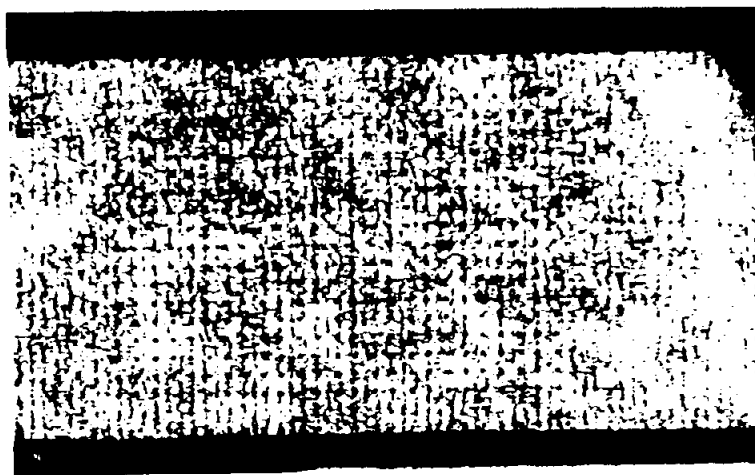


Fig. 9.1. Underformed(0% strain).

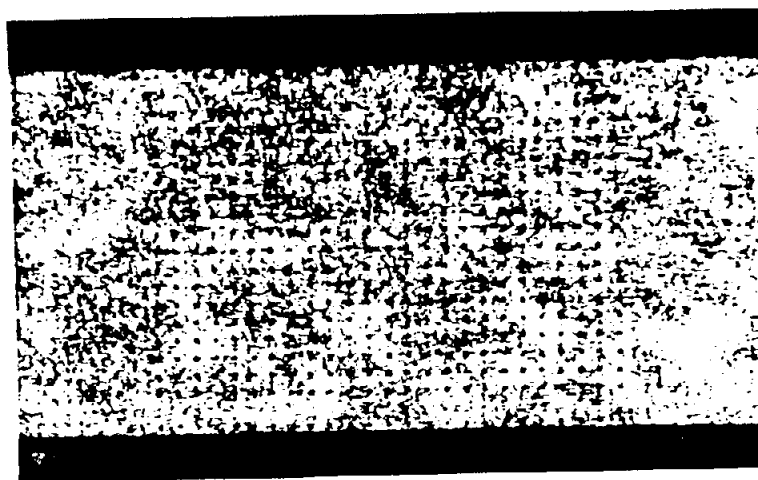


Fig. 9.2. Deformed(at 5.96% of strain).

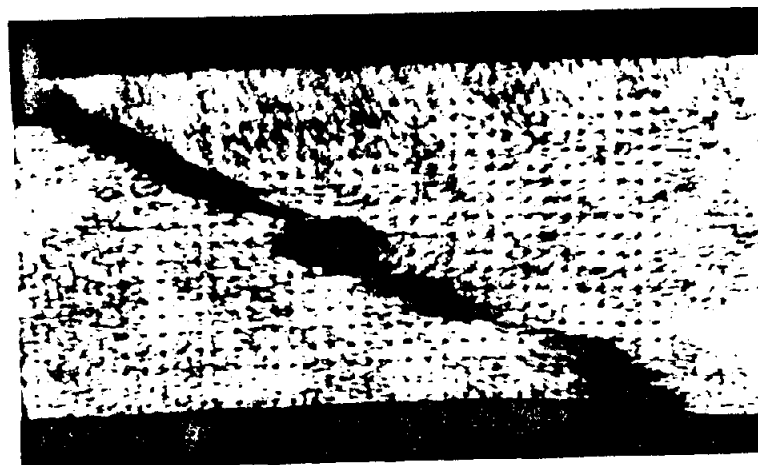


Fig. 9.3. At failure.

Fig. 9. Typical grid pattern in the underformed(unstrained) and deformed(strained) stages.

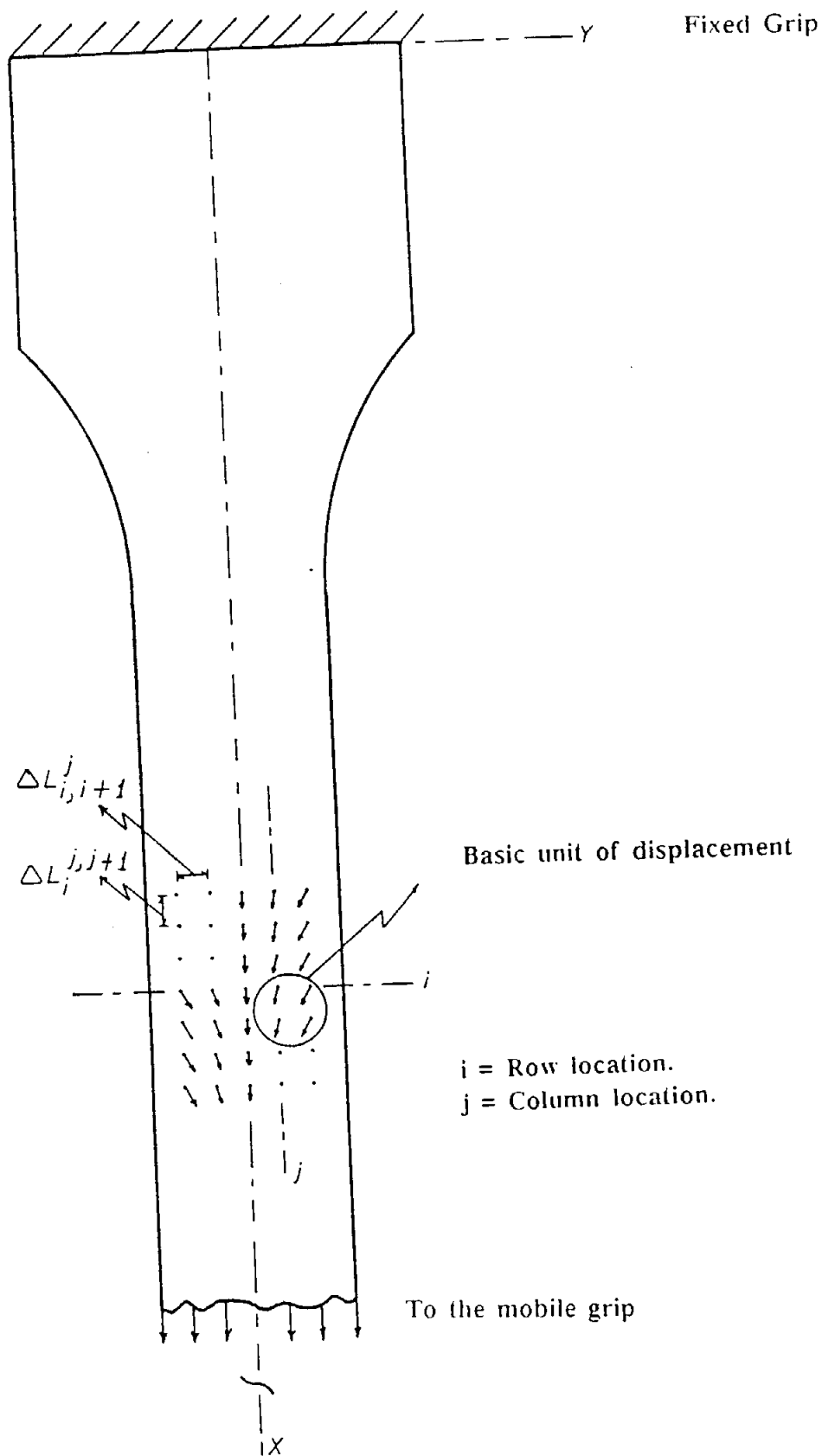


Fig. 10. Geometry of the specimen in uniaxial tensile testing.
 $\Delta L_{i,j,i+1}$ = Spacing between dots within a row (Y direction).
 $\Delta L_{i,j,j+1}$ = Spacing between dots within a column (x direction).

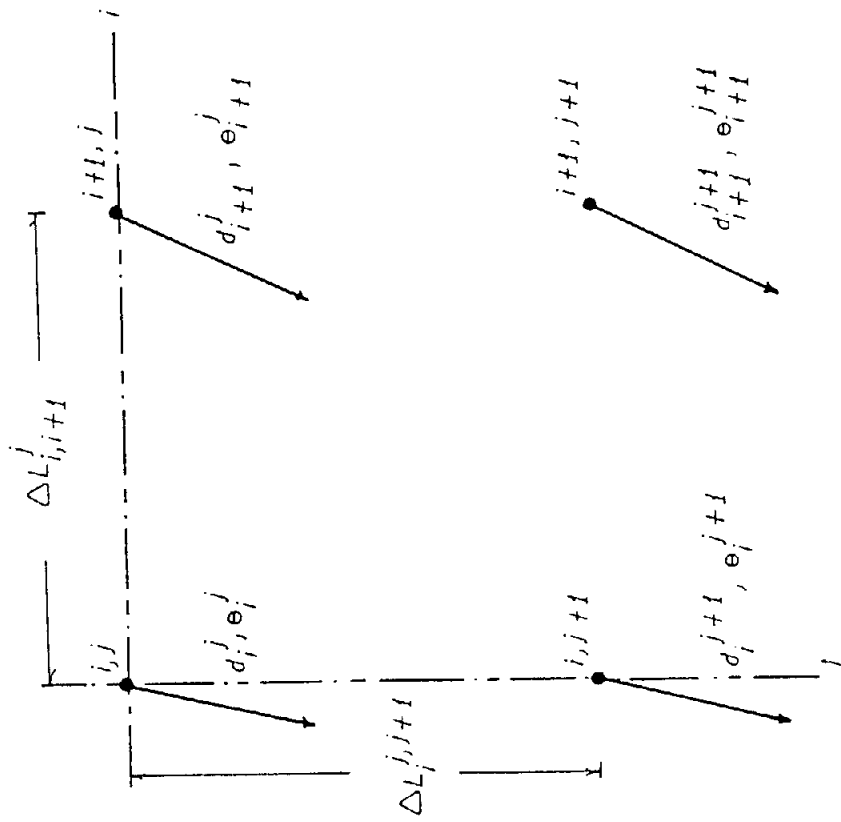


Fig. 11. Basic unit of displacement.
 $\Delta L_{i,j+1}^j$ = Spacing between dots in a row (y direction).
 $\Delta L_{i+1,j}^j$ = Spacing between dots in a column (x direction).

i = Row location.
 j = Column location.

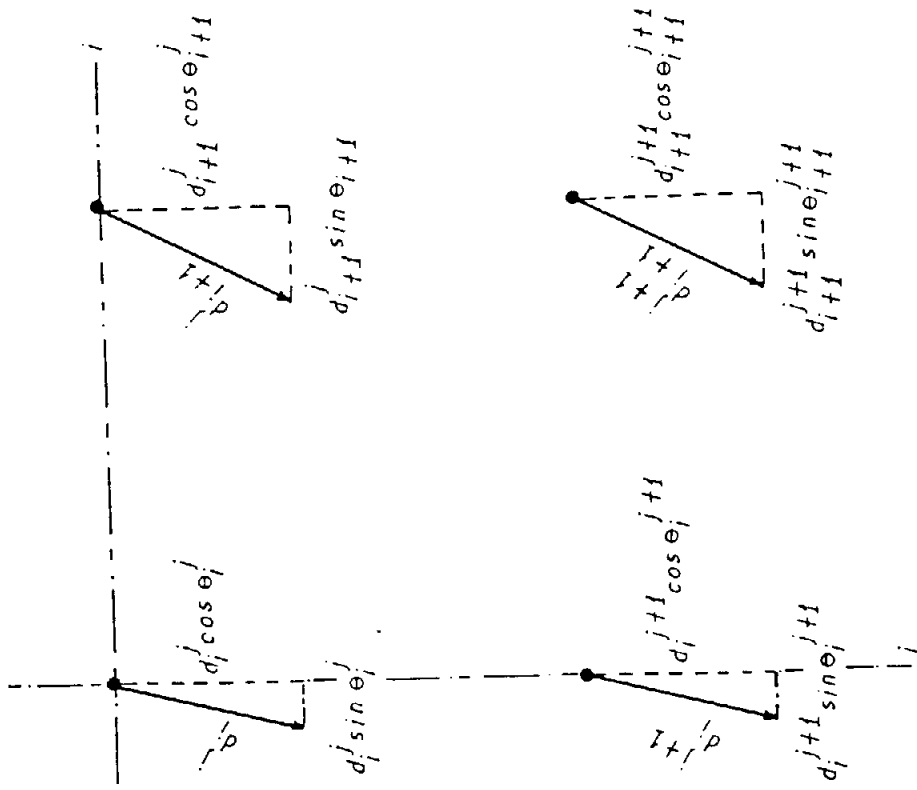


Fig. 12. Displacement vectors components for one basic unit.
 i = Row location.
 j = Column location.

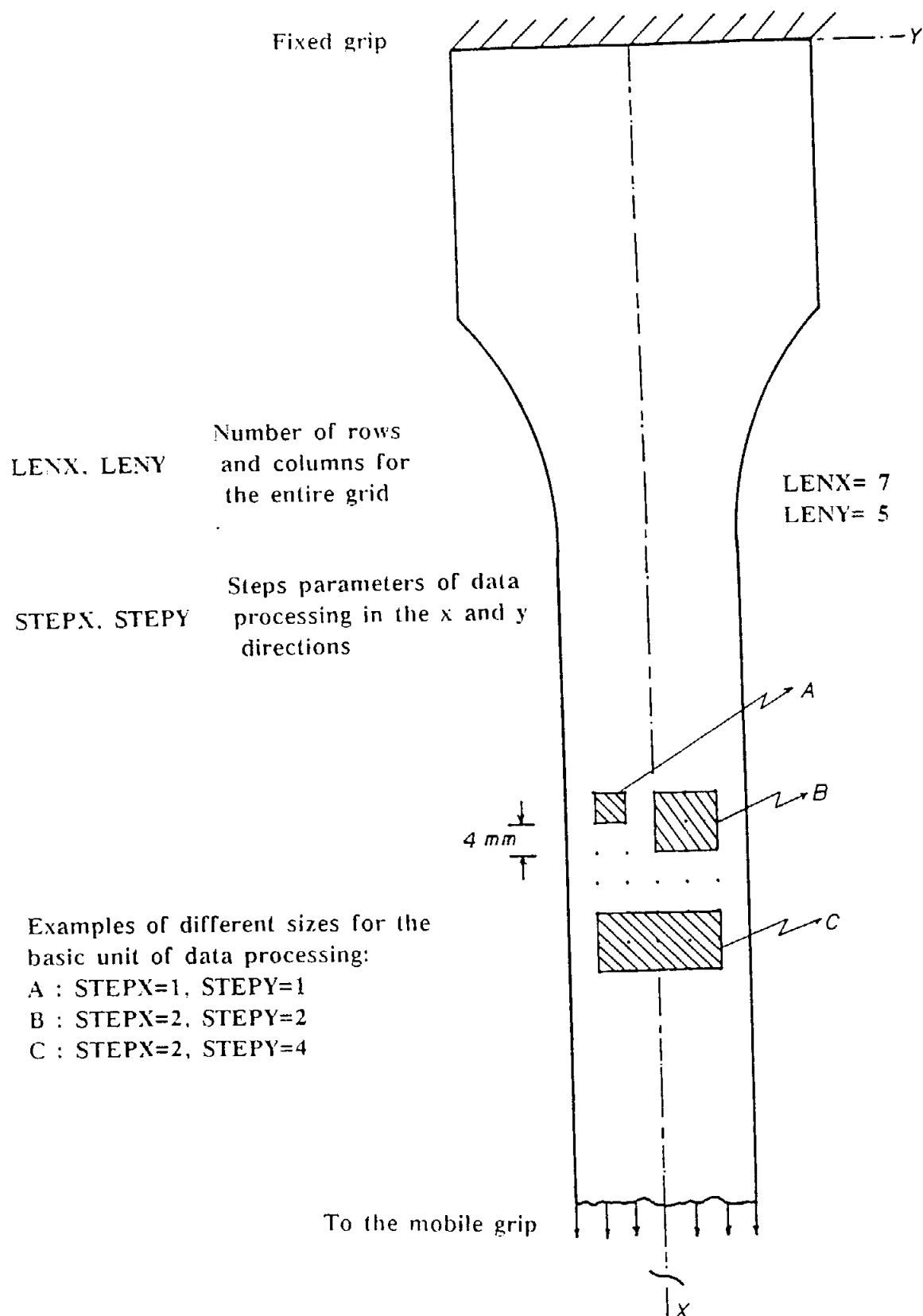
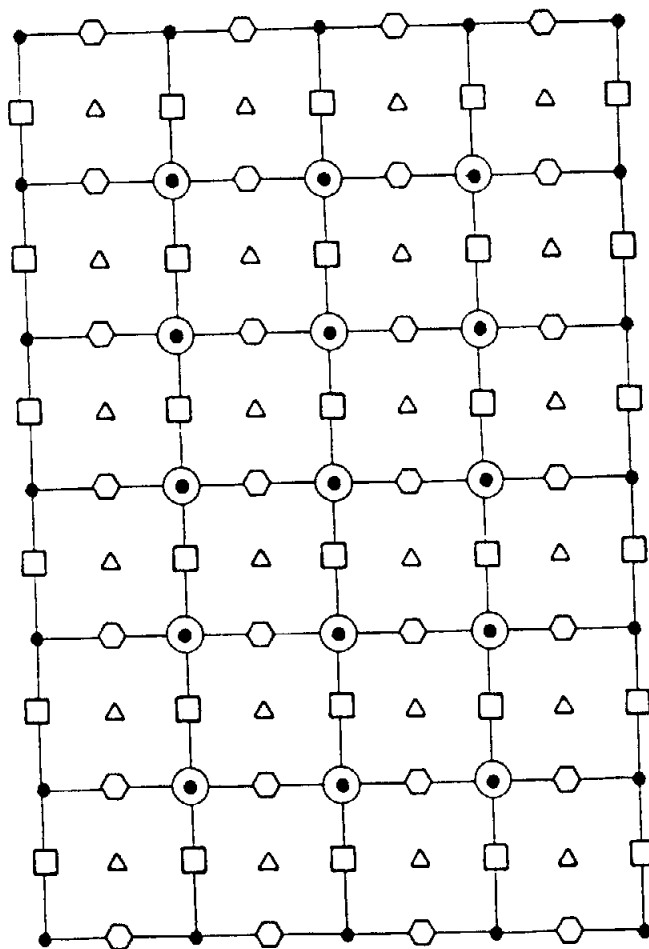


Fig. 13. Geometry and design for different basic units of processing in a uniaxial tensile specimen.

LENX= 7
LENY= 5

STEPX= 1
STEPLY= 1



SIMBOLS	NATURE OF INFORMATION	DIMENSION OF THE ARRAY
●	Displacement data	(LENX, LENY)
□	Axial strain	(LENX-STEPX, LENY)
⬡	Lateral strain	(LENX, LENY-STEPLY)
△	Shear + Principal strain	(LENX-STEPX, LENY-STEPLY)
○	Lateral contraction ratios	(LENX-2×STEPX, LENY-2×STEPLY)

Fig. 14. Array dimensions for strain calculations.

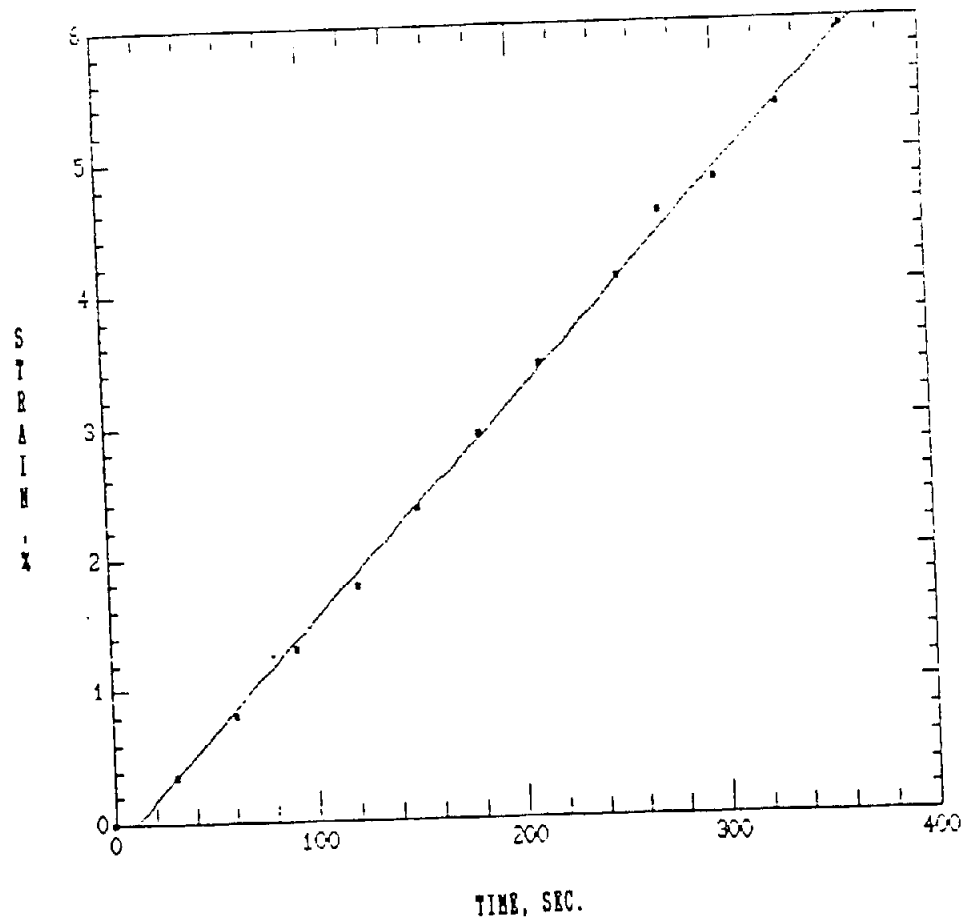


Fig. 15. Typical strain vs time relationship

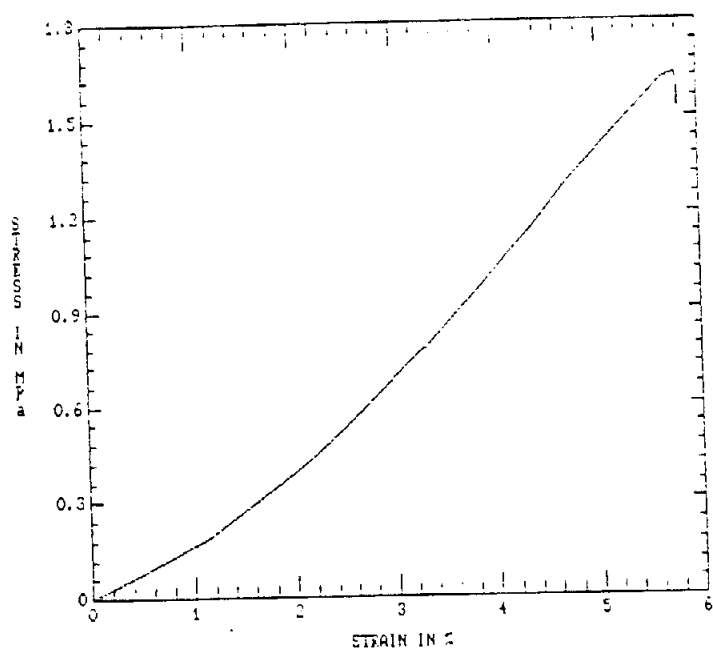


Fig. 16.1. Stress-strain relationship for MD specimens.

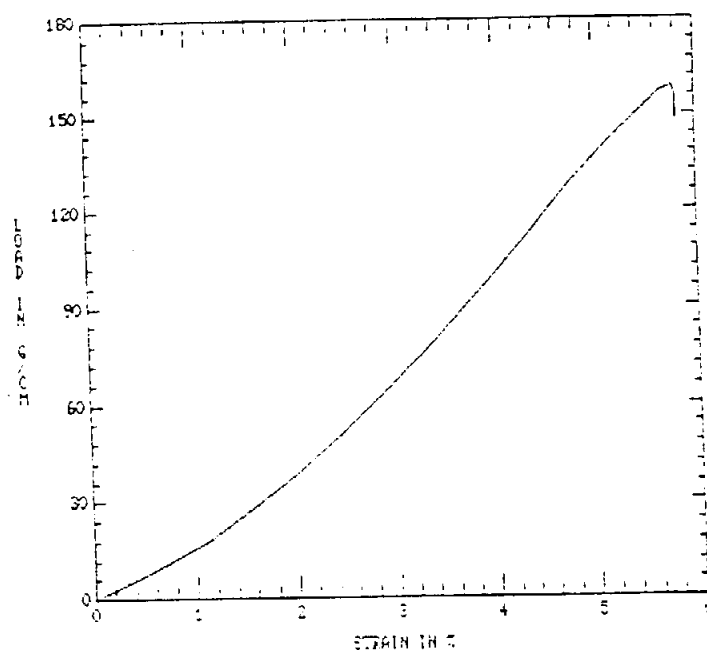


Fig. 16.2. Load-strain relationship for MD specimen.

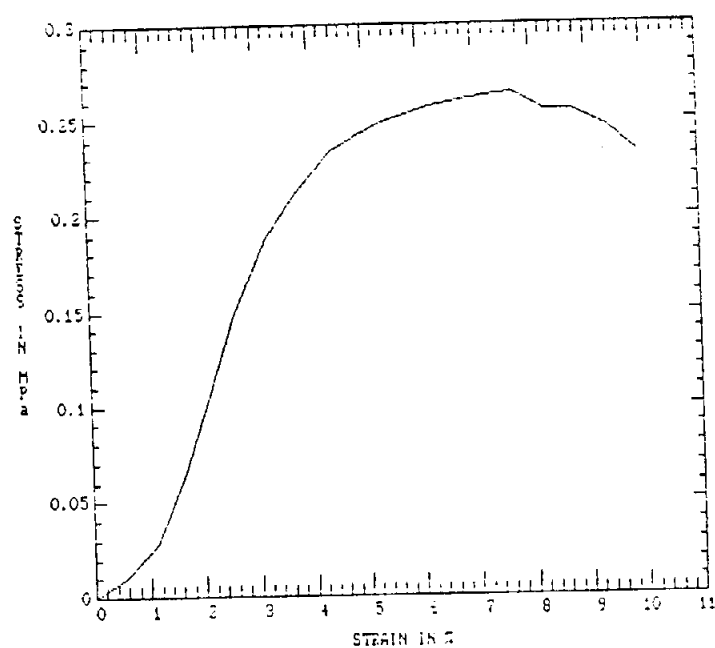


Fig. 16.3. Stress-strain relationship for CD specimens.

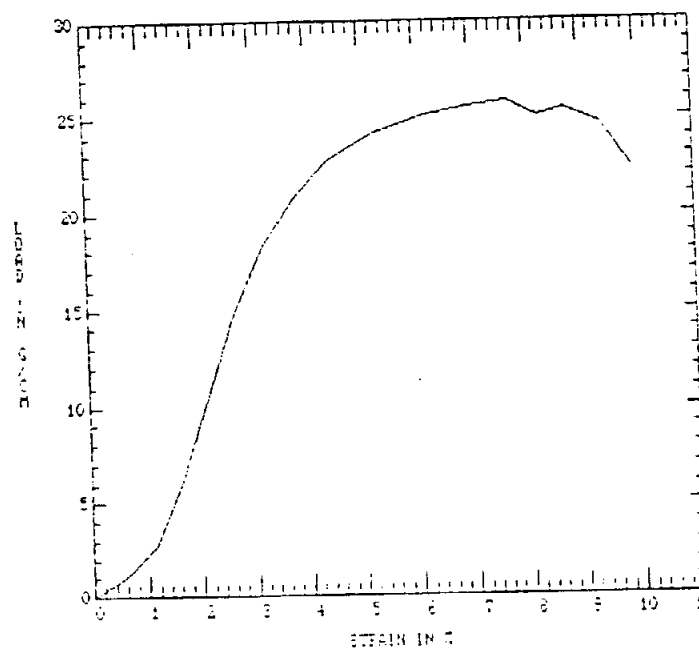


Fig. 16.4. Load-strain relationship for CD specimen.

Fig. 16. Typical relationship from the tensile test for the machine-made paper type A.

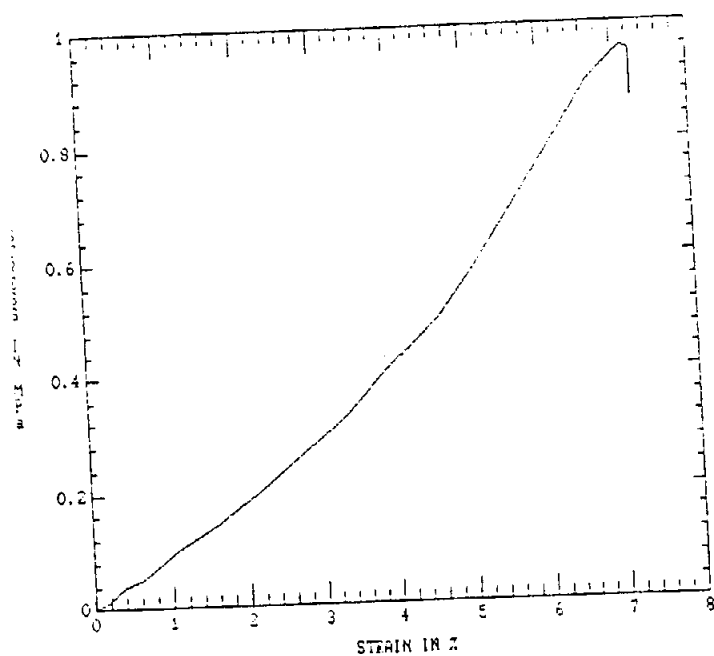


Fig. 17.1. Stress-strain relationship for MD specimens.

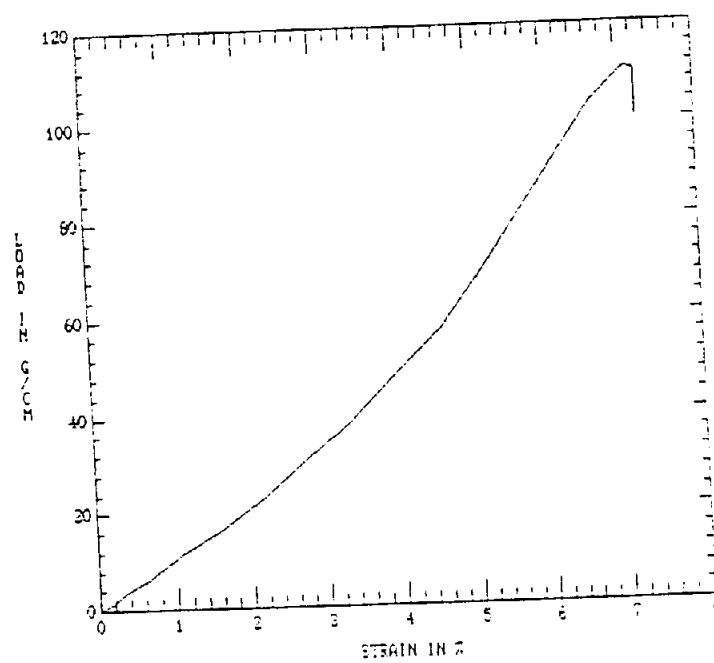


Fig. 17.2. Load-strain relationship for MD specimens.

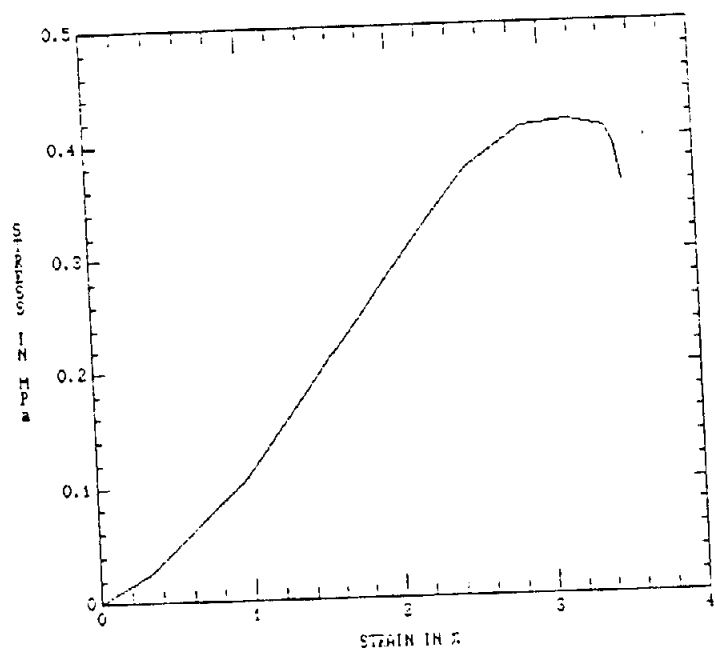


Fig. 17.3. Stress-strain relationship for CD specimens.

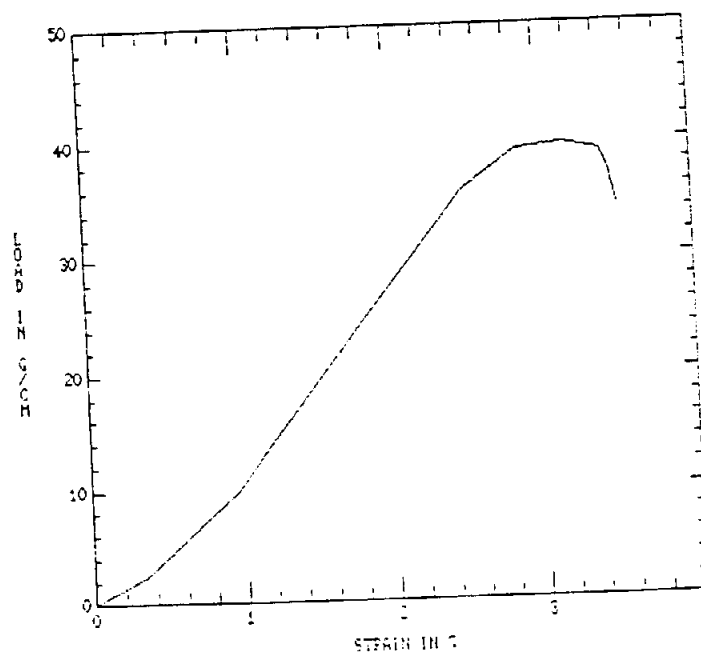


Fig. 17.4. Load-strain relationship for CD specimen.

Fig. 17. Typical relationship from the tensile test for the machine-made paper type B.

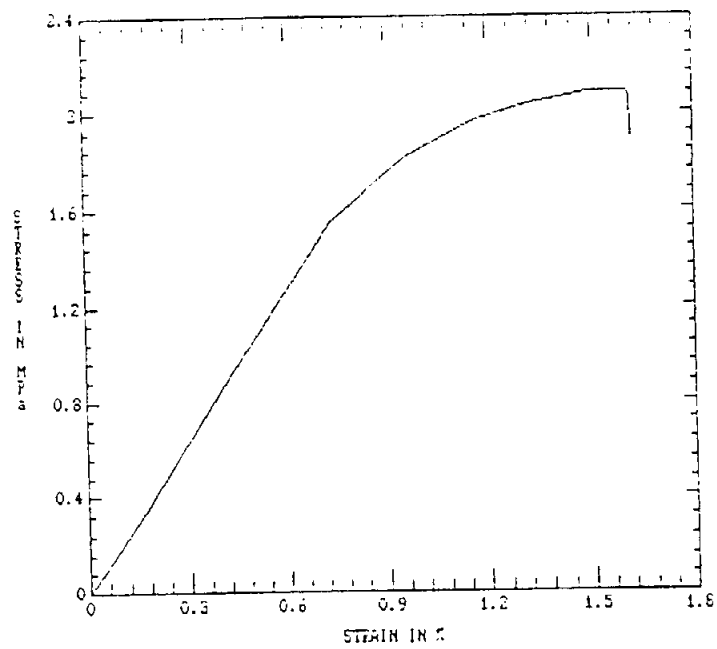


Fig. 18.1. Stress-strain relationship.

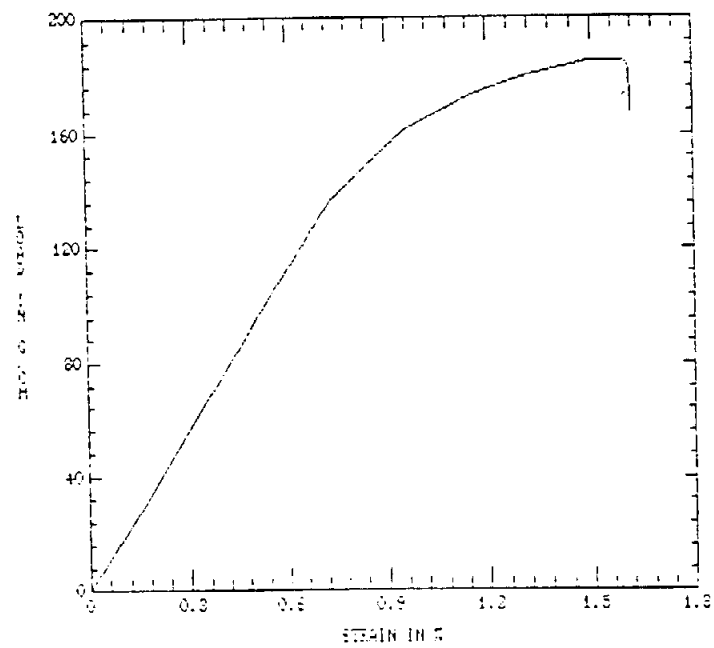
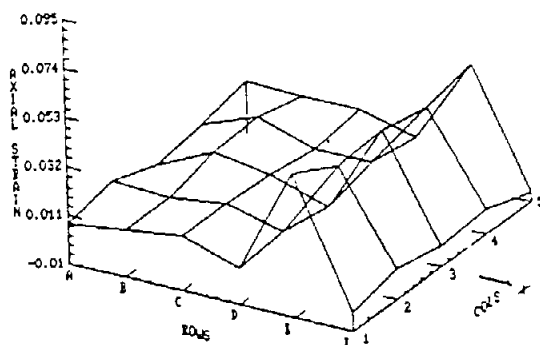


Fig. 18.2. Load-strain relationship.

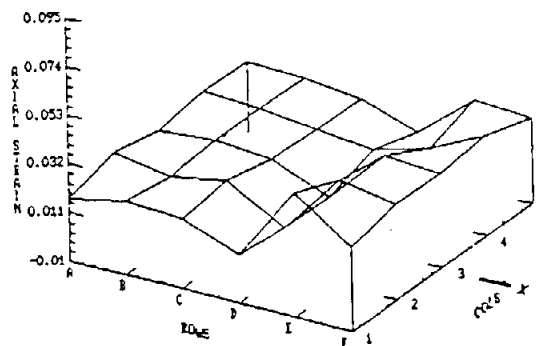
Fig. 18. Typical relationship from the tensile test for HANDSHEETS.



POSITIONAL STRAIN DATA

	ROW A	ROW B	ROW C	ROW D	ROW E	ROW F
Col. 5	0.01263	0.01139	0.01239	0.00582	0.04338	-0.00613
Col. 4	0.00786	0.01698	0.00897	0.00906	0.03843	0.00054
Col. 3	0.00438	0.01546	0.01201	0.00413	0.04279	-0.00144
Col. 2	0.01221	0.01011	0.01358	0.00709	0.04128	0.00297
Col. 1	0.00757	0.01020	0.01356	0.00559	0.05200	-0.00188

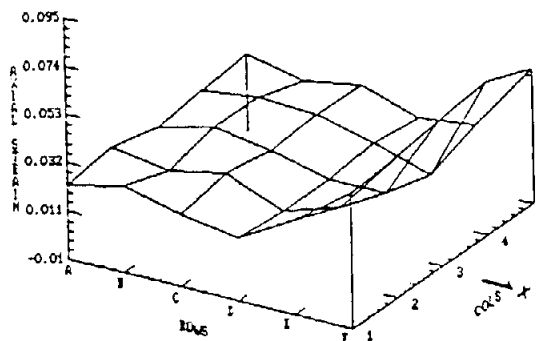
FIG. 19.1. Axial strain distribution at nominal axial strain level of 1.291%.



POSITIONAL STRAIN DATA

	ROW A	ROW B	ROW C	ROW D	ROW E	ROW F
Col. 5	0.02063	0.01944	0.01671	0.00850	0.02884	0.02706
Col. 4	0.02170	0.02023	0.01720	0.01489	0.02118	0.03320
Col. 3	0.01852	0.02033	0.01854	0.00783	0.03190	0.03030
Col. 2	0.02253	0.01841	0.02283	0.00875	0.03530	0.03142
Col. 1	0.01666	0.02155	0.02050	0.01061	0.04360	0.02621

FIG. 19.2. Axial strain distribution at nominal axial strain level of 2.129%.

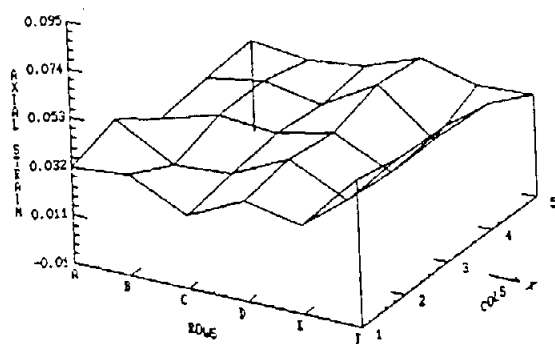


POSITIONAL STRAIN DATA

	ROW A	ROW B	ROW C	ROW D	ROW D	ROW F
Col. 5	0.02386	0.01861	0.02299	0.01470	0.01762	0.04840
Col. 4	0.02222	0.02489	0.02351	0.01714	0.00942	0.05667
Col. 3	0.01947	0.02586	0.02139	0.01522	0.01611	0.05408
Col. 2	0.02502	0.02017	0.02591	0.01564	0.02291	0.05075
Col. 1	0.02179	0.02759	0.02164	0.01773	0.03158	0.04940

FIG. 19.3. Axial strain distribution at nominal axial strain level of 2.543%.

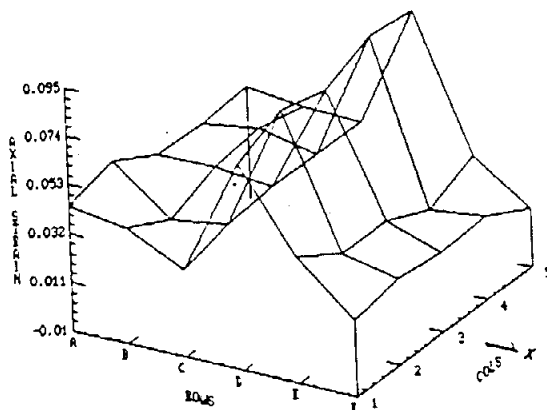
FIG. 19. Typical axial strain distribution for MD specimens, paper type A. Results are given in non-dimensional form using average parameters: STEPX=1, STEPY=1. Average parameters are described in item 3.6.



POSITIONAL STRAIN DATA

	ROW A	ROW B	ROW C	ROW D	ROW E	ROW F
Col. 5	0.02903	0.02660	0.02950	0.03889	0.03264	0.03424
Col. 4	0.02756	0.03174	0.02697	0.04122	0.02336	0.04457
Col. 3	0.02421	0.03125	0.02867	0.03466	0.02331	0.04886
Col. 2	0.03795	0.02357	0.02542	0.03776	0.02550	0.04998
Col. 1	0.03140	0.03374	0.02140	0.03378	0.02839	0.05410

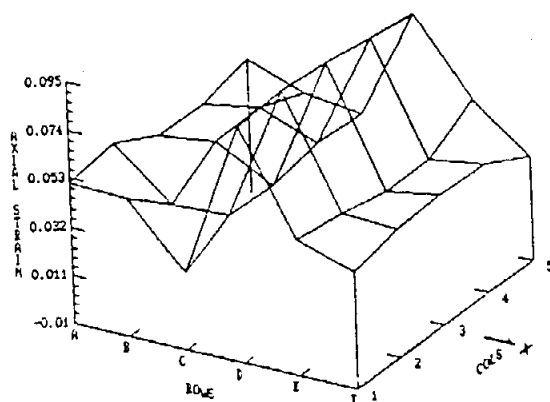
FIG. 19.4. Axial strain distribution at nominal axial strain level of 3.185%.



POSITIONAL STRAIN DATA

	ROW A	ROW B	ROW C	ROW D	ROW E	ROW F
Col. 5	0.03842	0.03574	0.03502	0.08911	0.03208	0.01463
Col. 4	0.03672	0.04055	0.03517	0.09211	0.02239	0.02541
Col. 3	0.03718	0.03773	0.03504	0.08268	0.03225	0.02448
Col. 2	0.04904	0.02902	0.03287	0.08773	0.03225	0.02700
Col. 1	0.04331	0.04019	0.02750	0.07881	0.04486	0.02337

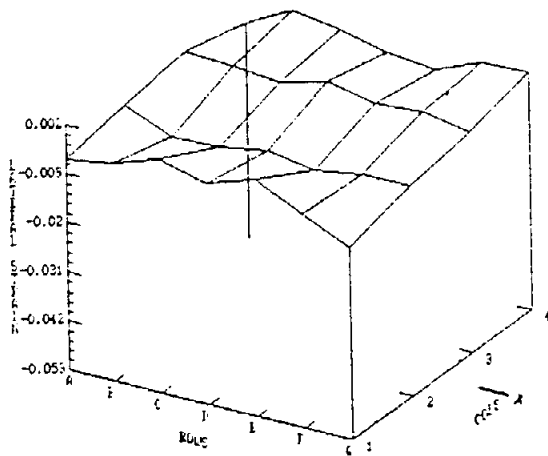
FIG. 19.5. Axial strain distribution at nominal axial strain level of 4.141%.



POSITIONAL STRAIN DATA

	ROW A	ROW B	ROW C	ROW D	ROW E	ROW F
Col. 5	0.04833	0.03931	0.03654	0.08509	0.05409	0.03540
Col. 4	0.04273	0.04712	0.03788	0.08849	0.04209	0.04572
Col. 3	0.04364	0.04637	0.03325	0.09232	0.04188	0.04686
Col. 2	0.05445	0.03357	0.03463	0.09435	0.04687	0.04596
Col. 1	0.05100	0.05042	0.02352	0.09248	0.04946	0.04135

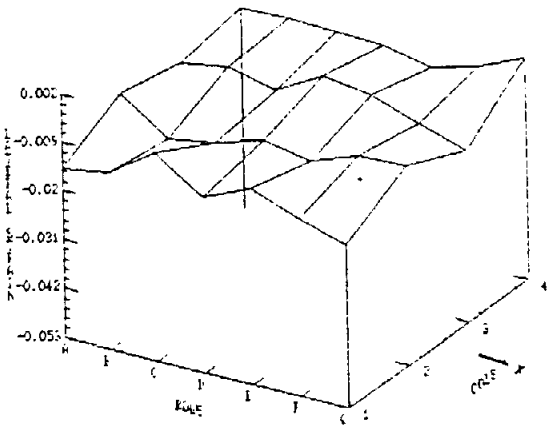
FIG. 19.6. Axial strain distribution at nominal axial strain level of 5.061%.



POSITIONAL STRAIN DATA

	ROW A	ROW B	ROW C	ROW D	ROW E	ROW F	ROW G
Col. 4	-0.00406	0.00161	-0.00011	-0.00280	-0.00425	0.00022	0.00073
Col. 3	-0.00094	-0.00150	-0.00250	0.00035	-0.00196	-0.00139	-0.00334
Col. 2	-0.00352	-0.00789	-0.00737	-0.00575	-0.00738	-0.00571	-0.00553
Col. 1	-0.00592	-0.00405	-0.00061	-0.00331	-0.00028	-0.00507	-0.01000

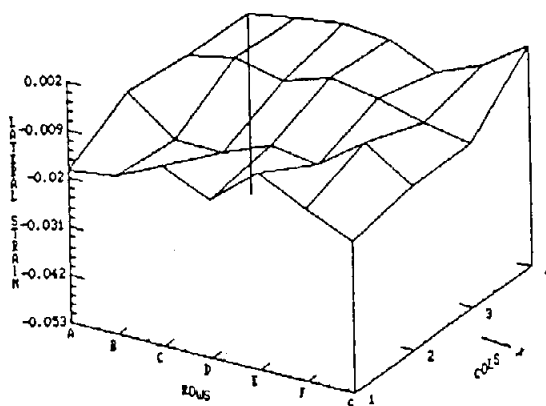
FIG. 20.1. Lateral strain distribution at nominal axial strain level of 1.291%.



POSITIONAL STRAIN DATA

	ROW A	ROW B	ROW C	ROW D	ROW E	ROW F	ROW G
Col. 4	-0.00778	-0.00737	-0.00760	-0.00788	-0.01037	-0.00752	-0.00294
Col. 3	-0.01020	-0.00866	-0.01112	-0.00522	-0.00714	-0.01101	-0.01424
Col. 2	-0.00753	-0.01527	-0.01365	-0.01027	-0.01233	-0.00857	-0.00826
Col. 1	-0.01505	-0.01336	-0.00608	-0.01350	-0.00897	-0.01325	-0.01613

FIG. 20.2. Lateral strain distribution at nominal axial strain level of 2.129%.

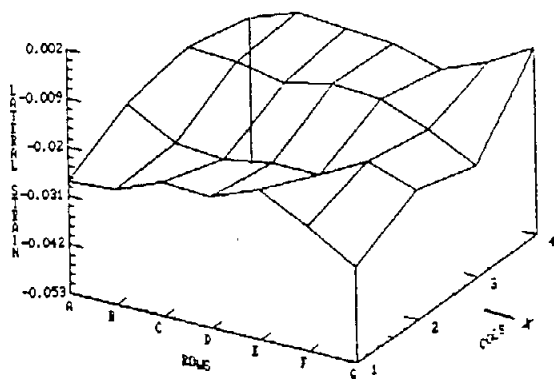


POSITIONAL STRAIN DATA

	ROW A	ROW B	ROW C	ROW D	ROW E	ROW F	ROW G
Col. 4	-0.01154	-0.00984	-0.00849	-0.00945	-0.01419	-0.01018	-0.00298
Col. 3	-0.01152	-0.00921	-0.01198	-0.00855	-0.01049	-0.01329	-0.01530
Col. 2	-0.01019	-0.01803	-0.01829	-0.01423	-0.01577	-0.00821	-0.01551
Col. 1	-0.01823	-0.01683	-0.01201	-0.01723	-0.00808	-0.01394	-0.01847

FIG. 20.3. Lateral strain distribution at nominal axial strain level of 2.543%.

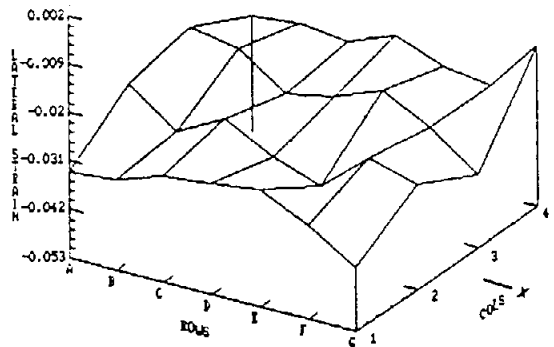
FIG. 20. Typical lateral strain distribution for MD specimens, paper type A. Results are given in non-dimensional form using average parameters: STEPX= 1, STEPY= 1. Average parameters are described in item 3.6.



POSITIONAL STRAIN DATA

	ROW A	ROW B	ROW C	ROW D	ROW E	ROW F	ROW G
Col. 4	-0.02016	-0.01615	-0.01736	-0.01771	-0.02111	-0.01676	-0.01072
Col. 3	-0.01687	-0.01761	-0.01980	-0.01730	-0.01805	-0.02202	-0.02773
Col. 2	-0.02006	-0.02632	-0.02715	-0.02529	-0.02553	-0.01984	-0.02375
Col. 1	-0.02762	-0.02712	-0.02278	-0.02349	-0.01909	-0.02484	-0.03139

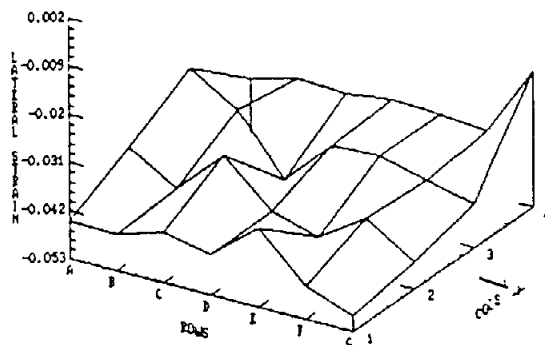
FIG. 20.4. Lateral strain distribution at nominal axial strain level of 3.165%.



POSITIONAL STRAIN DATA

	ROW A	ROW B	ROW C	ROW D	ROW E	ROW F	ROW G
Col. 4	-0.02659	-0.02570	-0.02697	-0.02270	-0.02702	-0.02844	-0.01655
Col. 3	-0.01975	-0.02197	-0.02936	-0.02709	-0.02276	-0.02829	-0.03641
Col. 2	-0.02307	-0.03132	-0.02542	-0.03157	-0.03541	-0.02593	-0.02936
Col. 1	-0.03360	-0.03278	-0.02925	-0.02816	-0.02659	-0.03170	-0.03863

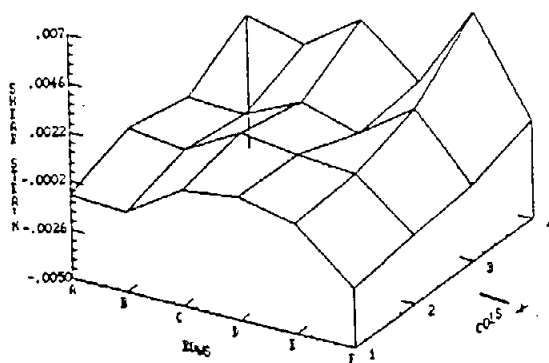
FIG. 20.5. Lateral strain distribution at nominal axial strain level of 4.141%.



POSITIONAL STRAIN DATA

	ROW A	ROW B	ROW C	ROW D	ROW E	ROW F	ROW G
Col. 4	-0.04057	-0.03756	-0.03828	-0.03688	-0.03741	-0.03858	-0.02196
Col. 3	-0.02877	-0.03535	-0.04875	-0.03811	-0.03761	-0.04035	-0.04272
Col. 2	-0.03732	-0.04391	-0.03352	-0.04333	-0.04646	-0.03958	-0.04671
Col. 1	-0.04431	-0.04481	-0.04146	-0.04374	-0.03492	-0.04565	-0.04952

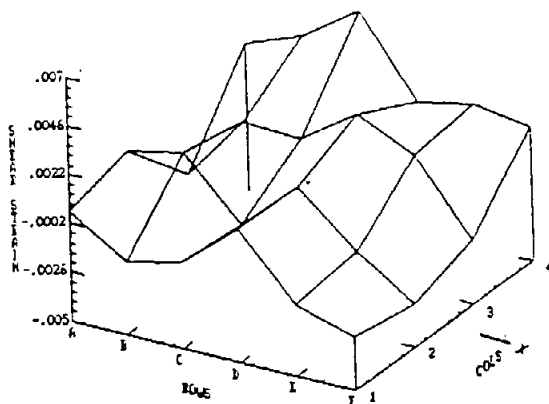
FIG. 20.6. Lateral strain distribution at nominal axial strain level of 5.061%.



POSITIONAL STRAIN DATA

	ROW A	ROW B	ROW C	ROW D	ROW E	ROW F
Col. 4	0.00159	0.00081	0.00270	0.00035	0.00450	-0.00018
Col. 3	-0.00303	-0.00051	0.00085	-0.00007	0.00181	-0.00122
Col. 2	0.00032	-0.00013	0.00138	0.00100	0.00074	-0.00156
Col. 1	-0.00084	-0.00108	0.00067	0.00102	0.00045	-0.00211

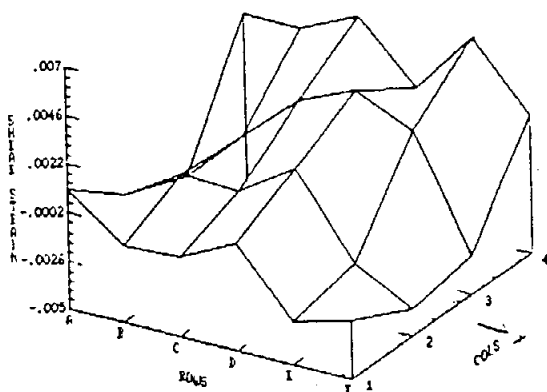
FIG. 21.1. Shear strain distribution at nominal axial strain level of 1.7917.



POSITIONAL STRAIN DATA

	ROW A	ROW B	ROW C	ROW D	ROW E	ROW F
Col. 4	0.00224	0.00335	0.00518	0.00141	0.00205	0.00161
Col. 3	-0.00207	0.00124	0.00104	0.00296	0.00160	-0.00188
Col. 2	0.00119	0.00185	-0.00105	0.00149	-0.00103	-0.00290
Col. 1	0.00032	-0.00142	-0.00074	0.00155	-0.00147	-0.00239

FIG. 21.2. Shear strain distribution at nominal axial strain level of 2.1297.

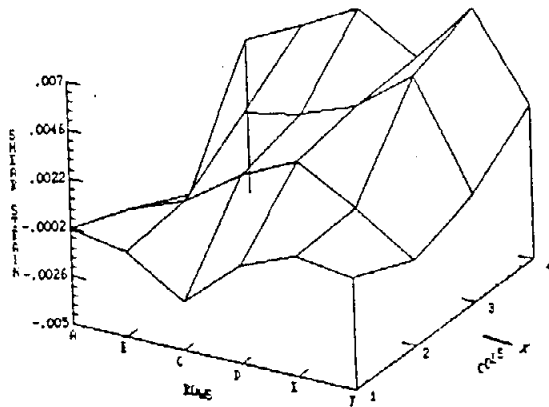


POSITIONAL STRAIN DATA

	ROW A	ROW B	ROW C	ROW D	ROW E	ROW F
Col. 4	0.00330	0.00331	0.00459	0.00171	0.00497	0.00184
Col. 3	-0.00269	0.00007	0.00247	0.00371	0.00242	-0.00301
Col. 2	-0.00145	0.00028	0.00012	0.00191	-0.00205	-0.00366
Col. 1	0.00087	-0.00113	-0.00100	0.00033	-0.00287	-0.00217

FIG. 21.3. Shear strain distribution at nominal axial strain level of 2.5431.

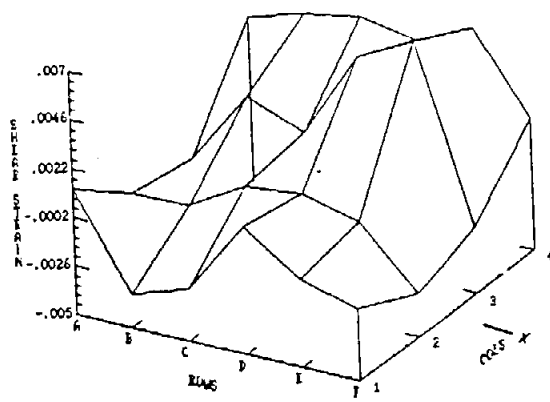
FIG. 21. Typical shear strain distribution for MD specimens, paper type A. Results are given in non-dimensional form using average parameters: STEPX= 1, STEPY= 1. Average parameters are described in item 3.6.



POSITIONAL STRAIN DATA

	ROW A	ROW B	ROW C	ROW D	ROW E	ROW F
Col. 4	0.00257	0.00390	0.00545	0.00365	0.00682	0.00261
Col. 3	-0.00288	0.00173	0.00237	0.00339	0.00554	0.00036
Col. 2	-0.00148	-0.00038	0.00152	0.00285	0.00124	-0.00075
Col. 1	-0.00030	-0.00076	-0.00264	-0.00017	0.00098	0.00057

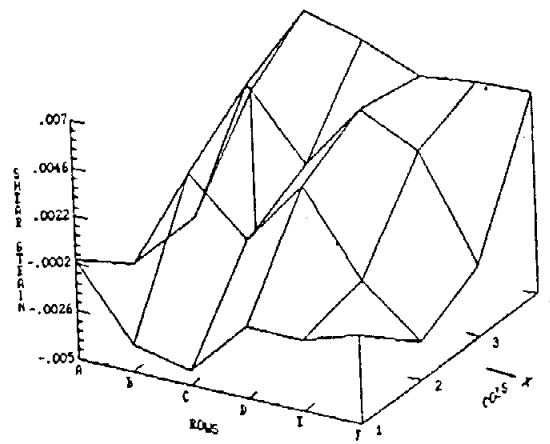
FIG. 21.4. Shear strain distribution at nominal axial strain level of 3.185%.



POSITIONAL STRAIN DATA

	ROW A	ROW B	ROW C	ROW D	ROW E	ROW F
Col. 4	0.00318	0.00399	0.00454	0.00395	0.00525	0.00148
Col. 3	-0.00160	0.00206	0.00100	0.00533	0.00673	-0.00174
Col. 2	-0.00113	-0.00113	0.00046	0.00075	0.00005	-0.00290
Col. 1	0.00122	-0.00338	-0.00245	0.00129	-0.00066	-0.00146

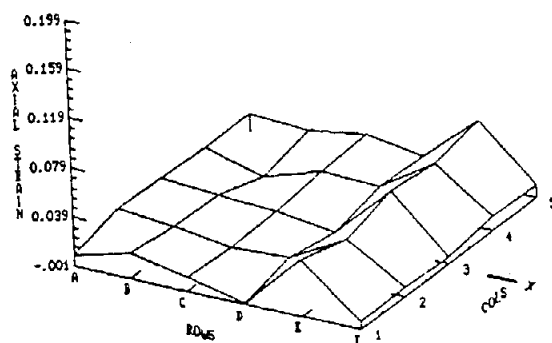
FIG. 21.5. Shear strain distribution at nominal axial strain level of 4.141%.



POSITIONAL STRAIN DATA

	ROW A	ROW B	ROW C	ROW D	ROW E	ROW F
Col. 4	0.00190	0.00653	0.00572	0.00460	0.00495	0.00509
Col. 3	-0.00222	0.00510	0.00172	0.00507	0.00371	-0.00137
Col. 2	-0.00242	0.00282	0.00013	0.00347	-0.00065	-0.00310
Col. 1	-0.00004	-0.00364	-0.00433	-0.00151	-0.00152	-0.00058

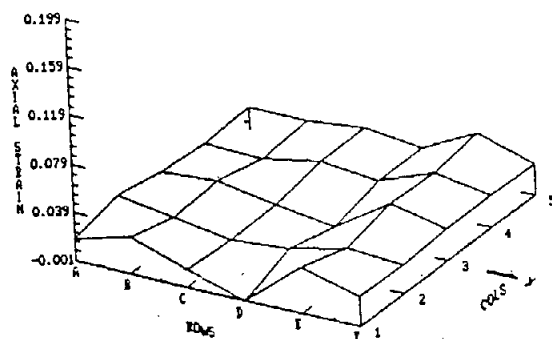
FIG. 21.6. Shear strain distribution at nominal axial strain level of 5.061%.



POSITIONAL STRAIN DATA

	ROW A	ROW B	ROW C	ROW D	ROW E	ROW F
Col. 5	0.01390	0.01016	0.01788	0.01068	0.05031	0.00906
Col. 4	0.01385	0.00839	0.01567	0.01333	0.04350	0.01019
Col. 3	0.01682	0.01352	0.01069	0.00399	0.04819	0.00435
Col. 2	0.01935	0.01538	0.00789	0.01003	0.03550	0.00636
Col. 1	0.00771	0.01967	0.01053	0.00035	0.04628	0.00553

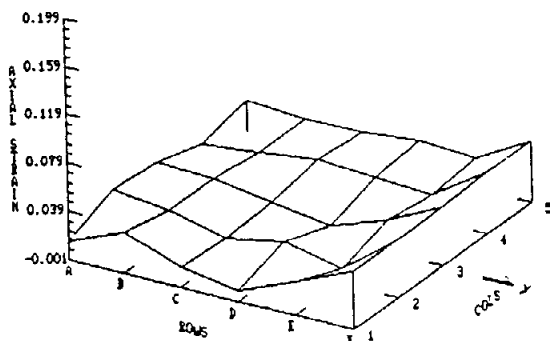
FIG. 22.1. Axial strain distribution at nominal axial strain level of 1.633%.



POSITIONAL STRAIN DATA

	ROW A	ROW B	ROW C	ROW D	ROW E	ROW F
Col. 5	0.01722	0.01768	0.02184	0.01689	0.03927	0.02433
Col. 4	0.01476	0.01376	0.02185	0.01583	0.03352	0.02548
Col. 3	0.01914	0.02295	0.01307	0.00543	0.03494	0.02457
Col. 2	0.02724	0.01903	0.01090	0.01353	0.02456	0.02243
Col. 1	0.01693	0.02879	0.01297	-0.00100	0.03683	0.02295

FIG. 22.2. Axial strain distribution at nominal axial strain level of 2.006%.

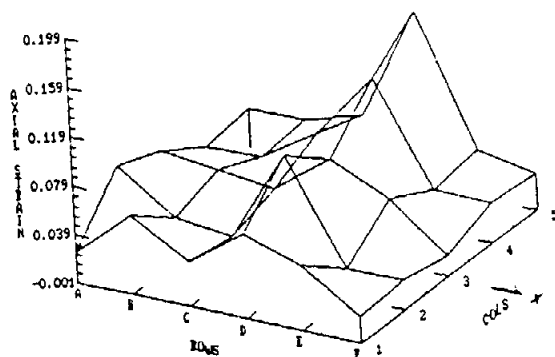


POSITIONAL STRAIN DATA

	ROW A	ROW B	ROW C	ROW D	ROW E	ROW F
Col. 5	0.02479	0.02118	0.02210	0.02651	0.02380	0.04845
Col. 4	0.01468	0.02009	0.02571	0.02246	0.01976	0.05063
Col. 3	0.02610	0.02545	0.01641	0.00857	0.02503	0.04811
Col. 2	0.03030	0.02482	0.01289	0.02202	0.01072	0.04691
Col. 1	0.01396	0.03243	0.01618	0.00714	0.02691	0.04628

FIG. 22.3. Axial strain distribution at nominal axial strain level of 2.502%.

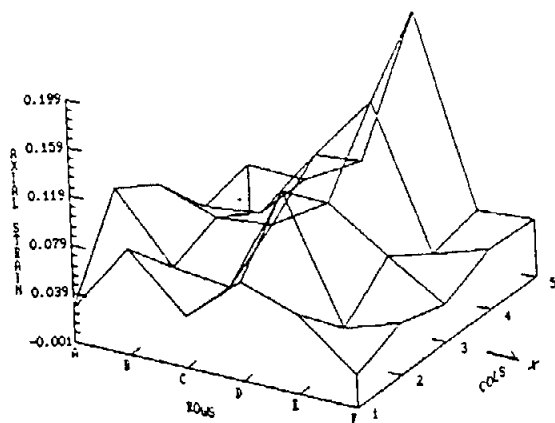
FIG. 22. Typical axial strain distribution for CD specimens, paper type A. Results are given in non-dimensional form using average parameters: STEPX= 1, STEPY= 1. Average parameters are described in item 3.6.



POSITIONAL STRAIN DATA

	ROW A	ROW B	ROW C	ROW D	ROW E	ROW F
Col. 5	0.03211	0.03209	0.04582	0.14157	0.03838	0.02860
Col. 4	0.02727	0.02984	0.05910	0.11360	0.03252	0.03177
Col. 3	0.05182	0.04667	0.04185	0.07553	0.05326	0.01575
Col. 2	0.06823	0.03533	0.03037	0.10679	0.02223	0.02337
Col. 1	0.02370	0.06495	0.03579	0.06937	0.05301	0.02068

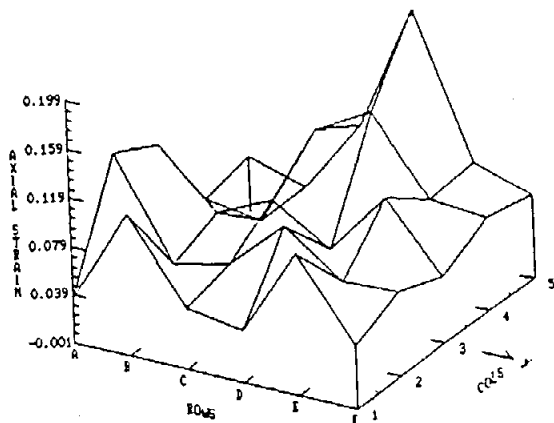
FIG. 22.4. Axial strain distribution at nominal axial strain level of 4.7432.



POSITIONAL STRAIN DATA

	ROW A	ROW B	ROW C	ROW D	ROW E	ROW F
Col. 5	0.03692	0.03480	0.06158	0.19724	0.04331	0.04608
Col. 4	0.02908	0.03517	0.09382	0.14850	0.03450	0.04908
Col. 3	0.07349	0.05882	0.06290	0.09158	0.05923	0.03026
Col. 2	0.09789	0.04471	0.03844	0.12772	0.02682	0.04119
Col. 1	0.02622	0.08680	0.04168	0.08009	0.06477	0.02664

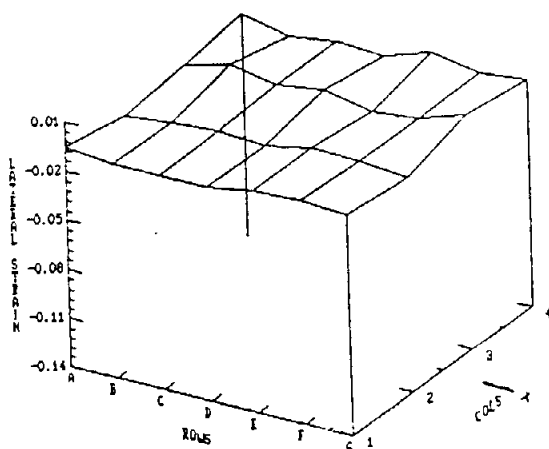
FIG. 22.5. Axial strain distribution at nominal axial strain level of 6.2661.



POSITIONAL STRAIN DATA

	ROW A	ROW B	ROW C	ROW D	ROW E	ROW F
Col. 5	0.04620	0.03122	0.09301	0.19837	0.08437	0.06842
Col. 4	0.03655	0.03025	0.11527	0.14131	0.08024	0.07559
Col. 3	0.10895	0.06376	0.08513	0.05526	0.10875	0.05377
Col. 2	0.12882	0.04845	0.05890	0.10109	0.06659	0.06778
Col. 1	0.03530	0.11596	0.04866	0.04116	0.11660	0.05101

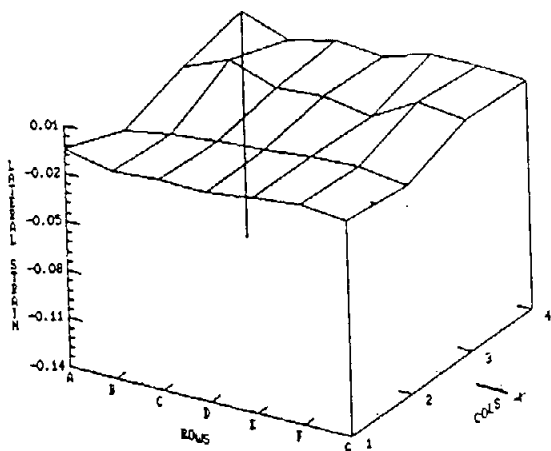
FIG. 22.6. Axial strain distribution at nominal axial strain level of 7.9402.



POSITIONAL STRAIN DATA

	ROW A	ROW B	ROW C	ROW D	ROW E	ROW F	ROW G
Col. 4	-0.00348	-0.01001	-0.00585	-0.00805	0.00197	-0.00328	-0.00111
Col. 3	-0.00844	-0.00028	-0.00645	-0.00193	-0.00832	-0.00604	0.00358
Col. 2	-0.01357	-0.01069	-0.00822	-0.00971	-0.00450	-0.00482	-0.00798
Col. 1	-0.00572	-0.00871	-0.00852	-0.00852	-0.00353	-0.00243	-0.00399

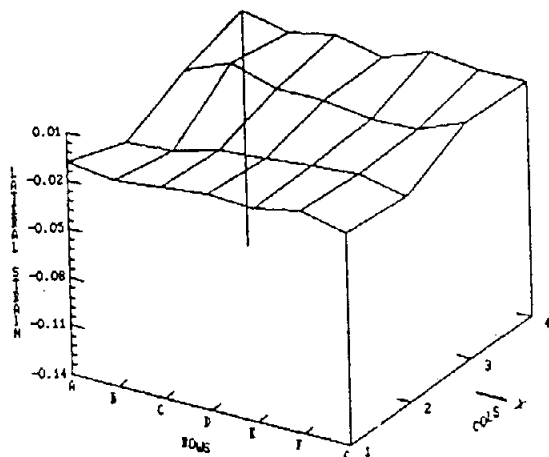
FIG. 23.1. Lateral strain distribution at nominal axial strain level of 1.633%.



POSITIONAL STRAIN DATA

	ROW A	ROW B	ROW C	ROW D	ROW E	ROW F	ROW G
Col. 4	0.00151	-0.00833	-0.00165	-0.00430	0.00425	0.00394	0.00261
Col. 3	-0.00643	0.00566	-0.00548	-0.00337	-0.00884	-0.00769	0.00415
Col. 2	-0.01961	-0.01546	-0.01248	-0.01040	-0.00754	-0.00644	-0.01077
Col. 1	-0.00472	-0.01175	-0.00933	-0.01022	-0.00678	-0.00340	-0.00658

FIG. 23.2. Lateral strain distribution at nominal axial strain level of 2.0087%.

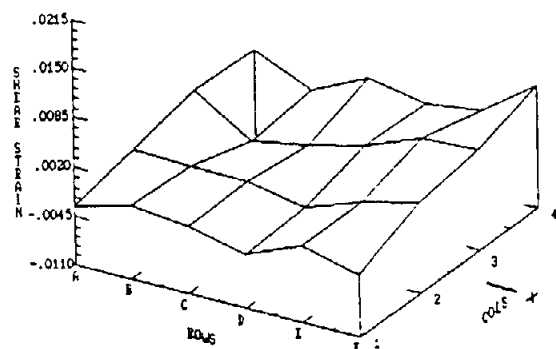


POSITIONAL STRAIN DATA

	ROW A	ROW B	ROW C	ROW D	ROW E	ROW F	ROW G
Col. 4	0.00651	-0.00022	0.00536	-0.00057	0.00990	0.00589	0.00591
Col. 3	-0.00477	-0.00743	-0.00162	-0.00108	-0.00567	-0.00528	0.00721
Col. 2	-0.02255	-0.02079	-0.01318	-0.01098	-0.00761	-0.00640	-0.01297
Col. 1	-0.00863	-0.01233	-0.00929	-0.00686	-0.00800	-0.00263	-0.00902

FIG. 23.3. Lateral strain distribution at nominal axial strain level of 2.50%.

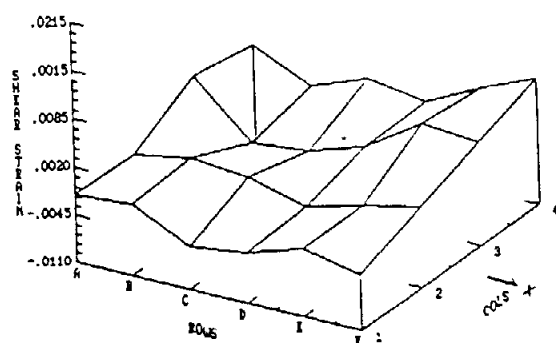
FIG. 23. Typical lateral strain distribution for CD specimens, paper type A. Results are given in non-dimensional form using average parameters: STEPX= 1, STEPY= 1. Average parameters are described in item 3.6.



POSITIONAL STRAIN DATA

	ROW A	ROW B	ROW C	ROW D	ROW E	ROW F
Col. 4	0.00032	-0.00297	0.00051	-0.00110	-0.00012	0.00503
Col. 3	0.00078	-0.00420	-0.00284	-0.00095	0.00183	0.00234
Col. 2	-0.00144	-0.00176	-0.00183	-0.00335	-0.00067	0.00124
Col. 1	-0.00307	-0.00105	-0.00204	-0.00393	-0.00094	-0.00290

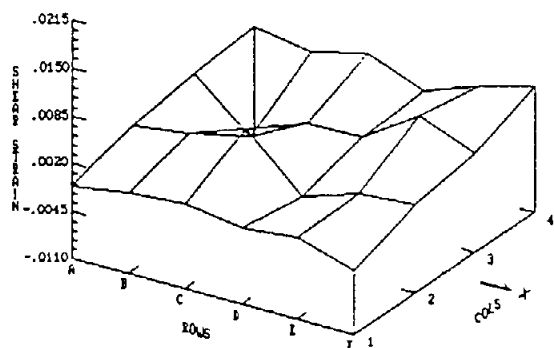
FIG. 24.1. Shear strain distribution at nominal axial strain level of 1.633%.



POSITIONAL STRAIN DATA

	ROW A	ROW B	ROW C	ROW D	ROW E	ROW F
Col. 4	0.00111	-0.00246	0.00040	-0.00090	0.00273	0.00588
Col. 3	0.00271	-0.00438	-0.00358	-0.00110	0.00369	0.00319
Col. 2	-0.00206	-0.00064	-0.00129	-0.00345	-0.00144	0.00015
Col. 1	-0.00181	-0.00116	-0.00522	-0.00412	-0.00175	-0.00357

FIG. 24.2. Shear strain distribution at nominal axial strain level of 2.008%.

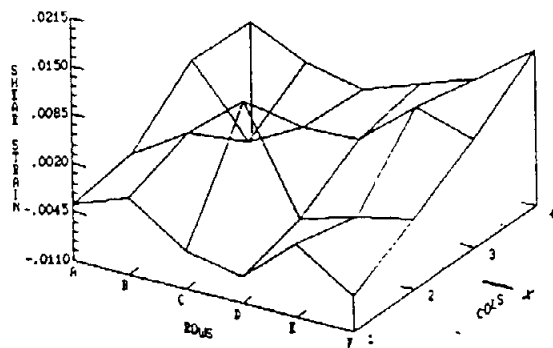


POSITIONAL STRAIN DATA

	ROW A	ROW B	ROW C	ROW D	ROW E	ROW F
Col. 4	0.00390	0.00266	0.00436	0.00147	0.00397	0.00603
Col. 3	0.00311	-0.00326	0.00056	0.00074	0.00571	0.00252
Col. 2	0.00162	0.00259	0.00535	-0.00179	0.00064	0.00110
Col. 1	-0.00101	0.00007	0.00059	-0.00059	0.00011	-0.00237

FIG. 24.3. Shear strain distribution at nominal axial strain level of 2.500%.

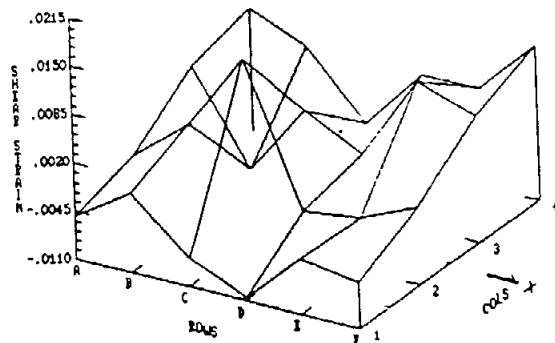
FIG. 24. Typical shear strain distribution for CD specimens, paper type A. Results are given in non-dimensional form using average parameters: STEPX= 1, STEPY= 1. Average parameters are described in item 3.6.



POSITIONAL STRAIN DATA

	ROW A	ROW B	ROW C	ROW D	ROW E	ROW F
Col. 4	0.00392	0.00047	-0.00127	0.00149	0.00397	0.00983
Col. 3	0.00448	-0.00465	-0.00065	-0.00029	0.00590	0.00342
Col. 2	-0.00257	0.00223	0.00846	-0.00545	-0.00322	-0.00151
Col. 1	-0.00360	-0.00070	-0.00597	-0.00754	-0.00121	-0.00625

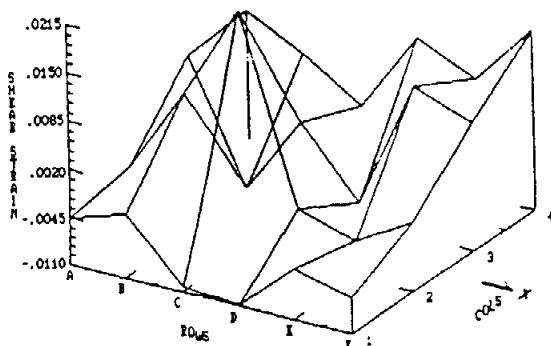
FIG. 24.4. Shear strain distribution at nominal axial strain level of 4.743%.



POSITIONAL STRAIN DATA

	ROW A	ROW B	ROW C	ROW D	ROW E	ROW F
Col. 4	0.00562	0.00214	-0.00614	0.00200	0.00212	0.00961
Col. 3	0.00340	-0.00851	0.00130	-0.00278	0.00869	0.00602
Col. 2	-0.00287	0.00339	0.01391	-0.00475	-0.00380	-0.00057
Col. 1	-0.00524	-0.00039	-0.00725	-0.01059	-0.00366	-0.00490

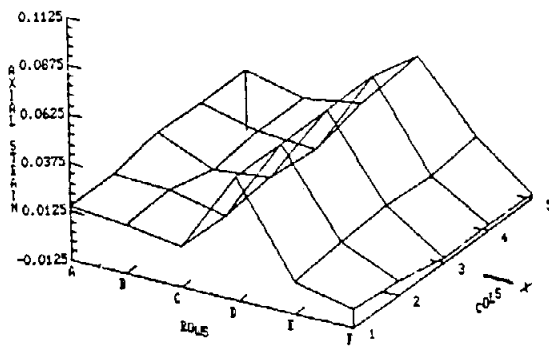
FIG. 24. Shear strain distribution at nominal axial strain level of 6.266%.



POSITIONAL STRAIN DATA

	ROW A	ROW B	ROW C	ROW D	ROW E	ROW F
Col. 4	0.00607	0.00240	-0.00264	0.00820	0.00477	0.01290
Col. 3	0.00593	-0.00988	-0.00074	-0.00824	0.00943	0.00641
Col. 2	-0.00355	0.00843	0.02138	-0.00326	-0.00590	-0.00143
Col. 1	-0.00459	-0.00225	-0.01036	-0.01092	-0.00408	-0.00609

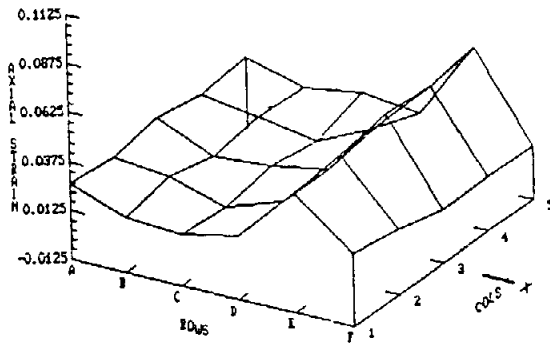
FIG. 24.6. Shear strain distribution at nominal axial strain level of 7.940%.



POSITIONAL STRAIN DATA

	ROW A	ROW B	ROW C	ROW D	ROW E	ROW F
Col. 5	0.01868	0.01059	0.01577	0.04633	0.01246	-0.01050
Col. 4	0.01828	0.01094	0.00834	0.05306	0.00847	-0.00901
Col. 3	0.01997	0.00767	0.01058	0.05241	0.01043	-0.01043
Col. 2	0.01490	0.01444	0.00788	0.05133	0.00782	-0.00559
Col. 1	0.01519	0.01299	0.00861	0.05135	0.00399	-0.00272

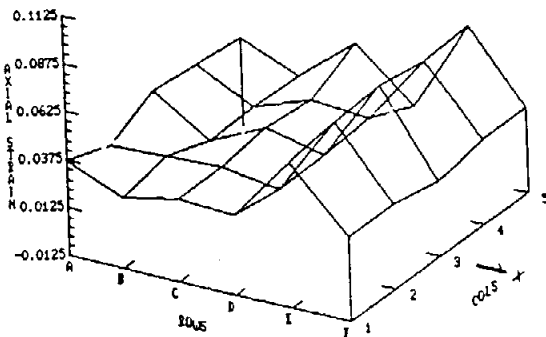
FIG. 25.1. Axial strain distribution at nominal axial strain level of 1.499%.



POSITIONAL STRAIN DATA

	ROW A	ROW B	ROW C	ROW D	ROW E	ROW F
Col. 5	0.02406	0.01554	0.02032	0.01685	0.05753	0.01493
Col. 4	0.02151	0.01748	0.01199	0.02573	0.05453	0.01581
Col. 3	0.02627	0.01410	0.01598	0.02203	0.05684	0.01517
Col. 2	0.02354	0.02084	0.01140	0.02135	0.05276	0.02131
Col. 1	0.02664	0.01549	0.01359	0.02033	0.04963	0.02536

FIG. 25.2. Axial strain distribution at nominal axial strain level of 2.510%.

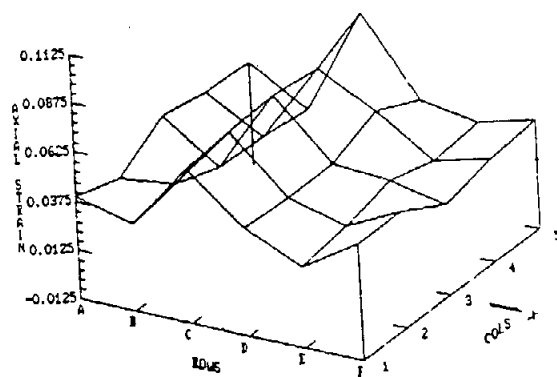


POSITIONAL STRAIN DATA

	ROW A	ROW B	ROW C	ROW D	ROW E	ROW F
Col. 5	0.03312	0.02055	0.04439	0.01833	0.06715	0.03171
Col. 4	0.03651	0.02121	0.03169	0.02846	0.06531	0.03139
Col. 3	0.03959	0.02018	0.03357	0.02652	0.06937	0.02681
Col. 2	0.02825	0.02923	0.03109	0.02606	0.06714	0.03141
Col. 1	0.03701	0.02478	0.03082	0.02872	0.06325	0.03121

FIG. 25.3. Axial strain distribution at nominal axial strain level of 3.604%.

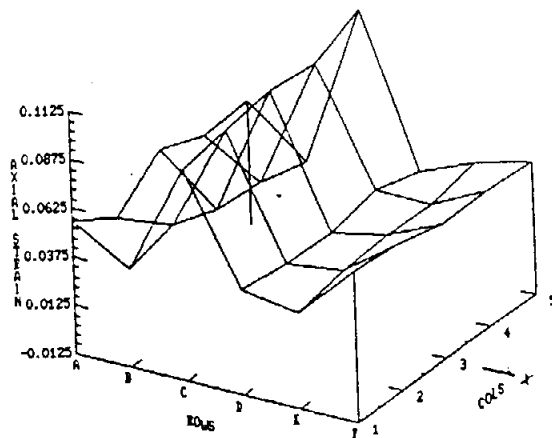
FIG. 25. Typical axial strain distribution for KD specimens, paper type B. Results are given in non-dimensional form using average parameters: STEPX= 1, STEPY= 1. Average parameters are described in ites 3.6.



POSITIONAL STRAIN DATA

	ROW A	ROW B	ROW C	ROW D	ROW E	ROW F
Col. 5	0.04003	0.02223	0.07857	0.04021	0.03512	0.04237
Col. 4	0.04131	0.02504	0.06701	0.05097	0.03225	0.04014
Col. 3	0.04626	0.02711	0.06968	0.04136	0.03994	0.03719
Col. 2	0.03167	0.03603	0.06847	0.04161	0.03350	0.04774
Col. 1	0.04039	0.03228	0.06649	0.04311	0.02951	0.04764

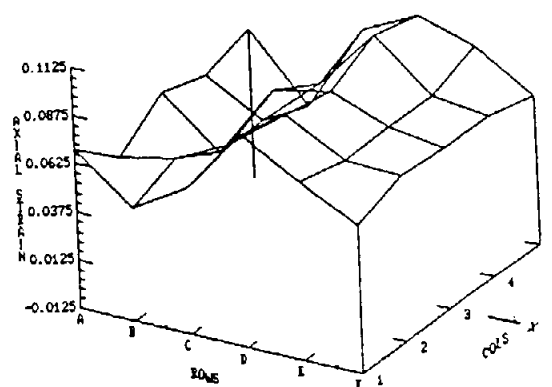
FIG. 25.4. Axial strain distribution at nominal axial strain level of 4.35%.



POSITIONAL STRAIN DATA

	ROW A	ROW B	ROW C	ROW D	ROW E	ROW F
Col. 5	0.05122	0.02715	0.11248	0.03628	0.04750	0.05545
Col. 4	0.04917	0.03324	0.10135	0.04313	0.04302	0.05731
Col. 3	0.05907	0.03554	0.10328	0.03786	0.04384	0.05608
Col. 2	0.04058	0.04428	0.09949	0.03878	0.04259	0.06254
Col. 1	0.05624	0.03815	0.09630	0.04167	0.03656	0.06528

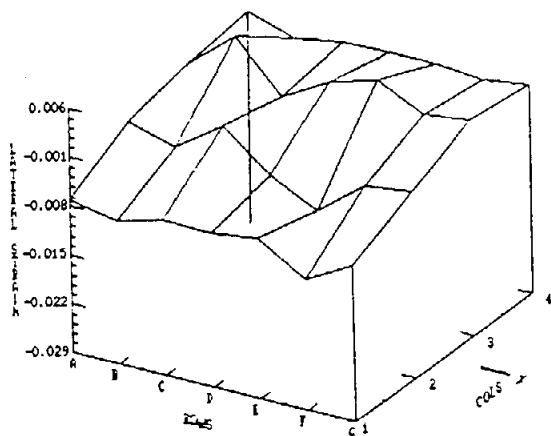
FIG. 25.5. Axial strain distribution at nominal axial strain level of 5.583%.



POSITIONAL STRAIN DATA

	ROW A	ROW B	ROW C	ROW D	ROW E	ROW F
Col. 5	0.06447	0.03168	0.07820	0.09204	0.08332	0.06459
Col. 4	0.05751	0.04104	0.06702	0.09816	0.07417	0.07058
Col. 3	0.06523	0.04150	0.08012	0.08692	0.07520	0.07047
Col. 2	0.04872	0.05537	0.06886	0.09177	0.07451	0.07331
Col. 1	0.06949	0.04625	0.06357	0.09779	0.07985	0.06447

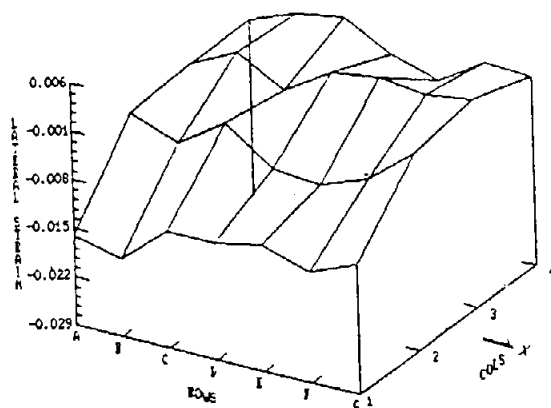
FIG. 25.6. Axial strain distribution at nominal axial strain level of 6.937%.



POSITIONAL STRAIN DATA

	ROW A	ROW B	ROW C	ROW D	ROW E	ROW F	ROW G
Col. 4	0.00165	-0.00062	0.00051	0.00081	0.00077	0.00014	0.00114
Col. 3	0.00012	0.00583	-0.00138	0.00254	0.00458	0.00115	0.00202
Col. 2	-0.00215	-0.00414	0.00062	-0.00471	-0.00817	-0.00287	-0.00192
Col. 1	-0.00718	-0.00845	-0.00665	-0.00684	-0.00588	-0.01012	-0.00658

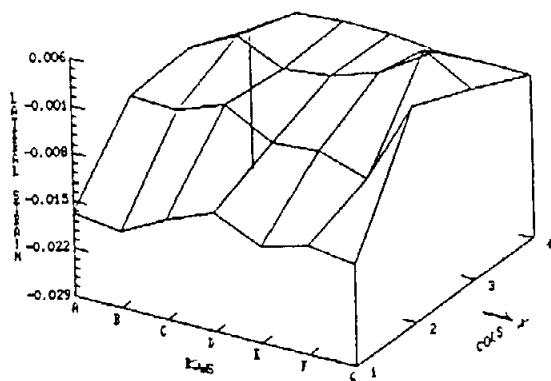
FIG. 26.1. Lateral strain distribution at nominal axial strain level of 1.499%.



POSITIONAL STRAIN DATA

	ROW A	ROW B	ROW C	ROW D	ROW E	ROW F	ROW G
Col. 4	-0.00328	-0.00086	0.00027	-0.00360	-0.00581	-0.00135	-0.00197
Col. 3	-0.00365	-0.00026	-0.00429	0.00012	0.00103	0.00013	0.00088
Col. 2	-0.00455	-0.00732	-0.00268	-0.00775	-0.00840	-0.00585	-0.00051
Col. 1	-0.01612	-0.01776	-0.01230	-0.01216	-0.01084	-0.01312	-0.01039

FIG. 26.2. Lateral strain distribution at nominal axial strain level of 2.510%.

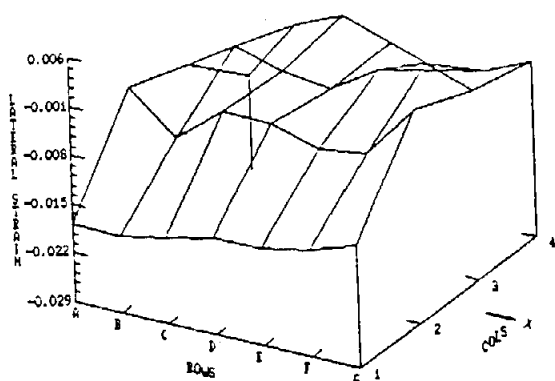


POSITIONAL STRAIN DATA

	ROW A	ROW B	ROW C	ROW D	ROW E	ROW F	ROW G
Col. 4	-0.00847	-0.00444	-0.00391	-0.00414	-0.00506	-0.00509	-0.00521
Col. 3	-0.00503	-0.00150	-0.00478	-0.00404	-0.00190	0.00292	-0.00112
Col. 2	-0.00570	-0.00606	-0.00355	-0.00761	-0.00722	-0.00960	0.00281
Col. 1	-0.01676	-0.01787	-0.01457	-0.01178	-0.01521	-0.01327	-0.01444

FIG. 26.3. Lateral strain distribution at nominal axial strain level of 3.604%.

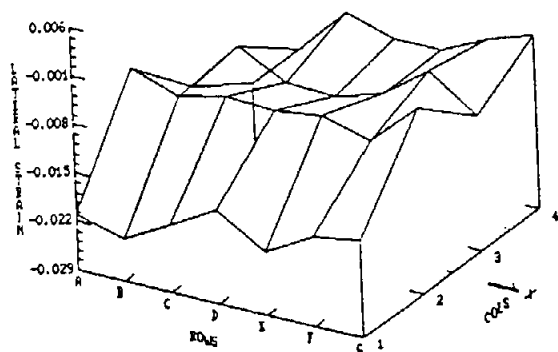
FIG. 26. Typical lateral strain distribution for MD specimens, paper type B. Results are given in non-dimensional form using average parameters: STEPX= 1, STEPY= 1. Average parameters are described in item 3.6.



POSITIONAL STRAIN DATA

	ROW A	ROW B	ROW C	ROW D	ROW E	ROW F	ROW G
Col. 4	-0.01538	-0.00651	-0.00362	-0.00593	-0.00842	-0.00675	-0.00391
Col. 3	-0.00769	-0.00343	-0.00545	-0.00617	-0.00197	0.00051	-0.00173
Col. 2	-0.00457	-0.01027	-0.00480	-0.00507	-0.00689	-0.00596	0.00188
Col. 1	-0.01777	-0.01813	-0.01668	-0.01512	-0.01521	-0.01371	-0.01137

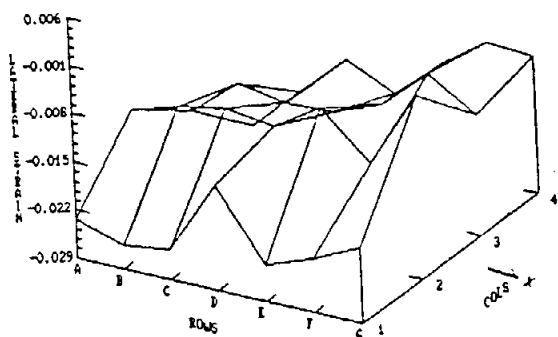
FIG. 26.4. Lateral strain distribution at nominal axial strain level of 4.35%.



POSITIONAL STRAIN DATA

	ROW A	ROW B	ROW C	ROW D	ROW E	ROW F	ROW G
Col. 4	-0.02088	-0.01432	-0.00731	-0.00959	-0.00950	-0.00645	-0.00422
Col. 3	-0.01515	-0.00759	-0.01122	-0.01166	-0.00964	-0.00470	-0.00965
Col. 2	-0.00608	-0.00860	-0.00696	-0.00747	-0.00655	-0.00859	-0.00211
Col. 1	-0.02112	-0.02307	-0.01934	-0.01562	-0.01993	-0.01615	-0.01517

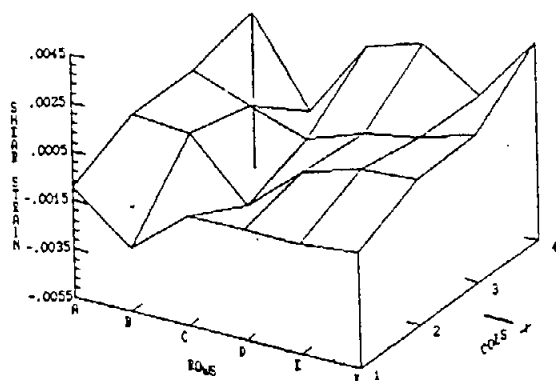
FIG. 26.5. Lateral strain distribution at nominal axial strain level of 5.583%.



POSITIONAL STRAIN DATA

	ROW A	ROW B	ROW C	ROW D	ROW E	ROW F	ROW G
Col. 4	-0.02871	-0.02206	-0.01586	-0.01909	-0.01334	-0.00868	-0.00915
Col. 3	-0.02031	-0.01457	-0.01591	-0.01561	-0.01292	-0.00683	-0.01114
Col. 2	-0.01368	-0.01180	-0.01042	-0.01139	-0.00725	-0.01363	-0.00215
Col. 1	-0.02342	-0.02571	-0.02482	-0.01383	-0.02380	-0.02128	-0.01816

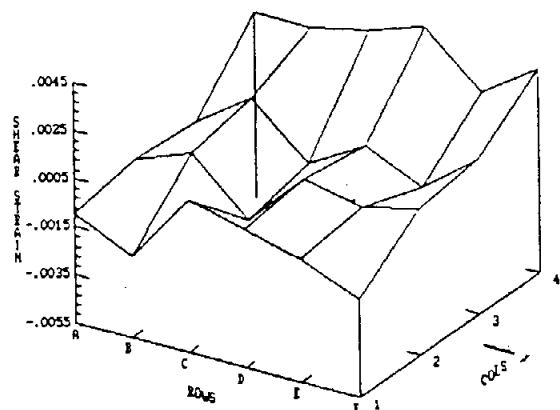
FIG. 26.6. Lateral strain distribution at nominal axial strain level of 6.987%.



POSITIONAL STRAIN DATA

	ROW A	ROW B	ROW C	ROW D	ROW E	ROW F
Col. 4	0.00101	-0.00255	0.00070	0.00140	-0.00018	0.00262
Col. 3	0.00026	-0.00060	-0.00137	-0.00055	-0.00009	0.00058
Col. 2	0.00027	0.00005	-0.00231	-0.00040	0.00031	0.00051
Col. 1	-0.00097	-0.00292	-0.00101	-0.00095	-0.00096	-0.00076

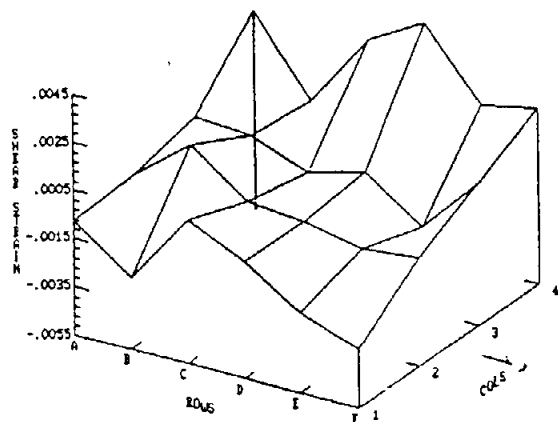
FIG. 27.1. Shear strain distribution at nominal axial strain level of 1.499%.



POSITIONAL STRAIN DATA

	ROW A	ROW B	ROW C	ROW D	ROW E	ROW F
Col. 4	0.00217	0.00216	0.00266	0.00338	0.00129	0.00292
Col. 3	-0.00063	0.00094	-0.00113	0.00021	-0.00086	0.00086
Col. 2	-0.00046	0.00042	-0.00178	0.00061	0.00000	0.00054
Col. 1	-0.00098	-0.00217	0.00081	0.00017	-0.00039	-0.00148

FIG. 27.2. Shear strain distribution at nominal axial strain level of 2.510%.

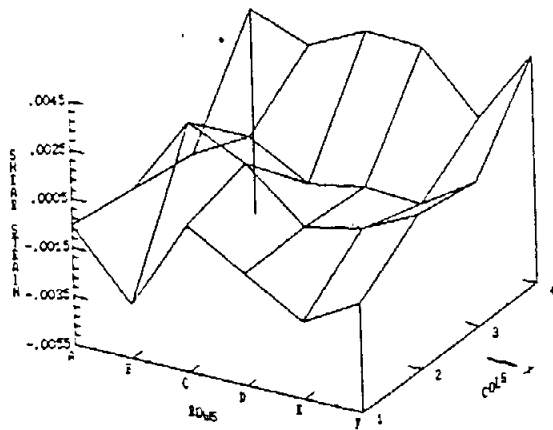


POSITIONAL STRAIN DATA

	ROW A	ROW B	ROW C	ROW D	ROW E	ROW F
Col. 4	0.00283	-0.00035	0.00280	0.00415	0.00131	0.00178
Col. 3	0.00010	-0.00005	-0.00097	-0.00033	-0.00205	0.00038
Col. 2	-0.00060	0.00128	-0.00050	-0.00069	-0.00120	-0.00096
Col. 1	-0.00081	-0.00252	0.00043	-0.00067	-0.00211	-0.00306

FIG. 27.3. Shear strain distribution at nominal axial strain level of 3.604%.

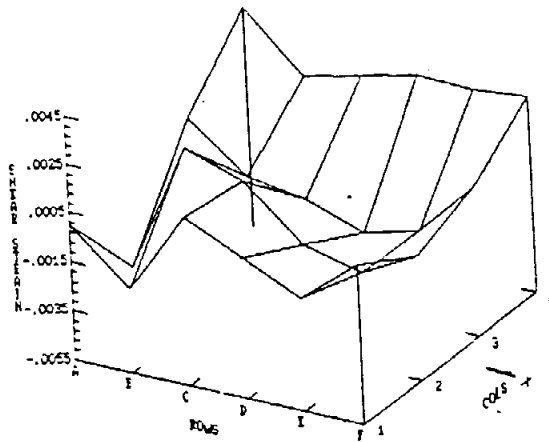
FIG. 27. Typical shear strain distribution for M0 specimens, paper type B. Results are given in non-dimensional form using average parameters: STEPX= 1, STEPY= 1. Average parameters are described in item 3.6.



POSITIONAL STRAIN DATA

	ROW A	ROW B	ROW C	ROW D	ROW E	ROW F
Col. 4	0.00298	0.00204	0.00318	0.00313	0.00073	0.00385
Col. 3	-0.00121	0.00007	-0.00131	-0.00086	-0.00104	0.00046
Col. 2	-0.00089	0.00241	0.00134	-0.00075	-0.00028	0.00086
Col. 1	-0.00058	-0.00330	0.00055	-0.00089	-0.00232	-0.00103

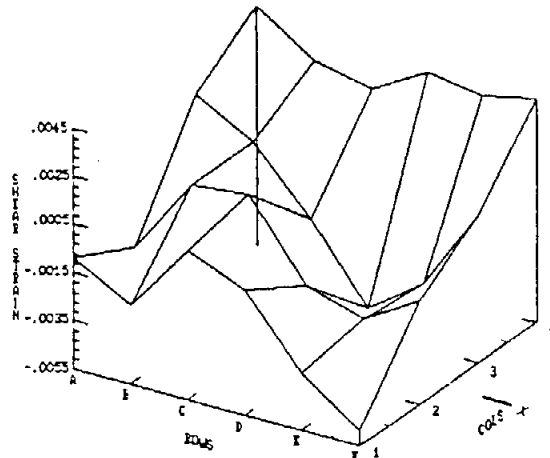
FIG. 27.4. Shear strain distribution at nominal axial strain level of 4.35%.



POSITIONAL STRAIN DATA

	ROW A	ROW B	ROW C	ROW D	ROW E	ROW F
Col. 4	0.00357	0.00123	0.00178	0.00235	0.00224	0.00248
Col. 3	0.00077	-0.00107	-0.00150	-0.00233	-0.00175	0.00058
Col. 2	-0.00353	0.00192	0.00104	-0.00100	-0.00164	-0.00039
Col. 1	0.00000	-0.00206	0.00135	0.00027	-0.00083	0.00106

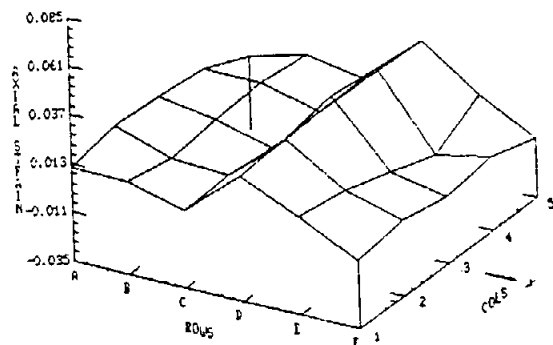
FIG. 27.5. Shear strain distribution at nominal axial strain level of 5.563%.



POSITIONAL STRAIN DATA

	ROW A	ROW B	ROW C	ROW D	ROW E	ROW F
Col. 4	0.00449	0.00285	0.00229	0.00361	0.00327	0.00382
Col. 3	0.00250	0.00118	-0.00144	-0.00444	-0.00283	0.00065
Col. 2	-0.00215	0.00110	0.00133	-0.00184	-0.00258	-0.00116
Col. 1	-0.00092	-0.00219	0.00063	-0.00032	-0.00317	-0.00486

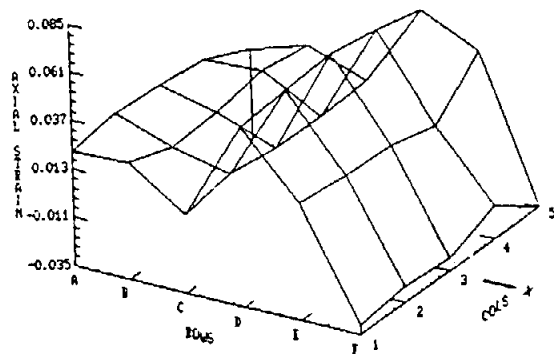
FIG. 27.6. Shear strain distribution at nominal axial strain level of 6.937%.



POSITIONAL STRAIN DATA

	ROW A	ROW B	ROW C	ROW D	ROW E	ROW F	
Col. 5	0.00162	0.00885	0.00305	0.02908	0.00887	-0.00576	2
Col. 4	0.01153	0.01160	0.00338	0.03198	-0.00448	0.00144	4
Col. 3	0.01396	0.00866	0.00114	0.03367	0.00262	-0.00275	3
Col. 2	0.01532	0.00619	0.00423	0.02894	0.00978	0.00181	1
Col. 1	0.01060	0.01052	0.00295	0.02593	0.01282	-0.00199	1

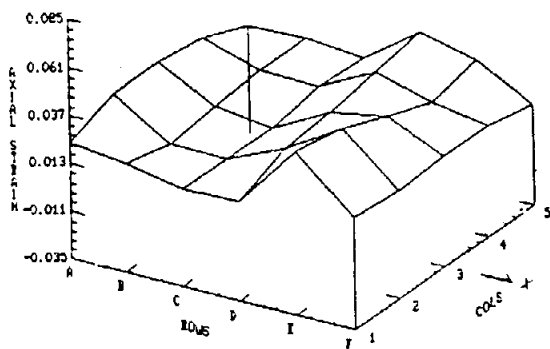
FIG. 28.1. Axial strain distribution at nominal axial strain level of 0.936%.



POSITIONAL STRAIN DATA

	ROW A	ROW B	ROW C	ROW D	ROW E	ROW F	
Col. 5	0.00811	0.01773	0.00639	0.04877	0.03507	-0.03476	
Col. 4	0.01885	0.02031	0.00499	0.05472	0.01371	-0.01920	
Col. 3	0.02256	0.01619	0.00483	0.05839	0.02010	-0.02857	
Col. 2	0.02469	0.01440	0.00792	0.05647	0.02067	-0.02729	
Col. 1	0.02125	0.02281	0.00322	0.05370	0.02328	-0.03017	

FIG. 28.2. Axial strain distribution at nominal axial strain level of 1.539%.

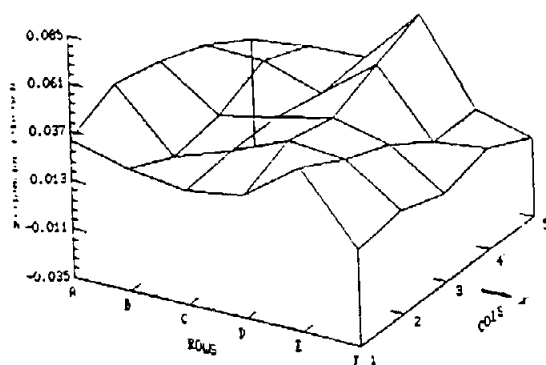


POSITIONAL STRAIN DATA

	ROW A	ROW B	ROW C	ROW D	ROW E	ROW F	
Col. 5	0.01834	0.01934	0.01680	0.03712	0.03090	0.01601	
Col. 4	0.02817	0.02004	0.01904	0.03277	0.02516	0.02048	
Col. 3	0.03259	0.01752	0.01362	0.02871	0.03390	0.02025	
Col. 2	0.03250	0.01347	0.01372	0.02574	0.04314	0.01885	
Col. 1	0.02342	0.02019	0.01413	0.01501	0.04716	0.02115	

FIG. 28.3. Axial strain distribution at nominal axial strain level of 2.362%.

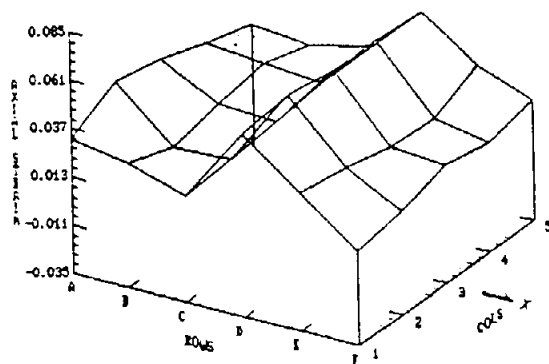
FIG. 28. Typical axial strain distribution for CD specimens, paper type B. Results are given in non-dimensional form using average parameters: STEPX= 1, STEPY= 1. Average parameters are described in item 3.6.



POSITIONAL STRAIN DATA

	ROW A	ROW B	ROW C	ROW D	ROW E	ROW F
Col. 5	0.01935	0.02267	0.02415	0.05251	0.01153	0.00442
Col. 4	0.03221	0.03112	0.02197	0.04309	0.01163	0.01464
Col. 3	0.04003	0.01960	0.02601	0.03221	0.02579	0.00839
Col. 2	0.04494	0.01497	0.02494	0.03694	0.03414	0.01554
Col. 1	0.03320	0.02552	0.02087	0.02521	0.04589	0.01303

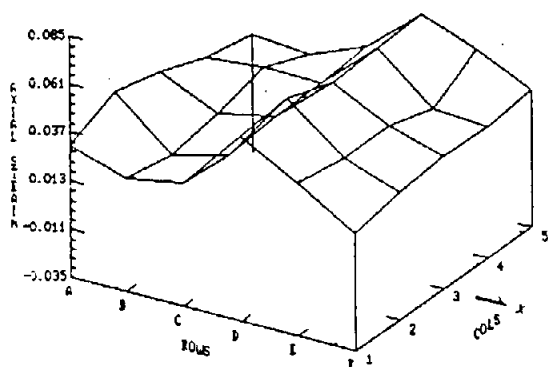
FIG. 28.4. Axial strain distribution at nominal axial strain level of 2.812%.



POSITIONAL STRAIN DATA

	ROW A	ROW B	ROW C	ROW D	ROW E	ROW F
Col. 5	0.02588	0.02263	0.02917	0.05422	0.03438	0.02405
Col. 4	0.03203	0.02977	0.02728	0.05353	0.02339	0.01882
Col. 3	0.03980	0.02483	0.02303	0.05652	0.02558	0.02335
Col. 2	0.04429	0.01896	0.02042	0.05969	0.03086	0.01672
Col. 1	0.03174	0.02688	0.01843	0.05535	0.03377	0.01213

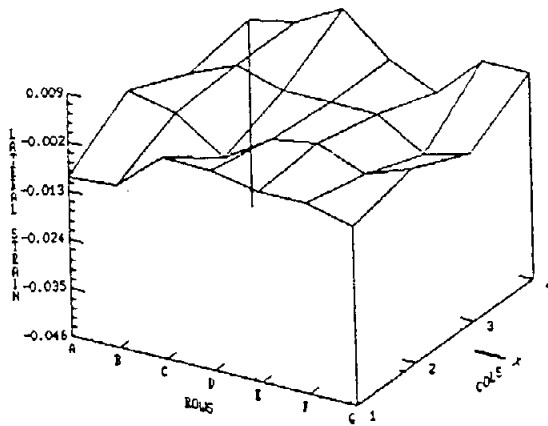
FIG. 28.5. Shear strain distribution at nominal axial strain level of 3.190%.



POSITIONAL STRAIN DATA

	ROW A	ROW B	ROW C	ROW D	ROW E	ROW F
Col. 5	0.02388	0.02128	0.03257	0.05623	0.04567	0.03342
Col. 4	0.02767	0.03023	0.03055	0.05481	0.03226	0.03003
Col. 3	0.03635	0.02251	0.02872	0.05320	0.03894	0.03126
Col. 2	0.04143	0.01771	0.02500	0.06086	0.03861	0.02890
Col. 1	0.02988	0.02166	0.02675	0.05723	0.04171	0.02351

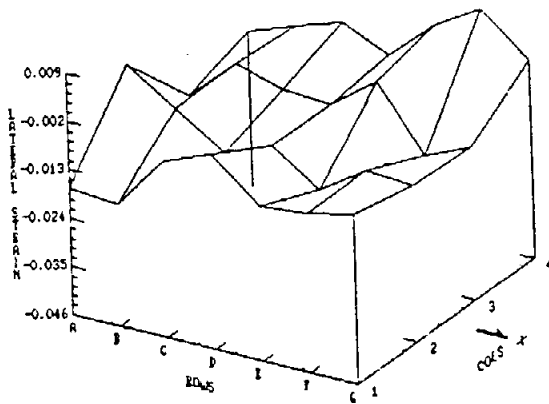
FIG. 28.6. Axial strain distribution at nominal axial strain level of 3.510%.



POSITIONAL STRAIN DATA

	ROW A	ROW B	ROW C	ROW D	ROW E	ROW F	ROW G
Col. 4	-0.00345	-0.00157	0.00409	-0.00434	-0.00927	0.00042	0.00061
Col. 3	-0.00607	-0.00137	-0.00452	-0.00468	-0.00441	-0.01081	-0.00821
Col. 2	-0.00025	-0.00265	-0.01004	-0.00327	-0.00145	-0.00571	-0.00167
Col. 1	-0.00986	-0.00923	-0.00031	-0.00066	-0.00266	-0.00264	-0.00554

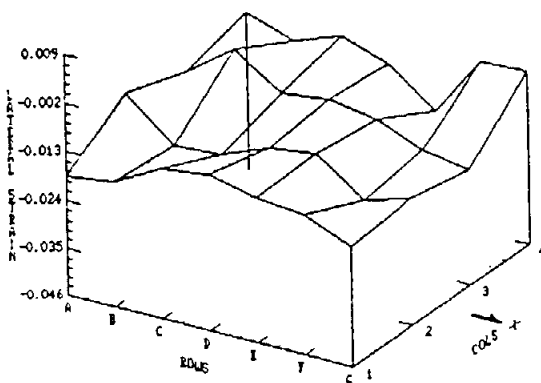
FIG. 29.1. Lateral strain distribution at nominal axial strain level of 0.936%.



POSITIONAL STRAIN DATA

	ROW A	ROW B	ROW C	ROW D	ROW E	ROW F	ROW G
Col. 4	-0.01074	-0.00663	-0.00309	-0.00817	0.00135	0.00778	-0.00121
Col. 3	-0.01565	-0.00571	-0.00904	-0.00938	-0.00176	-0.01582	-0.01128
Col. 2	0.00134	-0.00619	-0.01365	-0.00945	-0.01681	-0.00949	-0.01031
Col. 1	-0.01740	-0.01813	-0.00577	-0.00149	-0.01082	-0.00976	-0.00705

FIG. 29.2. Lateral strain distribution at nominal axial strain level of 1.539%.



POSITIONAL STRAIN DATA

	ROW A	ROW B	ROW C	ROW D	ROW E	ROW F	ROW G
Col. 4	-0.01030	-0.01396	-0.01011	-0.01362	-0.02152	-0.00759	-0.00690
Col. 3	-0.01438	-0.00643	-0.01341	-0.01198	-0.01380	-0.01784	-0.01977
Col. 2	-0.00948	-0.01846	-0.01773	-0.01364	-0.01209	-0.01973	-0.01667
Col. 1	-0.01855	-0.01708	-0.01151	-0.00996	-0.01262	-0.01358	-0.01817

FIG. 29.3. Lateral strain distribution at nominal axial strain level of 2.347%.

FIG. 29. Typical lateral strain distribution for CD specimens, paper type B. Results are given in non-dimensional form using average parameters: STEPX= 1, STEPY= 1. Average parameters are described in item 3.6.

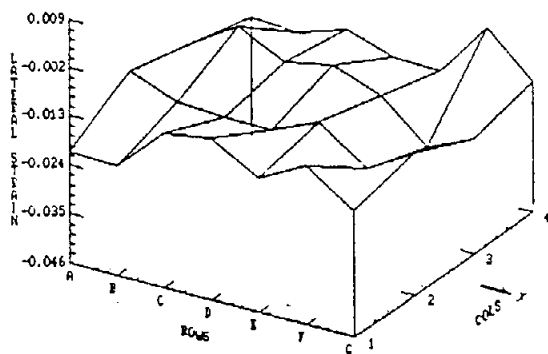


FIG. 29.4. Lateral strain distribution at nominal axial strain level of 2.812%.

POSITIONAL STRAIN DATA

	ROW A	ROW B	ROW C	ROW D	ROW E	ROW F	ROW G
Col. 4	-0.01864	-0.01934	-0.01579	-0.01932	-0.01966	-0.00692	-0.01654
Col. 3	-0.01542	-0.00853	-0.01392	-0.01159	-0.01598	-0.02458	-0.02015
Col. 2	-0.01228	-0.01645	-0.01694	-0.01719	-0.01249	-0.02006	-0.01393
Col. 1	-0.02099	-0.02153	-0.01116	-0.00928	-0.01582	-0.01002	-0.01751

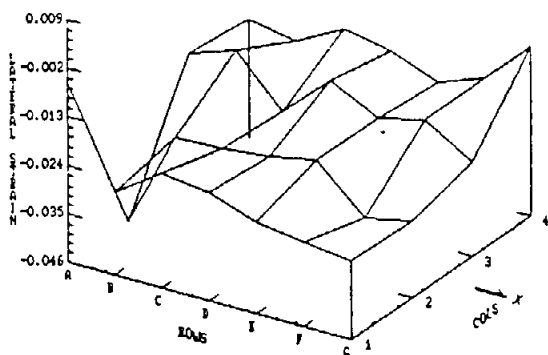


FIG. 29.5. Lateral strain distribution at nominal axial strain level of 3.190%.

POSITIONAL STRAIN DATA

	ROW A	ROW B	ROW C	ROW D	ROW E	ROW F	ROW G
Col. 4	-0.01904	-0.02119	-0.01564	-0.01744	-0.02183	-0.01784	-0.00791
Col. 3	-0.01731	-0.01369	-0.02466	-0.01483	-0.02048	-0.01779	-0.02478
Col. 2	-0.04599	-0.02405	-0.02365	-0.02260	-0.02058	-0.03062	-0.02851
Col. 1	-0.00510	-0.02706	-0.01990	-0.02140	-0.02527	-0.02706	-0.02836

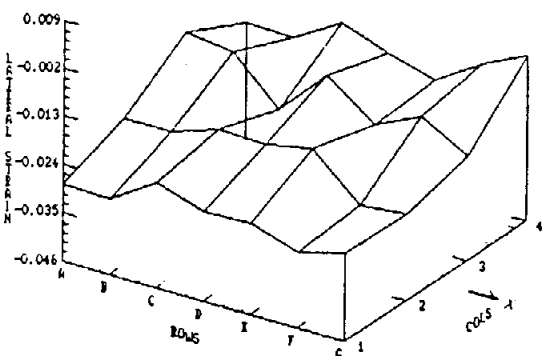
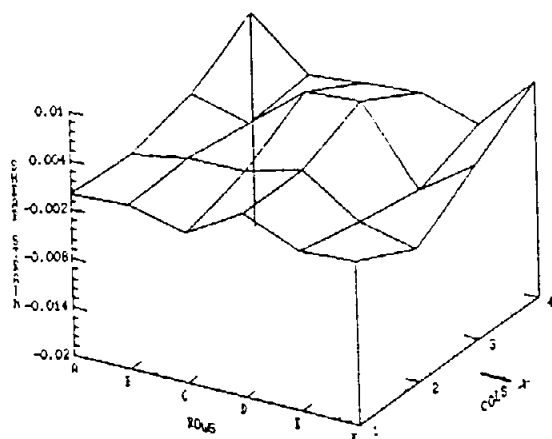


FIG. 29.6. Lateral strain distribution at nominal axial strain level of 3.510%.

POSITIONAL STRAIN DATA

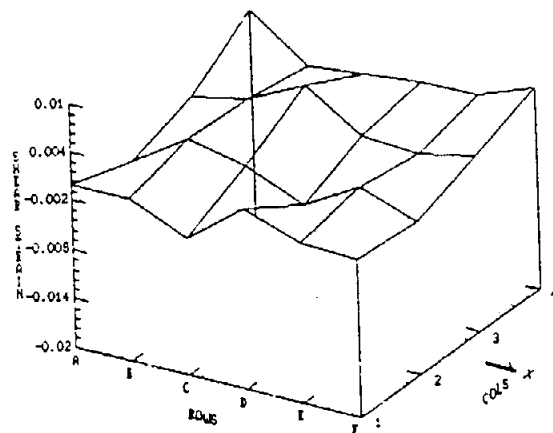
	ROW A	ROW B	ROW C	ROW D	ROW E	ROW F	ROW G
Col. 4	-0.01923	-0.01921	-0.01303	-0.01700	-0.02009	-0.01323	-0.00837
Col. 3	-0.01223	-0.01361	-0.02358	-0.01286	-0.02098	-0.01622	-0.02218
Col. 2	-0.02277	-0.02292	-0.01909	-0.01962	-0.01722	-0.02727	-0.02607
Col. 1	-0.02858	-0.02893	-0.02214	-0.02549	-0.02525	-0.02886	-0.02593



POSITIONAL STRAIN DATA

	ROW A	ROW B	ROW C	ROW D	ROW E	ROW F
Col. 4	0.00647	0.00032	0.00121	0.00163	-0.00047	0.00654
Col. 3	0.00150	-0.00035	0.00537	0.00584	-0.00321	0.00151
Col. 2	-0.00070	0.00071	0.00078	0.00260	-0.00191	-0.00358
Col. 1	-0.00012	0.00026	-0.00149	0.00259	-0.00029	0.00015

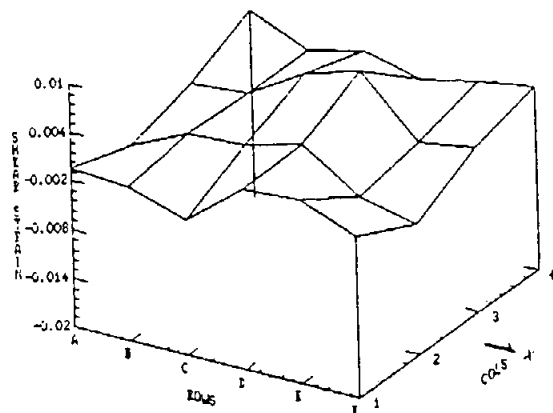
FIG. 30.1. Shear strain distribution at nominal axial strain level of 0.936%.



POSITIONAL STRAIN DATA

	ROW A	ROW B	ROW C	ROW D	ROW E	ROW F
Col. 4	0.00591	0.00065	0.00130	0.00203	0.00210	0.00478
Col. 3	0.00027	0.00167	0.00505	0.00069	0.00023	0.00167
Col. 2	-0.00246	0.00194	0.00035	-0.00274	0.00132	-0.00126
Col. 1	-0.00013	-0.00014	-0.00323	0.00198	-0.00023	-0.00056

FIG. 30.2. Shear strain distribution at nominal axial strain level of 1.539%.

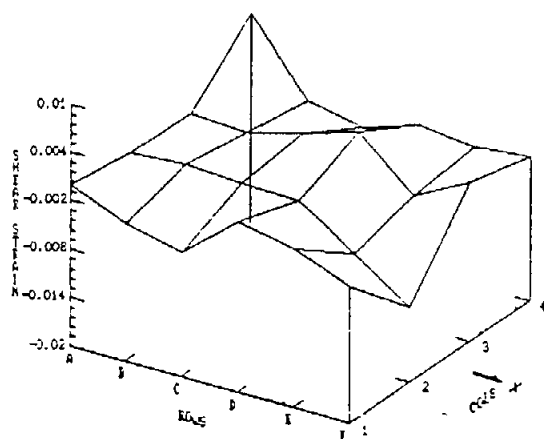


POSITIONAL STRAIN DATA

	ROW A	ROW B	ROW C	ROW D	ROW E	ROW F
Col. 4	0.00339	0.00007	0.00164	0.00000	0.00135	0.00240
Col. 3	-0.00063	-0.00009	0.00408	0.00625	-0.00076	0.00036
Col. 2	-0.00298	0.00034	0.00065	0.00257	-0.00230	-0.00392
Col. 1	-0.00044	-0.00102	-0.00340	0.00211	0.00251	-0.00024

FIG. 30.3. Shear strain distribution at nominal axial strain level of 2.382%.

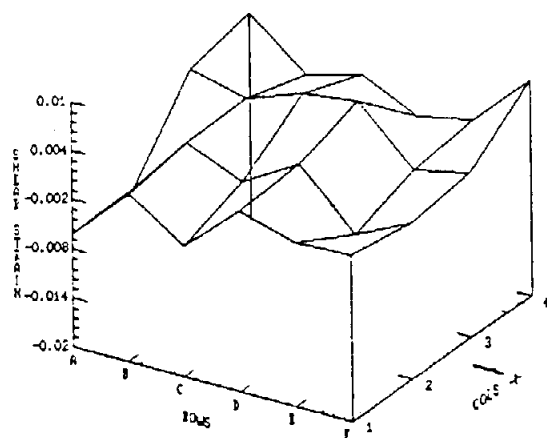
FIG. 30. Typical shear strain distribution for CD specimens, paper type B. Results are given in non-dimensional form using average parameters: $STEPY=1$, $STEPZ=1$. Average parameters are described in item 3.6.



POSITIONAL STRAIN DATA

	ROW A	ROW B	ROW C	ROW D	ROW E	ROW F
Col. 4	0.00599	-0.00284	-0.00435	-0.00209	-0.00284	-0.00205
Col. 3	-0.00124	-0.00183	0.00017	0.00210	-0.00392	-0.00031
Col. 2	-0.00114	-0.00071	-0.00108	-0.00134	-0.00616	-0.01073
Col. 1	-0.00014	-0.00302	-0.00453	0.00112	-0.00040	-0.00312

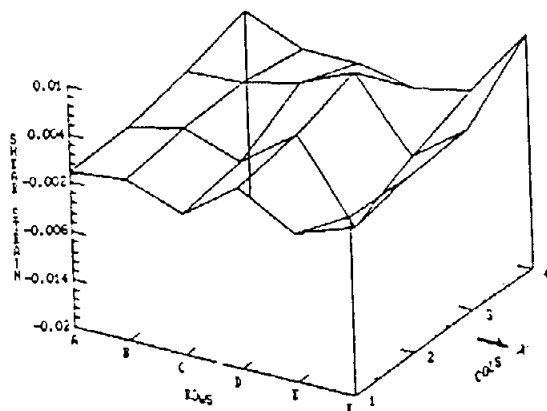
FIG. 30.4. Shear strain distribution at nominal axial strain level of 2.812%.



POSITIONAL STRAIN DATA

	ROW A	ROW B	ROW C	ROW D	ROW E	ROW F
Col. 4	0.00541	-0.00045	0.00148	-0.00183	-0.00028	0.00641
Col. 3	0.00365	0.00187	0.00431	0.00522	-0.00138	0.00017
Col. 2	-0.00636	0.00168	-0.00123	0.00266	-0.00413	-0.00097
Col. 1	-0.00621	0.00064	-0.00402	0.00196	0.00014	0.00044

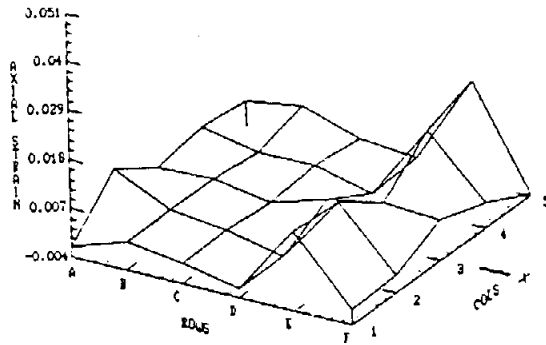
FIG. 30.5. Shear strain distribution at nominal axial strain level of 3.190%.



POSITIONAL STRAIN DATA

	ROW A	ROW B	ROW C	ROW D	ROW E	ROW F
Col. 4	0.00352	0.00041	0.00037	-0.00106	0.00051	0.00913
Col. 3	0.00112	0.00143	0.00319	0.00626	-0.00256	0.00258
Col. 2	-0.00037	0.00119	-0.00124	0.00376	-0.00599	0.00199
Col. 1	-0.00070	0.00006	-0.00245	0.00244	-0.00141	0.00233

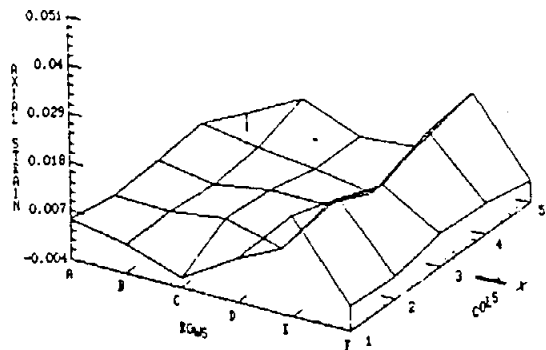
FIG. 30.6. Shear strain distribution at nominal axial strain level of 3.510%.



POSITIONAL STRAIN DATA

	ROW A	ROW B	ROW C	ROW D	ROW E	ROW F
Col. 5	0.00182	0.00380	-0.00067	-0.00174	0.01867	-0.00366
Col. 4	0.00313	0.00059	0.00087	-0.00249	0.01473	0.00149
Col. 3	0.00134	0.00200	0.00001	0.00358	0.00610	0.00515
Col. 2	0.00853	0.00247	0.00102	-0.00216	0.01324	0.00006
Col. 1	-0.00163	0.00263	0.00061	-0.00196	0.01403	-0.00049

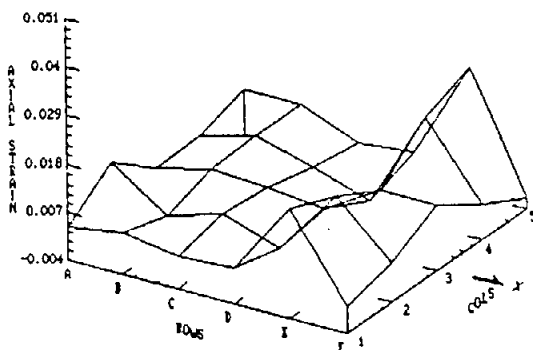
FIG. 31.1. Axial strain distribution at nominal axial strain level of 0.3032.



POSITIONAL STRAIN DATA

	ROW A	ROW B	ROW C	ROW D	ROW E	ROW F
Col. 5	0.00015	0.00657	0.00111	0.00226	0.01758	0.00098
Col. 4	0.00497	0.00286	0.00109	-0.00101	0.01637	0.00293
Col. 3	0.00382	0.00182	0.00373	0.00357	0.01141	0.00329
Col. 2	0.00331	0.00295	0.00446	0.00070	0.01539	0.00100
Col. 1	0.00511	0.00252	-0.00174	0.00580	0.01860	0.00182

FIG. 31.2. Axial strain distribution at nominal axial strain level of 0.4622.

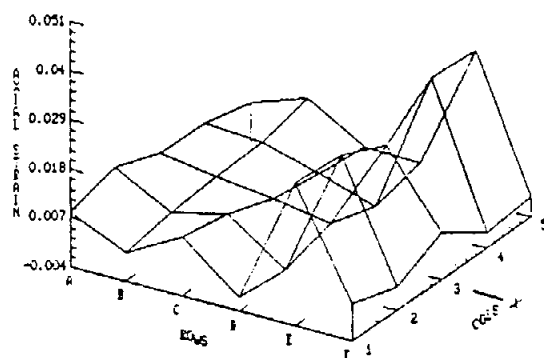


POSITIONAL STRAIN DATA

	ROW A	ROW B	ROW C	ROW D	ROW D	ROW F
Col. 5	0.00643	0.00645	0.00090	0.00202	0.02468	-0.00150
Col. 4	0.00301	0.00637	0.00273	-0.00163	0.02034	0.00404
Col. 3	0.00301	0.00604	0.00522	0.00357	0.01131	0.01126
Col. 2	0.01151	0.00243	0.00606	0.00159	0.01690	0.00476
Col. 1	0.00374	0.00563	0.00325	0.00417	0.02120	0.00222

FIG. 31.3. Axial strain distribution at nominal axial strain level of 0.6752.

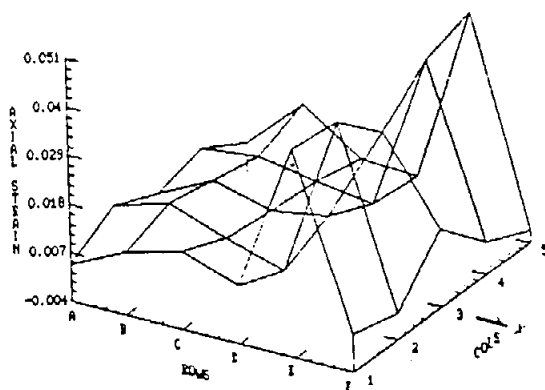
FIG. 31. Typical axial strain distribution for HANGSHEETS. Results are given in non-dimensional form using average parameters: STEPX= 1, STEPY= 1. Average parameters are described in item 3.6.



POSITIONAL STRAIN DATA

	ROW A	ROW B	ROW C	ROW D	ROW E	ROW F
Col. 5	0.00464	0.00914	0.00148	0.00144	0.02980	0.00051
Col. 4	0.00711	0.00628	0.00253	-0.00149	0.03109	-0.00037
Col. 3	0.00757	0.00566	0.00417	0.00203	0.02285	0.00661
Col. 2	0.01148	0.00472	0.00747	-0.00163	0.02781	0.00128
Col. 1	0.00805	0.00248	0.00928	-0.00101	0.02851	0.00452

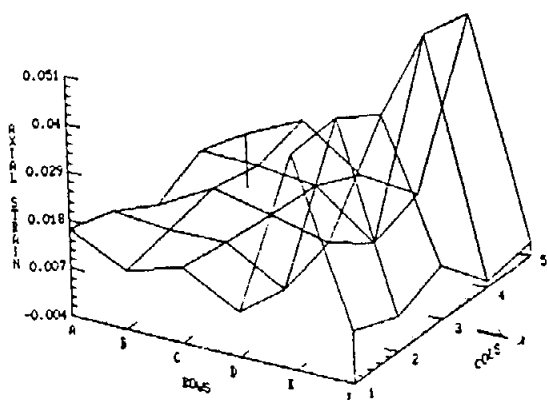
FIG. 31.4. Axial strain distribution at nominal axial strain level of 0.819%.



POSITIONAL STRAIN DATA

	ROW A	ROW B	ROW C	ROW D	ROW E	ROW F
Col. 5	0.00275	0.01459	0.00559	0.00451	0.04492	-0.00111
Col. 4	0.00903	0.01002	0.00756	0.00586	0.04125	0.00352
Col. 3	0.00582	0.01187	0.00847	0.01023	0.03243	0.01374
Col. 2	0.01021	0.01421	0.00950	0.00493	0.04194	0.00165
Col. 1	0.00447	0.01029	0.01356	0.00879	0.04306	0.00457

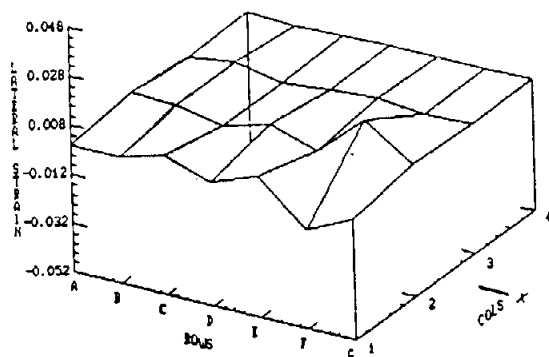
FIG. 31.5. Axial strain distribution at nominal axial strain level of 1.379%.



POSITIONAL STRAIN DATA

	ROW A	ROW B	ROW C	ROW D	ROW E	ROW F
Col. 5	0.00848	0.01460	0.00507	0.00405	0.04829	-0.00088
Col. 4	0.01188	0.01153	0.01018	-0.00002	0.05069	-0.00268
Col. 3	0.00665	0.01355	0.01083	0.00759	0.03968	0.00827
Col. 2	0.01260	0.01150	0.01176	0.00383	0.04638	0.00389
Col. 1	0.01580	0.00948	0.01334	0.00604	0.04565	0.00818

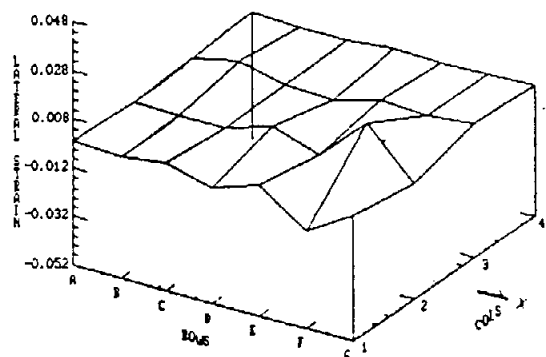
FIG. 31.6. Axial strain distribution at nominal axial strain level of 1.449%.



POSITIONAL STRAIN DATA

	ROW A	ROW B	ROW C	ROW D	ROW E	ROW F	ROW G
Col. 4	0.00061	-0.00063	0.00017	0.00114	0.00077	0.00133	0.00173
Col. 3	-0.00023	0.00283	-0.00122	0.00093	0.00238	0.00034	0.00123
Col. 2	0.00360	0.00286	-0.00074	0.00428	-0.00184	0.01569	0.00236
Col. 1	-0.00030	-0.00008	0.00478	-0.00117	0.00588	-0.01155	-0.00234

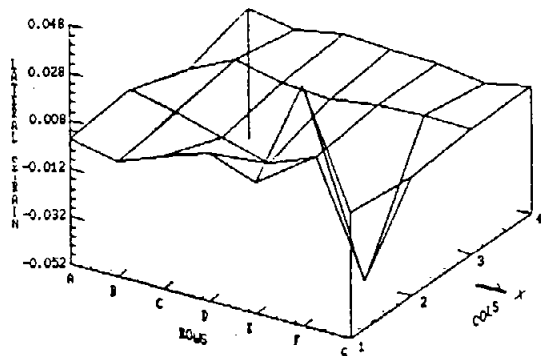
FIG. 32.1. Lateral strain distribution at nominal axial strain level of 0.3032.



POSITIONAL STRAIN DATA

	ROW A	ROW B	ROW C	ROW D	ROW E	ROW F	ROW G
Col. 4	-0.00006	-0.00112	-0.00109	0.00076	0.00032	0.00107	0.00195
Col. 3	-0.00097	0.00276	-0.00185	-0.00302	0.00196	0.00102	0.00321
Col. 2	-0.00188	-0.00274	-0.00253	0.00338	-0.00300	0.01456	-0.00408
Col. 1	-0.00095	-0.00238	0.00046	-0.00455	0.00196	-0.01242	-0.00043

FIG. 32.2. Lateral strain distribution at nominal axial strain level of 0.4621.

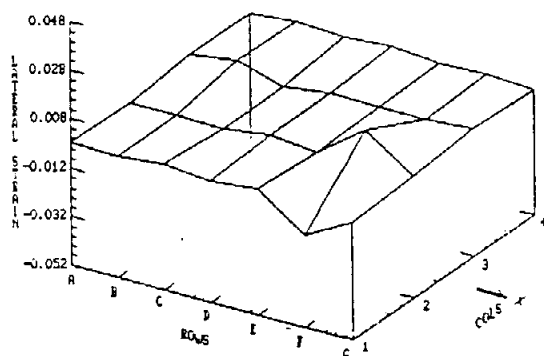


POSITIONAL STRAIN DATA

	ROW A	ROW B	ROW C	ROW D	ROW E	ROW F	ROW G
Col. 4	0.00289	-0.00131	0.00219	0.00079	0.00047	-0.00298	0.00096
Col. 3	-0.00522	0.00364	-0.00047	-0.00265	0.00018	0.00117	0.00042
Col. 2	0.00356	-0.00103	-0.00647	-0.01216	-0.00424	-0.05099	-0.00244
Col. 1	0.00061	-0.00407	0.00308	0.00967	0.00232	0.04771	0.00032

FIG. 32.3. Lateral strain distribution at nominal axial strain level of 0.6751.

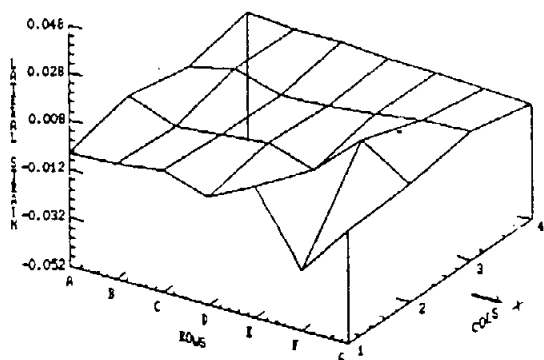
FIG. 32. Typical lateral strain distribution for HANDSHEETS. Results are given in non-dimensional form using average parameters: STEPX= 1, STEPY= 1. Average parameters are described in item 3.6.



POSITIONAL STRAIN DATA

	ROW A	ROW B	ROW C	ROW D	ROW E	ROW F	ROW G
Col. 4	-0.00049	0.00124	0.00029	0.00139	-0.00007	0.00078	-0.00059
Col. 3	-0.00023	0.00255	-0.00323	-0.00025	-0.00128	-0.00080	0.00005
Col. 2	-0.00244	-0.00298	-0.00305	-0.00090	-0.00274	0.01186	-0.00145
Col. 1	-0.00131	-0.00245	0.00005	-0.00193	0.00001	-0.01413	-0.00354

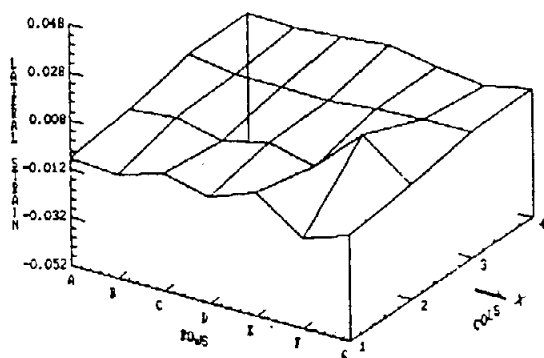
FIG. 32.4. Lateral strain distribution at nominal axial strain level of 0.819%.



POSITIONAL STRAIN DATA

	ROW A	ROW B	ROW C	ROW D	ROW E	ROW F	ROW G
Col. 4	0.00235	0.00029	0.00008	-0.00143	-0.00205	-0.00327	-0.00441
Col. 3	-0.00386	0.00090	-0.00525	-0.00403	-0.00233	0.00043	0.00090
Col. 2	0.00104	-0.00636	-0.00439	-0.00245	-0.00851	0.00888	-0.00366
Col. 1	-0.00534	-0.00481	-0.00246	-0.00812	0.00195	-0.02762	-0.00592

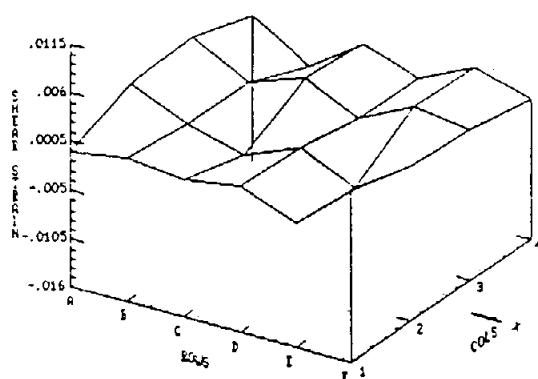
FIG. 32.5. Lateral strain distribution at nominal axial strain level of 1.379%.



POSITIONAL STRAIN DATA

	ROW A	ROW B	ROW C	ROW D	ROW E	ROW F	ROW G
Col. 4	0.00074	0.00045	0.00134	0.00388	-0.00015	-0.00279	0.00098
Col. 3	0.00113	-0.00211	-0.00173	-0.00263	-0.00046	0.00030	0.00025
Col. 2	-0.00460	-0.00264	-0.00712	-0.00269	-0.00675	0.01070	-0.00407
Col. 1	-0.00736	-0.00939	-0.00325	-0.00777	-0.00104	-0.01472	-0.00853

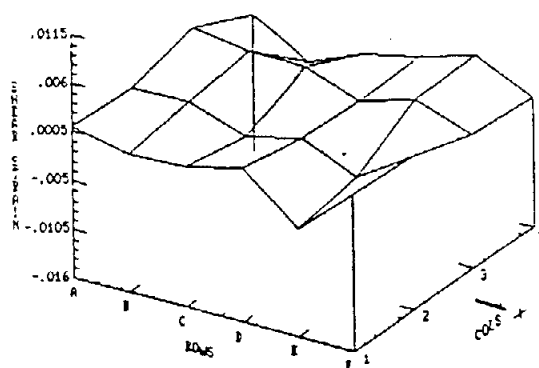
FIG. 32.6. Lateral strain distribution at nominal axial strain level of 1.449%.



POSITIONAL STRAIN DATA

	ROW A	ROW B	ROW C	ROW D	ROW E	ROW F
Col. 4	0.00078	-0.00351	0.00081	-0.00132	0.00161	-0.00012
Col. 3	0.00291	-0.00052	0.00165	-0.00108	0.00195	0.00112
Col. 2	0.00236	-0.00063	-0.00237	0.00030	-0.00263	0.00149
Col. 1	-0.00072	0.00025	-0.00048	0.00057	-0.00183	0.00343

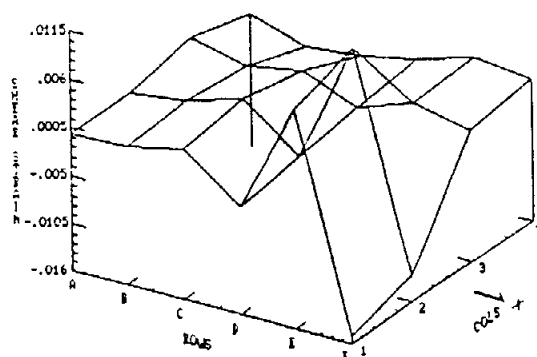
FIG. 33.1. Shear strain distribution at nominal axial strain level of 0.3032.



POSITIONAL STRAIN DATA

	ROW A	ROW B	ROW C	ROW D	ROW E	ROW F
Col. 4	-0.00065	-0.00424	-0.00164	-0.00027	0.00161	-0.00135
Col. 3	0.00271	0.00176	0.00169	-0.00051	0.00151	-0.00089
Col. 2	0.00072	0.00084	-0.00156	0.00009	-0.00264	0.00141
Col. 1	0.00098	-0.00045	-0.00018	0.00137	-0.00370	0.00183

FIG. 33.2. Shear strain distribution at nominal axial strain level of 0.4621.

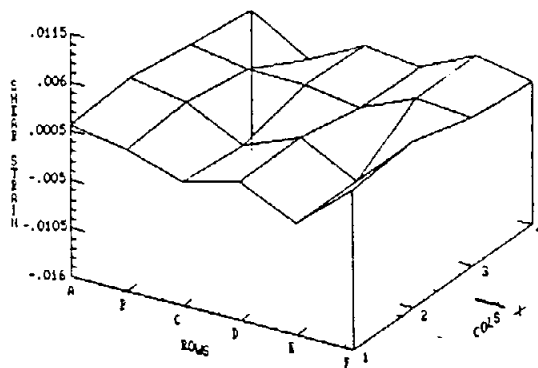


POSITIONAL STRAIN DATA

	ROW A	ROW B	ROW C	ROW D	ROW E	ROW F
Col. 4	-0.00094	-0.00287	-0.00236	-0.00098	0.00102	0.00022
Col. 3	0.00118	-0.00026	0.00086	-0.00164	0.00057	-0.00085
Col. 2	-0.00025	0.00044	0.00233	-0.00253	0.01146	-0.01285
Col. 1	-0.00028	-0.00001	0.00120	-0.00361	0.00935	-0.01502

FIG. 33.3. Shear strain distribution at nominal axial strain level of 0.6751.

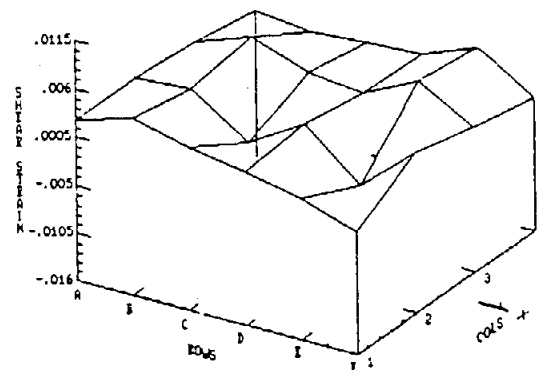
FIG. 33. Typical shear strain distribution for HANDSHEETS. Results are given in non-dimensional form using average parameters: STEPX= 1, STEPY= 1. Average parameters are described in item 3.6.



POSITIONAL STRAIN DATA

	ROW A	ROW B	ROW C	ROW D	ROW E	ROW F
Col. 4	-0.00015	-0.00394	-0.00071	-0.00150	0.00151	0.00014
Col. 3	0.00078	-0.00030	-0.00047	-0.00137	0.00142	0.00089
Col. 2	0.00180	0.00072	-0.00252	-0.00005	-0.00314	0.00287
Col. 1	0.00123	0.00004	-0.00192	-0.00011	-0.00316	0.00217

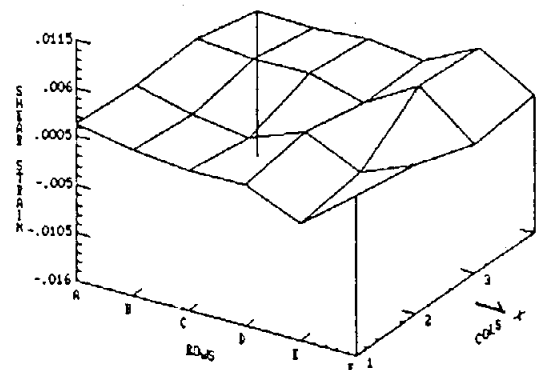
FIG. 33.4. Shear strain distribution at nominal axial strain level of 0.819%.



POSITIONAL STRAIN DATA

	ROW A	ROW B	ROW C	ROW D	ROW E	ROW F
Col. 4	0.00068	-0.00012	0.00028	0.00063	0.00312	-0.00084
Col. 3	0.00191	0.00411	0.00164	0.00118	0.00405	0.00050
Col. 2	0.00243	0.00298	-0.00146	0.00232	-0.00302	0.00235
Col. 1	0.00247	0.00433	0.00273	0.00151	0.00023	-0.00190

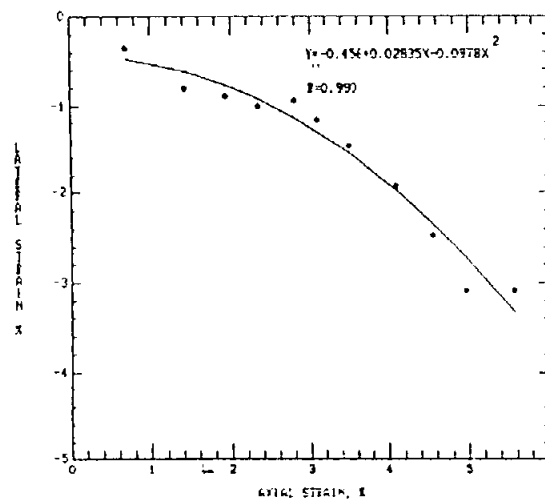
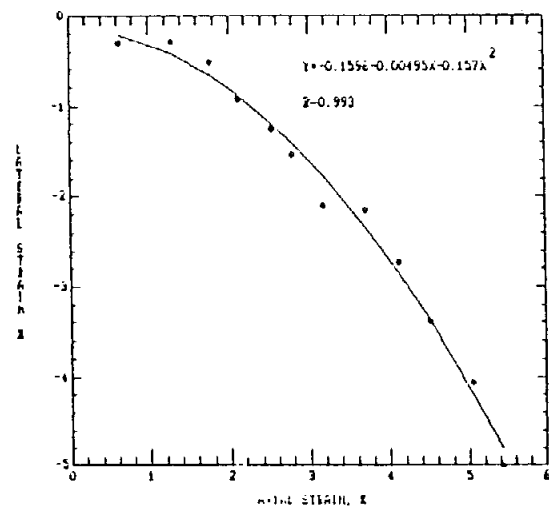
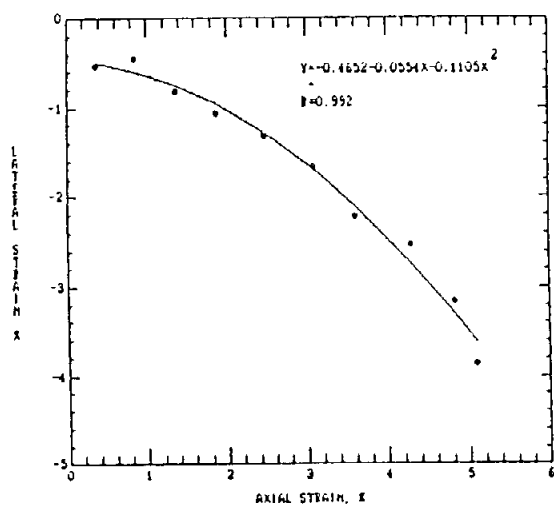
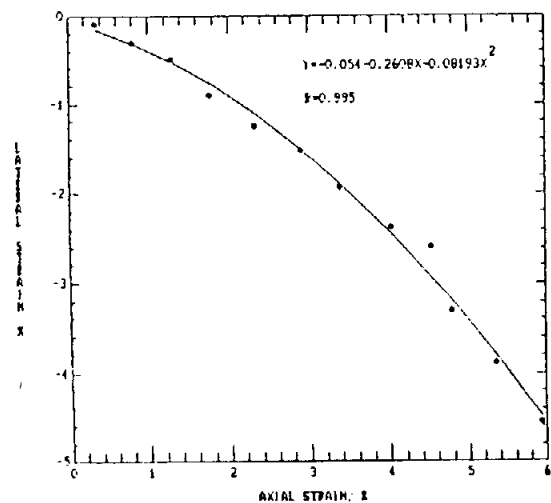
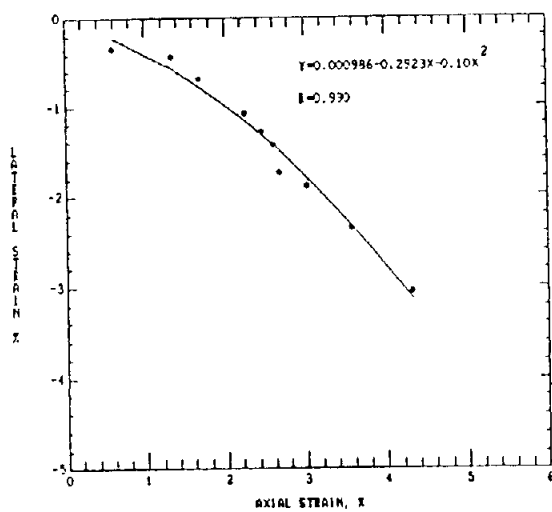
FIG. 33.5. Shear strain distribution at nominal axial strain level of 1.379%.

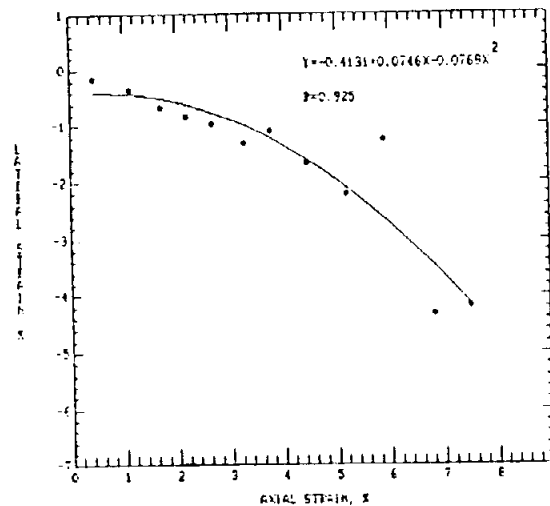
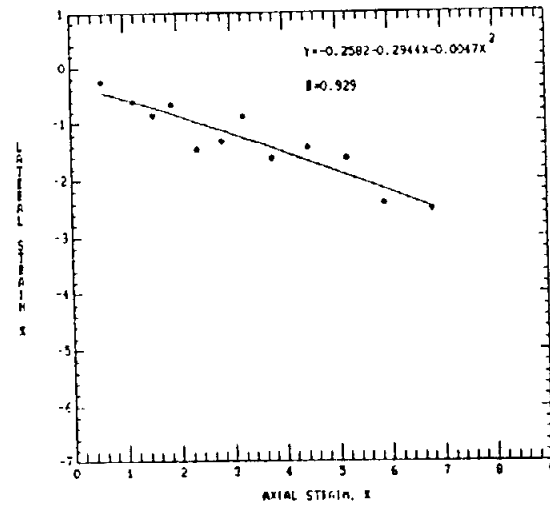
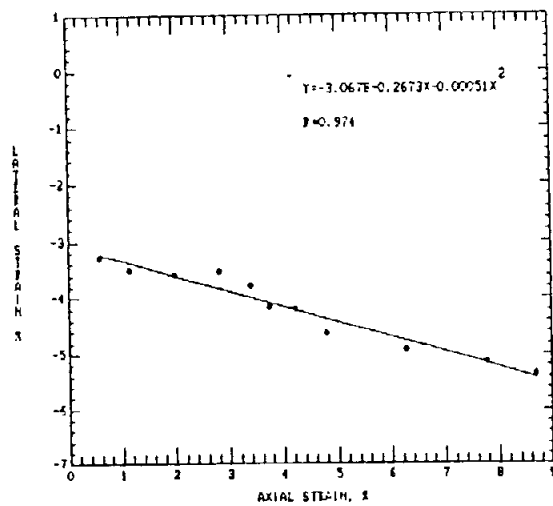
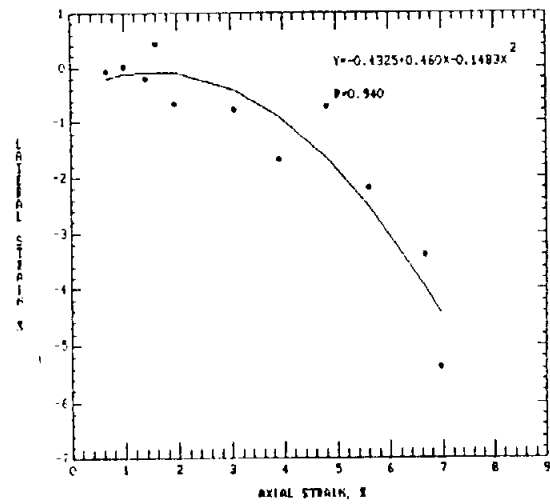
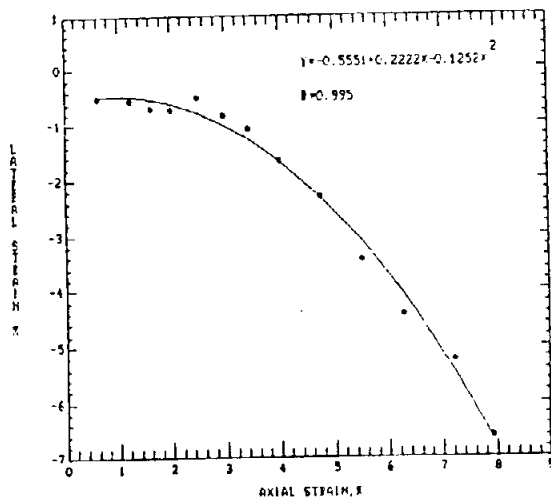


POSITIONAL STRAIN DATA

	ROW A	ROW B	ROW C	ROW D	ROW E	ROW F
Col. 4	0.00072	0.00047	0.00090	0.00006	0.00331	-0.00037
Col. 3	0.00223	0.00167	0.00179	0.00008	0.00371	-0.00130
Col. 2	0.00153	-0.00009	-0.00091	0.00149	-0.00136	0.00121
Col. 1	0.00199	0.00054	0.00003	0.00008	-0.00255	0.00237

FIG. 33.6. Shear strain distribution at nominal axial strain level of 1.449%.





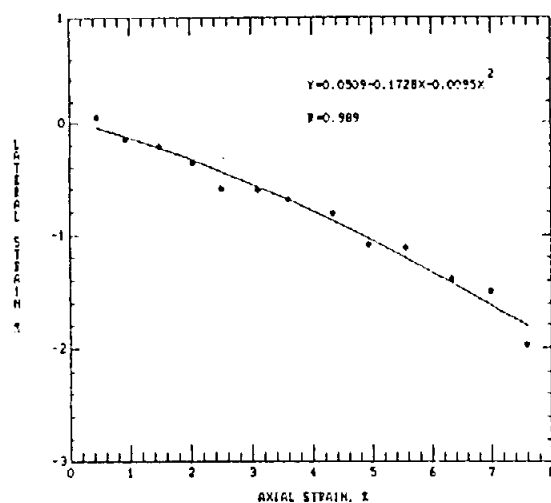


Fig. 36.1. Specimen no. 1

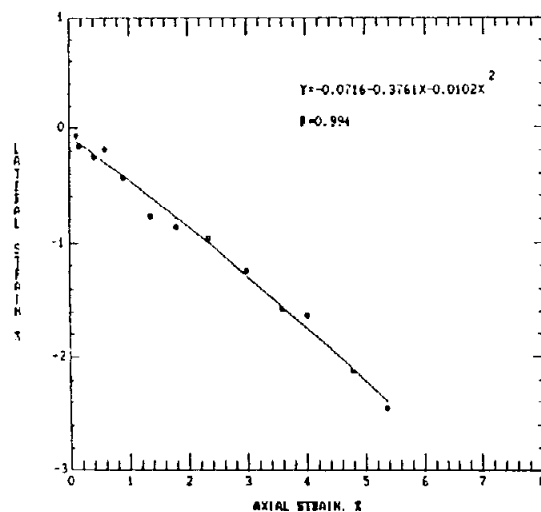


Fig. 36.2. Specimen no. 2

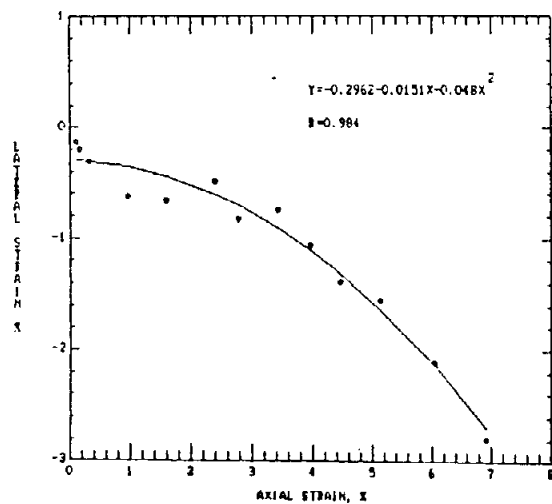


Fig. 36.3. Specimen no. 3

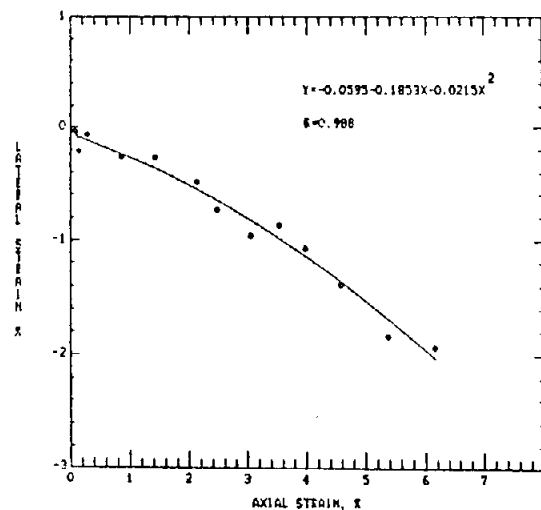


Fig. 36.4. Specimen no. 4

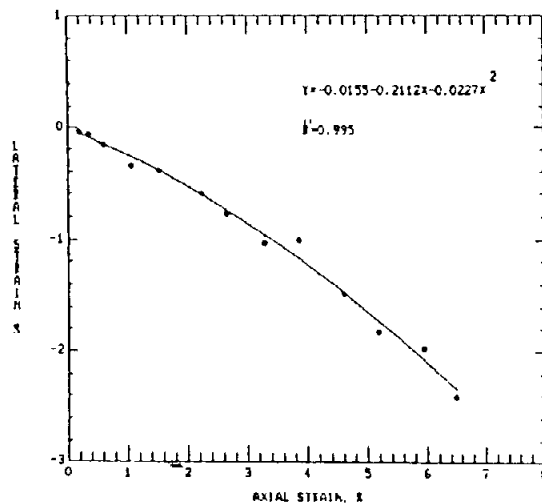


Fig. 36.5. Specimen no. 5

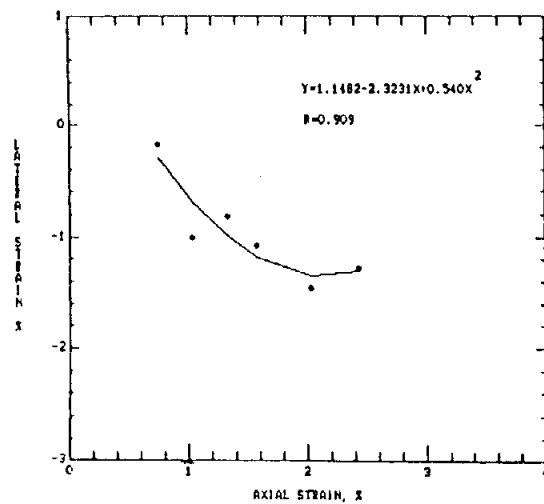
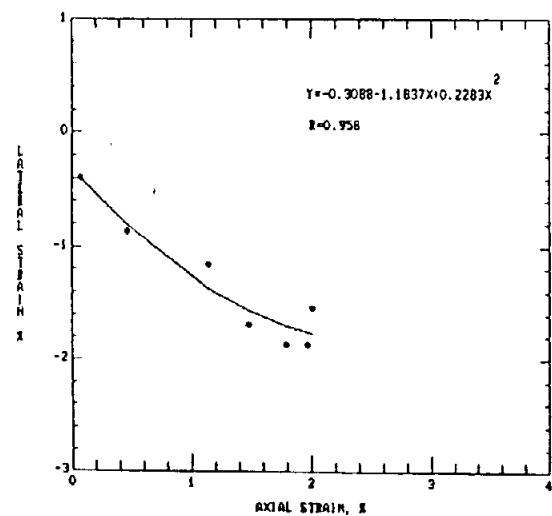
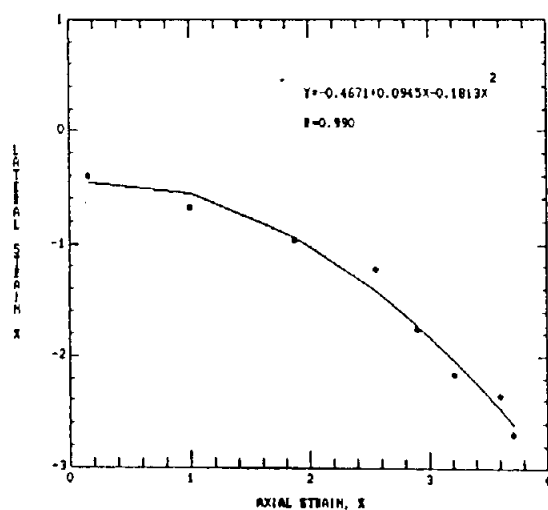
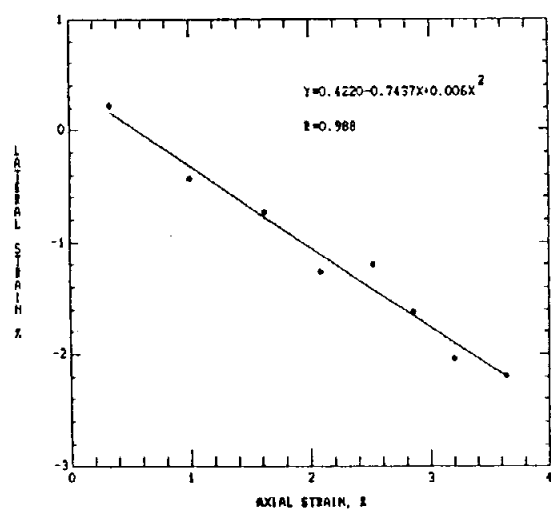
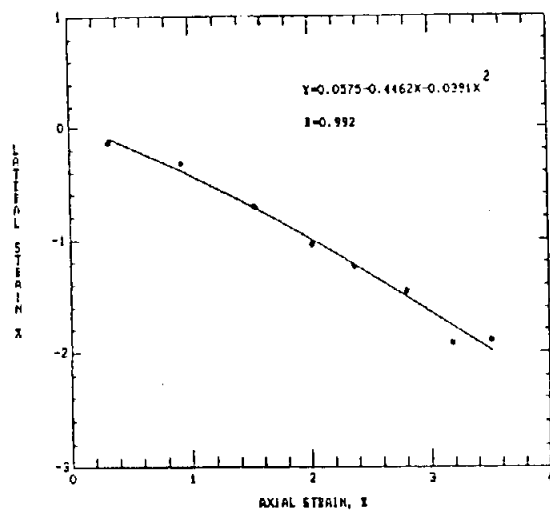


Fig. 37. Axial strain vs lateral strain, CD specimens, paper type B.

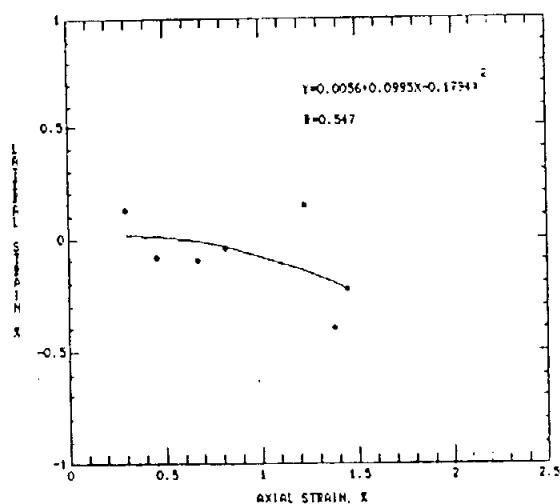


Fig. 38.1. Specimen no. 1

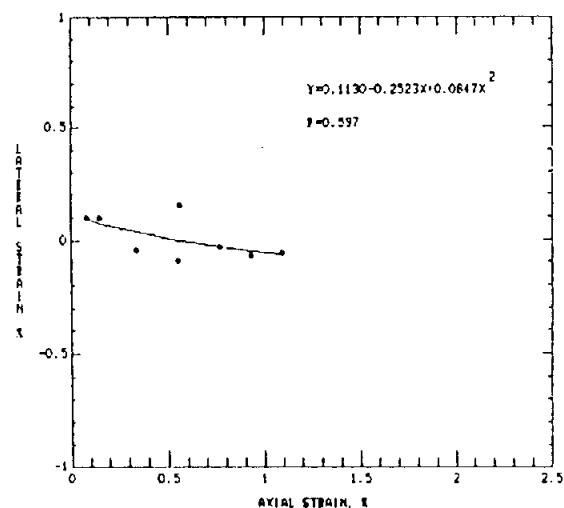


Fig. 38.2. Specimen no. 2

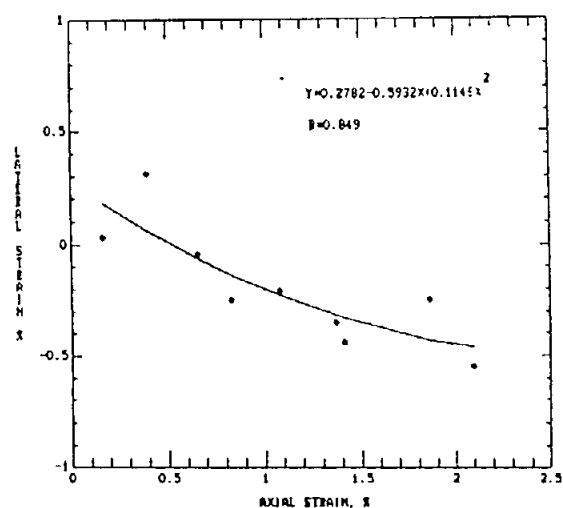


Fig. 38.3. Specimen no. 3

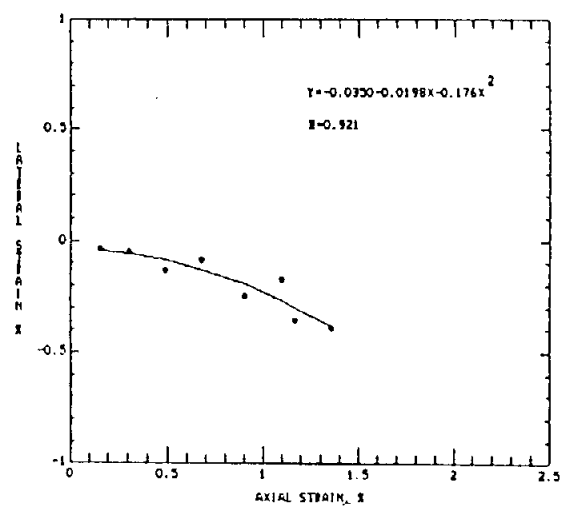


Fig. 38.4 Specimen no. 4

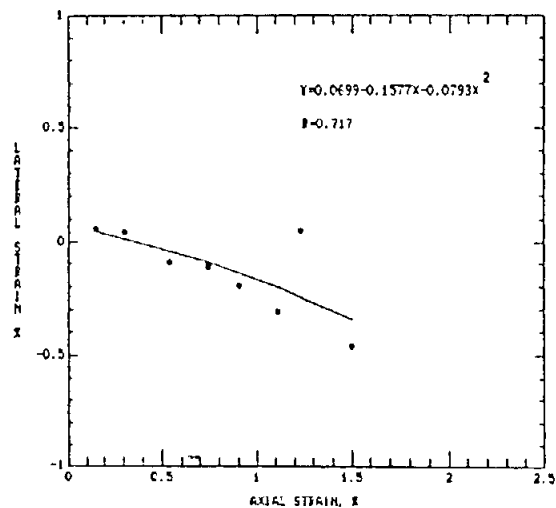


Fig. 38.5 Specimen no. 5

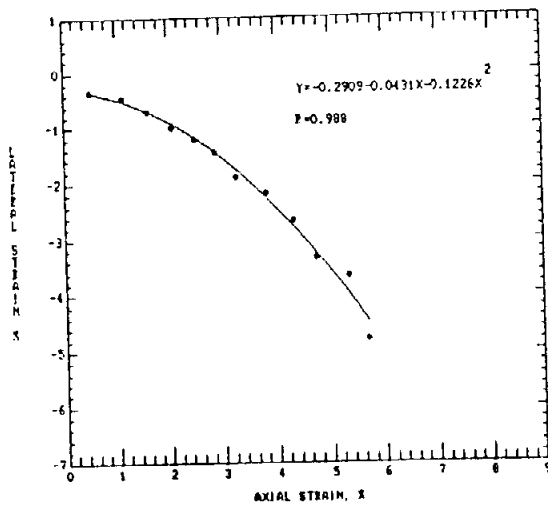


Fig. 39.1. Paper type A, MD specimens

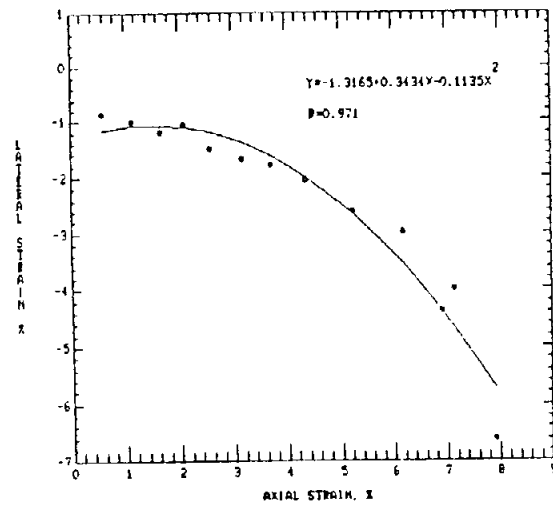


Fig. 39.2. Paper type A, CD specimens

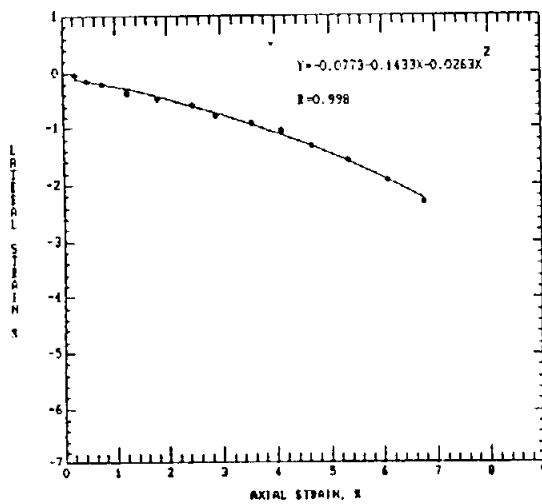


Fig. 39.3. Paper type B, MD specimens

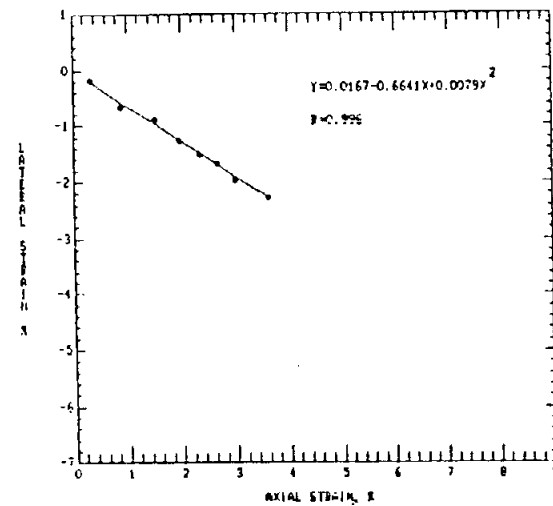


Fig. 39.4. Paper type B, CD specimens

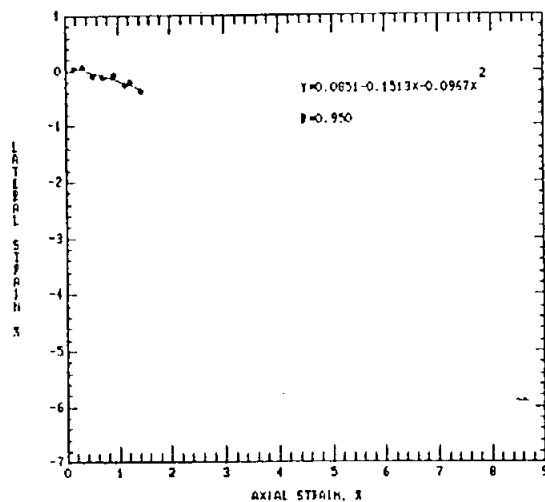


Fig. 39.5. HANDSHEET specimens

Fig. 39. Axial strain vs lateral strains. Average for 5 specimens
Paper type A: Higher fiber orientation distribution
Paper type B: Moderately fiber orientation distribution

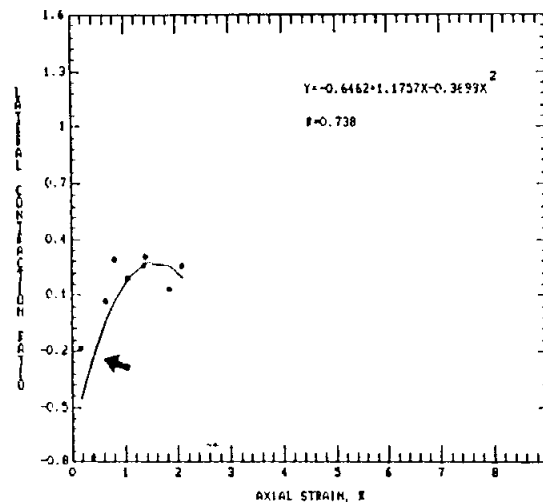
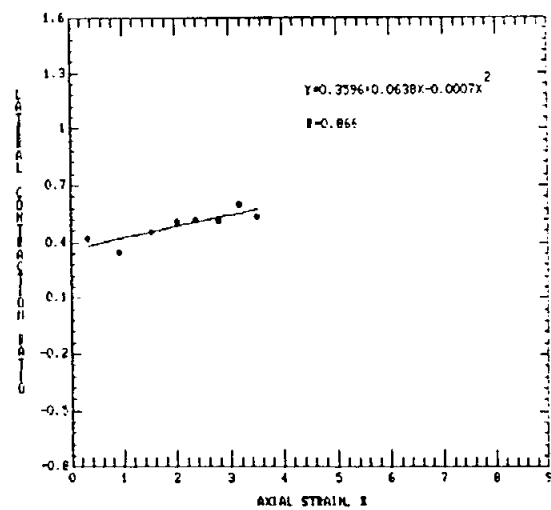
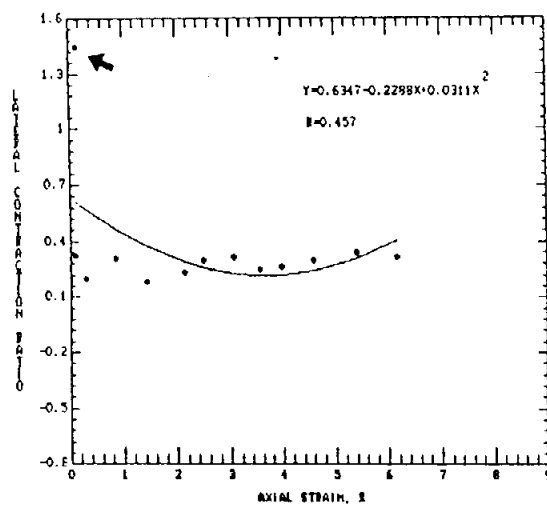
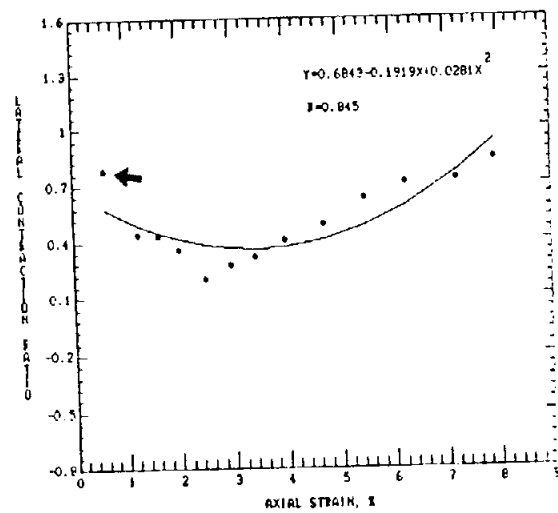
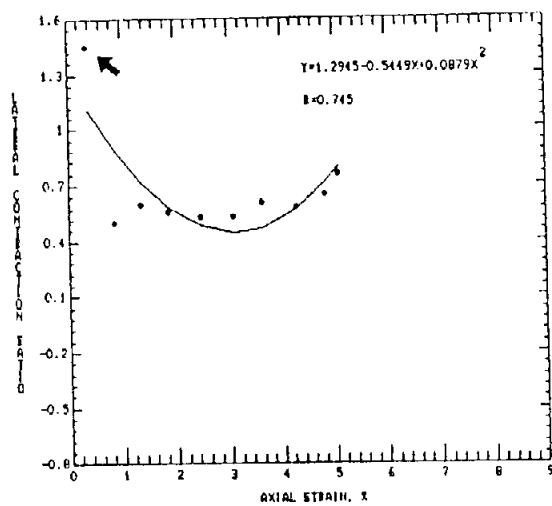


Fig.40. Typical axial strain-lateral contraction ratio relationship.

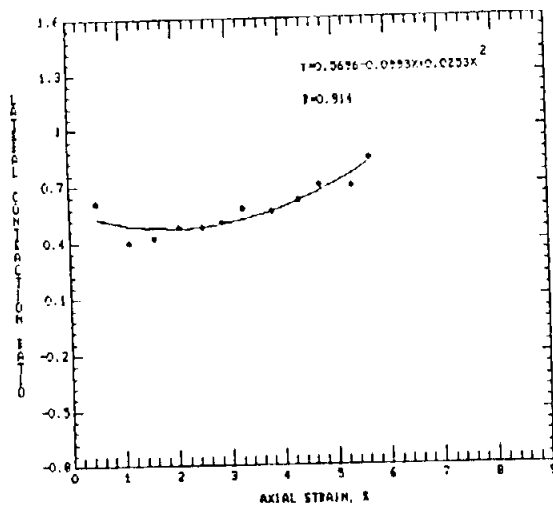


Fig. 41.1. Paper type A, MD specimens.

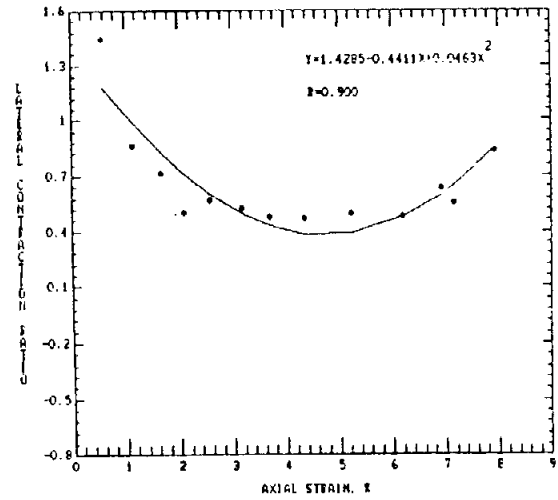


Fig. 41.2. Paper type A, CD specimens.

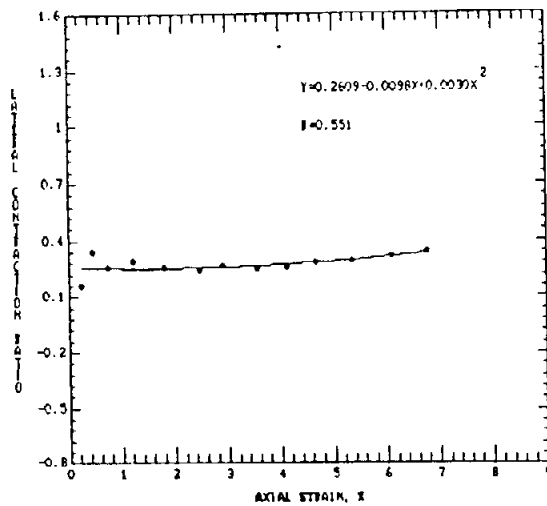


Fig. 41.3. Paper type B, MD specimens.

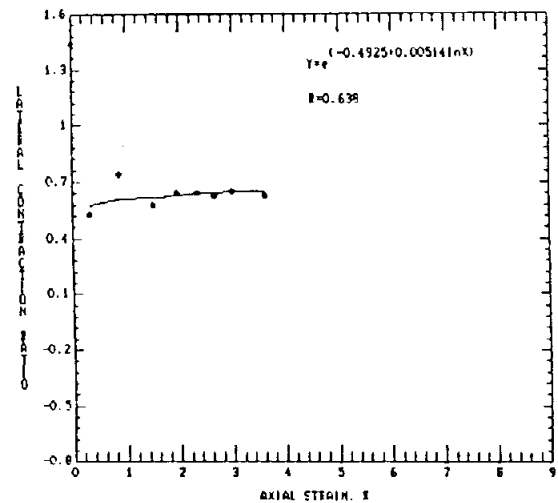


Fig. 41.4. Paper type B, CD specimens.

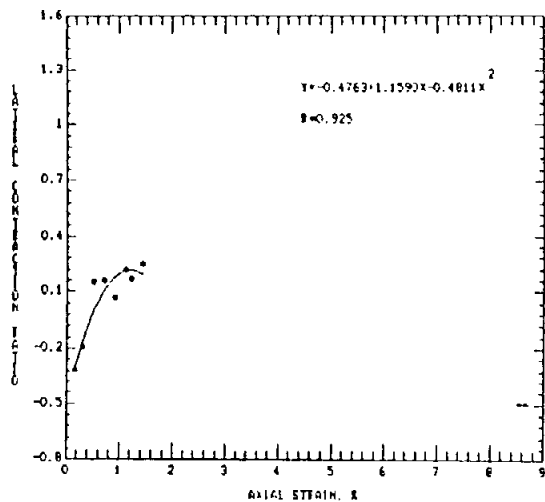


Fig. 41.5. HANDSHEET specimens.

Fig. 41. Axial strain - lateral contraction ratio relationship. Average for 5 specimens. Paper type A: Higher fiber orientation distribution. Paper type B: Moderately fiber orientation distribution.

3.11. Appendix A. Computer Programs Used for Data Acquisition
Control of the Mechanical Tests and Part of the Data
Acquired by the Keithley-DAS Interface System.

```

IST
2 PRINT" "
13 PRINT" "
20 PRINT" At present, acquiring data"
0 CALL INIT
40 CALL IONAME'("phocell",1,2,14,1,3)
41 CALL IONAME'("load",3,1,14,1,2)
0 CALL INTON'(50,"mil")
0 CALL ANIN'("str%",5000., "phocell,load",1,"try")
70 STAT%=0
0 CALL STATUS'("try",stat%)
0 IF STAT%=1 THEN GOTO 80
91 PRINT" name of the file to store"
92 INPUT" (file name)(filename)";FIL$
93 INPUT" file number";N#
94 OPEN "o",N#,FIL$
95 PRINT" ":PRINT" "
6 PER=0:PER1=0
00 FOR D=1 TO 5000
110 PER=0:PER1=0
120 CALL ARGETVAL'("str%",d,"phocell",per)
121 CALL ARGETVAL'("str%",d,"load",per1)
122 WRITE# N#,PER,PER1
150 NEXT D
62 CLOSE# N#
170 INPUT"If you want to see the data, type 1. Otherwise, type 0";TY#
172 IF TY#=0 GOTO 180
74 FOR B=1 TO 5000
75 PER=0:PER1=0
176 CALL ARGETVAL'("str%",b,"phocell",per)
177 CALL ARGETVAL'("str%",b,"load",per1)
78 PRINT PER,PER1
179 NEXT B
180 END

```

```

100 IST
10 INPUT" name of file to read";FIL$
20 INPUT" file number to read";N#
30 INPUT" numner of data points (length*2)";NN#
40 N1#=NN#/2
55 DIM ARRAY(N1#,2),ARRY(N1#,2)
60 OPEN "1",N#,FIL$
70 FOR I=1 TO NN#
85 INPUT# N#,PER
90 II%=I/2:K=II%
100 IF I=II%*2 GOTO 55
110 ARRAY(K,1)=PER :GOTO 56
120 ARRAY(K,2)=PER
130 NEXT I
140 CLOSE# N# :LENGTH=N1#
150 INPUT"If you want to see all the data, type 1. Otherwise,type 0";FL#
160 IF FL#=0 GOTO 100
170 FOR J=1 TO N1#
180 PRINT ARRAY(J,1),ARRAY(J,2)
190 NEXT J
200 INPUT"if you want to stop here, type 0. Otherwise type 1";PA#
210 IF PA#=0 GOTO 1000
220 INPUT"From what row do you want to see";PB#
230 INPUT"Until what row do you want to see";PC#
240 FOR M=PB# TO PC#
250 PRINT ARRAY(M,1),ARRAY(M,2)
260 NEXT M
270 INPUT"If you want to keep all the data, type 1. Otherwise type 0";FG#
280 IF PG#=0 GOTO 150
290 GOTO 580
300 INPUT"from what row do you want to remove out";PD#
310 INPUT"Until what row do you want to remove out";PE#
320 PD#=PD#-1:PE#=PE#+1:PF#=PE#-PD#-1:N1#=N1#-PE#
330 IF PD#<1 GOTO 220
340 FOR N=1 TO PD#
350 ARRY(N,2)=ARRAY(N,2):ARRY(N,1)=ARRAY(N,1)
360 PRINT ARRY(N,1),ARRY(N,2)
370 NEXT N
380 FOR NN=PE# TO LENGTH
390 NM=NN-PF#
400 ARRY(NM,1)=ARRAY(NN,1):ARRY(NM,2)=ARRAY(NN,2)
410 PRINT ARRY(NM,1),ARRY(NM,2)
420 NEXT NN
430 PRINT" ":PRINT" ":PRINT"Length of the data file":PRINT N1#
440 INPUT"name of the file to store the new data";FILES
450 INPUT"file number";NN#
460 OPEN "o",NN#,FILES
470 FOR J1=1 TO N1#
480 WRITE# NN#,ARRY(J1,1),ARRY(J1,2)
490 NEXT J1
500 CLOSE# NN#
510 INPUT"If you want to stop here, type 1, otherwise type 0";BE#
520 IF BE#=0 GOTO 58
530 END

```

RUN

name of file to read? b:ths3.10h

file number to read? 1

number of data points (length*2)? 2000

If you want to see all the data, type 1. Otherwise, type 0? 0

From what row do you want to see? 200

Until what row do you want to see? 250

7715 7259

7717 7261

7717 7261

7717 7262

7718 7262

7717 7262

7718 7263

7717 7264

7717 7264

7717 7265

7717 7266

7717 7266

7717 7268

7718 7267

7717 7268

7718 7269

7718 7270

7718 7270 .

7717 7271

7717 7271

7717 7272

7754 ← 7272 ←

7730 7274

7722 7274

7719 7275

7718 7275

7717 7275

7717 7277

7717 7277

7717 7277

7716 7278

7716 7279

7716 7280

7716 7280

7716 7281

7716 7281

7716 7282

7716 7283

7716 7283

7716 7283

7716 7284

7716 7284

7715 7285

7716 7286

7715 7286

7715 7288

7716 7288

7716 7288

7716 7289

7716 7289

7717 7290

If you want to keep all the data, type 1. Otherwise type 0? 1

If you want to stop here, type 1, otherwise type 0? 1

3.12. Appendix B. Computer Programs Used for Semi-automatic
Processing of Grid Photographies.

```

SOFTWARE[00]
[00] SOFTWARE
[01] ' ' ' ' ' ' ' ' ' '
[02] '*****'
[03] '*****'
[04] '***** DOT MATRIX TECHNIQUE *****'
[05] '*****'
[06] '*****'
[07] ' ' ' ' ' '
[08] '*****'
[09] '***** SEMI-AUTOMATIC PROCESSING OF GRID PHOTOGRAPHIES *****'
[10] '***** by RUBENS CHAVES DE OLIVEIRA Feb. 88 *****'
[11] '*****'
[12] ' ' ' ' ' ' ' ' ' ' 'PRESS ENTER TO CONTINUE' ' PAUSE+M
[13] OPTIONS
[14] ' ' ' ' ' '
[15] '

```

```

OPTIONS[00]
[00] OPTIONS; OPT:=CARTE; BRAN
[01] BEGIN:
[02] CARTE:=0 ' '
[03] 'THIS IS THE MAIN MENU. IF YOU DO NOT KNOW HOW TO GO ON or IF THIS IS THE'
[04] 'FIRST TIME YOU RUN THIS SOFTWARE TYPE D FOR DESCRIBE.'
[05] M+?' ' OPT+M
[06] +(OPT#?'D')/CONTI
[07] DESCR1
[08] CONTI:
[09] '
[10] 'IMPORTANT: BEFORE DIGITIZING LOCATE THE PROJECTOR APPROPRIATELY.' ' '
[11] ' 1)- To go in the procedure DOTDTZ, type 1.'
[12] ' 2)- To go in the procedure FREAD2, type 2.'
[13] ' 3)- To go in the procedure DWRITE, type 3.'
[14] ' 4)- To go in the procedure FREAD, type 4.'
[15] ' 5)- To go in the procedure RENAME, type 5.'
[16] ' 6)- To go in the procedure MISTAKE, type 6.'
[17] ' 7)- To go in the procedure ERASE, type 7.'
[18] ' 8)- To exit the program, type 8.'
[19] 'ENTER THE NUMBER OF YOUR CHOICE.'
[20] CARTE+0
[21] +(CARTE=8)/END
[22] BRAN+23+CARTE
[23] +BRAN
[24] DOTDTZ ' +BEGIN
[25] FREAD2 ' +BEGIN
[26] DWRITE ' +BEGIN
[27] FREAD ' +BEGIN
[28] RENAME ' +BEGIN
[29] MISTAKE ' +BEGIN
[30] ERASE ' +BEGIN
[31] END:
[32] '

```



```

      =DESCRIBED
[10] DESCRIP;PAUSE
[11] '      '
[12] 'THIS SOFTWARE MAKES THE ACQUISITION OF GRID PATTERNS IN A SEMI-AUTOMATIC'
[13] 'PROCEDURE'
[14] '      '
[15] '      THE MAIN FUNCTIONS ARE DESCRIBED...      '
[16] '      '
[17] 'DOTDTZ: This function makes the acquisition of X and Y coord. of grid'
[18] '      photographs obtained by the DOT MATRIX TECHNIQUE and using '
[19] '      the ALTEK digitizer table. It calls the function LABELDTZ which'
[20] '      makes the acquisition of X and Y coord. of dotlines-label which'
[21] '      are used to align the photographs with digitizer axis that we'
[22] '      know to be in correct X-Y plane.'
[23] '      '
[24] 'FREAD2: This function makes the reading of the X and Y coord. data file'
[25] '      and display it in a column form or in a condensed matrix form,'
[26] '      representing the real location of the dots on the paper sample.'
[27] '      '
[28] 'ALIGN3: This function makes the alignment of the photographs(negative)'
[29] '      by calculating the slope of dotlines-label which are used to '
[30] '      rotate and then translate the rough X and Y coord. data.'
[31] '      '
[32] 'PRESS ENTER TO CONTINUE.'
[33] PAUSE+D
[34] '      '
[35] 'DWRITE: This function makes the writing of your displacement data.'
[36] '      '
[37] 'DREAD: This function makes the reading of your displacement data.'
[38] '      '
[39] 'RENAME: This function renames your data file, if necessary.'
[40] '      '
[41] 'MISTAKE: This function replace wrong data in your data file. To use this'
[42] '      function you must have obtained your correct data previously.'
[43] '      To obtain the correct data you must go in the DOTDTZ procedure.'
[44] '      Then, you type it in.'
[45] '      '
[46] 'ERASE: This function erases wrong data file.'
[47] '      '
[48] '      '
[49] '      '
[50] 'PRESS ENTER TO CONTINUE.'
[51] PAUSE+D
[52] '      '
[53] '      SUGGESTIONS FOR DIGITIZING PROCEDURE. . .'
[54] '      '
[55] 'NOTE: For convenience during the digitizing procedure, follow the arrow'
[56] '      as stated below:'
[57] '      '
[58] '      '
[59] '      GRID PATTERN'
[60] '      '
[61] '      '
[62] '      '
[63] '      '
[64] '      '
[65] '      '
[66] '      '
[67] '      '
[68] '      '
[69] '      '
[70] '      '
[71] '      '
[72] '      '
[73] '      '
[74] '      '
[75] '      '
[76] '      '
[77] '      '
[78] '      '
[79] '      '
[80] '      '
[81] '      '
[82] '      '
[83] '      '
[84] '      '
[85] '      '
[86] '      '
[87] '      '
[88] '      '
[89] '      '
[90] '      '
[91] '      '
[92] '      '
[93] '      '
[94] '      '
[95] '      '
[96] '      '
[97] '      '
[98] '      '
[99] '      '
[100] '      '

```

[illegible]

```

DOTDTZ:
[10] DOTDTZ;N;NAME;AFB;DATA;TRANS;BUTTON;XVAL;YVAL;X;Y;I;MATRIX1;GO;INF;GAGEL;LENX;LENY
[11] MORE:'PRESS ENTER TO DIGITIZE THE LABEL or ** G ** FOR THE GRID-PATTERN:'
[12] BUFFER
[13] GO=0  $\diamond$   $\rightarrow$  (GO='G')/JUMP1
[14] LABELDTZ
[15] JUMP1:'HOW MANY DOTS DO YOU WISH TO DIGITIZE PER GRID-PATTERN?'  $\diamond$  N1=0
[16] 'HOW MANY MEASUREMENTS PER DOT DO YOU WISH TO DIGITIZE?'  $\diamond$  N=0
[17] 'START DIGITIZING THE GRID-PATTERN'  $\diamond$  I1=0  $\diamond$  XX=YY=N1=0
[18] LOOP1:I=0  $\diamond$  ARB=(N,30)=0  $\diamond$  X=Y=N=0
[19] LOOP:I=I+1
[100] ARB[I];I= 1 1 1 0 1 30 DARBIN ''  $\diamond$  DSOUND 4500 100
[110] DATA=ARB[I];
[120] DATA=DATA[(DATA/I3)+1]+I/I3]
[130] TRANS=DATA[DATA+DIO]
[140] BUTTON=I+TRANS
[150] ('THE BUTTON PRESSED WAS '),BUTTON
[160] XVAL=((TRANS[I2+I5])=100)*2.54  $\diamond$  YVAL=((TRANS[I8+I5])=100)*2.54
[170] ('THE X,Y COORD. OF THE DOT IS ',(XVAL),( ' '), (YVAL)
[180] XI[I]=XVAL
[190] YI[I]=YVAL
[200]  $\rightarrow$  (I<N)/LOOP  $\diamond$  DSOUND 3000 300
[210] I1=I1+1
[220] XX[I1]=(+/X)=X  $\diamond$  YY[I1]=(+/Y)=Y  $\diamond$   $\rightarrow$  (I1<N1)/LOOP1
[230] '***** THE X,Y COORD. OF THE DOTS ARE (in mm) *****'
[240] MATRIX1=XX,[1.5]YY  $\diamond$  MATRIX1  $\diamond$  DSOUND 3000 300  $\diamond$  FY
[250] 'Tension or Cyclic, Exp. No., H or L or HS, Machine Plane, Sample No.'
[260] 'ENTER NAME OF THE NEW FILE TO STORE THIS DATA:(Drive Number then File)'
[270] NAME=0  $\diamond$  NAME OFCREATE 1951  $\diamond$  MATRIX1 OFAPPEND 1951
[280] 'DO YOU WANT INPUT A GAGEL, LENX AND LENY FOR THIS FILE?(if not type N)'
[290] INF=0  $\diamond$   $\rightarrow$  (INF='N')/JUMP
[300] 'ENTER THE GAGE LENGTH FOR THIS FILE:'  $\diamond$  GAGEL=0
[310] 'ENTER THE LENX FOR THIS FILE:'  $\diamond$  LENX=0
[320] 'ENTER THE LENY FOR THIS FILE:'  $\diamond$  LENY=0
[330] GAGEL OFAPPEND 1951  $\diamond$  LENX OFAPPEND 1951  $\diamond$  LENY OFAPPEND 1951
[340] JUMP:OFUNTIE 1951  $\diamond$  'DO YOU WISH TO CONTINUE DIGITIZING? (Y or N)'
[350]  $\rightarrow$  ('Y'=1+0)=MORE
[360] OPTIONS
[370]  $\nabla$ 

```

```

BUFFER:
[10] BUFFER;R
[11] ATHIS FUNCTION EMPTIES DATA IN BUFFER.
[12] R= 1 1 1 0 0 32000 DARBIN ''  $\diamond$  DERAISE 'R'
[13]  $\nabla$ 

```

```

      ▽LABELDTIME
[00] LABELDTIME:NAME;ARB;DATA:TRANS:BUTTON:XVAL:YVAL;X:Y;I;MATRIX1
[11] 'HOW MANY DOTS DO YOU WANT TO DIGITIZE FOR THE LINE-LABEL?' ◊ N1+0
[12] 'HOW MANY MEASUREMENTS PER DOT DO YOU WISH TO DIGITIZE?' ◊ N+0
[13] 'START DIGITIZING THE DOTLINE-LABEL' ◊ I1+0 ◊ XX+YY+N1+0
[14] LOOP1:I+0 ◊ ARB+(N,30)+0 ◊ X+Y+N+0
[15] LOOP:I+I+1
[16] ARB[I;J]+ 1 1 1 0 1 30 DARBIN '' ◊ DSOUND 4500 100
[17] DATA+ARB[I;J]
[18] DATA+DATA[(DATA+13)+1)+1+13]
[19] TRANS+DATA+DATA+0101
[100] BUTTON+1+TRANS
[111] ('THE BUTTON PRESSED WAS '),BUTTON
[121] XVAL+((TRANS[2+15])÷100)×2.54 ◊ YVAL+((TRANS[3+15])÷100)×2.54
[131] ('THE X,Y COORD. OF THIS DOT IS ',(XVAL),(YVAL))
[141] X[I;J]+XVAL
[151] Y[I;J]+YVAL
[161] +(I(N)/LOOP ◊ DSOUND 3000 300
[171] I1+I1+1
[181] XX[I1]+(X/X)÷pX ◊ YY[I1]+(Y/Y)÷pY ◊ +(I1(N1)/LOOP1
[191] '***** THE X,Y COORD. OF THE DOTLINE IS (in mm) *****'
[201] MATRIX1+XX,[1.5]YY ◊ MATRIX1
[211] DSOUND 3000 300 ◊ FY
[221] 'LB,Tension or Cyclic, Exp. No.,H or L or S, Machine Plane, Sample No.'
[231] 'ENTER NAME OF THE NEW FILE TO STORE THIS DATA:(Drive Number then File)'
[241] NAME+0 ◊ NAME OFCREATE 1951
[251] MATRIX1 OFAPPEND 1951 ◊ OFUNTIE 1951

```

```

      ▽CORR[0]
[00] CORR
[11] 'ENTER LABEL FILE NAME TO READ:' ◊ LABEL+0
[21] LABEL OFTIE 1954 ◊ MATRIX1+OFREAD 1954,1 ◊ OFUNTIE 1954
[31] MATX+MATRIX1[;1] ◊ MATY+MATRIX1[;2]
[41] MATX+MATX-((+/MATX)÷pMATX) ◊ MATY+MATY-((+/MATY)÷pMATY)
[51] SOMXY+(MATX×MATY) ◊ SOMXY+(+/SOMXY) ◊ SOMX+(MATX×2) ◊ SOMX+(+/SOMX)
[61] SOMY+(MATY×2) ◊ SOMY+(+/SOMY) ◊ r+SOMXY÷((SOMX×SOMY)+0.5)
[71] r
[81] EQ+MATRIX1[;2]÷MATRIX1[;1]×0.1 ◊ 0 1 ◊ MATXST+EQ[1]+(EQ[2]×MATRIX1[;1])
[91] DEVY+(MATRIX1[;2]-MATXST)×2 ◊ SY+((+/DEVY)÷(MATRIX1[;1]-2))×0.5
[101] MATXAUG+(+/MATRIX1[;1])÷MATRIX1[;1] ◊ DEVX+(MATRIX1[;1]-MATXAUG)×2
[111] SOMDEVX+(+/DEVX)×0.5 ◊ SB+SY÷SOMDEVX ◊ T+(((EQ[2])×2)×0.5)÷SB
[121] T
[131] ▽

```

```

      *FREAD2[00]
[00] FREAD2;NAME:GAGEL;GO:A;PAUSE;B;LENX;LENY;EXIT
[10] 'DO YOU WANT TO SEE THE DATA IN CONDENSED MATRIX FORM? (If not, type N)'
[20] GO=D *+(GO='N')/JUMP
[30] BEGIN: *FY
[40] 'ENTER THE NAME OF THE FILE TO BE READ:' *NAME=D
[50] NAME DFTIE 1951
[60] GAGEL*DFREAD 1951,2 * 'THE GAGEL FOR THIS FILE IS:' * GAGEL
[70] LENX*DFREAD 1951,3 * 'THE LENX FOR THIS FILE IS:' * LENX
[80] LENY*DFREAD 1951,4 * 'THE LENY FOR THIS FILE IS:' * LENY
[90] 'PRESS ENTER TO CONTINUE:' * PAUSE=D
[100] '***** THE X COORD. OF THE GRID ARE *****'
[110] NAME*DFREAD 1951,1 * A+NAMEC;13 * A*(LENX,LENY)*A * A *
[120] 'PRESS ENTER TO CONTINUE' * PAUSE=D
[130] '***** THE Y COORD. OF THE GRID ARE *****'
[140] B+NAMEC;23 * B*(LENX,LENY)*B * B *
[150] 'PRESS ENTER TO CONTINUE' * PAUSE=D
[160] DFUNTIE 1951
[170] 'IS IT THE FILE THAT YOU WANT TO USE? (IF NOT, AND IF YOU WANT TO TRY'
[180] 'AN OTHER ONE TYPE THE LETTER N.)'
[190] EXIT=D *+(EXIT='N')/BEGIN
[200] *END
[210] JUMP:FREAD1
[220] END:
[230] OPTIONS

```

```

      *FREAD1[00]
[00] FREAD1;NAME:SC;NC;IC;I;PAUSE;EXIT
[10] BEGIN:
[20] FY
[30] 'ENTER THE NAME OF THE FILE TO BE READ:' *NAME=D
[40] NAME DFTIE 1951
[50] 'ENTER THE STARTING COMPONENT TO BE READ:' *SC=D
[60] 'ENTER THE NUMBER OF COMPONENT TO BE READ:' *NC=D
[70] 'ENTER THE INCREMENT IN COMPONENT TO BE READ:' *IC=D
[80] I=SC-IC
[90] LOOP:I+I+IC *+(I=2)/JUMP2 *+(I=3)/JUMP3 *+(I=4)/JUMP4
[100] ('***** X, Y COORD. OF THE GRID NUMBER ',(I),(' ARE *****')) *+JUMP
[110] JUMP2:'THE GAGE LENGTH FOR THIS FILE IS:' *+JUMP
[120] JUMP3:'THE LENX FOR THIS FILE IS:' *+JUMP
[130] JUMP4:'THE LENY FOR THIS FILE IS:' *+JUMP
[140] JUMP:NAME*DFREAD 1951,1
[150] NAME * ' ' * 'PRESS ENTER TO CONTINUE' * PAUSE=D
[160] *(I*(SC+(NC-1)*IC)/LOOP
[170] DFUNTIE 1951
[180] 'IS THAT THE FILE THAT YOU WANT TO USE? (IF NOT, AND IF YOU WANT TO TRY'
[190] 'AN OTHER ONE TYPE THE LETTER N.)'
[200] EXIT=D *+(EXIT='N')/BEGIN
[210] *

```

```

      *FYLDB
[100] FY
[110] FILE=DFLIB 1 * FILE=FILE;(8+(100) * F1+DFLIB 1 * F+FILE10*10 * IN+(F+80)
[120] FILE=(F)*FILE * T+(IN*80)-F * FILE*(T/4) '
[130] FILE=FILE.FIL * FILE=(IN.80)*FILE * FILE
[140] *

      *DWRITEID3
[200] DWRITE
[210] BEGIN: * FY0
[220] ALIGN3
[230] D+(((X1-X0)*2)+((Y1-Y0)*2))*0.5 * +((Y1-Y0)=0)/JUMP1
[240] THETA+(((300((Y1-Y0)+(X1-X0))*180)+91
[250] 'DO YOU WANT TO SEE THE DATA? (if not type N)' * SEE=* * +((SEE='N')/JUMP
[260] '***** DISPLACEMENT VALUES(in mm) *****' * DD+(LENX,LENY)*D * 7 3 *DI
[270] ' ' * 'PRESS ENTER TO CONTINUE' * PAUSE*D * '
[280] '***** ANGLE VALUES(in degree) *****' * TT+(LENX,LENY)*THETA * 7 3 *TT
[290] ' ' * 'PRESS ENTER TO CONTINUE' * PAUSE*D * ' * +JUMP
[300] JUMP1: '*** THERE IS NO DISPLACEMENT VECTOR, and NO DISPLACEMENT ANGLE ***'
[310] JUMP:DFUNTIME 1951,1952 * DFUNTIME 1954,1955
[320] 'IS IT THE DATA FILE THAT YOU WANT TO USE?(if not, and if you want to try'
[330] 'an other one type the letter N)'
[340] GO=* * +((GO='N')/BEGIN
[350] DFLIB 1
[360] ORDER=ORDER+1
[370] '
[380] 'ARE YOU SURE THAT YOU WANT TO CREATE A NEW FILE? (if not type N)'
[390] CH=* * +((CH='N')/0
[400] '
[410] 'ENTER NAME OF THE FILE TO STORE THIS DATA: (Give no. then File)'
[420] NAME=* * NAME DFCREATE ORDER * NAME DFAPPEND ORDER
[430] '
[440] 'ENTER THE NAME OF THE SAMPLE:'
[450] COM1+' Sample Name: ',*
[460] 'ENTER THE DATE:'
[470] COM2+' *** Date: ',*
[480] 'ENTER THE NATURE OF THE TEST, (Tension, Cyclic):'
[490] COM3+' *** Test in: ',*
[500] 'ENTER YOUR FIRST NAME:'
[510] COM4+' Proces. by: ',*
[520] 'ENTER THE CROSS HEAD STRAIN, and EXPOSURE NUMBER:'
[530] COM5+' *** Cross Head strain, and Exp. No.: ',*
[540] 'IF YOU WANT ENTER SOME SPECIAL COMMENTS:'
[550] COM6+' Spec. Comments: ',*
[560] COM=COM1, COM2, COM3, COM4, COM5, COM6
[570] COM DFAPPEND ORDER
[580] LENX DFAPPEND ORDER * LENY DFAPPEND ORDER
[590] GAGEL DFAPPEND ORDER * GGS DFAPPEND ORDER
[600] D DFAPPEND ORDER * THETA DFAPPEND ORDER
[610] DFUNTIME ORDER
[620] '
[630] 'DO YOU WISH TO CONTINUE? (Y or N)'
[640] +('Y'=1)*BEGIN
[650] OPTIONS
[660] *

```

```

      @FYO[0]
[00] FYO
[10] FILE=@FLIB 0 0 FILE+FILE[;(8+10)] 0 FI=@DLIB 0 0 F+FI[10×10 0 IN+(F+80)
[20] FILE+(F)@FILE 0 T+(IN×80)-F 0 FI+(T)@' '
[30] FILE+FILE,FI 0 FILE+(IN,80)@FILE 0 FILE

```

```

      @DREAD[0]
[00] DREAD;CASE;NUM;EXI;NOM;PAUSE;NAME;COMMENT;RESSPA;RESROT
[10] BEGIN:
[20] FYO 0 OFNUMS
[30] 'ENTER THE NAME OF THE FILE THAT YOU WANT TO READ:'
[40] NOM=@
[50] 'ENTER A FILE TIE NUMBER FOR THAT FILE:'
[60] NUM=@
[70] NOM OFTIE NUM
[80] '
[90] '
[100] NAME=@DREAD NUM,1 0 COMMENT=@DREAD NUM,2
[110] LENX=@DREAD NUM,3 0 LENY=@DREAD NUM,4
[120] GAGEL=@DREAD NUM,5 0 GGS=@DREAD NUM,6
[130] RESSPA=@DREAD NUM,7 0 RESROT=@DREAD NUM,8
[140] NAME
[150] '
[160] COMMENT
[170] '
[180] 'DO YOU WANT TO HAVE A LOOK ON THE INITIAL DATA ? (If not type a N). '
[190] CASE=@ 0 +(CASE='N')/POP
[200] '
[210] '***** DISPLACEMENT VALUES (in mm) *****'
[220] OUTPUT RESSPA
[230] 'PRESS ENTER TO CONTINUE.'
[240] PAUSE=@
[250] '
[260] '***** ANGLE VALUES (in degree) *****'
[270] OUTPUT RESROT
[280] 'PRESS ENTER TO CONTINUE.'
[290] PAUSE=@
[300] POP:
[310] '
[320] '
[330] '
[340] 'IS IT THE FILE THAT YOU WANT TO USE ? (If not, and if you want to try'
[350] 'an other one type a N.)'
[360] EXI=@ 0 +(EXI='N')/BEGIN
[370] OPTIONS
[380] ▽

```

```

      @OUTPUT[0]
[00] OUTPUT VECT:K;SUBS;PROD;INT;TABRES
[10] K+SUBS+PROD+0 @ INT+10 @ PROD+LENX*LENY
[20] SUBS+PROD-@VECT @ INT+VECT
[30] +(SUBS=0)/END
[40] LOOP:K+K+1
[50] INT+INT,0
[60] +(K(SUBS)/LOOP
[70] END:
[80] TABRES+(LENY,LENX)@INT @ 8 3 @ (QTABRES)
[90] ▽

```

```

      @RENAME[0]
[00] RENAME
[10] FY
[20] 'ENTER THE NAME OF THE FILE TO BE RENAMED:(Drive no. then File)' @ NAME+@
[30] NAME OFTIE 1951
[40] 'ENTER A NEW NAME FOR THIS FILE:(Drive no. then File)' @ NEWNAME+@
[50] NEWNAME OFRENAME 1951 @ OFUNTIE 1951
[60] OPTIONS
[70] ▽

```

```

      @ALIGN3[0]
[00] ALIGN3
[10] 'DO YOU WANT TO KEEP THE FIRST LABEL and FIRST GRID FILE?(If yes type Y)'
[20] GO+@ @ +(GO='Y')/JUMP1
[30] 'ENTER NAME OF THE **FIRST LABEL FILE** TO BE READ:' @ LABEL+@
[40] LABEL OFTIE 1954 @ LINEH+DFREAD 1954,1 @ x01+LINEH[;1] @ y01+LINEH[;2]
[50] HO+y01@x01+.* @ 1 @ THETAL+(-3)@ (HO[2])
[60] x01+LINEH[8;1] @ y01+LINEH[8;2] @ THETARP+(-3)@ (y01÷x01)
[70] DTHETA+(THETARP-THETAL) @ r+((x01*2)+(y01*2))*0.5
[80] x01+r*(2@DTHETA) @ y01+r*(1@DTHETA) @ DIFX0+(250-x01) @ DIFY0+(300-y01)
[90] A -----
[100] 'ENTER NAME OF THE **FIRST GRID FILE** TO BE READ:' @ NAME+@
[110] NAME OFTIE 1951 @ NAME+DFREAD 1951,1 @ XO+NAME[;1] @ YO+NAME[;2]
[120] GAGEL+DFREAD 1951,2 @ LENX+DFREAD 1951,3 @ LENY+DFREAD 1951,4
[130] THETAD+(-3)@ (YO÷XO) @ r+((XO*2)+(YO*2))*0.5 @ DTHETA+(THETAD-THETAL)
[140] XO+r*(2@DTHETA) @ YO+r*(1@DTHETA) @ XO+DIFX0+XO @ YO+DIFY0+YO
[150] A -----
[160] JUMP1:'ENTER NAME OF THE **NEXT LABEL FILE** TO BE READ:' @ LABEL+@
[170] LABEL OFTIE 1955 @ LINEH+DFREAD 1955,1 @ x01+LINEH[;1] @ y01+LINEH[;2]
[180] HO+y01@x01+.* @ 1 @ THETAL+(-3)@ (HO[2])
[190] x01+LINEH[8;1] @ y01+LINEH[8;2] @ THETARP+(-3)@ (y01÷x01)
[200] DTHETA+(THETARP-THETAL) @ r+((x01*2)+(y01*2))*0.5
[210] x01+r*(2@DTHETA) @ y01+r*(1@DTHETA) @ DIFX1+(250-x01) @ DIFY1+(300-y01)
[220] A -----
[230] 'ENTER NAME OF THE **NEXT GRID FILE** TO BE READ:' @ NAME+@
[240] NAME OFTIE 1952 @ NAME+DFREAD 1952,1 @ XI+NAME[;1] @ YI+NAME[;2]
[250] THETAD+(-3)@ (YI÷XI) @ r+((XI*2)+(YI*2))*0.5 @ DTHETA+(THETAD-THETAL)
[260] XI+r*(2@DTHETA) @ YI+r*(1@DTHETA) @ XI+DIFX1+XI @ YI+DIFY1+YI
[270] ▽

```


✶MISTAKE00

```

001 MISTAKE;I;VALUE;GAGEL;LENX;LENY;GO;DATA;A;R;C;B;N;MATRIX1
011 BEGIN:FY
021 'ENTER THE NAME OF THE FILE TO CORRECT:(Drive no. then File)' & NAME&D
031 NAME DFTIE 1951
041 CONT:'PRESS ENTER TO CORRECT INITIAL PARAMETERS or TYPE D TO CORRECT DATA:'
051 GO&D & +(GO='D')/JUMPD
061 MORE:'ENTER, 2 TO MODIFY GAGEL, 3 TO MODIFY LENX, 4 TO MODIFY LENY:' & I&D
071 'THE PRESENT VALUE IS:' & NAME&DREAD 1951,1 & NAME
081 'ENTER YOUR NEW VALUE TO BE REPLACED:' & VALUE&D & VALUE DFREPLACE 1951,1
091 'DO YOU WANT TO CORRECT MORE? (Y or N)' & +( 'Y'=1&D)&MORE
101 GAGEL&DREAD 1951,2 & 'THE NEW GAGEL FOR THIS FILE IS:' & GAGEL
111 LENX&DREAD 1951,3 & 'THE NEW LENX FOR THIS FILE IS:' & LENX
121 LENY&DREAD 1951,4 & 'THE NEW LENY FOR THIS FILE IS:' & LENY
131 'DO YOU WANT TO CONTINUE?(If not type N)' & GO&D & +(GO='N')/END & +YES
141 JUMPD:GAGEL&DREAD 1951,2 & LENX&DREAD 1951,3 & LENY&DREAD 1951,4
151 YES:'***** THE X COORD. OF THE GRID IN MATRIX FORM ARE *****'
161 DATA&DREAD 1951,1 & A&DATA[;1] & A&(LENX,LENY)&A & A & ''
171 'PRESS ENTER TO CORRECT ENTIRE X-ROW or P TO CORRECT INDIVIDUAL X-ELEMENT:'
181 GO&D & +(GO='P')/JUMPX
191 'ENTER THE ROW LOCATION NUMBER TO BE CORRECTED:' & R&D
201 'ENTER THE VALUES IN A VECTOR FORM:' & VALUE&D & A&R;]+VALUE
211 JUMPA:'** THE NEW X COORD. OF THE GRID IN MATRIX FORM ARE **' & A & +JUMP1
221 JUMPX:'ENTER A ROW AND THEN A COLLUMN LOCATION NUMBER FOR THAT ELEMENT:'
231 R&D & C&D & 'ENTER THE VALUE FOR THAT ELEMENT:' & VALUE&D
241 A&R;C]+VALUE & +JUMPA
251 JUMP1:' ' & '***** THE Y COORD. OF THE GRID IN MATRIX FORM ARE *****'
261 B&DATA[;2] & B&(LENX,LENY)&B & B & ''
271 'PRESS ENTER TO CORRECT ENTIRE Y-ROW or P TO CORRECT INDIVIDUAL Y-ELEMENT:'
281 GO&D & +(GO='P')/JUMPY
291 'ENTER THE ROW LOCATION NUMBER TO BE CORRECTED:' & R&D
301 'ENTER THE VALUES IN A VECTOR FORM:' & VALUE&D & B&R;]+VALUE
311 JUMPB:'** THE NEW Y COORD. OF THE GRID IN MATRIX FORM ARE **' & B & +JUMP2
321 JUMPY:'ENTER A ROW AND THEN A COLLUMN LOCATION NUMBER FOR THAT ELEMENT:'
331 R&D & C&D & 'ENTER THE VALUE FOR THAT ELEMENT:' & VALUE&D
341 B&R;C]+VALUE & +JUMPB
351 JUMP2:N&(LENX)x(LENY) & A&(N,1)&A & B&(N,1)&B & MATRIX1&A,B
361 MATRIX1 DFREPLACE 1951,1
371 'DO YOU WANT TO CONTINUE CORRECTING THIS FILE? (If yes type Y )'
381 GO&D & +(GO='Y')/CONT
391 END: & DFUNTIE 1951
401 'DO YOU WANT TO CORRECT OTHER FILES? (Y or N)'
411 +( 'Y'=1&D)&BEGIN
421 OPTIONS

```

✶ERASE00

```

001 ERASE
011 FY
021 'ENTER THE NAME OF THE FILE TO BE ERASED:(Drive no. then File)' & NAME&D
031 NAME DFTIE 1951 & NAME DFERASE 1951 & DFUNTIE 1951
041 OPTIONS
051 ?

```

```

      WWSPRINTED]
[00] WSPRINT;CR;ANS;NAME;NN;I;TEMP;F;LN;M;LINES;PAGE;FN;WS;PG;PAGES;BLOCK
[10] CR+DTCLF
[20] ANS+ASK '      PRINT ALL FUNCTIONS IN YOUR WS ? '
[30] +( 'N'=1+ANS)/LO
[40] NAME+DNL 3
[50] NAME+NAME[4,71]Q(' ',DAVE[86+170])\NAME;]
[60] NN+1+NAME
[70] +START
[80] LO:NN+ASK '      ENTER NUMBER OF FUNCTIONS TO PRINT : '
[90] NAME+(NN,15)Q' '
[100] I+1
[110] L1:TEMP+(ASK '      ENTER NAME OF FUNCTION ',(20+31),' : ')
[120] NAME[I;J+15+TEMP,15]Q' '
[130] +L1+1NN[21+I+1
[140] START:'      SET PAPER TO NEW PAGE , ENTER ' Q E
[150] I+1
[160] L2:F+OCR NAME[I;J
[170] N+1+QF
[180] LN+3Q(1,N)QO,\N-1
[190] LN+((N,1)Q'('),LN,(N,1)Q')'
[200] M+LN,((N,2)Q' '),F
[210] M[I;J5]Q' ' Q M[I;5]Q'Q'
[220] LINES+LN
[230] PAGE+Q
[240] FN+(50Q' '),('FUNCTION : '),NAME[I;J
[250] WS+(50Q' '),('WORKSPACE : '),11+DWSID
[260] PG+(50Q' '),('PAGE : ')
[270] PAGES+FN+50
[280] L3:LINES+((PAGE+Q)X50)+LINES
[290] +L4+1502Q LINES
[300] BLOCK+LINES[150]
[310] +L5
[320] L4:BLOCK+LINES
[330] L5:PAGE+PAGE+1
[340] 1QCR Q FN Q WS Q PG,(3PAGE),'/',3PAGES Q 1QCR
[350] M[BLOCK;]
[360] 8QCR
[370] +L3+1PAGES>PAGE
[380] +(50+QBLOCK)/END
[390] (49-QBLOCK)QCR
[400] END:+L2+1NN[21+I+1
[410] ' ' Q '      END OF JOB '
[420] Q

```

```

      WASK[0]
[00] Z+ASK N
[10] Q+N+,N
[20] Z+(QN)+Q
[30] Q

```

CHAPTER 4

EXPERIMENTAL MEASUREMENTS: PRECISION AND ACCURACY OF THE DOT MATRIX TECHNIQUE

- 4.1. Introduction
- 4.2. Errors in the Determination of Applied Load
- 4.3. Errors in the Determination of Cross-sectional Area of
the Specimens
 - 4.3.1. Errors in Width Determination
 - 4.3.2. Errors in Thickness Determination
- 4.4. Errors in Strain Computations
 - 4.4.1. Errors in the Determination of Modulus of
Elasticity due to Strain Computations
 - 4.4.2. Errors in the Determination of the Axial Strain
Field
 - 4.4.3. Errors in the Determination of Lateral
Contraction Ratios
- 4.5. Effect of Moisture Content of the Exposed Photograph
Films on Data Processing
- 4.6. Final Remarks
- 4.7. Literature

4.1. INTRODUCTION

The objective of this chapter is to quantify errors that can affect the accuracy and precision of measurements. We are concerned with the fact that if we measure something repeatedly we obtain different results, even if our determinations are made under conditions controlled as closely as possible. To characterize the measurements of testing procedures, a distinction should be made between accuracy and precision [1]. Accuracy is the closeness of measurements to the "true" or actual value of the quantity being measured. In other words, it is the difference between the test value and the true value. It is not always practical to measure accuracy because the "true value" must be determined by some idealized method. The term precision refers to the closeness with which the measurements agree with each other. This is a measure of the variation that can be expected when repeated tests are made on the same specimen.

Precision errors are sometimes called random or accidental errors, which can be evaluated by applying certain statistical concepts and techniques. Accuracy errors are referred to as systematic errors and are usually reduced through calibration, which will improve the performance of the measuring device [2]. In cases where a systematic error is not completely eliminated, it then becomes part of the random

error or uncertainty and is therefore assessed statistically [3, 4].

If one accepts the statistical parameters that describe the characteristics of a distribution of data that are associated with accuracy and precision, the errors of our experiment may be described by using simple statistic procedures rather than more sophisticated error analysis. If we describe the data deviation about the mean (\bar{X}) to be $[\bar{X} \pm (1.96 \times \text{standard deviation})]$ as an error, there will be a 95% probability [5] that the results will fall in that interval. As it expresses the reliability of our estimate of a parameter, the narrower the interval, the more precise the estimate.

In our experimental approach, the sources of errors that could generate inaccuracies and imprecisions in our results may be grouped in two categories: sources associated with the data acquisition for stress computation, and those occurring in the data processing for strain analysis. However, they are interactive; also, they may occur randomly and unpredictably during data acquisition. For example, the modulus of elasticity, E , is calculated from the stress-strain curve as follows:

$$E = \sigma / \epsilon \quad \sigma = F/A, \text{ then, } E = (F/A)/\epsilon$$

Therefore, the precision in E depends on the accuracy of the determination of the force F , the cross-sectional area A , and the technique for the measurement of the strain ϵ .

4.2. ERRORS IN THE DETERMINATION OF APPLIED LOAD

The force F (LOAD) was calculated by using the average calibration equation obtained from 20 calibrations. The standard estimation error of the equation is 0.446g. The standard deviation of the standard estimation error of F , calculated from 20 calibration equations, is 0.092g. Therefore, an error of $[0.446 \pm (1.96 \times 0.092g)]$ can be expected when F is calculated. It represents less than 2% of the failure load for CD test specimens and a negligible percentage for MD and handsheet specimens.

The correlation coefficient of the output of the load cell to the calibration weights was 0.9999, in all cases, during the calibration procedure.

4.3. ERRORS IN THE DETERMINATION OF CROSS-SECTIONAL AREA OF THE SPECIMENS

The errors involved in the calculation of the cross sectional area of the specimens may be grouped into two categories: (a) error in width measurements, and (b) error in thickness determination.

4.3.1. ERRORS IN WIDTH DETERMINATION

The error of measurement of the width of the specimens was calculated from a series of measurements made on one specimen. The mean (\bar{X}) value of the measurements is 20.11mm, and the standard deviation equals 0.045mm. The ratio of the standard deviation to the mean value of the measurements is less than 0.3%. Therefore, a deviation from the mean equal to $[\bar{X} \pm (1.96 \times 0.045\text{mm})]$ can be expected. This small error occurs because of the softness of the paper specimens used in this study, which made it difficult to position the micrometer on the exact edges of the specimen without bending it.

4.3.2. ERRORS IN THICKNESS DETERMINATION

As described in item 3.4, chapter 3, the thicknesses of the specimens were determined by use of an ocular microscope scale, which we consider reasonably accurate for our purpose. Here we attribute most of the variability of data to the heterogeneity of paper rather than to the accuracy and precision of the instrumental measurements; if such

errors do occur, they are masked by the effect of non-homogeneity of the sheet thickness. Ten sets of 80 data points each were taken for the thickness measurement of a given specimen by following the sampling procedure illustrated in Fig. 6 in chapter 3. For each set of data (80 data points), a mean thickness value and standard deviation were determined. Again, a mean of the mean thickness and of the standard deviation were calculated. The ratio of the standard deviation to the mean is 6.8%, which defines the variation in our data acquisition procedure.

4.4. ERRORS IN STRAIN COMPUTATIONS

The main source of strain computation errors may be the digitizing procedure used to collect the displacement data for strain calculations, where the influence of personal decisions might take place. As described in item 3.5 in chapter 3, the image of the dot matrix is enlarged onto a digitizing table and the dots are digitized by locating the digitizer cursor in the center of the dot. The cursor contains crosshairs to guide the operator in placing it at the center. However, the dots are not always perfectly circular and in some cases their edges may appear fuzzy. Therefore, special

care and attention are required when digitizing.

To investigate the effect of personal decisions or bias in centering the cursor on the dot, four different digitizing procedures were devised and then performed on the same set of photographs taken from one specimen. For each procedure, the displacement data acquisition was independently repeated ten times (10 replications per digitizing procedure). Then the strain was computed for each individual replication. In fact, this method not only tests operator dependence; it also describes the precision and accuracy of the dot matrix technique in determining mechanical properties.

The differences in the four procedures are:

- a) procedure # 1: each individual dot was digitized only once over the entire matrix.
- b) procedure # 3: each individual dot was digitized three times consecutively, and the arithmetic mean of these three x-y values was considered the x-y coordinate for that specific dot.
- c) procedure # 5: in this case, each individual dot was digitized five times consecutively, and the arithmetic mean of these five x-y values was considered the x-y coordinate for that specific dot.
- d) procedure # 10: following the same procedure, each individual dot (over the entire matrix, 7x5

dots) was digitized ten times, and the arithmetic mean of these ten x-y values was considered the x-y coordinate for that specific dot.

4.4.1. ERRORS IN THE DETERMINATION OF MODULUS OF ELASTICITY DUE TO STRAIN COMPUTATIONS

The errors in the determination of the modulus of elasticity were obtained by reproducing ten stress-strain relationships for each individual digitizing procedure, corresponding to the number of replications per procedure. This was done only for one CD test specimen. The modulus of elasticity is the slope of the linear portion of the stress-strain relationship obtained for each individual replication carried out per procedure. However, in all cases, the same values of load applied to the specimen were used for stress computations. The corresponding axial strains during the test were calculated by measuring the displacement between only two dots located at the center of the test specimen, with a distance of 24mm between them. The results are shown in Table 1 and in graphic form in Figs. 1 through 5.

From Table 1 one can observe the improvement in the

data dispersion by comparing the statistical parameters that describe the characteristics of data distributions. However, the differences between procedures are very small, and the test for comparison of means proved not to be significant at the level of 5%.

Table 1. Moduli of Elasticity Obtained for Different Digitizing Procedures and their Characteristic Distributions.

	Procedure # 1	Procedure # 3	Procedure # 5	Procedure # 10
Replications	10	10	10	10
Mean (MPa)	7.572	7.617	7.625	7.639
Variance	0.0125	6.323E-3	4.078E-3	1.6118E-3
Standard Deviation	0.1117	0.0795	0.0638	0.0401
Coefficient of Variation (%)	1.545	1.043	0.836	0.525

As previously described, accuracy is referenced to a certain "true" value. However, in some situations the "true" value does not occur in practice. But, usually the mean value is accepted as a "true" or actual value [6]. This is the method applied in this study; the precision and accuracy of the four distinct digitizing procedures are shown in Fig. 1,

where the horizontal line across the data is the arithmetic mean of the entire population. Therefore, based on concepts of precision and accuracy, procedure # 1 is less precise than the others, but all of them are of similar reasonable accuracy. The arithmetic mean for each specific procedure was calculated, and is shown by the horizontal line across the respective data in Figs. 2 through 5. Again, procedure # 1 shows less precision than the others, and in this case, it appears to be less accurate as well. Procedure # 10 is more precise and accurate than the others, but in view of the small degree of improvement indicated in Table 1, it would seldom appear to be worth the large extra effort in data collection and processing.

4.4.2. ERRORS IN THE DETERMINATION OF THE AXIAL STRAIN FIELD

In the investigation of the precision and accuracy of the dot matrix technique in determining axial strain distributions, only one photograph of the strained specimen at approximately 1% strain was considered. However, with the use of a 7 x 5 grid and the average step parameters $STEPX = 1$ and $STEPLY = 1$ (as described in item 3.6, chapter 3) for the basic unit of strain calculations, a mean value of the strain field

was obtained. This was repeated ten times for each digitizing procedure used to collect the data. The ten mean values for each specific digitizing procedure are shown in graphic form in Figs. 6 through 10. The mean of these ten mean values and their characteristics of distribution are shown in Table 2.

Although the difference in means between procedures is not statistically significant at the 5% level, we should be careful in choosing a digitizing procedure, since the objective is to measure strains; one must consider if large or small displacements are to be measured, and whether a large or small number of data are to be collected.

The data dispersion about the mean of the entire population is shown in Fig. 6, and the data dispersion about

Table 2. Characteristic of Distribution of the Axial Strain Field.

	Procedure # 1	Procedure # 3	Procedure # 5	Procedure # 10
Replications	10	10	10	10
Mean (%)	1.045	1.038	1.046	1.045
Variance	6.378E-4	2.758E-4	1.804E-4	1.464E-4
Standard Deviation	0.0253	0.0166	0.0134	0.0121
Coefficient of Variation (%)	2.421	1.600	1.281	1.158

their individual means are shown in Figs. 7 through 10. From these figures we can see that all the procedures are accurate. However, from Table 2 one can observe that if procedure #1 is used, we run the risk of having an actual mean value for axial strain field in the range of $[1.045 \pm (1.96 \times 0.0253\%)]$. But the range of error for procedure #5 is $[1.046 \pm (1.96 \times 0.0134\%)]$ which corresponds to a reduction of almost 50% in error of precision. Therefore, if procedure # 1 is used for small strain measurements, a large precision error may be involved; this error can be significantly reduced if one of the other digitizing procedures is used.

4.4.3. ERRORS IN THE DETERMINATION OF LATERAL CONTRACTION RATIOS

Since the determination of lateral contraction ratios involves calculations of axial, lateral and shear strains to calculate the principal axes of strain, and consequently the principal strain components, the correct handling of the digitizing cursor is very important. The precision and accuracy of our experiment to determine this property is shown in Figs. 11 through 15. In these figures the data points represent a mean value obtained from a 7 x 5 grid.

STEPX = 2 and STEPY = 2 were used for the average step parameters to obtain the lateral contraction ratios, as described in item 3.6, chapter 3. Ten replications were done for each specific digitizing procedure. Procedure # 1 appears to be less accurate than the others.

The test of significance of the difference between averages of Table 3 data showed no difference between procedures. The F test for comparison of variance of data between procedures demonstrates it to be a case of heterogeneous variance only when procedure # 1 was compared with the others at the 5% significance level. As we consider the dispersion of the data about the mean errors in the range

Table 3. Characteristic of Distribution of Lateral Contraction Ratios.

	Procedure # 1	Procedure # 3	Procedure # 5	Procedure # 10
Replications	10	10	10	10
Mean	0.136	0.146	0.161	0.156
Variance	1.339E-3	3.743E-4	2.871E-4	2.376E-4
Standard Deviation	0.0366	0.01935	0.0169	0.0154
Coefficient of Variation (%)	26.91	13.25	10.50	9.87

of $[\bar{X} \pm (1.96 \times \text{standard deviation})]$, characteristic of each specific digitizing procedure, it is seen that such errors are not negligible. The use of digitizing procedure # 1 caused the highest variability of data. Although the use of the other digitizing procedures improved the reproducibility of the data (as can be seen by comparison of coefficients of variation), this error is still substantial. For instance, a coefficient of variation of 10.50% occurred using digitizing procedure # 5. Since the precision errors are random or accidental, we can attribute their occurrence to semi-automatic data processing of the photographs. We believe though, that this error can be substantially reduced if fully automatic data processing is used for the dot matrix technique.

4.5. EFFECT OF MOISTURE CONTENT OF THE EXPOSED PHOTOGRAPH FILMS ON DATA PROCESSING

Since the dimensional stability of photographic film may be affected by its moisture content, we set up an experiment in order to investigate this effect on the strain measurements. The lateral contraction ratio was the property chosen to be measured, since its determination involves calculations of two principal strain components; these strains

could be affected by longitudinal and transverse dimensional instability of the films.

In this experiment we used the same photographs and the same procedures used to calculate the lateral contraction ratios described in the previous item. However, in this case we varied the moisture content of the photographs (negatives). This was achieved by immersing photographs in water at 23 ± 1 C for one hour, after which the excess water was removed. Then the photographs were processed using digitizing procedure # 5. The mean value for the lateral contraction ratios obtained over the 7 x 5 grid was considered the datum for one replication. Ten replications were performed. This procedure was repeated using an immersion time of 24 hours.

The statistics for each treatment of the photographs are shown in Table 4. From this table, the test of significance of the difference between averages of the photographs immersed for one hour in water showed no difference from those conditioned according to ref. [7], at the level of 5% of significance. However, at this level the average for photographs immersed 24 hours in water is significantly different from the others.

In order to make comparisons between photographs immersed in water with those conditioned according to ref. [7], a plot of data and means is shown in Fig. 16. In this figure, all of the data for the 24-hour immersion samples are located below the horizontal line, which represents the mean

Table 4. Effect of Immersion in Water of the Exposed Photographs on the Characteristic Distribution of Lateral Contraction Ratios (L.C.R.).

	Conditioned	1 hour immersion	24 hours immersion
Replications	10	10	10
Mean L.C.R.	0.161	0.153	0.115
Variance	2.871E-4	3.955E-4	1.921E-4
Standard Deviation	0.0169	0.0199	0.0139
Coefficient of Variation (%)	10.50	13.01	12.09

of the data obtained for the photographs conditioned according to ref. [7]. Although 24 hours of immersion in water makes the acquired data lack accuracy, they are still precise. The moisture contents for the photographs conditioned according to ref. [7] and the treatments of 1 hour and 24 hours immersed in water were 1.41%, 4.14% and 10.92% respectively. The moisture content was determined from a set of 10 photographs according to the procedures of ref. [8].

4.6. FINAL REMARKS

Although we have conducted a relatively unsophisticated analysis of errors, we believe the results reported in this chapter provide a satisfactory understanding of the problems in analyzing the data.

Since the errors occur randomly in an unpredictable way over the entire system of data processing, we think it is inappropriate to algebraically add the errors from different sources, in order to determine the errors involved in the determination of one specific property. However, we should expect that, in general, the total error in computing one specific property would be the sum of separate contributions of the error from different sources. In fact, we show that a logical and indirect way of adding the separate contributions is to analyze the errors over the final properties to be measured.

Many sources of errors might be avoided or reduced if a fully automatic data processing system were available. Even though human judgement has many advantages, certainly human error is a factor to be considered in digitizing the coordinate data by the digitizing table used in this experiment. Certainly, the next step in potential future applications of the dot matrix system would be to improve the quality of data acquisition by the dot matrix technique.

4.7. LITERATURE

1. BEERS, Yardley. Introduction to the theory of error.
Reading, Mass., Addison-Wesley, 1957. 66p.
2. TOPPING, J. Errors of observation and their treatment.
New York, Reinhold Publ., 1960. 119p.
3. BENDAT, Julius S. & PIERSON, Allen G. "Statistical errors
in random data analysis." In: Random data: Analysis and
measurement procedures. New York, Wiley-Interscience,
1971. chapter 6, pp. 170-213.
4. WOODWARD, Robert S. Probability and theory of errors.
4th.ed. New York, J. Wiley, 1906. 47p. (Mathematical
Monographs, no. 7)
5. KENNEDY, John B. & NEVILLE, Adam M. "Use of normal
distribution." In: Basic statistical methods for
engineers and scientists. 3rd. edition. New York,
Harper & Row, 1986. chapter 11, pp. 190-232, especially
section "Confidence interval estimation", pp. 209-215.
6. BARFORD, N.C. Experimental measurements: Precision, error
and truth. 2nd.ed. Chichester, J. Wiley, 1987. 159p.
7. TAPPI T 402. Standard conditioning and testing atmospheres
for papers, board, pulp handsheets and related products,
TAPPI, 1982.
8. TAPPI T 412 om-83. Moisture in paper and paperboard. TAPPI,
1983. 2p.

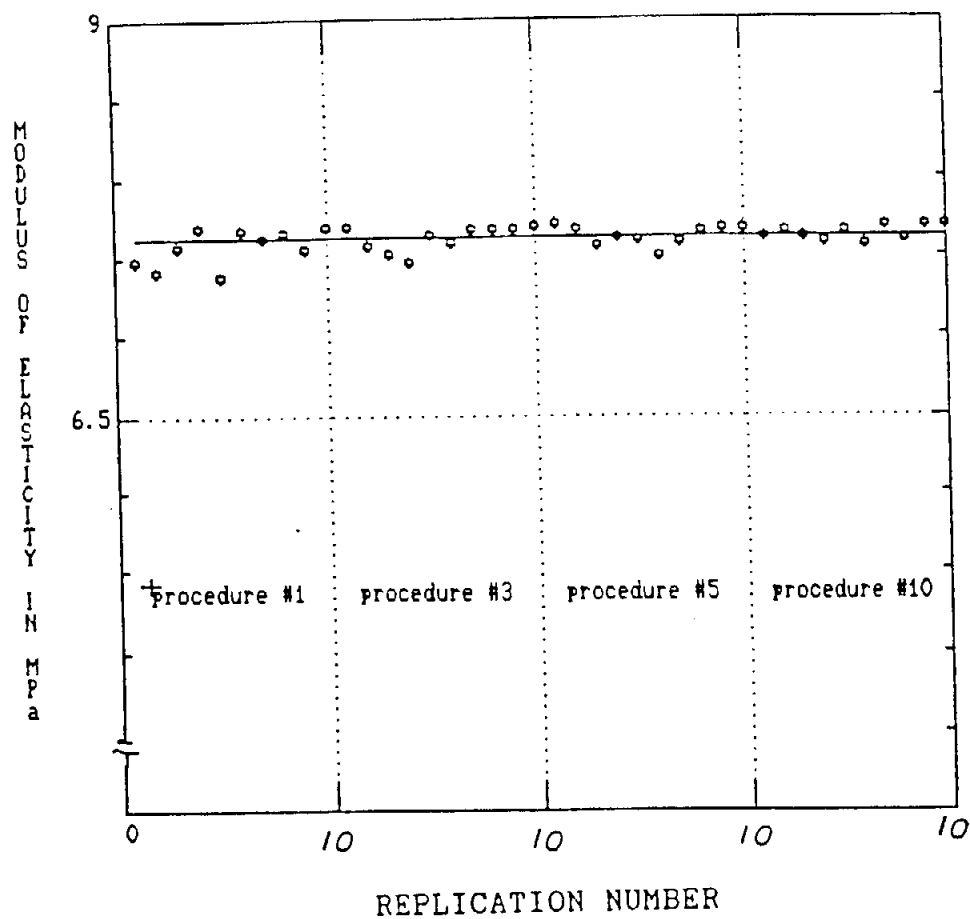


Fig. 1. Precision and accuracy of four digitizing procedures for the determination of modulus of elasticity.

Horizontal line= mean value of the entire data ("true" mean of the population).

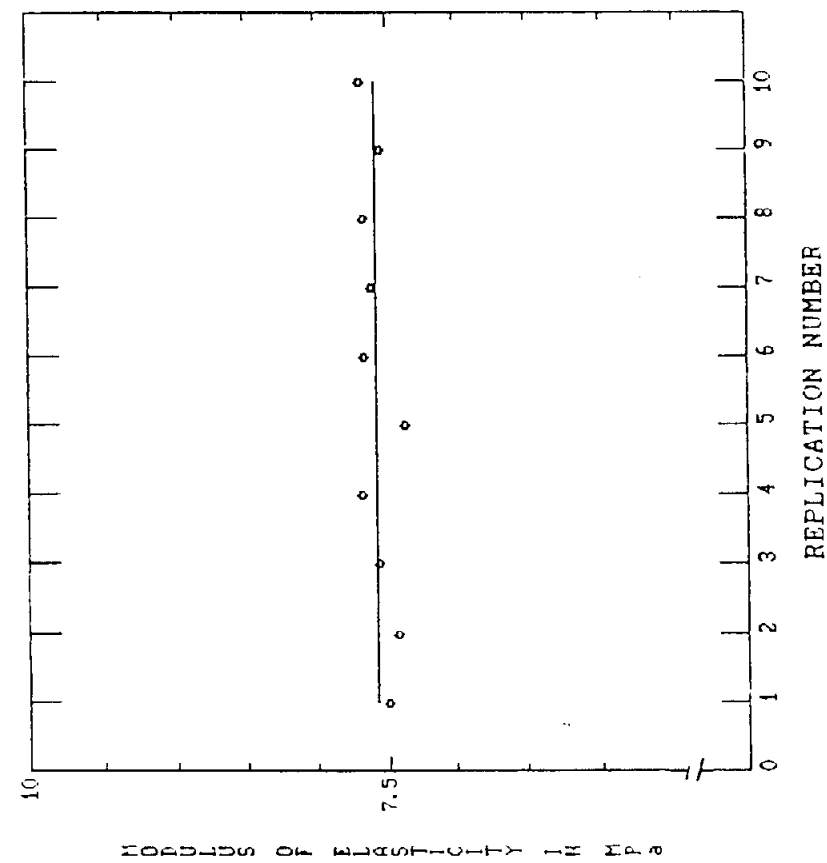


Fig. 2. Precision and accuracy in the determination of modulus of elasticity using digitizing procedure #1.
Horizontal line= mean.

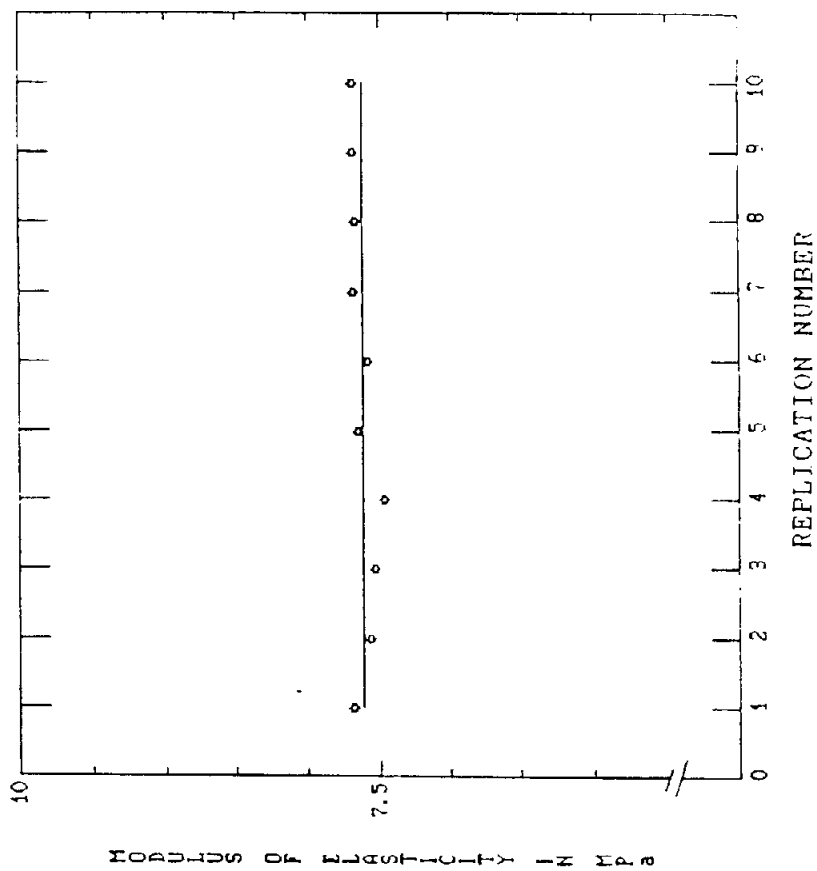


Fig. 3. Precision and accuracy in the determination of modulus of elasticity using digitizing procedure # 3.
Horizontal line= mean.

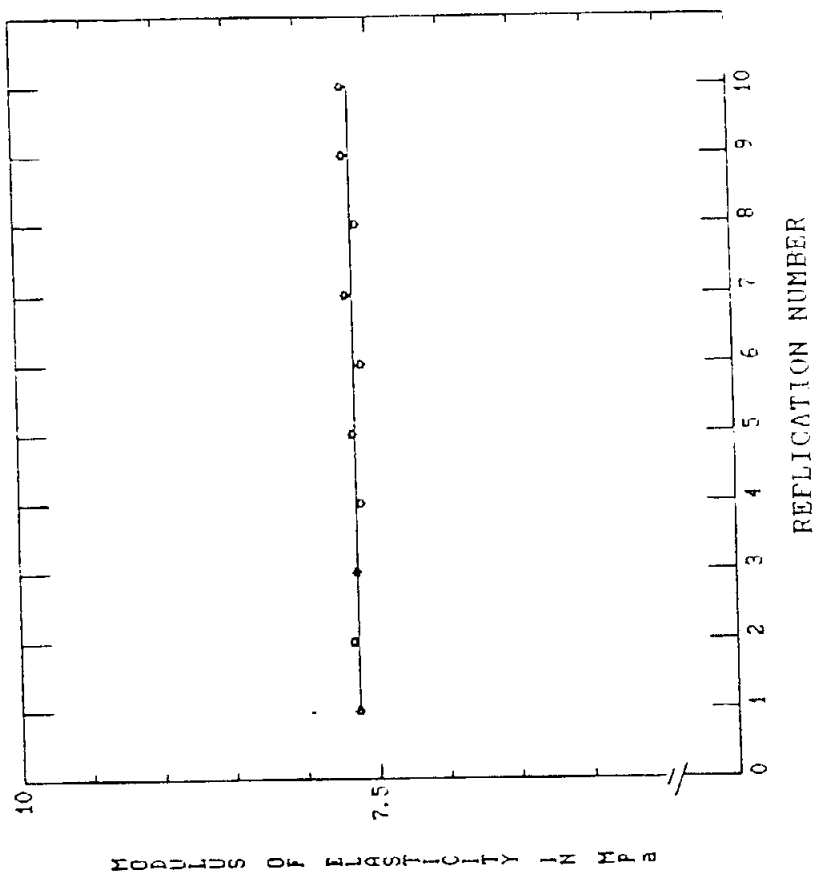


Fig. 5. Precision and accuracy in the determination of modulus of elasticity using digitizing procedure #10. Horizontal line= mean.

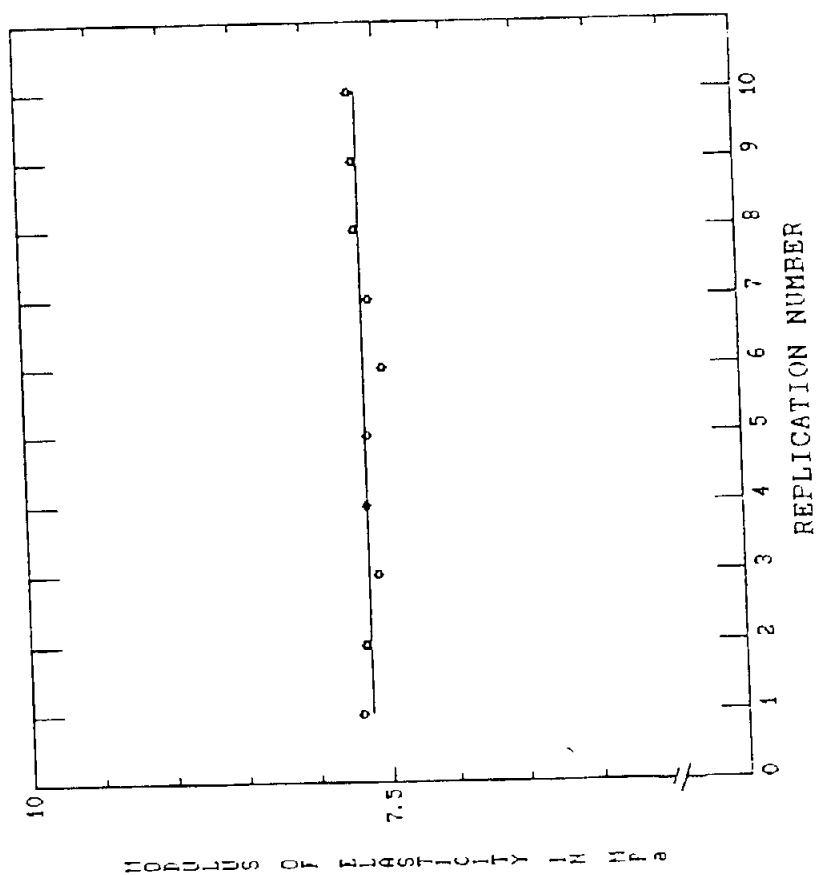


Fig. 4. Precision and accuracy in the determination of modulus of elasticity using digitizing procedure #5. Horizontal line= mean.

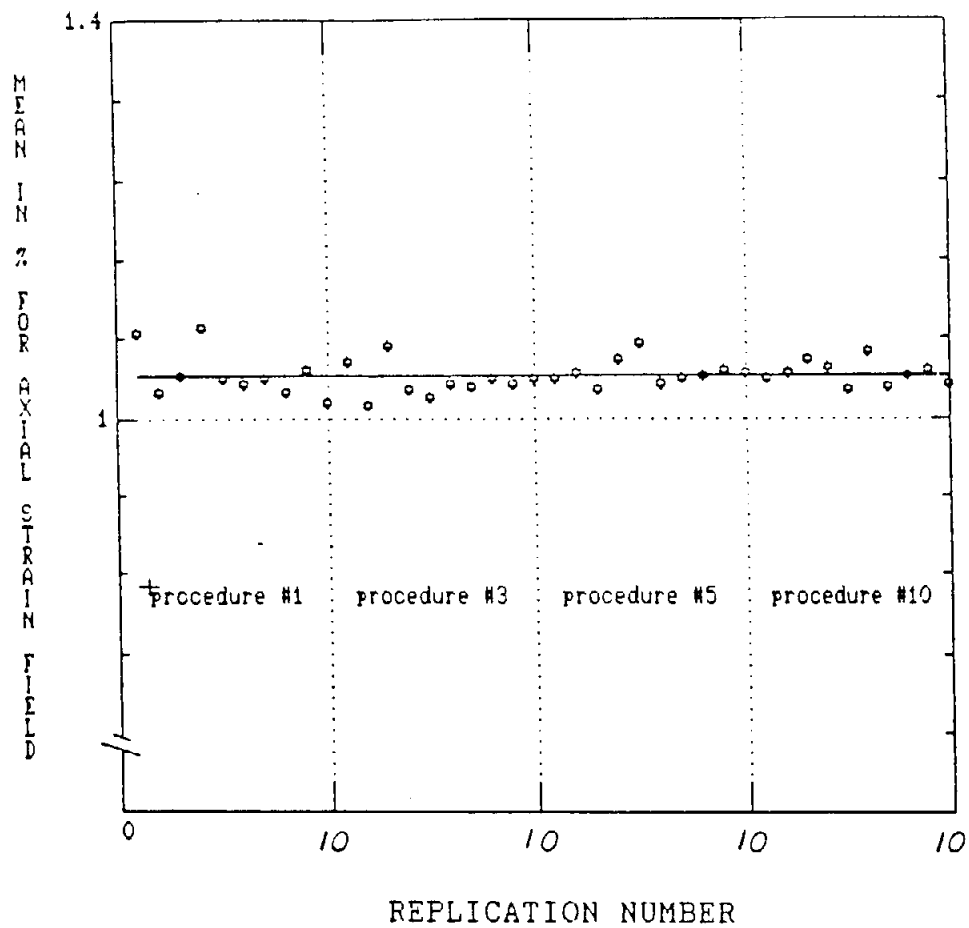


Fig. 6. Precision and accuracy of four digitizing procedures for the determination of axial strain field.

Horizontal line= mean value of the entire data ("true" mean of the population).

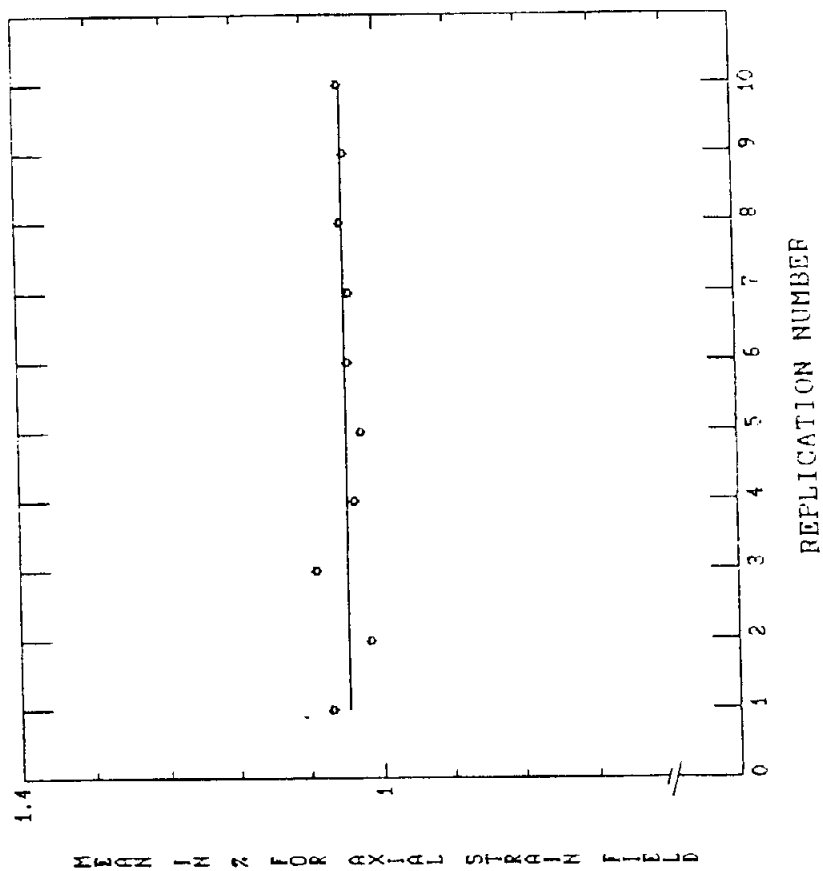


Fig. 8. Precision and accuracy in the determination of axial strain field using digitizing procedure # 3. Horizontal line= mean.

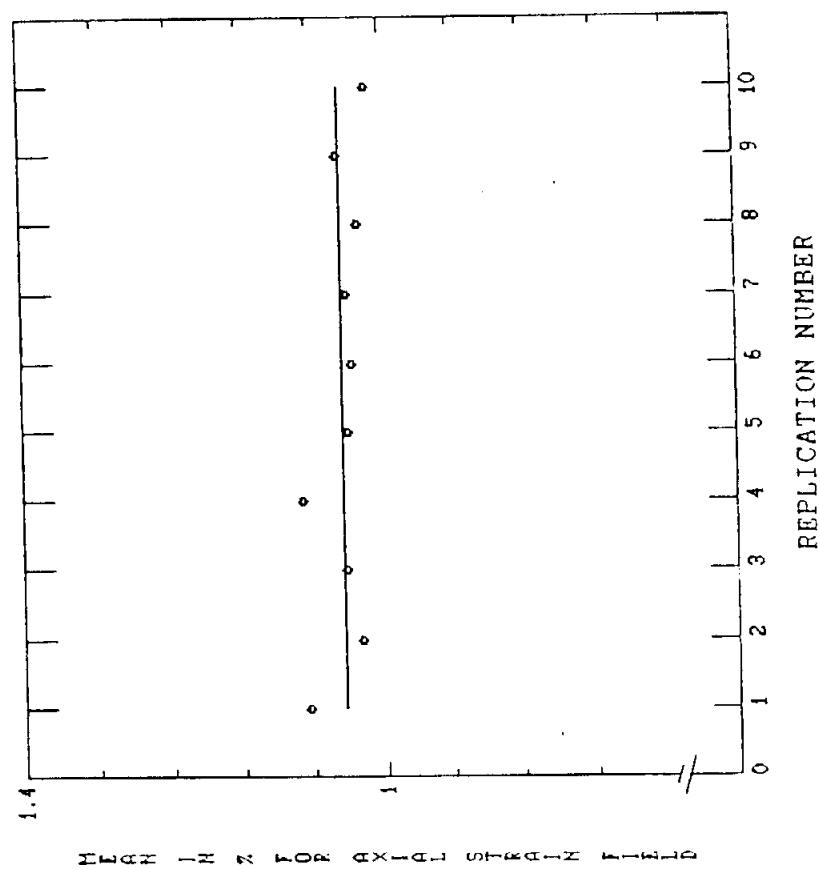


Fig. 7. Precision and accuracy in the determination of axial strain field using digitizing procedure # 1. Horizontal line= mean.

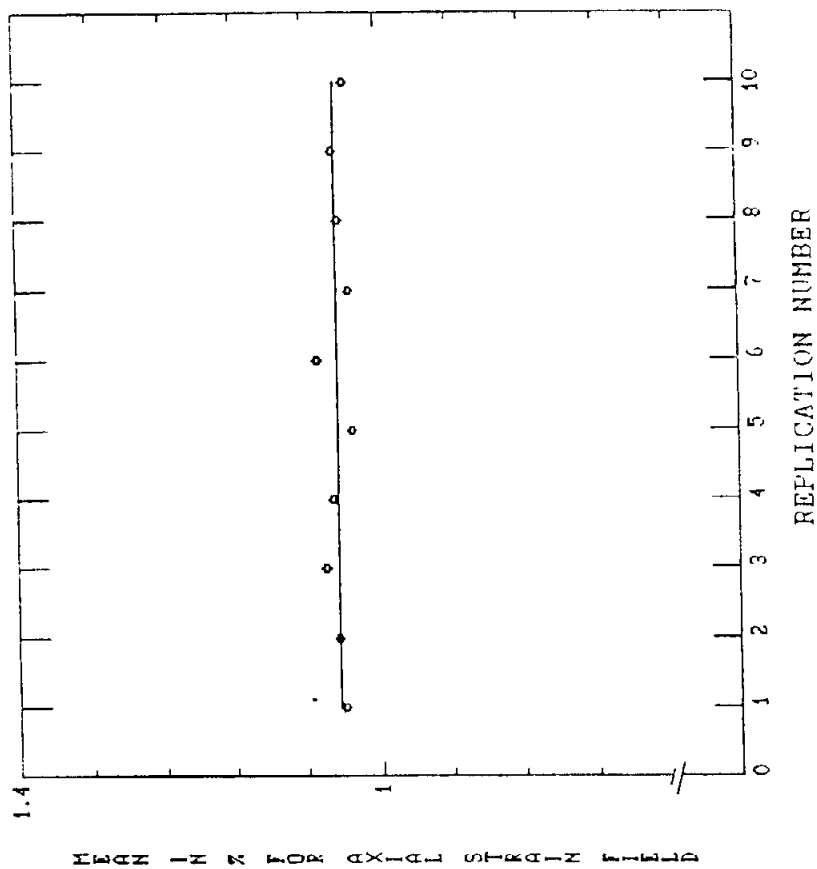


Fig. 9. Precision and accuracy in the determination of axial strain field using digitizing procedure # 5. Horizontal line= mean.

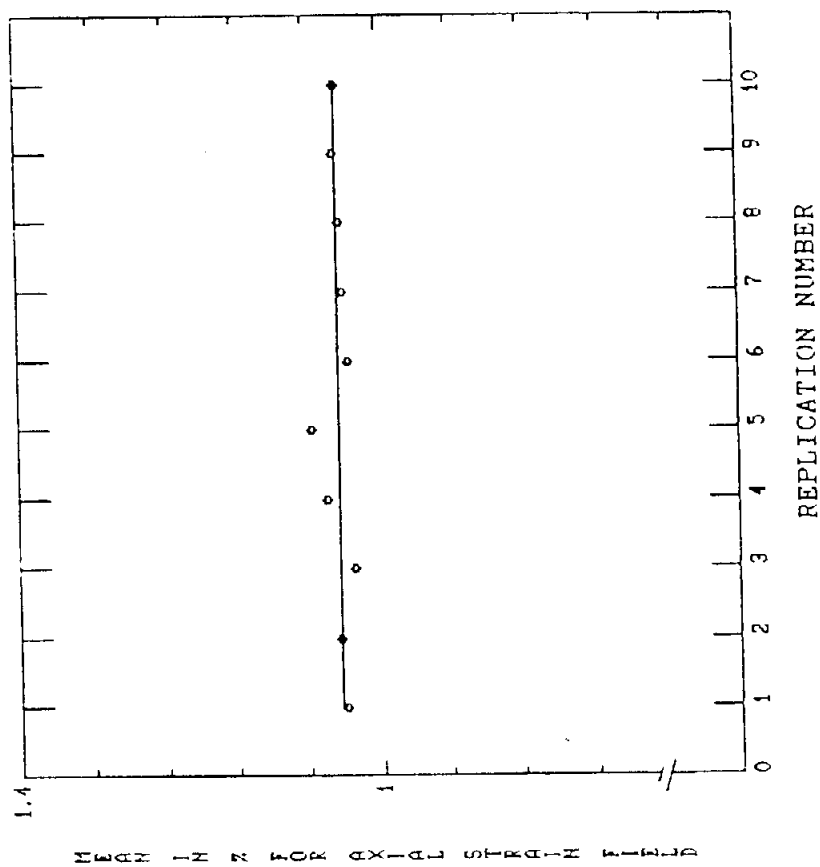


Fig. 10. Precision and accuracy in the determination of axial strain field using digitizing procedure # 10. Horizontal line= mean.

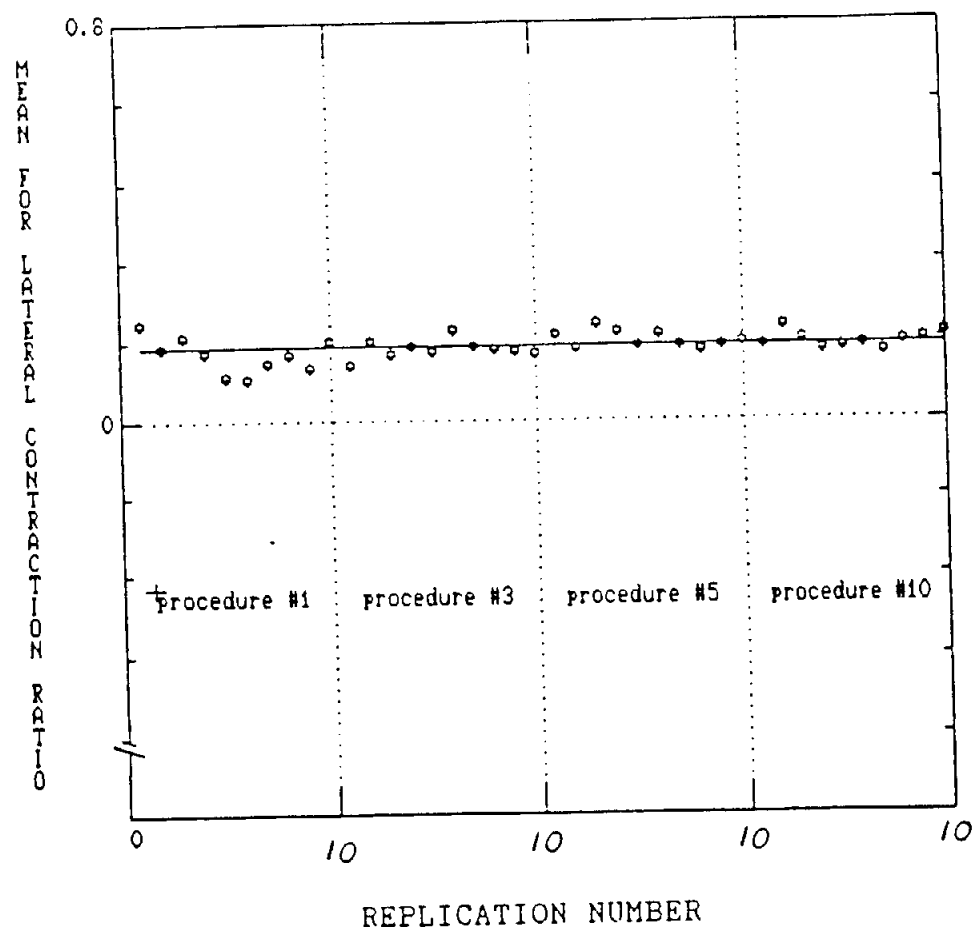


Fig. 11. Precision and accuracy of four digitizing procedures for the determination of lateral contraction ratios.

Horizontal line= mean value of entire data("true" mean of the population).

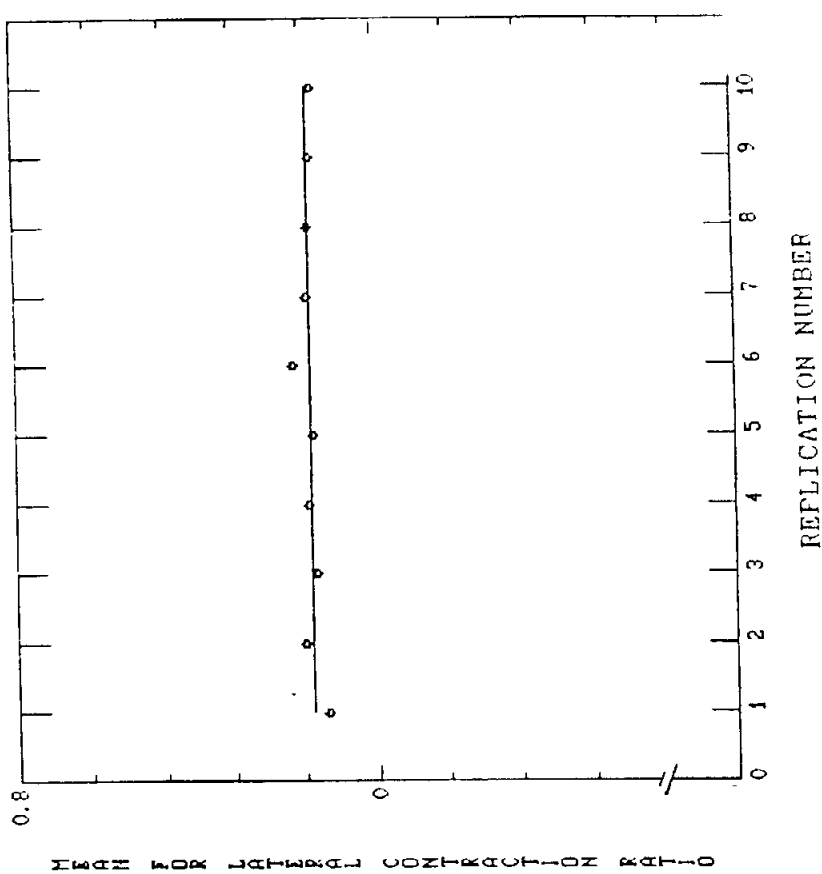


Fig. 13. Precision and accuracy in the determination of lateral contraction ratios using digitizing procedure #3. Horizontal line= mean.

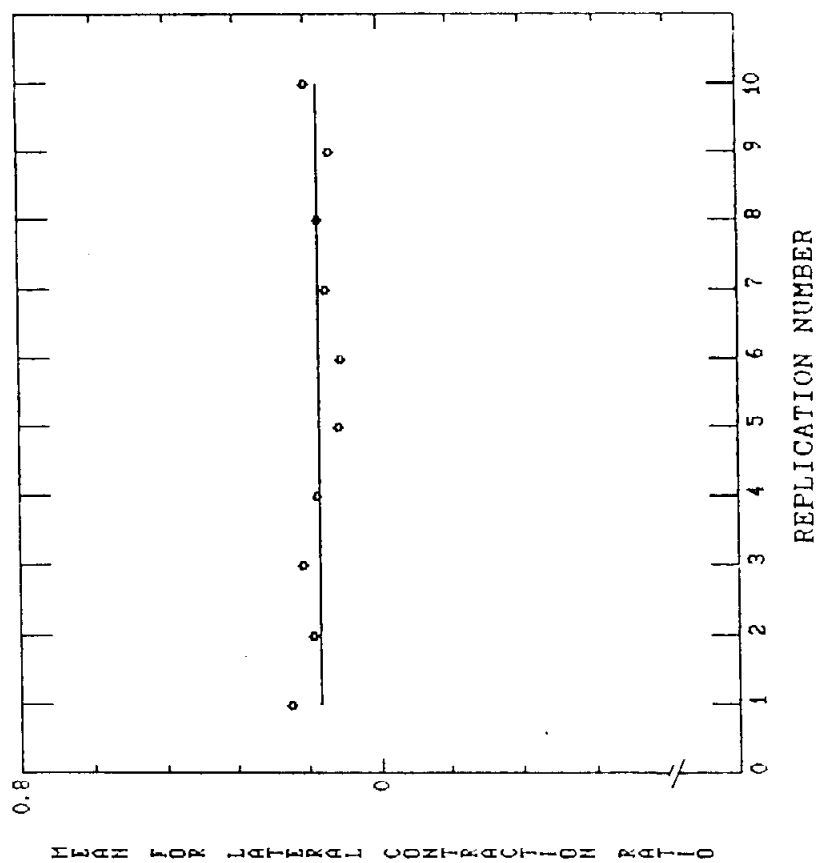


Fig. 12. Precision and accuracy in the determination of lateral contraction ratios using digitizing procedure #1. Horizontal line= mean.

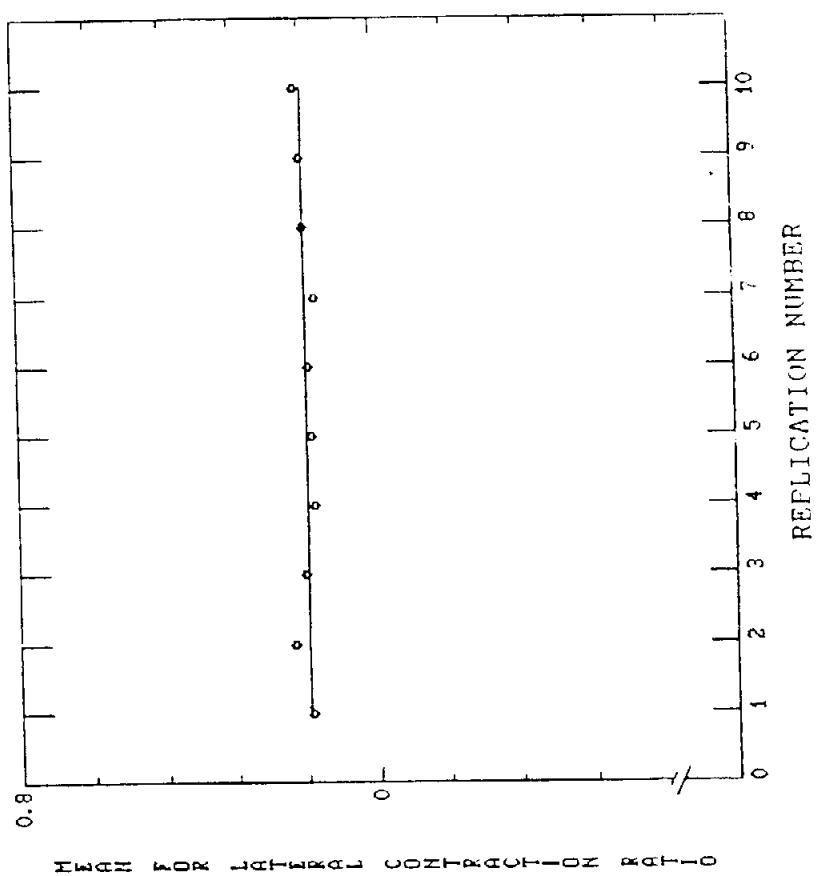


Fig. 14. Precision and accuracy in the determination of lateral contraction ratios using digitizing procedure #5. Horizontal line= mean.

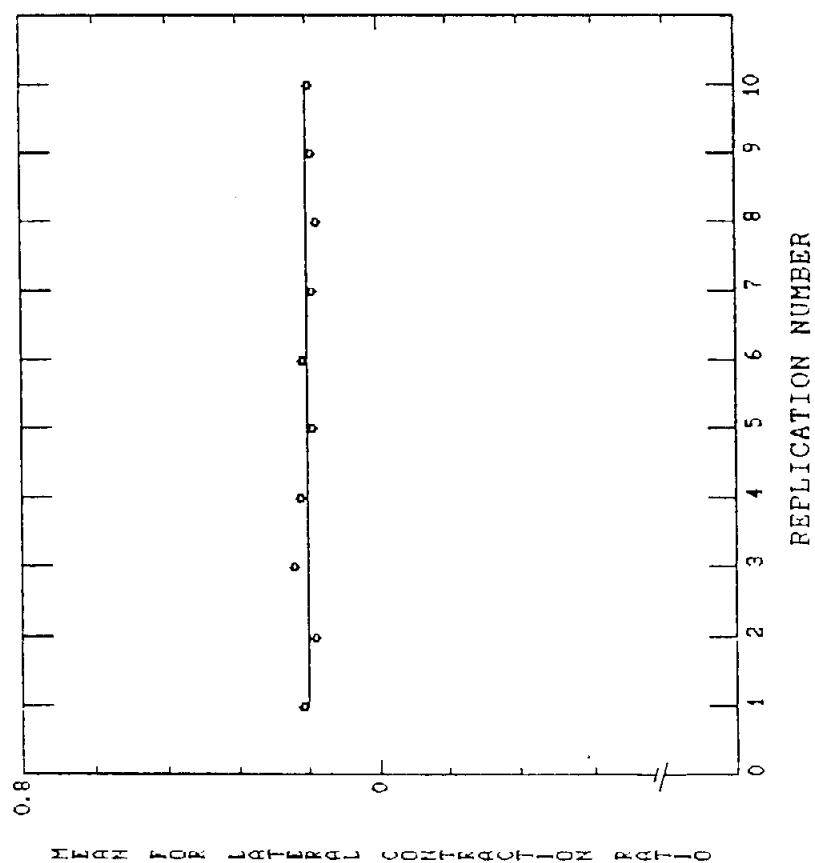


Fig. 15. Precision and accuracy in the determination of lateral contraction ratios using digitizing procedure #10. Horizontal line= mean.

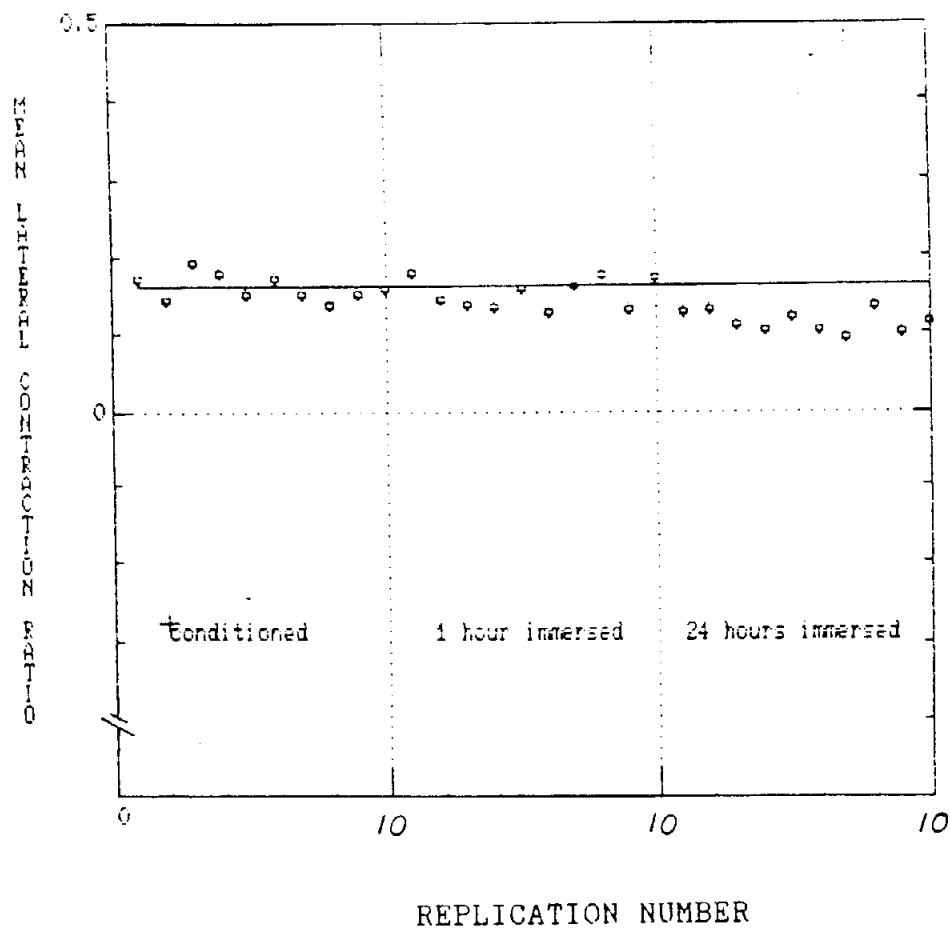


Fig. 16. Effect of moisture content of the exposed photographs on the precision and accuracy of the determination of lateral contraction ratios.

Horizontal line= mean of data from the photographs conditioned according to ref. [7].

Conditioned: the photographs were conditioned according to ref. [7].

1 and 24 hours immersed: the photographs were immersed in water at $23 \pm 1^\circ \text{C}$.

NOTE: the displacement data for all conditions were obtained using the digitizing procedure # 5.

CHAPTER 5

THE APPLICATION OF DOT MATRIX TECHNIQUE TO EVALUATE THE EFFECTS OF STRUCTURE ON THE MECHANICAL PROPERTIES OF PAPER

- 5.1. Introduction
- 5.2. Relationship between grammage and film absorbance
- 5.3. Experimental approach for mass distribution
characterization
- 5.4. Characterization of two-dimensional strain field
distribution
- 5.5. Relationship between grammage and strain
- 5.6. Conclusion
- 5.7. Literature
- 5.8. Appendix A
- 5.9. Appendix B
- 5.10. Appendix C
- 5.11. Appendix D
- 5.12. Appendix E
- 5.13. Appendix F
- 5.14. Appendix G

5.1. INTRODUCTION

Paper is a thin web composed of fibers aligned at various angles, yielding numerous interfiber contacts at which the fibers may be bonded together. Sheet structure in the web is usually characterized by the nature of the individual fibers, their arrangement with respect to one another, and the extent to which they are bonded. Thus the properties of the web reflect its structure, which in turn depends on the nature and pretreatment of the fibers and on the process used to form and finish the network. Paper's end uses are limited basically by its properties.

Some important network parameters that are often considered in theories relating to mechanical properties are: grammage, sheet density and mass distribution; orientation, size and distribution of flocs; fiber density, length, width, thickness (including its ratios) and curliness; fiber segment length (distance between bond centroids) and cross-sectional shape (including area, wall thickness and degree of collapse); fiber orientation distribution; mechanical properties of individual fibers; relative bonded area and the mechanical nature of the interfiber bond. Other important parameters are surface charges and effect of drying restraints [1-5].

A method that allows structure to be related to mechanical properties will bring significant contributions to

the evaluation and understanding of the relationship between structural changes and property changes.

The ability of the dot matrix technique to characterize two-dimensional strain fields enables us, by also using a beta-radiography technique, to obtain point-to-point correlations between grammage and strain fluctuations.

This chapter reports on the application of these techniques as experimental tools to help understand the nature of the inhomogeneity of the strain field as a function of mass distribution.

5.2. RELATIONSHIP BETWEEN GRAMMAGE AND FILM ABSORBANCE

In the paper field the term mass distribution usually means local variations in grammage. The three existing principal methods for determining local grammage are weighing, absorption of light, and absorption of radiation. Their advantages and disadvantages are discussed by Norman [6]. A comparison of various types of mass sensing technologies (visible light, submillimeter laser, alpha-rays, beta-rays, gamma-rays, soft x-rays and gravimetry) was presented by Cresson [7].

The beta-radiography method appears to be at

present the most appropriate technique for grammage sensing. The main advantages of the technique are that it correlates well with mass, it is non-destructive, and it is applicable over a large grammage range. For our application the local grammage in lightweight paper specimens could be obtained by this method with a minimum of handling, thereby avoiding damage. The same specimens were used later for strain measurements.

Generally, the technique of beta-radiography consists of sandwiching the paper sheet between a radioactive source and an x-ray film. The beta radiation transmitted through the sheet is recorded on the film. The film is analyzed by densitometry and the distribution of optical density (film absorbance) is used to calculate the corresponding mass distribution in the paper sheet.

The transmission of beta radiation through matter is related to the grammage (W) by the following equation [6]:

$$T = e^{-\mu W} \quad [1]$$

where,

T = transmission factor

μ = absorption coefficient

W = grammage

The proportionality of the optical density or absorbance $A = \ln(1/T)$ of a film to the amount of radiation transmitted by the exposed specimen has been demonstrated by

Norman and Wahren [8,9]. It is related to the grammage, W , by the equation

$$A_w = cte^{-\mu W} + A_\infty \quad [2]$$

If one takes the logarithm of the normalized absorbance of the film, equation [2] can be rearranged as follows:

$$\ln(A_w - A_\infty) = \ln ct - \mu W \quad [3]$$

where,

A_w = absorbance of the film corresponding to absorption by the sample

A_∞ = absorbance of the unexposed film (film background corresponding to infinite grammage)

c = proportionality factor

t = exposure time

For zero grammage ($W=0$), the solution for ct equation [2] becomes

$$ct = A_0 - A_\infty \quad [4]$$

Substituting equation [4] into equation [3] and solving for grammage, W , yields

$$\mu W = \ln(A_0 - A_\infty) - \ln(A_w - A_\infty)$$

$$W = \frac{1}{\mu} \{ \ln[(A_0 - A_\infty)/(A_w - A_\infty)] \} \quad [5]$$

where,

W = grammage, g/m^2

A = absorbance of fully exposed film (without paper sample)

μ = absorption coefficient of the paper, m^2/g .

The equations [3] and [5] describe for the radiographic process the relationship between film optical density (film absorbance) and the local grammage of the specimen. The grammage, W , in equation [5] is thus a function of film optical density (absorbance), which is determined experimentally for each individual radiograph. The mass distribution is therefore derived from the film by the distribution of its optical density.

The absorption coefficient, μ , which describes the attenuation of the beta particles through the matter and is therefore characteristic of the particular absorber [10], was determined experimentally for papers used in this study and for the Mylar step wedge used for monitoring the radiographic system. It was determined according to equation [3] from a linear regression of the logarithm of corrected optical densities on the corresponding grammage. The corrected optical density is the optical density, A_w , minus the film background, A_∞ . The regression was achieved by exposing to the beta source five step samples ranging from 0 to 100 g/m^2 for the papers and seven step samples ranging from 0 to 50 g/m^2 for the Mylar. The optical density of each step was calculated as

the average of 50 random measurements on that specific step. Three replications were done for each sample. The average value of absorption coefficient, μ , for the machine-made samples was $328 \text{ cm}^2/\text{g}$ with a standard deviation of $8.6 \text{ cm}^2/\text{g}$; for handsheet samples it was $335 \text{ cm}^2/\text{g}$ with a standard deviation of $4.8 \text{ cm}^2/\text{g}$; and for mylar samples, it was $352 \text{ cm}^2/\text{g}$ with a standard deviation of $2.3 \text{ cm}^2/\text{g}$. The values of absorption coefficient found for these papers compare reasonably well with an average value of $337 \text{ cm}^2/\text{g}$ found by Cresson [7] for different types of pulp materials, and for the value of $320 \text{ cm}^2/\text{g}$ suggested by Norman & Wahren [9] for paper materials.

5.3. EXPERIMENTAL APPROACH FOR MASS DISTRIBUTION CHARACTERIZATION

Sources of error in the beta-radiographic method are numerous. The most important of these (and suggested remedies) can be found in references [7 and 11]. Among them the most relevant parameters that define the efficiency of the radiographic system are: type of film, exposure time, type and freshness of developer and fixer, development time, temperature of the baths, degree of agitation, source of the

beta radiation, and characteristics of the densitometer (aperture, wavelength).

A schematic of the chamber used to obtain the beta-radiographs of the paper specimens is shown in Fig.1. The chamber (28 x 14 x 1.5 cm) was made of aluminum plates (1/4in thick). The beta-source (Carbon-14 polymer source, in sheet form with dimensions 10.2 x 10.2 x 0.1 cm and nominal activity 228 MBq, 6.17 mCi) was large enough to accomodate both the mylar step wedges (used for monitoring the radiographic process), and three paper specimens. The film used to record the radiation was Industrex-R. A exposure time of 8 hours was used. The sensitometric curve of the film (Optical Density - Log Exposure curve) is shown in Appendix A. This curve was obtained by exposing the film to the beta-radiation for different exposure times. In this curve the optical density scale is defined as the difference between the density of the exposed part of the film and its background density. For each given exposure time, the optical densities (Absorbances) of the films were obtained using the MacBeth TD-504 transmission densitometer [12] with the operating conditions described in Appendix B, which were the same conditions used to scan the radiographs obtained for characterization of mass distribution of the paper specimens. The standard radiographic development procedure is described in Appendix C.

The papers used in this study were a machine made paper and a handsheet. To avoid a possible effect of the crepe

on the determination of local grammage, the surface of the machine made tissue was flattened using a hot iron. To know some characteristics of formation before starting the experiment, a floc analysis was carried out on the paper sheets. These same sheets were later used to prepare the test specimens for grammage and strain analysis. The floc analysis was done by using the M/K 3-D sheet analyser [13]. The results are presented in Appendix D.

The procedure used to determine the areal mass distribution -- that is, the local grammage variation in the specimens -- is as follows: Since a wrinkle-free specimen is required, the specimens were designed according to the approach developed in Chapter 2. The center area (24x16 mm) of the narrow rectangular section of the necked-down specimens was chosen for this study. Fig. 2 illustrates the procedure. Before inserting the specimens into the radiographic chamber it was necessary to place on the specimen three reference marks (1mm square pieces of self-adhesive tape heavy enough to totally absorb the beta-radiation) in plane with two orientation dot-columns (25 dots 1mm apart sprayed on the edges of the specimen using the airbrush technique described in Chapter 3. The purpose of these orientation dot-columns will be discussed in the following section). These reference marks and the orientation dot-columns were placed outside the test area of the specimen. Therefore, they do not interfere with the mass distribution determination. After the

radiographic process was completed the images of the paper specimen and of the three reference marks were produced in the film, showing a distinct contrast between them. The images of the three reference marks were then used to align the radiographs for the scanning procedure in a correct x-y plane with the standard square aperture of the densitometer. This was achieved by matching the image of the three reference marks on the radiographs with the other three corresponding marks made on the densitometer diffuse plate (frame), which was also in plane with the orientation dot-columns sprayed on the specimen edges.

The scanning was done by attaching the radiographs to the frame of an x-y MC2000 programable translation stage [14] (operation conditions described in Appendix B), which was fully computer-controlled. The translation of the radiograph was done over the standard square aperture of the densitometer in an intermittent stepwise basis of 1mm squares until it covered the entire 384 mm^2 area under study. An IBM personal computer was used to control the translation stage and to store the acquired data from each individual translation step for grammage calculation. Therefore, with the acquired data (optical densities) from each radiograph a matrix corresponding to 24x16 grammage data points was generated per paper specimen. These were obtained with use of the software shown in Appendix E.

5.4. CHARACTERIZATION OF TWO-DIMENSIONAL STRAIN FIELD DISTRIBUTION

In this section we describe the procedure used for characterization of a spatially varying two-dimensional strain field (axial, lateral and shear strains) corresponding locally to the grammage of the specimen, using the dot matrix method.

After the radiographic process was completed, the template was again superimposed onto the specimen by matching the dot-columns on the specimen with the respective orientation column of holes on the template used to produce them. This was achieved by fixing the paper specimen on a piece of cardboard, and with the help of a stereo microscope the registry was easily done (manually). Then the specimen was prepared by spraying the matrix of dots on it, using the airbrushing procedure described in Chapter 3. A matrix of 25x17 dots 1mm apart was generated on the specimen, where each set of four dots corresponds to a basic unit of data processing (basic unit of displacement) covering a local area equivalent to 1mm square, which matches to the respective local area used to scan the radiographs by the stepwise procedure described in the previous section. Other different sizes and shapes of basic units of data processing are shown in Fig. 13 in Chapter 3.

From the pattern of dots sprayed onto the specimen,

the strains were calculated by the method and algorithms described in Chapter 3. However, in this application the data array dimensions used for strain calculations are shown in Fig.3. From this figure one can see that from 425 displacement data points ($LENX=25$, $LENY=17$) is generated a matrix of 24×17 data points for axial strain; 25×16 for lateral strain and 24×16 for shear strain. However, in order to better represent the value for axial and lateral strain per mm squares, and also to match the array dimension of strain data (axial and lateral strain) with the same dimension of the data array for grammage (a matrix of 24×16 data points per specimen) the mean value from two adjacent axial strain values and from two adjacent lateral strain values were obtained per mm squares (from four displacement data points). This rendered per specimen matrices of 24×16 data points for axial and lateral strains, respectively. For the shear strains such an averaging process was not necessary since it had previously been done by the algorithm used to calculate them (equation 11 in Chapter 3). Therefore, considering the spatially varying data in 1mm squares, a number of 384 data points were obtained for axial, lateral and shear strains, respectively, which equals the number of data points for grammage obtained in corresponding locations on the specimen.

The stage of the tensile test where the data for strain field distribution were obtained for correlation analysis is indicated by the arrows on the load per unit of

width versus strain curves shown in Appendix F for the machine made paper (MD and CD) and for handsheets.

5.5. RELATIONSHIP BETWEEN GRAMMAGE AND STRAIN

Elucidation of the pointwise correlation between local mass and corresponding paper properties has attracted considerable interest. Any provable relationship between local grammage and spatially varying strains should help us to understand the inhomogeneous nature of paper mechanical properties. In this study, the pointwise correlation matrices were generated between the grammage and locally corresponding axial, lateral and shear strain by the simplest and most frequently used correlation technique. The correlation coefficient was used to find the degree of association between them.

Correlation techniques can be used in various ways other than the approach used in this study. As suggested by Dodson [15] structural statistics over finite zones can be deduced by integrating point autocorrelation functions from other structural parameters already known, which can yield a correlation between the mass distribution and the strain distribution. If statistical information is known on the array

of strain data and their relationship with structural parameters, it is possible to estimate the mean and variance of mass by using the strain information. However, for one to work on statistical geometric modelling of paper, a larger amount of experimental data and other experimental approaches are needed in order to take into account other structural parameters such as local fiber orientation, degree of bonding etc. We are planning to establish in the future, with the methods and procedures developed in this dissertation, a basis for predicting the nature and mechanical consequences of paper inhomogeneity. For now, we think that the multiple correlation statistical technique is still a very powerful tool for estimation of paper behavior as a prelude to getting involved in more complex mechanical modelling.

As described above, the data acquisitions for grammage and strains were experimentally obtained on a 1mm square basis. In order to verify the existence of correlation by considering different spatial periodicities, a method that employs spatial average parameters was used to obtain progressively more stable data from the grammage and strain arrays. This was achieved by following the mathematical procedure described below. The array dimensions for correlation are summarized in Table 1.

Table 1. Array Dimensions for Correlation Analysis.

SPATIAL PARAMETERS	NUMBER OF DATA POINTS	DIMENSIONS OF ARRAY			
		Grainage	Axial Strain	Lateral Strain	Shear Strain
1mm squares	384	(LENY,LENY)	(LENY,LENY)	(LENY,LENY)	(LENY,LENY)
2mm squares	345	(LENY-1,LENY-1)	(LENY-1,LENY-1)	(LENY-1,LENY-1)	(LENY-1,LENY-1)
3mm squares	308	(LENY-2,LENY-2)	(LENY-2,LENY-2)	(LENY-2,LENY-2)	(LENY-2,LENY-2)
4mm squares	273	(LENY-3,LENY-3)	(LENY-3,LENY-3)	(LENY-3,LENY-3)	(LENY-3,LENY-3)

For LENY=24, LENY=16; which are the number of rows (x direction) and columns (y direction) of the entire array of data obtained in 1mm squares basis according to fig.3 and the statement below:

G = Grainage obtained per mm square

$\left[\square_i^j + \square_{i+1}^j \right] \div 2 = \text{AIS} = \text{Average axial strain per mm square in a row (y direction) obtained by the APL function (TAKEASTR) shown in Appendix E.}$

$\left[\square_i^j + \square_i^{j+1} \right] \div 2 = \text{LTS} = \text{Average lateral strain per mm square in a column (y direction) obtained by the APL function (TAKEELSTR) shown in Appendix E.}$

$\triangle = \text{SHS} = \text{Average shear strain per mm square calculated by equation 11 in Chapter 3.}$

By making VAR = G, AXS, LTS and SHS in the algorithms below, the spatial average procedure was obtained by 2mm, 3mm

and 4mm squares for grammage, axial, lateral and shear strain, respectively.

For spatial average per 2mm squares with $1 \leq i \leq 15$ (y-direction) and $1 \leq j \leq 23$ (x-direction):

$$[\text{VAR}_i^j + \text{VAR}_{i+1}^j + \text{VAR}_i^{j+1} + \text{VAR}_{i+1}^{j+1}] \div 4$$

For spatial average per 3mm squares with $1 \leq i \leq 14$ (y-direction) and $1 \leq j \leq 22$ (x-direction):

$$[\text{VAR}_i^j + \text{VAR}_{i+1}^j + \text{VAR}_{i+2}^j + \text{VAR}_i^{j+1} + \text{VAR}_{i+1}^{j+1} + \text{VAR}_{i+2}^{j+1} + \text{VAR}_i^{j+2} + \text{VAR}_{i+1}^{j+2} + \text{VAR}_{i+2}^{j+2}] \div 9$$

For spatial average per 4mm squares with $1 \leq i \leq 13$ (y-direction) and $1 \leq j \leq 21$ (x-direction):

$$[\text{VAR}_i^j + \text{VAR}_{i+1}^j + \text{VAR}_{i+2}^j + \text{VAR}_{i+3}^j + \text{VAR}_i^{j+1} + \text{VAR}_{i+1}^{j+1} + \text{VAR}_{i+2}^{j+1} + \text{VAR}_{i+3}^{j+1} + \text{VAR}_i^{j+2} + \text{VAR}_{i+1}^{j+2} + \text{VAR}_{i+2}^{j+2} + \text{VAR}_{i+3}^{j+2} + \text{VAR}_i^{j+3} + \text{VAR}_{i+1}^{j+3} + \text{VAR}_{i+2}^{j+3} + \text{VAR}_{i+3}^{j+3}] \div 16$$

These mathematical procedures were performed by the APL functions (SAP2, SAP3 and SAP4, respectively) shown in Appendix E.

The relationship between grammage and strains obtained by the cross correlations generated between the variables under study is presented in Tables 2, 3 and 4. In

the correlation analysis, the sign convention for strain has been taken into account. Therefore, tensile strain is denoted as positive and compressive strain is denoted as negative values. The degree of association that exists between them, expressed by the corresponding correlation coefficient, proves the existence of a close mathematical relation between the variables. But before we go further it is important to realize that this does not necessarily imply causation. Thus, a correlation coefficient which is high indicates that the variables tend to change together either in the same or in the opposite direction. Otherwise, when a low correlation coefficient is obtained, the conclusion that the independent variable does not influence the quantity being measured is not necessarily correct [16]. It is possible that other factors exist, masking or nullifying the effect of the independent variable.

In general, the correlation between mass and strain on a pointwise basis was not as high as might be expected. Owing to the great difficulty of isolating other local effects of factors such as flocculation, fiber orientation, number and extent of free fiber lengths, number of fiber crossings, etc., it is not yet possible to describe in precise terms the contribution of the mass distribution to the heterogeneity of the strain field. At this stage of our research, especially in case of lightweight paper, we question whether the behavior of the sheet is directly or indirectly induced by the

pointwise variation in grammage. The lower grammage regions that result from localized smaller values of specimen thickness yield smaller cross sectional areas, which may strain more as a direct consequence of the higher stress level developed in these regions. However, the effects of other factors such as a lower number of interfiber bonds and consequently a longer free fiber length may cause these thinner spots to experience larger deformations, which are indirectly the consequence of a lower amount of mass.

Table 2 shows the correlation matrices obtained for test specimens on a 1mm square basis. In this table one can see that the negative sign of the correlation coefficient clearly indicates that changes in axial strain relate in a logical and opposite order to grammage variations. Values ranging from -0.339 to -0.633 were found for machine made paper and values from -0.299 to -0.416 were obtained for handsheet specimens. However, the positive sign of the correlation coefficient for lateral strain shows that this variable changes in the same direction of the grammage. But it should be inferred that the lateral strains are essentially negative strains. Values from 0.320 to 0.596 were obtained for machine made paper and values from 0.268 to 0.354 for handsheet specimens.

In general, the lowest correlation was found for shear strain versus grammage, axial and lateral strain. It might be explained by the positive and negative shear strains

obtained inside the grid area of the specimen under tension. The positive and negative shear strains tend to compensate each other in the plane of the specimens, reducing or nullifying the somation factor in the formula used in the analysis to calculate the correlation coefficient [16]. Theoretically, we should expect correlation zero. However, possibly due to heterogeneity of the paper material and/or processing errors involved in the technique, values near to zero were found. In general, values varying from -0.004 to -0.172 were obtained for machine made paper and values from -0.001 to 0.068 were found for handsheet specimens.

The negative sign of correlation coefficient obtained for axial strain versus lateral strain shows that the lateral strain changes in opposite direction to each other, since lateral strains are essentially negative strains.

In general, higher correlation was obtained for machine made paper than for handsheets. A possible explanation may lie in the greater inhomogeneity of mass distribution of the machine made paper, which locally may cause a correspondingly larger response to the inhomogeneity of the strain field. This is reinforced by Table 3.

Table 3 shows the correlation matrices generated from the average of the three test specimens on 1, 2, 3 and 4mm squares basis. In this Table, one can see that the correlation coefficients for grammage, axial, lateral and shear strains in the correlation matrices, in the majority of

the cases, increase in magnitude as the spatial average parameters increase from 1mm to 4mm squares. For convenience in visualizing the effect of the spatial periodicities on the degree of association between grammage and axial, lateral and shear strains, plots of correlation coefficients versus spatial average parameters are given in Figures 4.1, 4.2 and 4.3 for the machine made paper (MD and CD) and handsheet, respectively. From these figures, it seems that in the inhomogeneous mass and strain fields, the method of spatial average parameters appears to make the data more stable for correlation analysis, which may improve the correlation between mass and strains. However, in certain cases, if spatial average parameters larger than 3mm squares are used to process the data, the increment of the correlation is leveled off or even reduced to a value lower than that obtained by considering the data in 1mm squares. The shear strain presented the lowest correlation for all spatial average parameters whether compared to axial and lateral strains.

In order to verify whether the location on the specimen has some defined effect on the correlation between mass and strain, correlation matrices were generated using the data acquired from two different locations, but still inside the grid area of the specimens. This was accomplished by processing two columns of data obtained on a 1mm squares basis from the outermost portion of the specimens and two columns obtained from the inner portion of the specimens along the

axial direction. The results are shown in Table 4. It seems that by our experimental approach the randomness of mass and corresponding strain variations on 1mm squares are not affected by geometrical location in the test specimen. Although the correlation coefficients are different from those obtained by considering the entire data array, it can be seen that the correlation still occurs and no defined trend for compromising, masking or nullifying the correlation between mass and strains can be inferred. In our experimental approach the outermost rectangular finite element (1mm square elements) was located on the specimen at 2mm from the specimen edges, which appears to be enough to avoid a possible effect of drastic difference in boundary condition that could be imposed on the rectangular finite element if one of its sides was on the free edges of the specimen. A finite element study of stress and strain behavior of a low grammage spot in paper during elongation carried out by Kimura and Shimizu [17] shows that the effect of the location on the concentrations of stress and strain was negligible as long as the thin spot was inside the edges by more than the distance of its own width.

The randomness of the mass and axial, lateral and shear strain distribution for the machine made paper (MD and CD) and handsheet specimens are represented in tri-dimensional graphic form in Figures 5, 6, 7 and 8, respectively. These graphics were plotted by using the data distribution on a 1mm squares basis obtained from three typical test specimens for

each type of paper. The greater inhomogeneity of mass distribution of the machine made paper than for handsheet can be seen by comparison of Figures 5.1 and 5.2 with Figure 5.3, and the respective standard deviations (SD) inserted in the Figures. For all variables, that is, for grammage, axial, lateral and shear strain distribution, it was found higher standard deviation for machine made paper than for handsheet.

Following similar trend, the greater inhomogeneity of the axial, lateral and shear strain distribution for machine made paper compared to handsheet is shown within the respective Figures 6, 7 and 8. These observations reinforce our previous discussion in which the randomness of mass distribution cause a correspondingly larger response to the inhomogeneity of the strain field. For machine made paper, the greater inhomogeneity was found for the specimens tested in CD direction.

Scatter plots for machine made paper (MD and CD) and for handsheet specimens showing variation of axial, lateral and shear strains as functions of mass distribution are shown in Figures 9 through 26. Figures 9, 10 and 11 show the relationship between grammage and axial strain on 1mm square basis for MD, CD and handsheet specimens, respectively. From these figures one can see that, in general, local points of higher grammage tend to strain less than points of lower grammage. This opposite trend reinforces the previous discussion of the correlation between grammage and strains

which is emphasized by the correlation equation inserted in the figures. However, other different trends are observable. Some local points of equal value in grammage strain more, or strain less, in what seems to be a random fashion. This is the typical case that the stress and strain behavior of a certain spot appears to result from a complicated combination of effects of various structural parameters. Other spots with large difference in grammage between them present similar strain values. This is in agreement with graphs of experimental values of relative areal dilation against areal density reported by Dodson [18] on the deformation of commercial bonded fibrous networks. Dodson also found a significant correlation of local deformation with the local areal density of mass. A possible explanation may lie in the reinforcing effect of heavier spots on the mechanical response of light spots found by Kimura and Shimizu [17] and by Thorpe [19] from computer simulation studies of the tensile behavior of paper based on finite element analysis.

Figures 12, 13 and 14 show the relationship between grammage and axial strain for MD, CD and handsheet specimens on 1, 2, 3 and 4mm square basis, respectively. From these figures one can see that, in general, as a result of the averaging stepwise process applied over the data obtained on a 1mm square basis, the trend in the scattering of the data was reduced. It made the data more stable for correlation and reinforced our previous discussion about the results presented

in Table 3. Although this averaging process reduces the number of data points as the average step parameters increase, it combines other spatially varying data for correlation.

The relationship between grammage and lateral strain on 1mm square basis for MD, CD and handsheet specimens is presented in Figures 15, 16 and 17, respectively. As in general, the lateral strains are essentially negative strains, local points of higher grammage tend to strain more than points of lower grammage. This is shown by the positive sign of correlation coefficient and is reinforced by both, the positive slope of the correlation equation and its fitted line inserted in the figures. However, other different trends are also observable in the same fashion it does for axial strain. That is, some local points of equal value in grammage strain more, or strain less, in what seems to be a random fashion. Other spots with large differences in grammage between them present similar strain values.

Figures 18, 19 and 20 show the relationship between grammage and lateral strain for MD, CD and handsheet specimens, respectively, on 1, 2, 3 and 4mm square basis. In similar fashion to axial strain, the average stepwise parameters reduce the scattering of the data as it increases from 1 to 4mm square basis. This can be seen by comparison of the figures relative to the average obtained from 1mm to 4mm square basis, for MD, CD and handsheets. The positive sign of correlation coefficient and its respective correlation

equations inserted in the figures indicates that the lateral strain increases in the same direction of grammage. This was expected, since lateral strains are essentially negative strains.

Figures 21, 22 and 23 show the relationship between grammage and shear strain for MD, CD and handsheet specimens, respectively. The scattering of the data showing positive and negative strain distributions reinforces our previous discussion about the balancing effect of positive and negative sign of shear strains responsible for the low correlation to grammage variation. Although small correlation has been found to grammage, the average stepwise process applied over the data for shear strains unexpectedly increased its correlation to grammage and made the data more stable. The results are shown in Figs. 24 and 25 for machine made paper and in Fig. 26 for handsheet specimens. However, we believe that the mathematical stepwise procedure tend to nullify the balancing effect of negative and positive shear, since it was applied over the average data obtained on 1mm square basis from three individual paper specimens. Therefore, the increase in correlation may not represent a real correlation between grammage and shear, but only a disbalancing on positive and negative values for shear strains caused by the average mathematical procedure.

5.6. CONCLUSION

With the Dot Matrix and Beta-radiography techniques, we have been able to discover a fine trend toward periodicities in mass and strain distribution. With the experimental methods and procedures developed in this chapter, we found that axial and lateral sheet strains exhibit a considerable degree of relationship to mass distribution. However, causality must be determined by considering other factors as well. The correlations between mass and strains, which were not as high as we expected, appears to indicate the significant participation of a combination of other structural parameters in the complicated mechanical phenomena. Relationships ascribed to strain variation may in fact be related, at least in part, to some other structural parameters. The machine made paper, as it was expected, presented greater inhomogeneity of mass and strains than the handsheets.

The stepwise procedures applied over the data obtained on 1mm square basis tend to stabilize the data for correlation analysis and to improve the correlation between grammage and strains. In general, a best correlation is reached if the average over finite zones is obtained on 3 or 4mm square basis.

We hope this chapter has reasonably shown the

usefulness of the technique as a potential experimental tool. It will be used in the future in combination with other methods, procedures and available techniques [1, 7, 20] to form an experimental basis for prediction of the nature and mechanical consequences of paper inhomogeneity, by taking into account other structural parameters in the sheet that could be responsible for variations in strain behavior. This method is especially useful in the case of lightweight paper, for which the application of other displacement measurement techniques is limited.

5.7. LITERATURE

1. MARK, R. E. "Structure and structural anisotropy." In: MARK, Richard E. (ed.). Handbook of physical and mechanical testing of paper and paperboard. New York, M.Dekker, 1983. vol.2, chapter 24, pp.283-377.
2. DODSON, C.T.J. & HERDMAN, P.T. "Mechanical properties of paper." In: RANCE, H.F. (ed.). Handbook of paper science. Amsterdam, Elsevier, 1982. vol.2, chapter 7, pp. 71-126.
3. CORTE, H. "The structure of paper." In: RANCE, H.F. (ed.). Handbook of paper science. Amsterdam, Elsevier, 1982. vol.2, chapter 9, pp. 175-282.
4. NORMAN, Bo; FELLERS, C.; ANDERSSON, H.; HOLLMARK, H.; BRISTOW, J.A.; PAULER, N. "Paper structure." In: BRISTOW, J. Anthony & KOLSETH, Petter (eds.). Paper structure and properties. New York, M.Dekker, 1986. Part II, pp.121-224. (International Fiber Science and Technology Series, 8)

5. HTUN, M.; RIGDAHL, M.; HOLLMARK, H.; de RUVO, A.; FELLERS, C.; KOLSETH, P.; CARLSSON, L. "Mechanical properties in relation to structure." In: BRISTOW, J. Anthony & KOLSETH, Petter (eds.). **Paper structure and properties.** New York, M.Dekker, 1986. Part III, pp.227-363. (International Fiber Science and Technology Series, 8)
6. NORMAN, Bo. "The formation of paper sheets." In: BRISTOW, J. Anthony & KOLSETH, Petter (eds.). **Paper structure and properties.** New York, M.Dekker, 1986. Chapter 6, pp. 123-150. (International Fiber Science and Technology Series, 8).
7. CRESSON, Thierry Marcel. **The sensing, analysis and simulation of paper formation.** Syracuse, State University of New York, College of Environmental Science and Forestry, 1988. 82p. (Ph.D. Thesis)
8. NORMAN, Bo & WAHREN, Douglas. "The measurement of mass distribution in paper sheets using a beta radiographic method." *Svensk papperstidning*, 77(11): 397-406, 1974.
9. NORMAN, Bo & WAHREN, Douglas. "Mass distribution and sheet properties of paper." In: BOLAM, F.M. (ed.). **The fundamental properties of paper related to its uses.** London, Tech. Sect., B.P. & B.M.A., 1976. pp.7-70.
10. EVANS, Robley D. "Beta-Ray spectra". In: **The atomic nucleus.** McGraw-Hill, 1955. Chapter 17, pp. 536-566.
11. SARA, Heikki. **The characterization and measurement of paper formation with standard deviation and power spectrum.** Helsinki, Helsinki University of Technology (Otaniemi), 1978. 162p. (Doctor of Technology Thesis)
12. KOLLMORGEN CORPORATION. **Macbeth Color & Photometry Division. Operator's manual for Transmission Densitometer, model TD-504.** Revised Feb. 1973. [6p.]
13. KALLMES, O.J. "A new rapid technique for measuring the basis weight variations of paper on the micro-scale." [Preprint of paper to be published in] *Paper Age*, Aug. 1988. [8p.]
14. DAEDAL INC. **MC2000 & MC2100 Instruction manual.** Harrison City, Pa., 15636 USA. [69p.]
15. DODSON, C.T.J. **A universal law of formation.** [Text of a lecture given at PAPRICAN, Pointe Claire, 24 November 1989] 9p.

16. KENNEDY, J.B. & NEVILLE, A.M. **Basic statistical method for engineers and scientists.** 3rd. ed. New York, Harper & Row, 1986. 613p.
17. KIMURA, Minoru & SHIMIZU, Hiroshi. "Stress and strain behavior of low grammage spot in paper during elongation." *Jpn. Tappi*, 39(8): 55-62, 1985.
18. DODSON, C.T.J. "The statistical analysis of patterns of deformation in flat bonded fibrous networks." *J. Phys. D: Appl. Phys.* (3): 269-276, 1970.
19. THORPE, J.L. "Paper as an orthotropic thin plate." *Tappi*, 64(3): 119-121, 1981.
20. BOULAY, R.; DROUIN, B. & GAGNON, R. "Measurement of local fibre orientation variations." *Journal of Pulp and Paper Science*, 12(6): J177-J181, Nov. 1986.

Table 2. Correlation Matrices generated per Test Specimen in 1mm Square Basis

MACHINE DIRECTION (MD)												
	SPECIMEN NO. 1				SPECIMEN NO. 2				SPECIMEN NO. 3			
	Grammage	Axial	Lateral	Shear	Grammage	Axial	Lateral	Shear	Grammage	Axial	Lateral	Shear
Grammage	1.000	-0.588	0.476	-0.065	1.000	-0.339	0.389	-0.058	1.000	-0.633	0.596	-0.034
Axial (1)	-0.588	1.000	-0.611	0.076	-0.339	1.000	-0.416	0.058	-0.633	1.000	-0.734	-0.004
Lateral (2)	0.476	-0.611	1.000	-0.014	0.389	-0.416	1.000	-0.121	0.596	-0.734	1.000	-0.032
Shear (3)	-0.065	0.076	-0.014	1.000	-0.058	0.058	-0.121	1.000	-0.034	-0.004	-0.032	1.000
CROSS MACHINE DIRECTION (CD)												
	SPECIMEN NO. 1				SPECIMEN NO. 2				SPECIMEN NO. 3			
	Grammage	Axial	Lateral	Shear	Grammage	Axial	Lateral	Shear	Grammage	Axial	Lateral	Shear
Grammage	1.000	-0.352	0.403	-0.172	1.000	-0.478	0.455	-0.040	1.000	-0.503	0.320	-0.111
Axial (1)	-0.352	1.000	-0.175	0.015	-0.478	1.000	-0.489	0.066	-0.503	1.000	-0.428	0.097
Lateral (2)	0.403	-0.175	1.000	-0.013	0.455	-0.489	1.000	-0.130	0.320	-0.428	1.000	0.006
Shear (3)	-0.172	0.015	-0.013	1.000	-0.040	0.066	-0.130	1.000	-0.111	0.097	0.006	1.000
HANDSHEETS												
	SPECIMEN NO. 1				SPECIMEN NO. 2				SPECIMEN NO. 3			
	Grammage	Axial	Lateral	Shear	Grammage	Axial	Lateral	Shear	Grammage	Axial	Lateral	Shear
Grammage	1.000	-0.318	0.354	0.068	1.000	-0.300	0.287	0.016	1.000	-0.416	0.269	0.025
Axial (1)	-0.318	1.000	-0.411	-0.040	-0.299	1.000	-0.291	-0.001	-0.416	1.000	-0.444	0.024
Lateral (2)	0.354	-0.411	1.000	-0.009	0.287	-0.291	1.000	0.047	0.268	-0.444	1.000	0.003
Shear (3)	0.068	-0.040	-0.009	1.000	0.016	-0.001	0.047	1.000	0.025	0.024	0.003	1.000

(1), (2), (3): Axial, Lateral and Shear Strains, respectively.

Table 3. Correlation Matrices Generated from the Average of Three Test Specimens in 1, 2, 3 and 4mm Squares Basis

MACHINE DIRECTION (MD)																
1mm SQUARE				2mm SQUARES				3mm SQUARES				4mm SQUARES				
Grammage	Axial	Lateral	Shear	Grammage	Axial	Lateral	Shear	Grammage	Axial	Lateral	Shear	Grammage	Axial	Lateral	Shear	
Grammage	1.000	-0.533	0.490	-0.066	1.000	-0.586	0.549	-0.159	1.000	-0.559	0.519	-0.248	1.000	-0.493	0.391	-0.342
Axial (1)	-0.533	1.000	-0.647	0.075	-0.586	1.000	-0.707	0.147	-0.559	1.000	-0.736	0.184	-0.493	1.000	-0.741	0.195
Lateral (2)	0.490	-0.647	1.000	-0.063	0.549	-0.707	1.000	-0.154	0.519	-0.736	1.000	-0.239	0.391	-0.741	1.000	-0.263
Shear (3)	-0.060	0.075	-0.063	1.000	-0.159	0.147	-0.154	1.000	-0.248	0.184	-0.239	1.000	-0.342	0.195	-0.263	1.000
CROSS MACHINE DIRECTION (CD)																
1mm SQUARE				2mm SQUARES				3mm SQUARES				4mm SQUARES				
Grammage	Axial	Lateral	Shear	Grammage	Axial	Lateral	Shear	Grammage	Axial	Lateral	Shear	Grammage	Axial	Lateral	Shear	
Grammage	1.000	-0.473	0.466	-0.118	1.000	-0.585	0.576	-0.212	1.000	-0.640	0.671	-0.293	1.000	-0.639	0.735	-0.347
Axial (1)	-0.473	1.000	-0.407	0.134	-0.585	1.000	-0.478	0.213	-0.640	1.000	-0.544	0.296	-0.639	1.000	-0.589	0.371
Lateral (2)	0.466	-0.407	1.000	-0.116	0.576	-0.478	1.000	-0.234	0.671	-0.544	1.000	-0.309	0.735	-0.589	1.000	-0.357
Shear (3)	-0.118	0.134	-0.116	1.000	-0.212	0.213	-0.234	1.000	-0.293	0.296	-0.309	1.000	-0.347	0.371	-0.357	1.000
HANDSHEETS																
1mm SQUARE				2mm SQUARES				3mm SQUARES				4mm SQUARES				
Grammage	Axial	Lateral	Shear	Grammage	Axial	Lateral	Shear	Grammage	Axial	Lateral	Shear	Grammage	Axial	Lateral	Shear	
Grammage	1.000	-0.317	0.308	0.038	1.000	-0.345	0.353	-0.076	1.000	-0.354	0.370	-0.127	1.000	-0.376	0.353	-0.175
Axial (1)	-0.316	1.000	-0.397	-0.027	-0.345	1.000	-0.559	0.027	-0.354	1.000	-0.677	0.061	-0.376	1.000	-0.714	0.102
Lateral (2)	0.308	-0.397	1.000	0.035	0.353	-0.559	1.000	0.083	0.370	-0.677	1.000	0.137	0.353	-0.714	1.000	0.127
Shear (3)	0.038	0.027	0.035	1.000	-0.076	0.027	0.083	1.000	-0.127	0.061	0.137	1.000	-0.175	0.102	0.127	1.000
1), (2), (3): Axial, Lateral and Shear Strains, respectively.																

(1), (2), (3): Axial, Lateral and Shear Strains, respectively.

Table 4. Correlation Matrices Generated from the Average of Three Test Specimens in 1mm Square Basis for Two Different Locations Within the Test Area

MACHINE DIRECTION (MD)								
	ALONG THE EDGES OF THE SPECIMENS				ALONG THE CENTER OF THE SPECIMENS			
	Grammage	Axial	Lateral	Shear	Grammage	Axial	Lateral	Shear
Grammage	1.000	-0.365	0.515	0.044	1.000	-0.502	0.407	-0.050
Axial (1)	-0.365	1.000	-0.748	0.097	-0.502	1.000	-0.536	-0.113
Lateral (2)	0.515	-0.748	1.000	-0.128	0.407	-0.536	1.000	-0.095
Shear (3)	0.044	0.097	-0.128	1.000	-0.050	-0.113	-0.095	1.000

CROSS MACHINE DIRECTION (CD)								
	ALONG THE EDGES OF THE SPECIMENS				ALONG THE CENTER OF THE SPECIMENS			
	Grammage	Axial	Lateral	Shear	Grammage	Axial	Lateral	Shear
Grammage	1.000	-0.384	0.640	-0.171	1.000	-0.410	0.659	0.055
Axial (1)	-0.384	1.000	-0.496	0.031	-0.410	1.000	-0.388	-0.087
Lateral (2)	0.640	-0.496	1.000	-0.054	0.659	-0.388	1.000	-0.093
Shear (3)	-0.171	0.031	-0.054	1.000	0.055	-0.087	-0.093	1.000

HANDSHEETS								
	ALONG THE EDGES OF THE SPECIMENS				ALONG THE CENTER OF THE SPECIMENS			
	Grammage	Axial	Lateral	Shear	Grammage	Axial	Lateral	Shear
Grammage	1.000	-0.279	0.458	0.042	1.000	-0.283	0.400	-0.087
Axial (1)	-0.279	1.000	-0.463	-0.028	-0.283	1.000	-0.331	0.104
Lateral (2)	0.458	-0.463	1.000	0.032	0.400	-0.331	1.000	-0.140
Shear (3)	0.042	-0.028	0.032	1.000	-0.087	0.104	-0.140	1.000

(1), (2), (3): Axial, Lateral and Shear Strains, respectively.

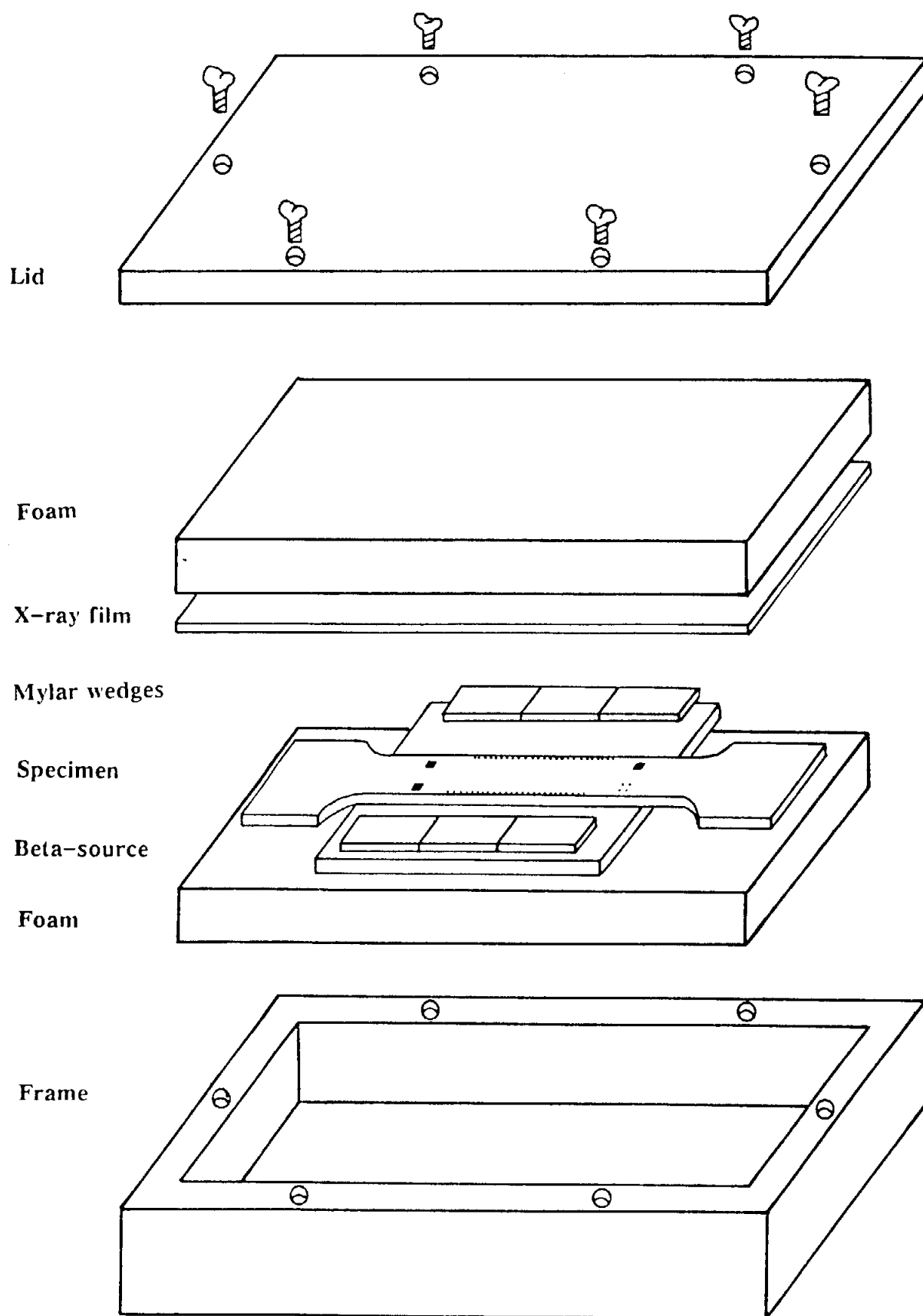


Fig. 1. Schematics of the beta-radiography chamber.
The fig. shows only one paper specimen.

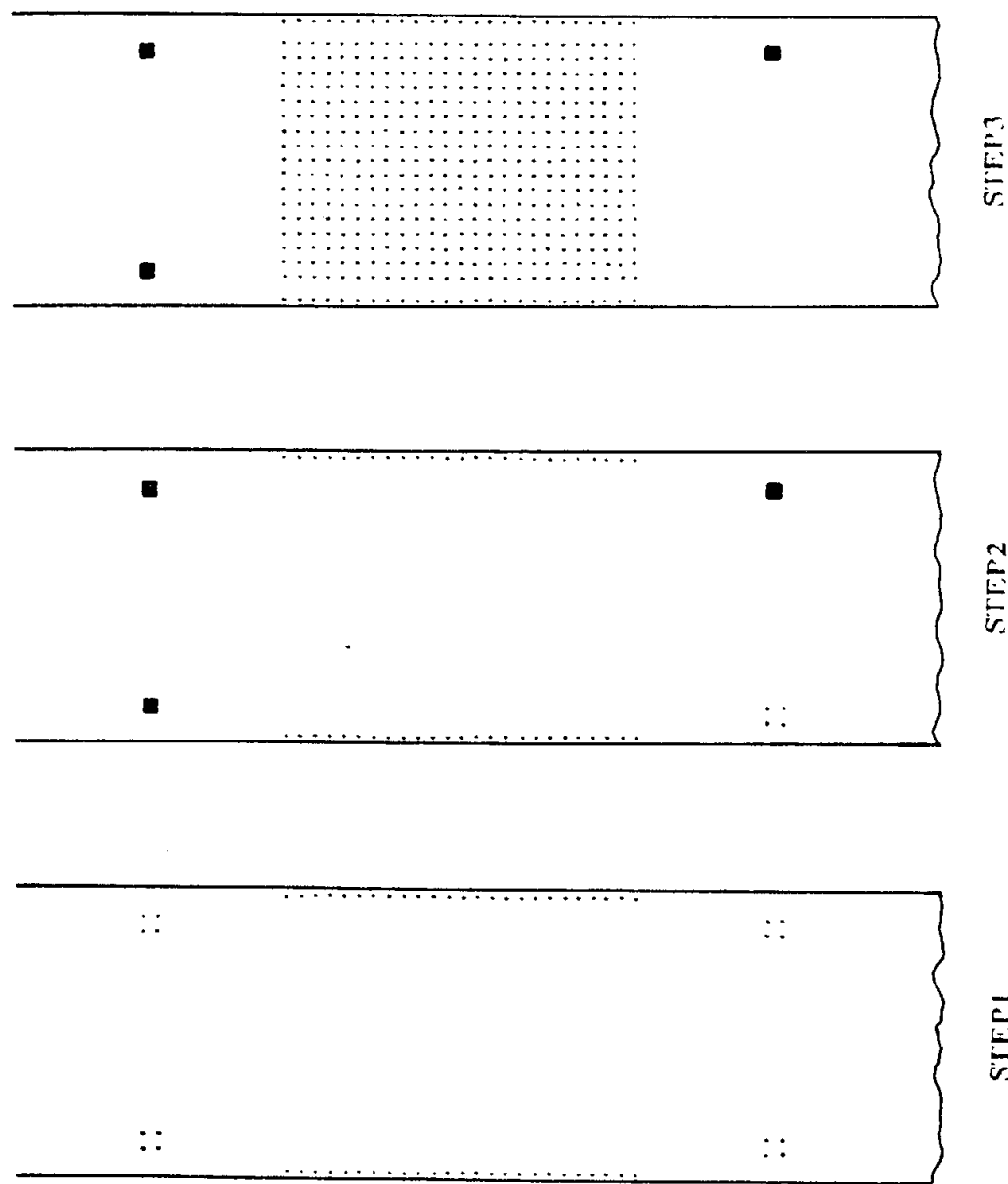
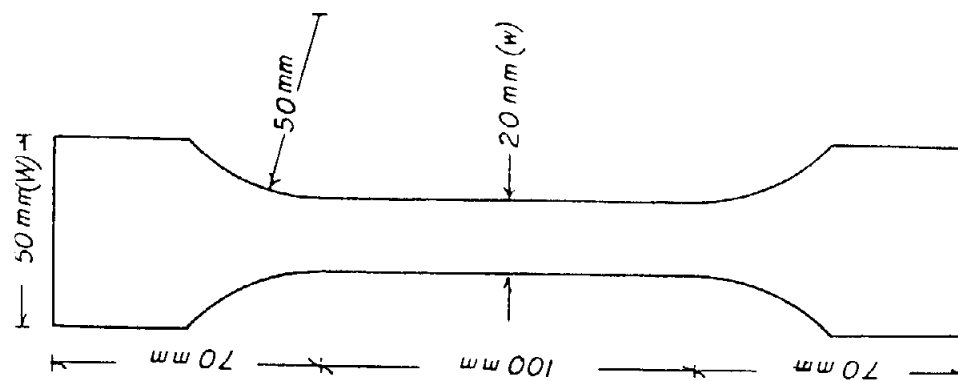


Fig. 2. Preparation of the necked-down specimen for beta-radiography and for the tensile test.
 STEP1: Center portion of the specimen with the two orientation columns of dots in plane with four-dots reference marks used to superimpose the three pieces of self-adhesive tape of 1mm square as shown in STEP2.
 STEP2: Specimen used for beta-radiography.
 STEP3: Specimen used for tensile test, showing the dot matrix used for strain field determination.

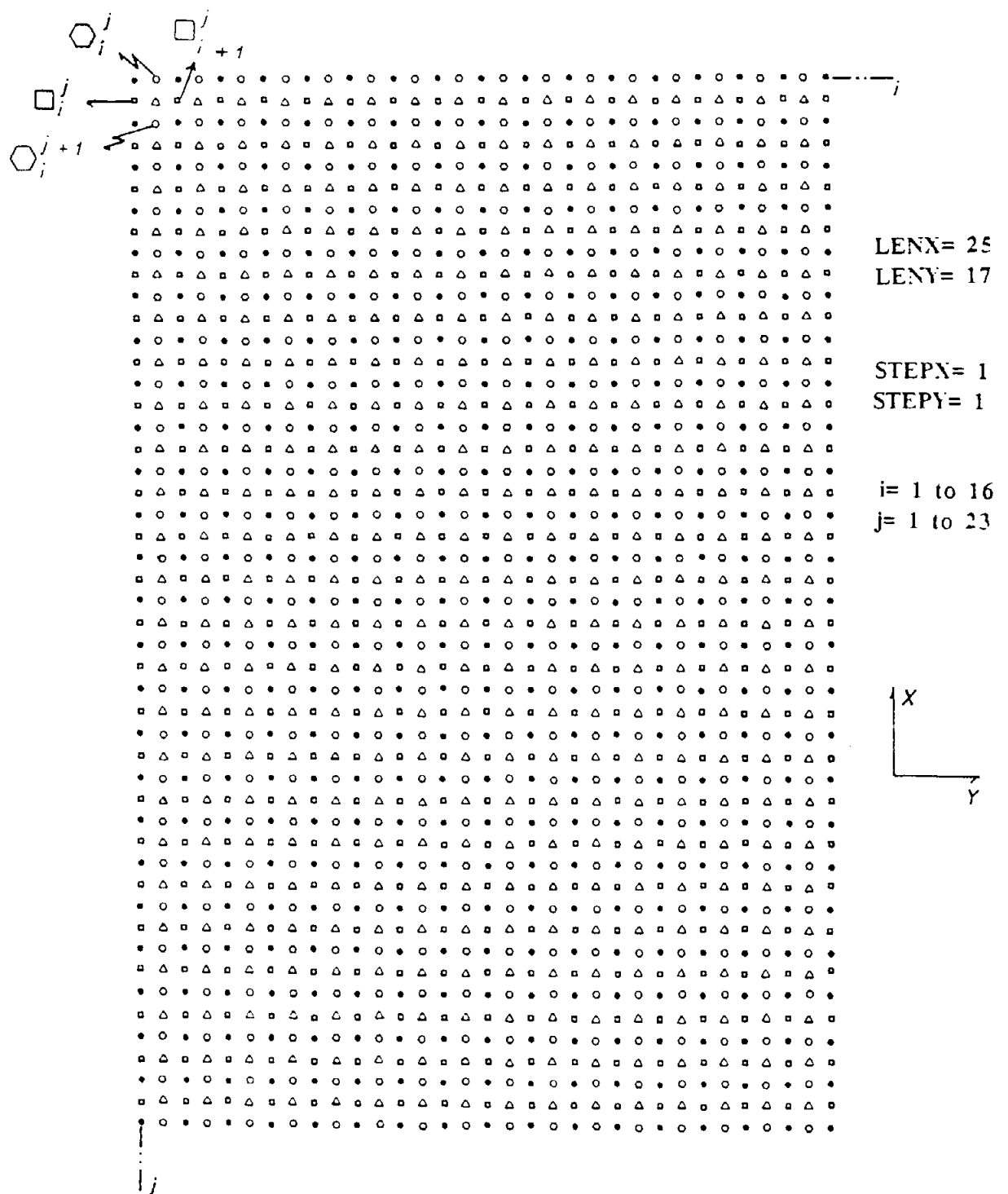


Fig. 3. Array dimensions for strain calculations.

SIMBOLS	NATURE OF INFORMATION	DIMENSIONS OF ARRAY
•	Displacement data	(LENX,LENY)
□	Axial strain	(LENX-STEPX,LENY)
○	Lateral strain	(LENX,LENY-STEPLY)
△	Shear strain	(LENX-STEPX,LENY-STEPLY)

NOTE: LENX, LENY, STEPX and STEPLY are defined in Chapter 3.

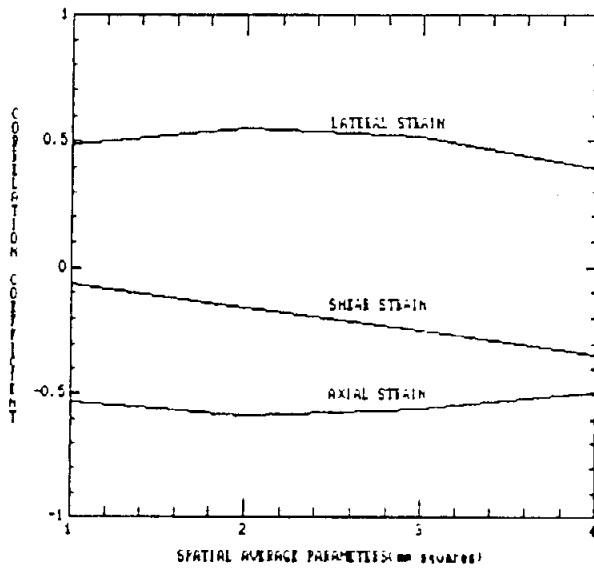


Fig. 4.1. MD specimens.

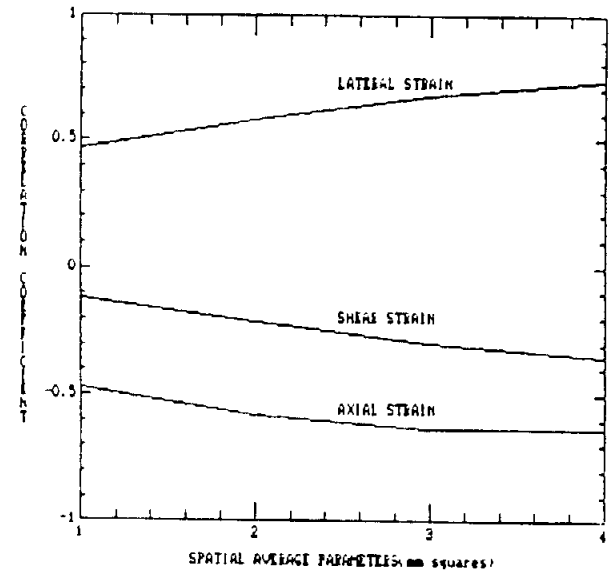


Fig. 4.2. CD specimens.

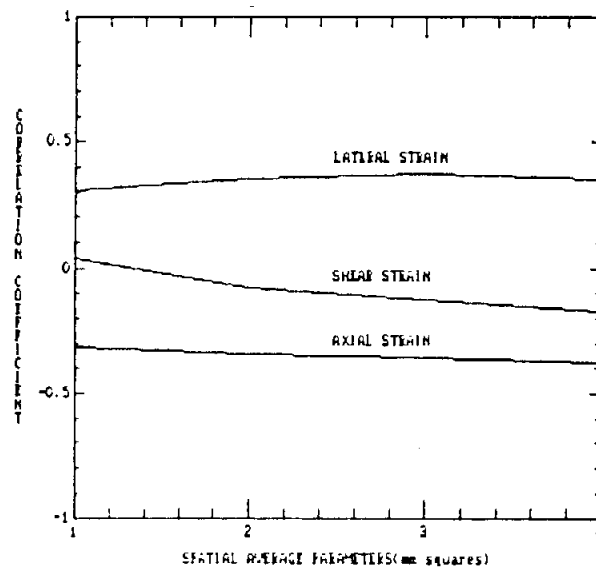


Fig. 4.3. Handsheets.

Fig. 4. Influence of the spatial average parameters on the correlation between grammage and strains.

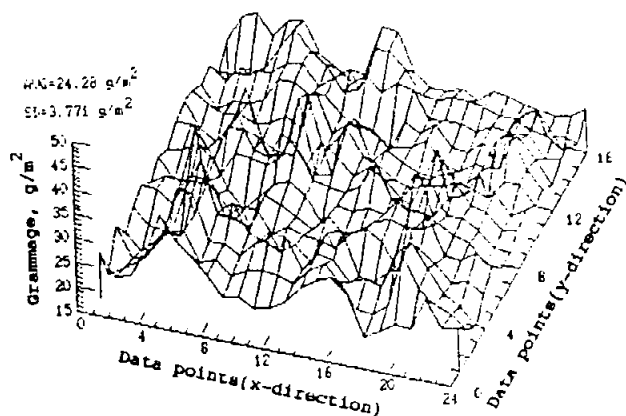


Fig. 5.1. Typical 3-D view for MD specimens (MD specimen no. 2)

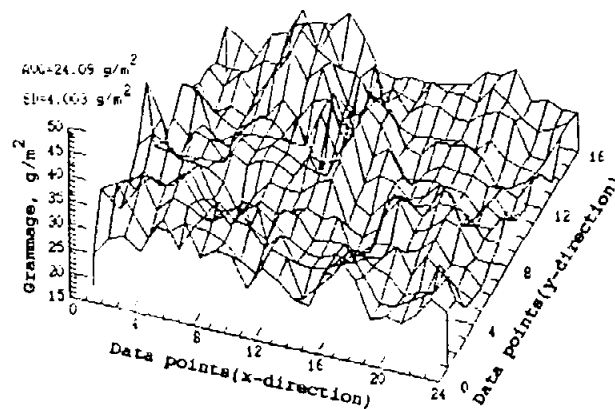


Fig. 5.2. Typical 3-D view for CD specimens (CD specimen no. 3)

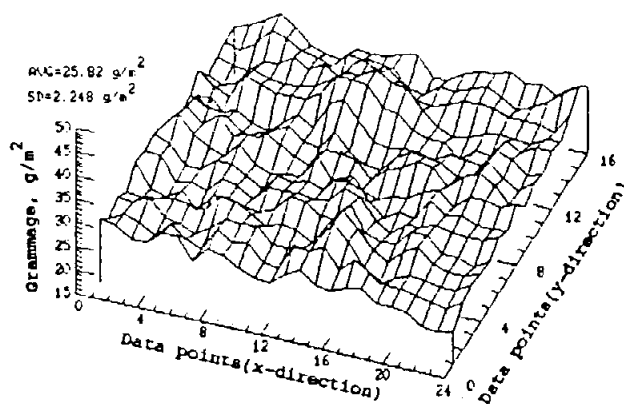


Fig. 5.3. Typical 3-D view for Handsheet specimens (HANDSHEET specimen no. 1)

Fig. 5. Typical 3-dimensional (3-D) view of the grammage distribution on 1 mm square basis for machine made paper and handsheet.

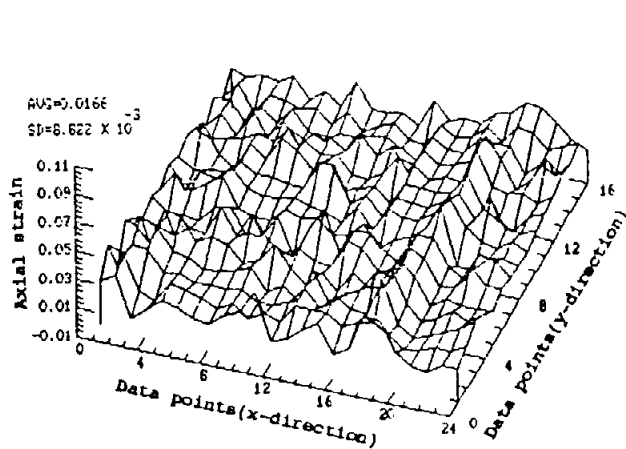


Fig. 6.1. Typical 3-D view for MD specimens (MD specimen no. 2)

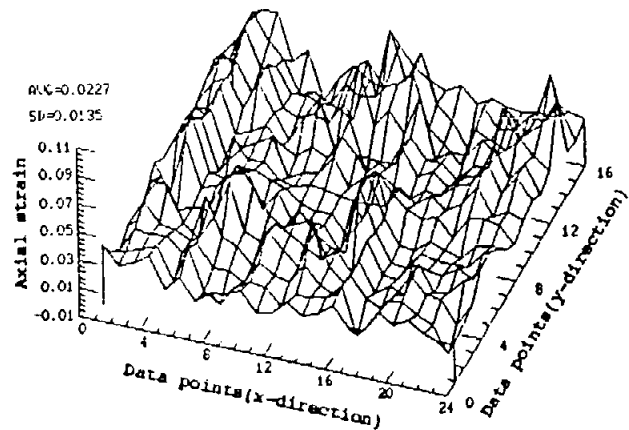


Fig. 6.2. Typical 3-D view for CD specimens (CD specimen no. 3)

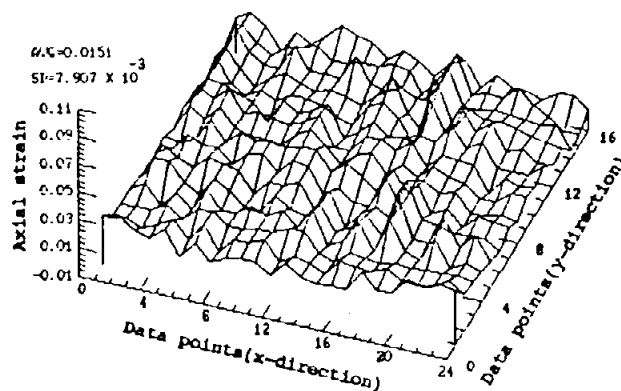


Fig. 6.3. Typical 3-D view for Handsheet specimens (HANDSHEET specimen no. 1)

Fig. 6. Typical 3-dimensional (3-D) view of the axial strain distribution on 1 mm square basis for machine made paper and handsheet.

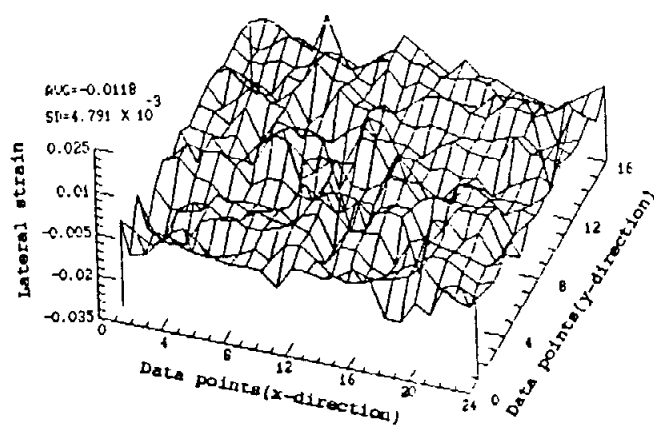


Fig. 7.1. Typical 3-D view for MD specimens (MD specimen no. 2)

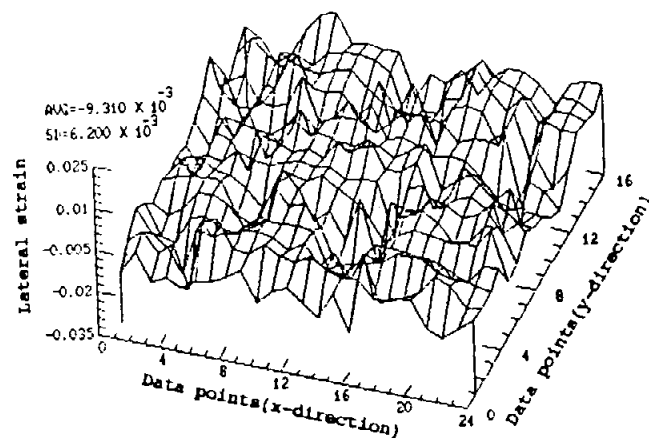


Fig. 7.2. Typical 3-D view for CD specimens (CD specimen no. 3)

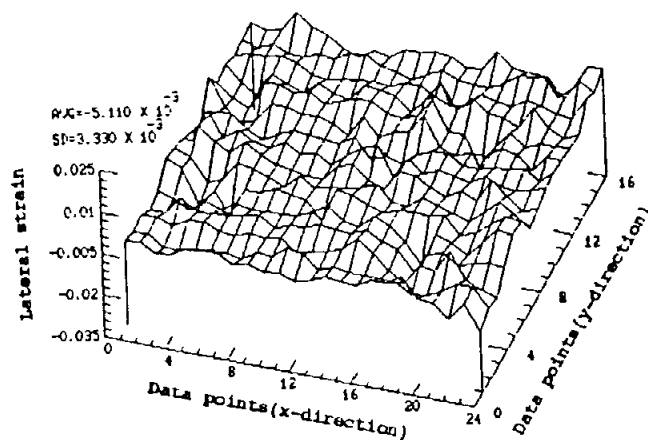


Fig. 7.3. Typical 3-D view for Handsheet specimens (HANDSHEET specimen no. 1)

Fig. 7. Typical 3-dimensional (3-D) view of the lateral strain distribution on 1 mm square basis for machine made paper and handsheet.

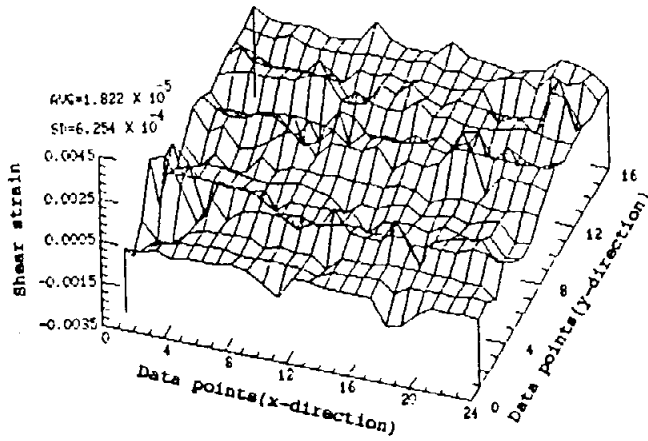


Fig. 8.1. Typical 3-D view for MD specimens (MD specimen no. 2)

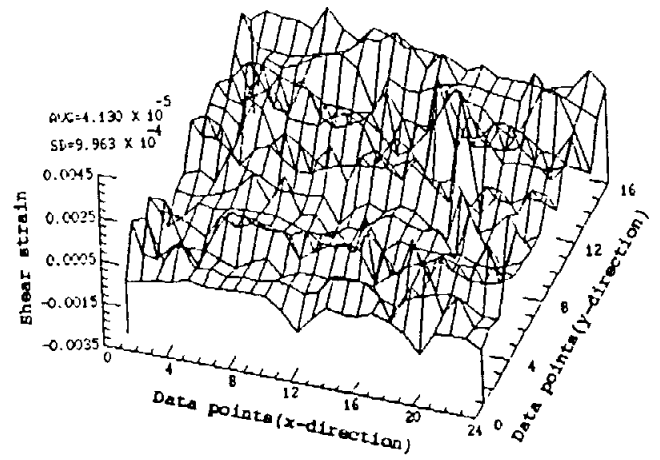


Fig. 8.2. Typical 3-D view for CD specimens (CD specimen no. 3)

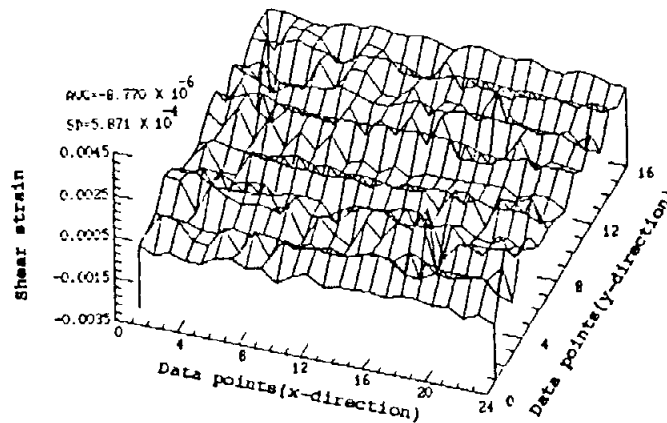


Fig. 8.3. Typical 3-D view for Handsheet specimens (HANDSHEET specimen no. 1)

Fig. 8. Typical 3-dimensional (3-D) view of the shear strain distribution on 1 mm square basis for machine made paper and handsheet.

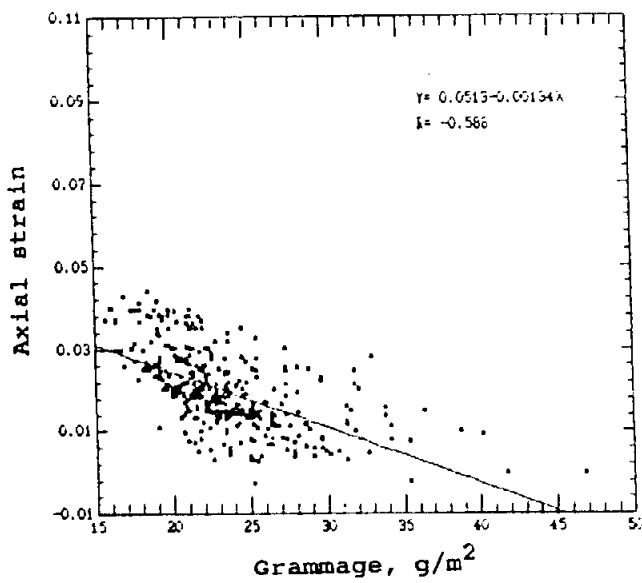


Fig. 9.1. MD specimen no. 1.

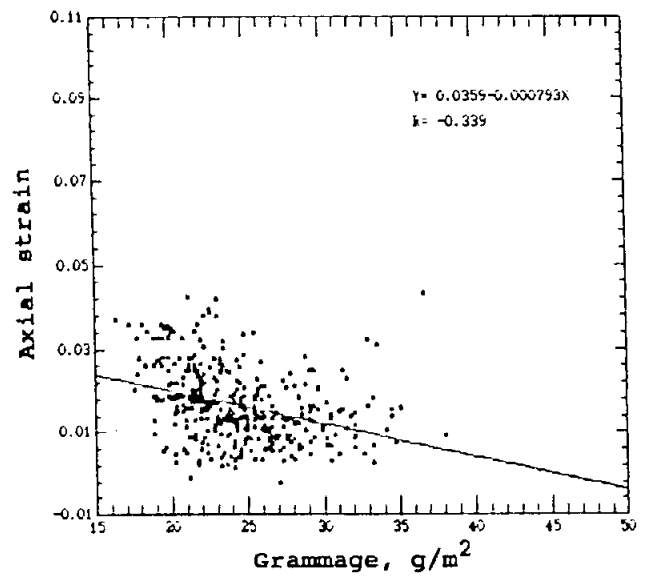


Fig. 9.2. MD specimen no. 2.

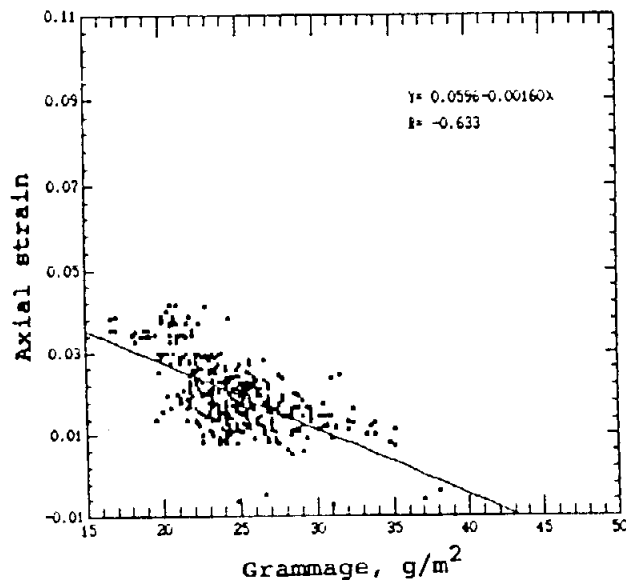


Fig. 9.3. MD specimen no. 3.

Fig. 9. Relationship between grammage and axial strain for MD specimens on 1 mm square basis.

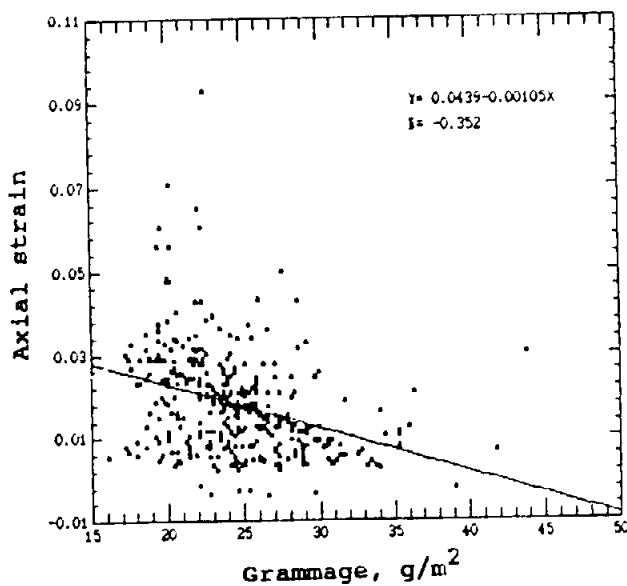


Fig. 10.1. CD specimen no. 1.

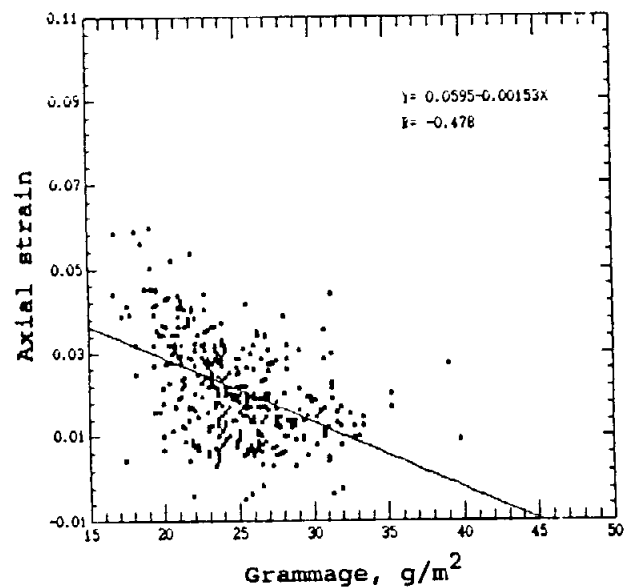


Fig. 10.2. CD specimen no. 2.

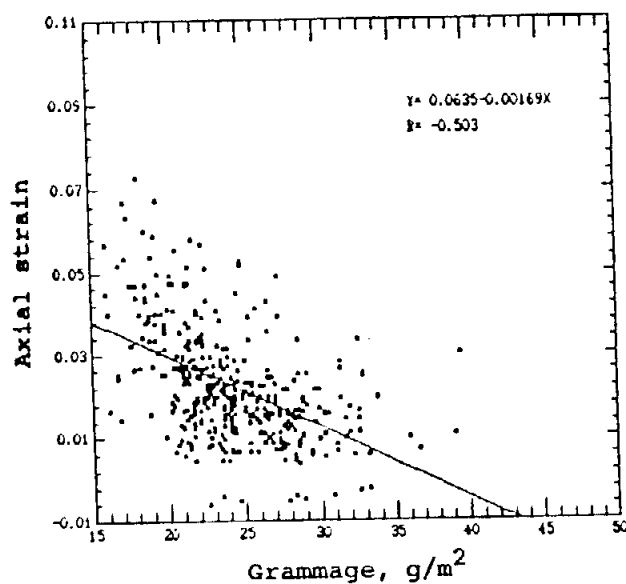


Fig. 10.3. CD specimen no. 3.

Fig. 10. Relationship between grammage and axial strain for CD specimens on 1 mm square basis.

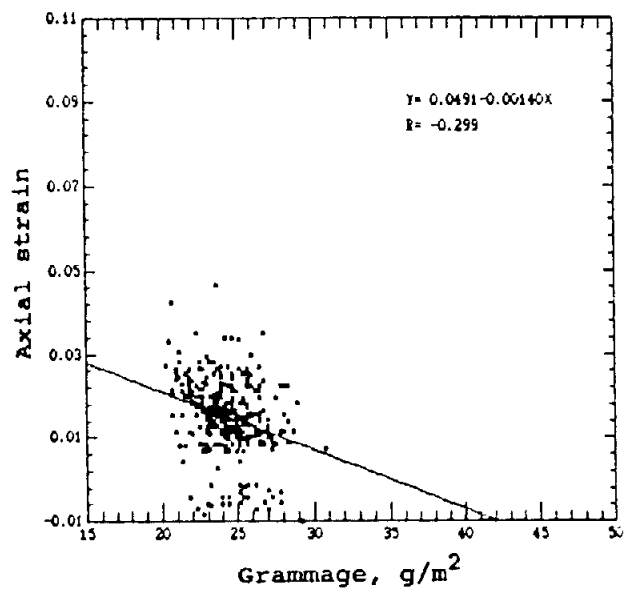
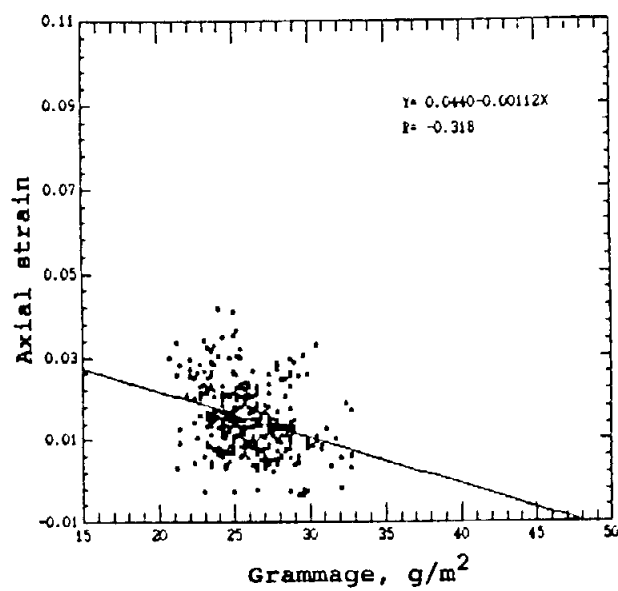


Fig. 11.1. HANDSHEET specimen no. 1. Fig. 11.2. HANDSHEET specimen no. 2

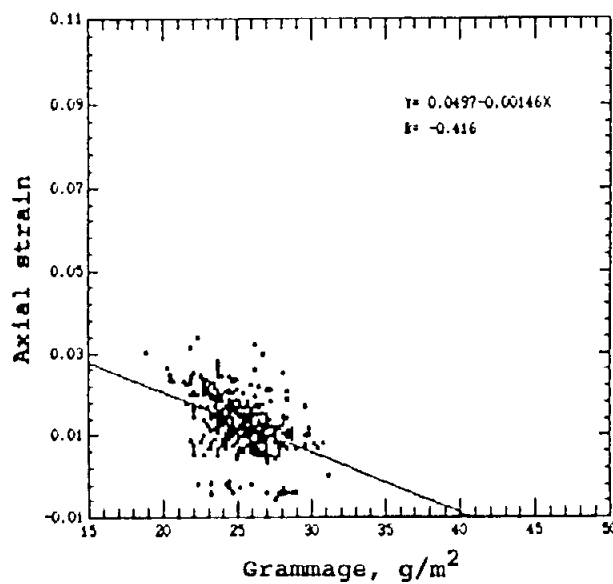


Fig. 11.3. HANDSHEET specimen no. 3.

Fig. 11. Relationship between grammage and axial strain for HANDSHEET specimens on 1 mm square basis.

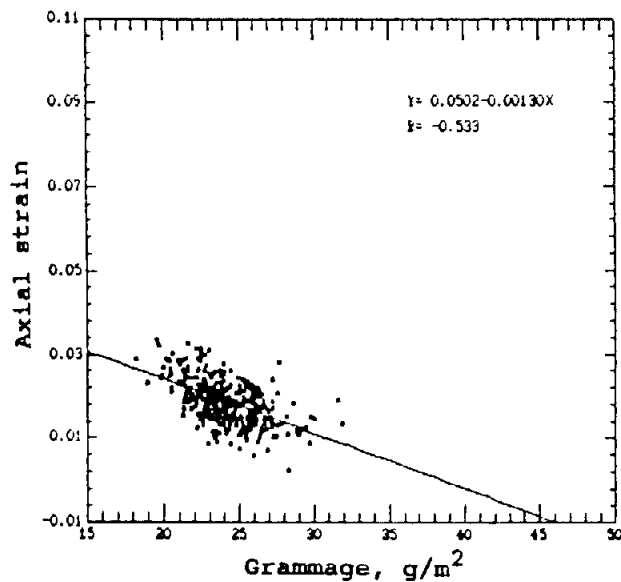


Fig. 12.1. Average from three specimens on 1 mm square basis.

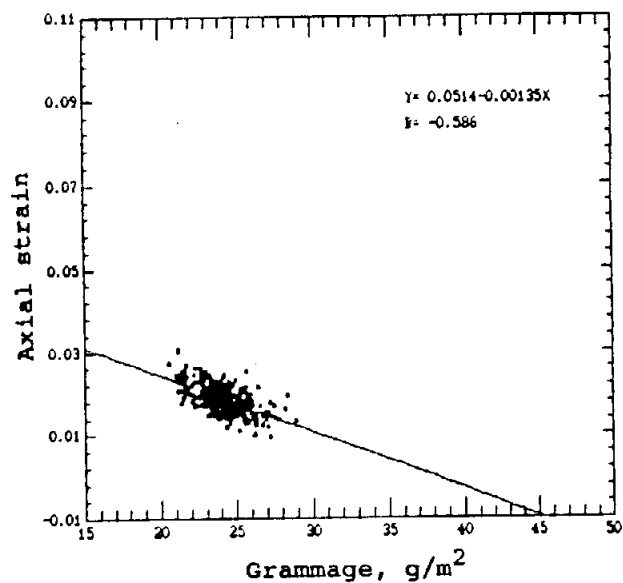


Fig. 12.2. Average from three specimens on 2 mm squares basis.

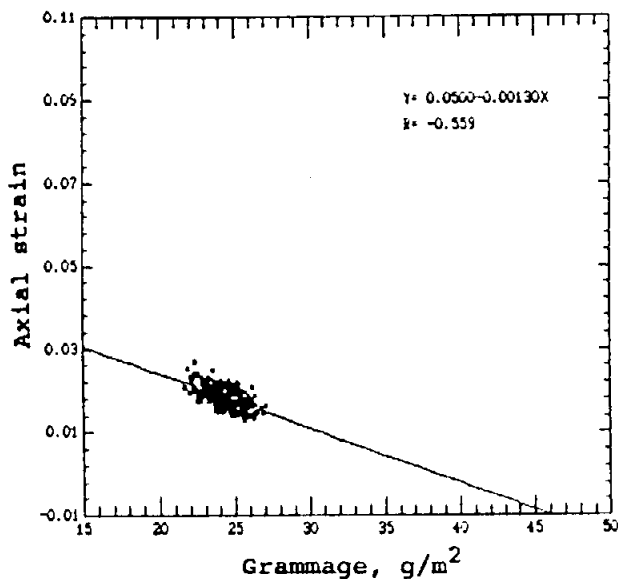


Fig. 12.3. Average from three specimens on 3 mm squares basis.

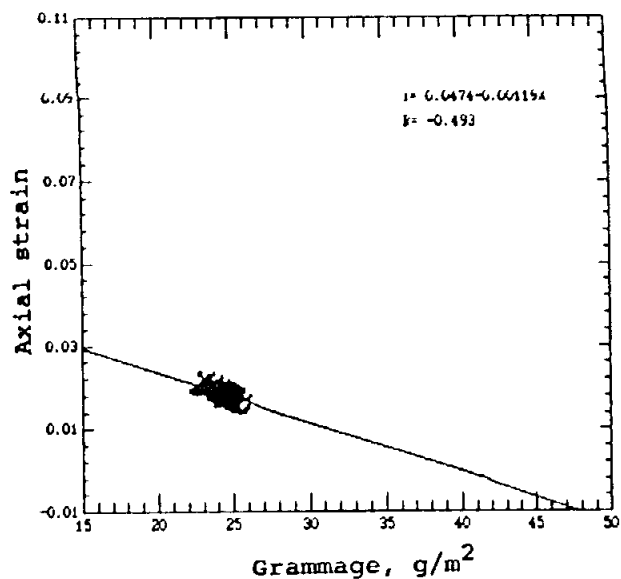


Fig. 12.4. Average from three specimens on 4 mm squares basis.

Fig. 12. Relationship between grammage and axial strain for MD specimens on 1, 2, 3 and 4 mm squares basis.

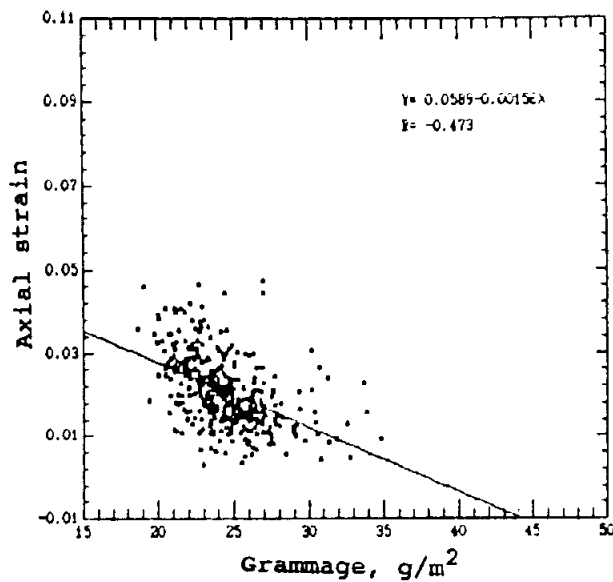


Fig. 13.1. Average from three specimens on 1 mm square basis.

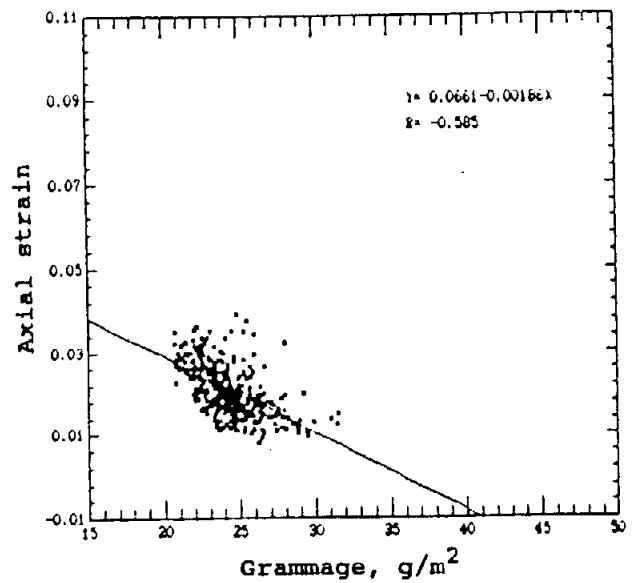


Fig. 13.2. Average from three specimens on 2 mm squares basis.

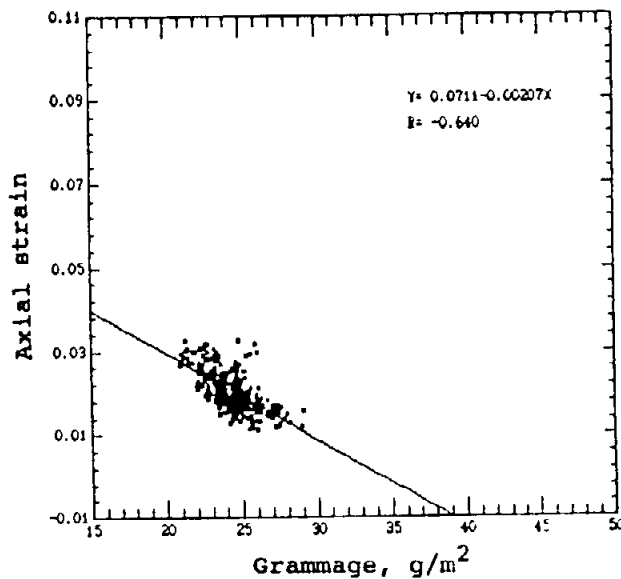


Fig. 13.3. Average from three specimens on 3 mm squares basis.

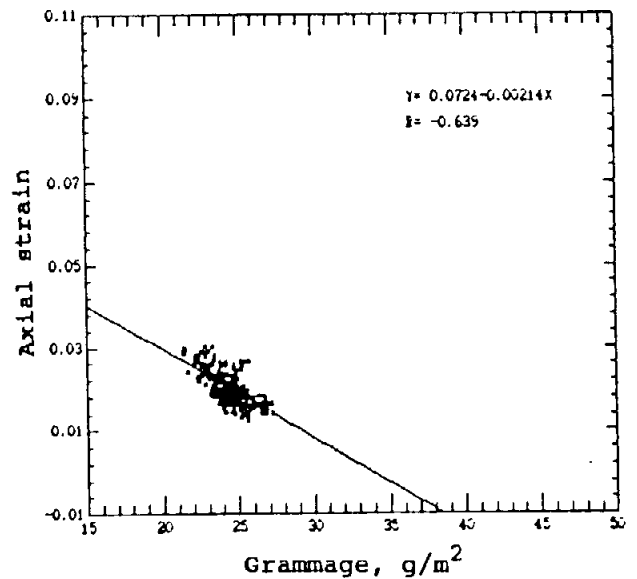


Fig. 13.4. Average from three specimens on 4 mm squares basis.

Fig. 13. Relationship between grammage and axial strain for CD specimens on 1, 2, 3 and 4 mm squares basis.

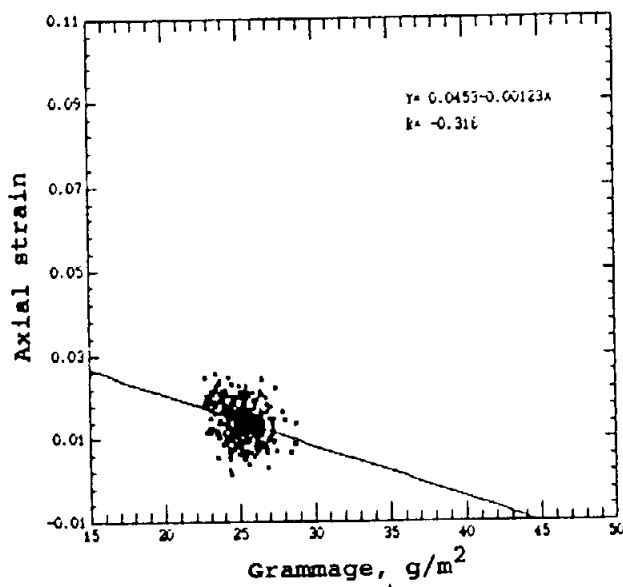


Fig. 14.1. Average from three specimens on 1 mm squares basis.

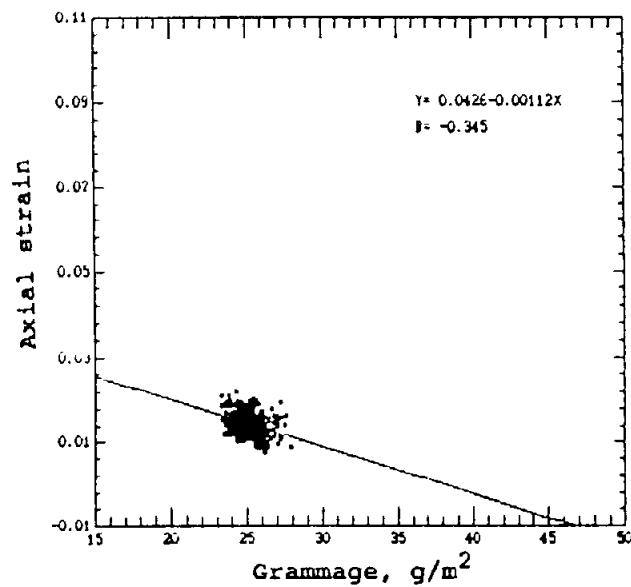


Fig. 14.2. Average from three specimens on 2 mm squares basis..

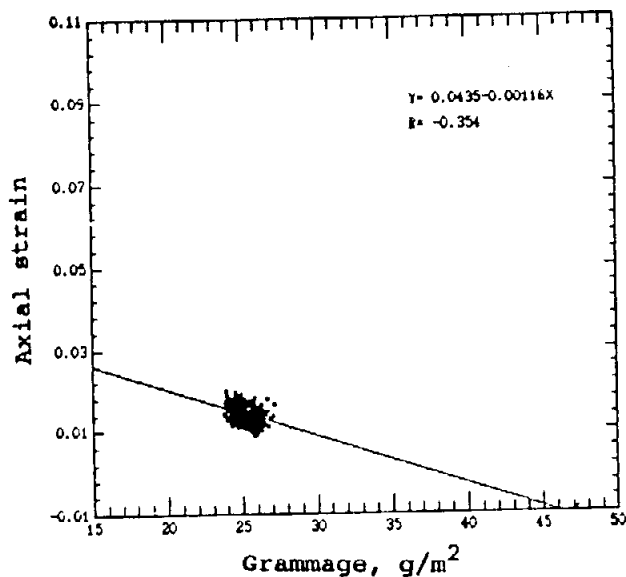


Fig. 14.3. Average from three specimens on 3 mm squares basis.

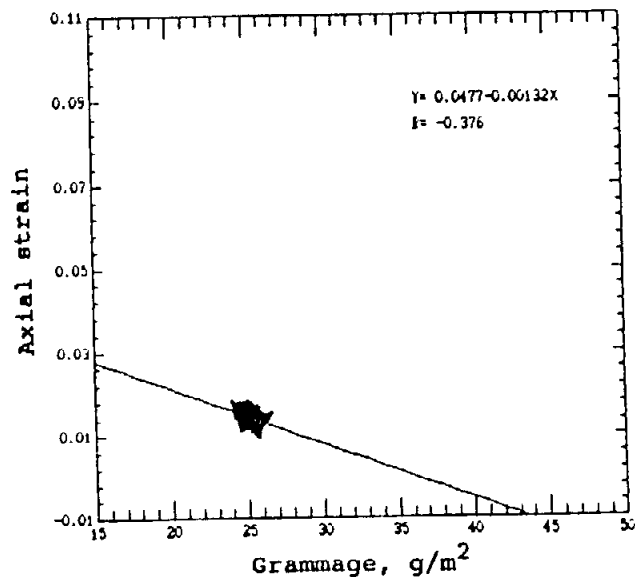


Fig. 14.4. Average from three specimens on 4 mm squares basis.

Fig. 14. Relationship between grammage and axial strain for HANDSHEET specimens on 1, 2, 3 and 4 mm squares basis.

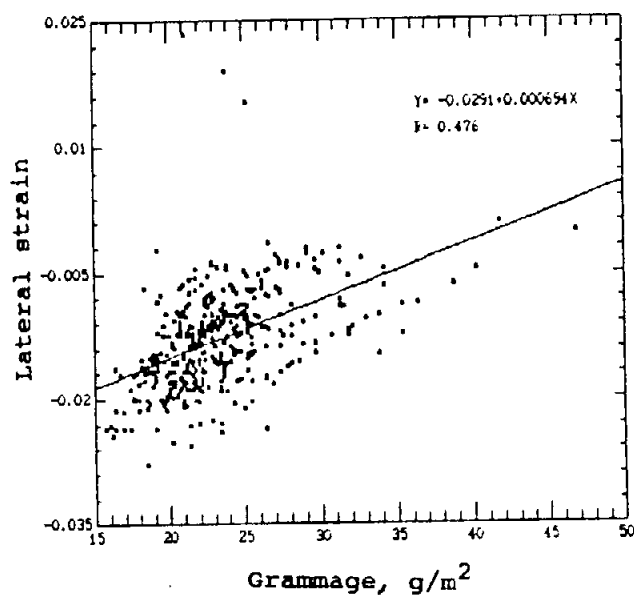


Fig. 15.1. MD specimen no. 1.

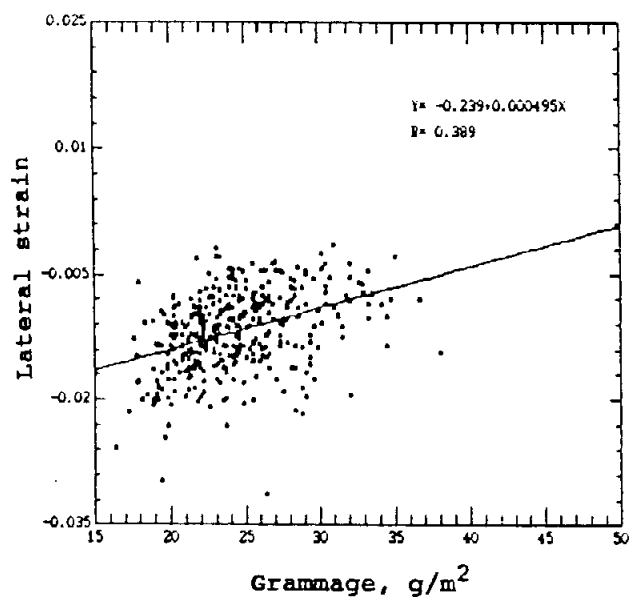


Fig. 15.2. MD specimen no. 2.

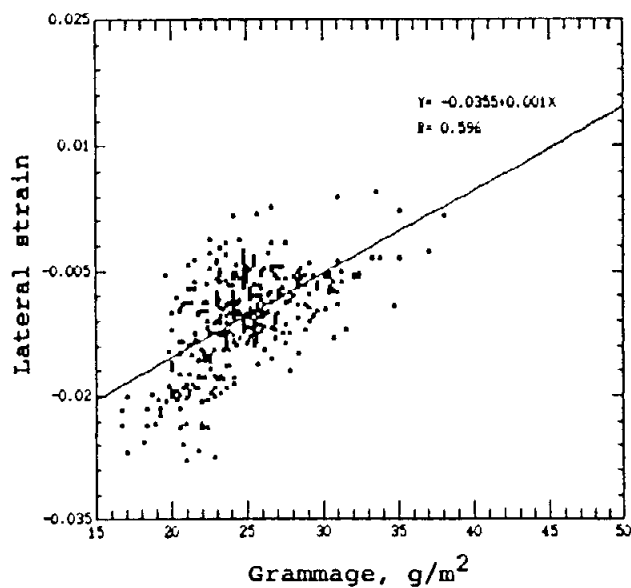


Fig. 15.3. MD specimen no. 3.

Fig. 15. Relationship between grammage and lateral strain for MD specimens on 1 mm square basis.

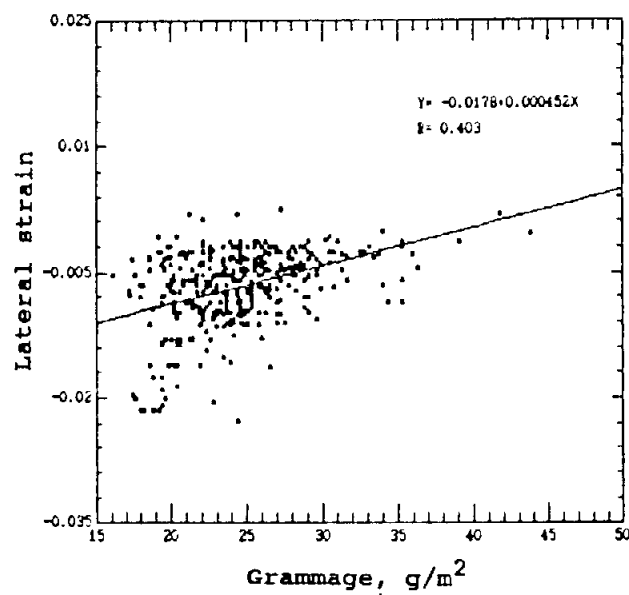


Fig. 16.1. CD specimens no. 1.

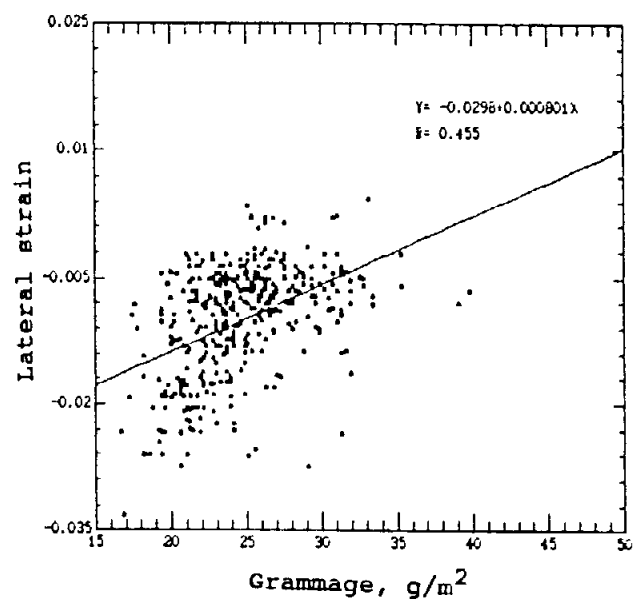


Fig. 16.2. CD specimen no. 2.

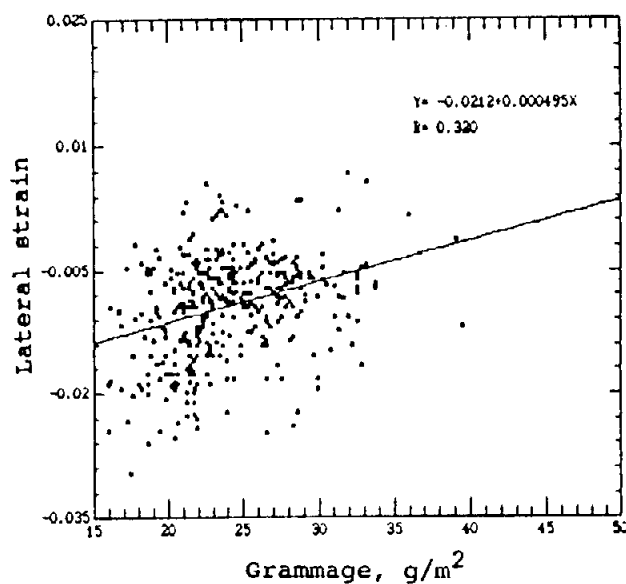


Fig. 16.3. CD specimen no. 3.

Fig. 16. Relationship between grammage and lateral strain for CD specimens on 1 mm square basis.

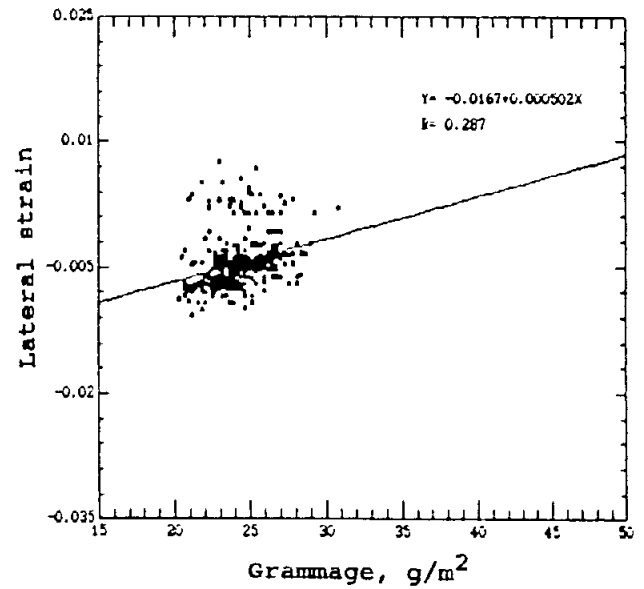
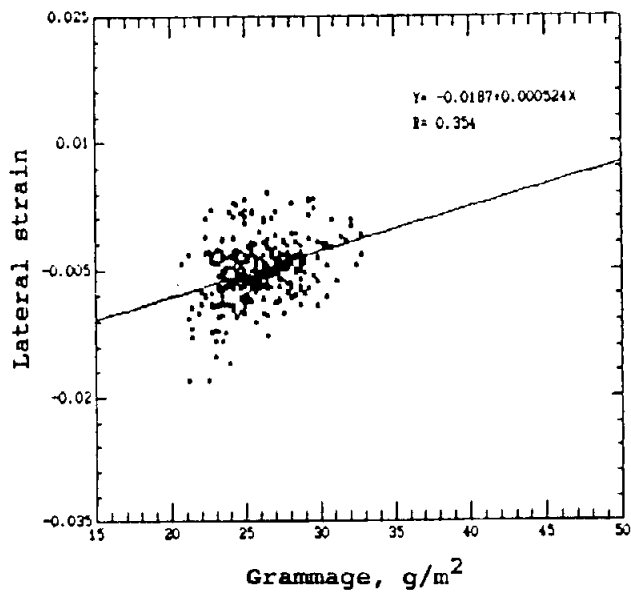


Fig. 17.1. HANDSHEET specimen no. 1. Fig. 17.2. HANDSHEET specimen no. 2.

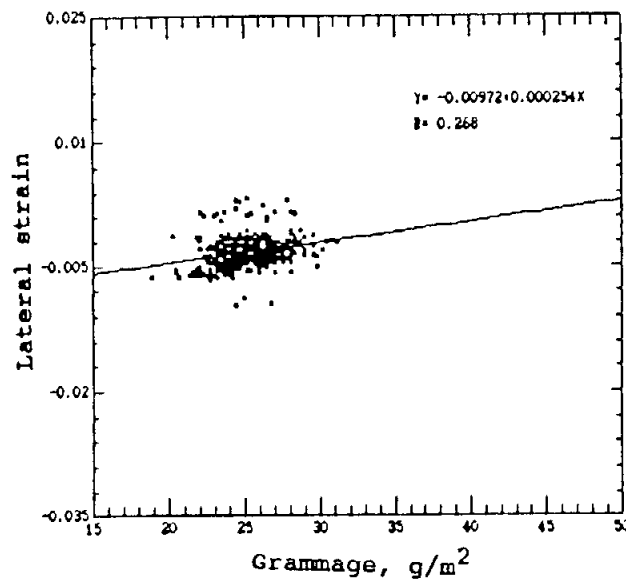


Fig. 17.3. HANDSHEET specimen no. 3.

Fig. 17. Relationship between grammage and lateral strain for HANDSHEET specimens on 1 mm square basis.

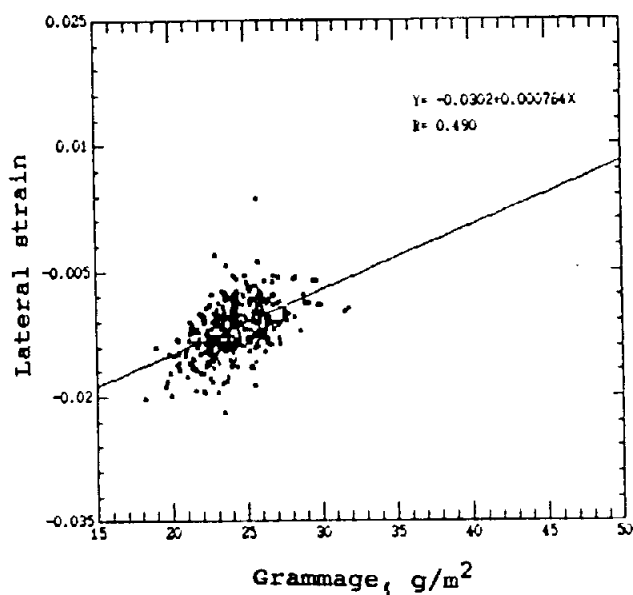


Fig. 18.1. Average from three specimens on 1 mm square basis.

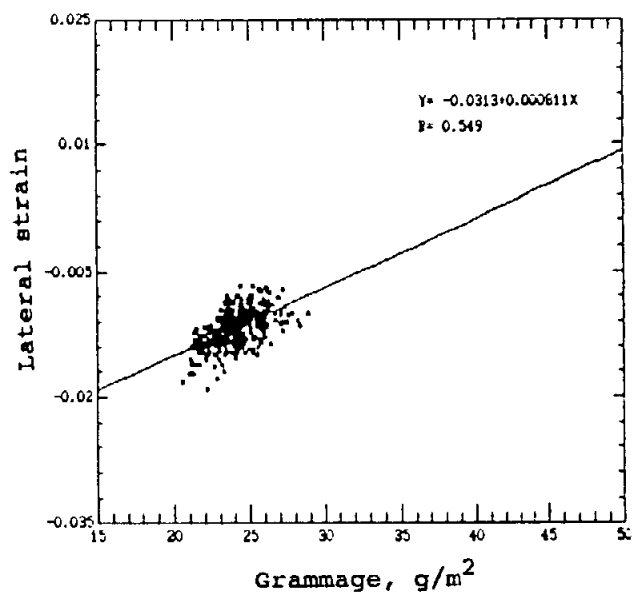


Fig. 18.2. Average from three specimens on 2 mm square basis.

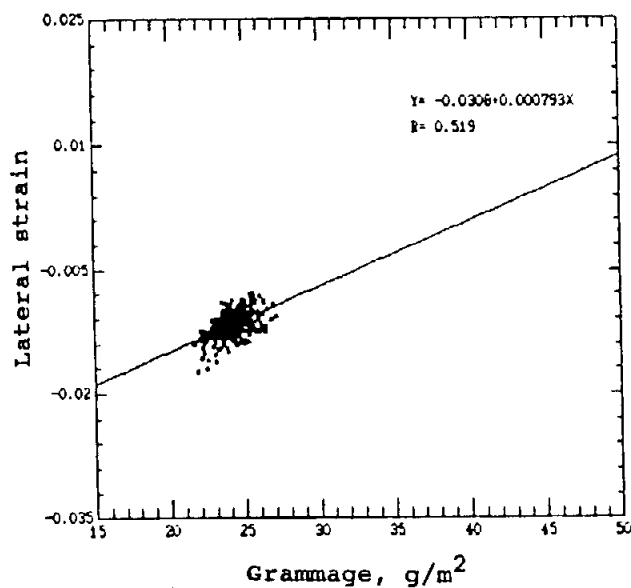


Fig. 18.3. Average from three specimens on 3 mm square basis.

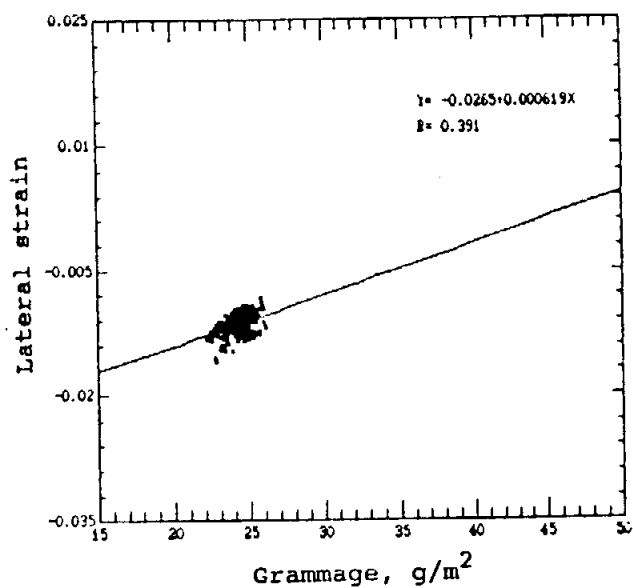


Fig. 18.4. Average from three specimens on 4 mm square basis.

Fig. 18. Relationship between grammage and lateral strain for MD specimens on 1, 2, 3 and 4 mm squares basis.

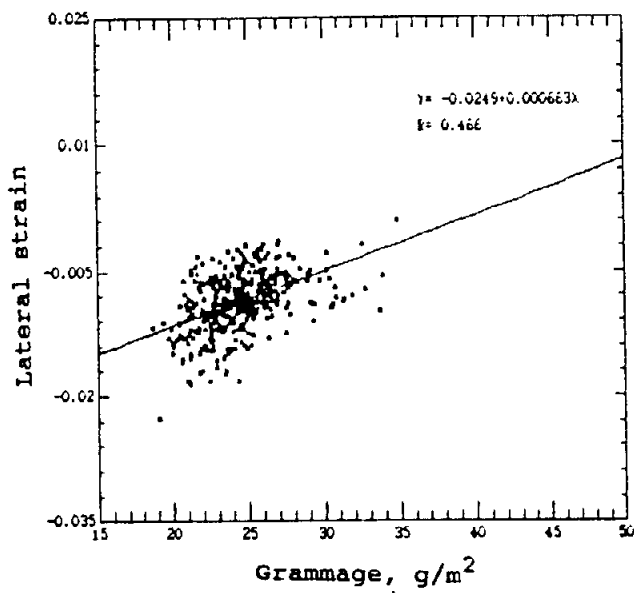


Fig. 19.1. Average from three specimens on 1 mm square basis.

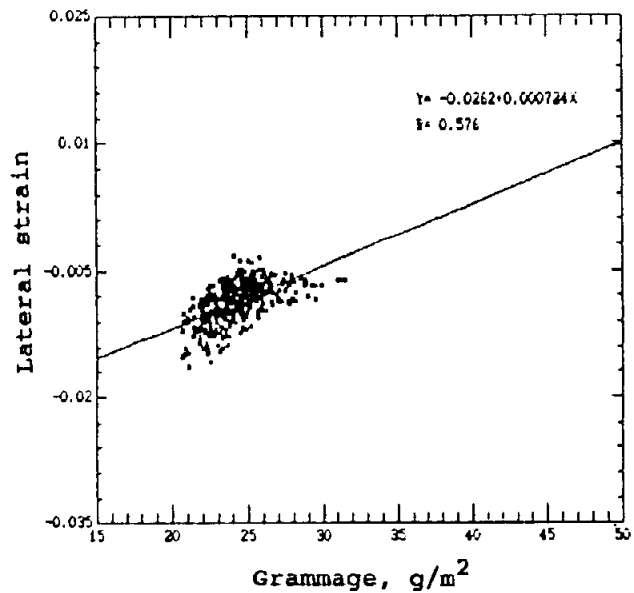


Fig. 19.2. Average from three specimens on 2 mm squares basis.

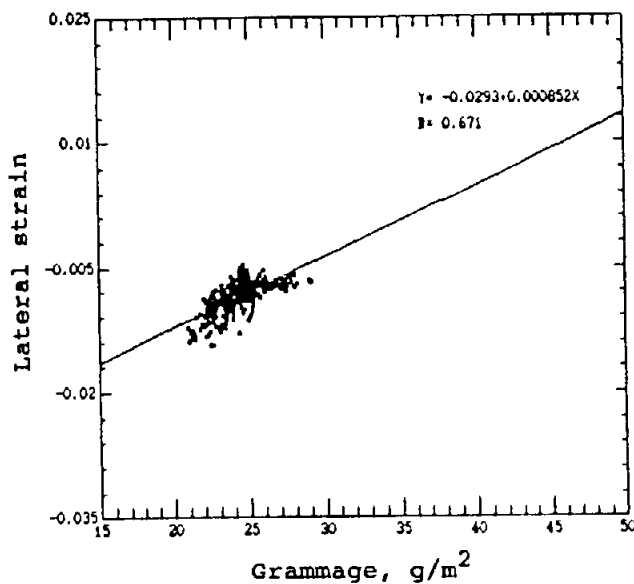


Fig. 19.3. Average from three specimens on 3 mm squares basis.

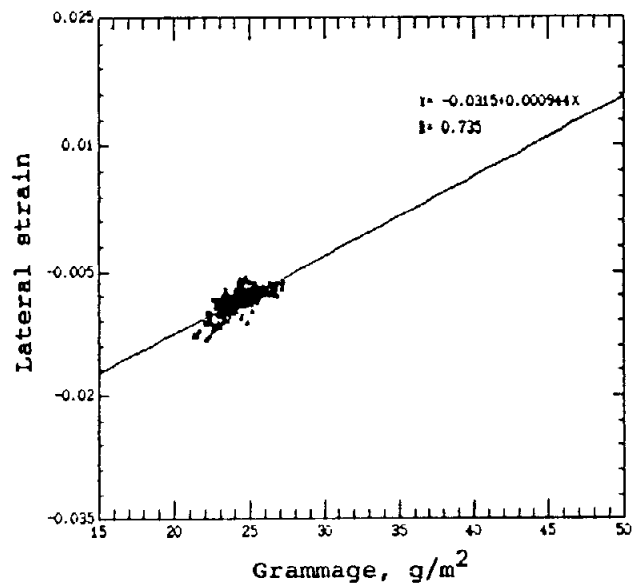


Fig. 19.4. Average from three specimens on 4 mm squares basis.

Fig. 19. Relationship between grammage and lateral strain for CD specimens on 1, 2, 3 and 4 mm squares basis.

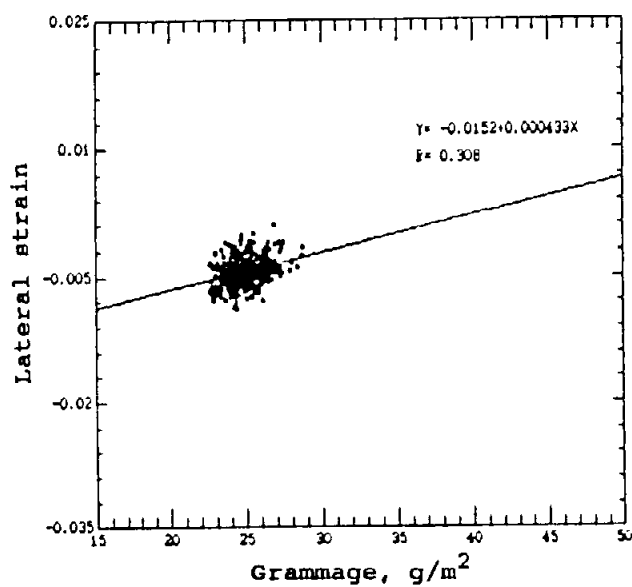


Fig. 20.1. Average from three specimens on 1 mm square basis.

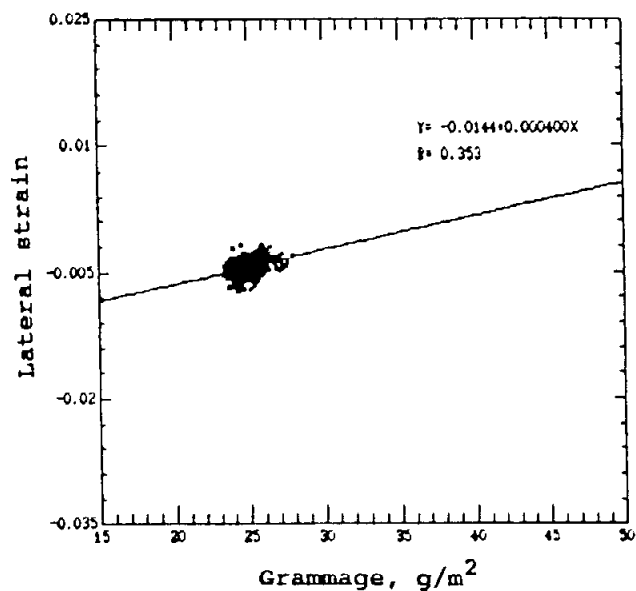


Fig. 20.2. Average from three specimens on 2 mm squares basis.

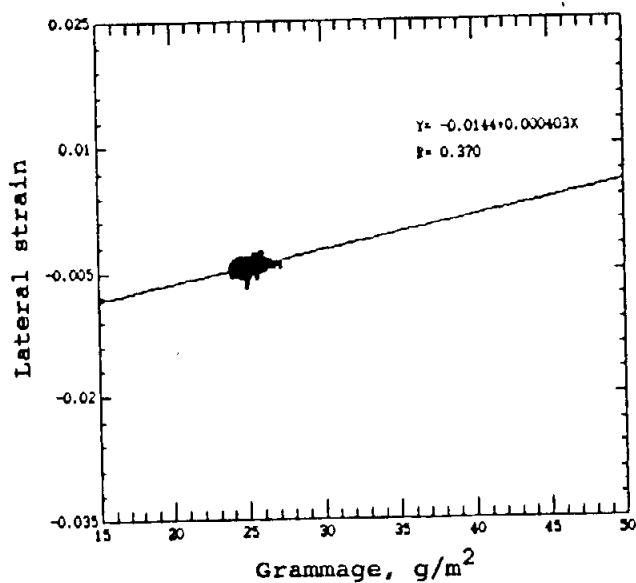


Fig. 20.3. Average from three specimens on 3 mm squares basis.

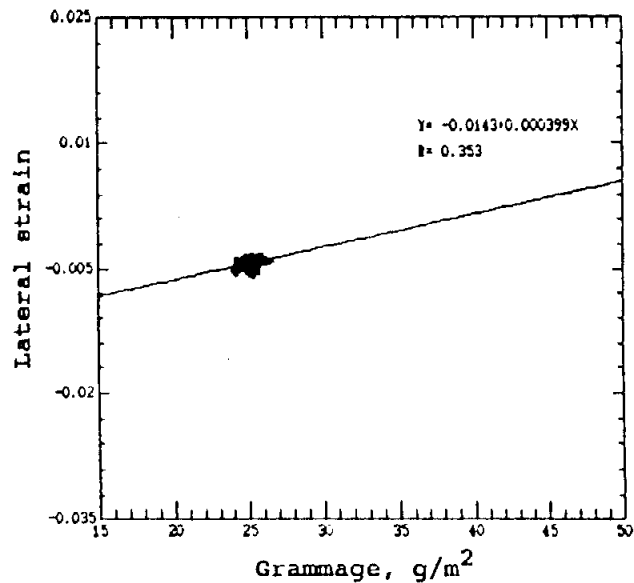


Fig. 20.4. Average from three specimens on 4 mm squares basis.

Fig. 20. Relationship between grammage and lateral strain for HANDSHEET specimens on 1, 2, 3 and 4 mm squares basis.

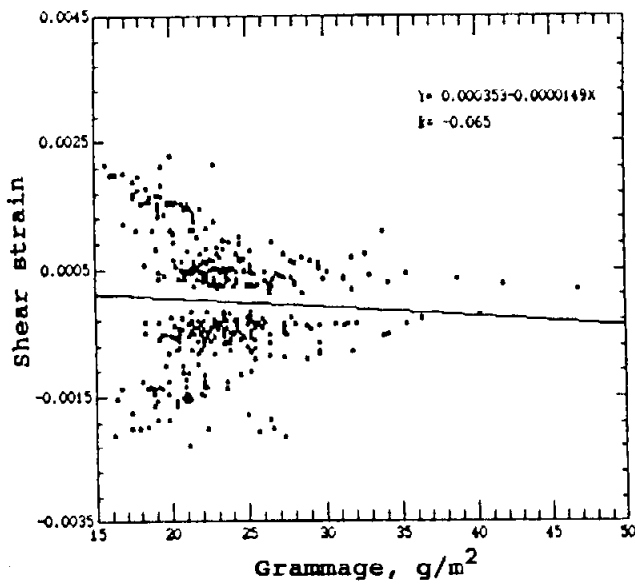


Fig. 21.1. MD specimen no. 1.

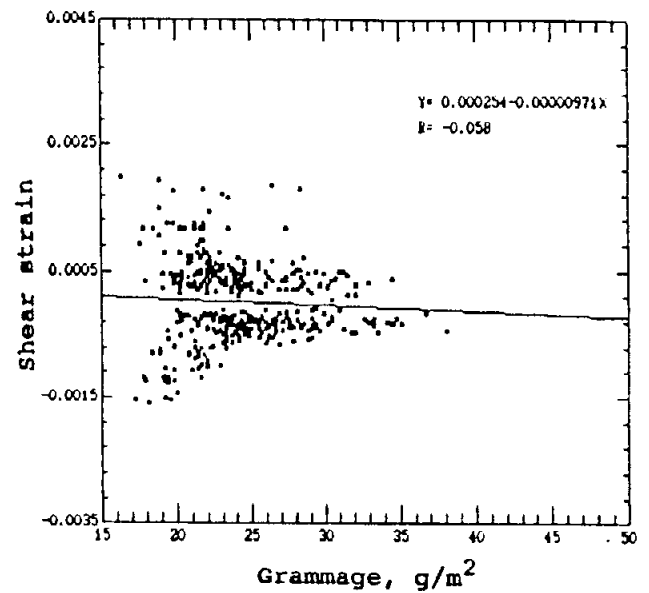


Fig. 21.2. MD specimen no. 2.

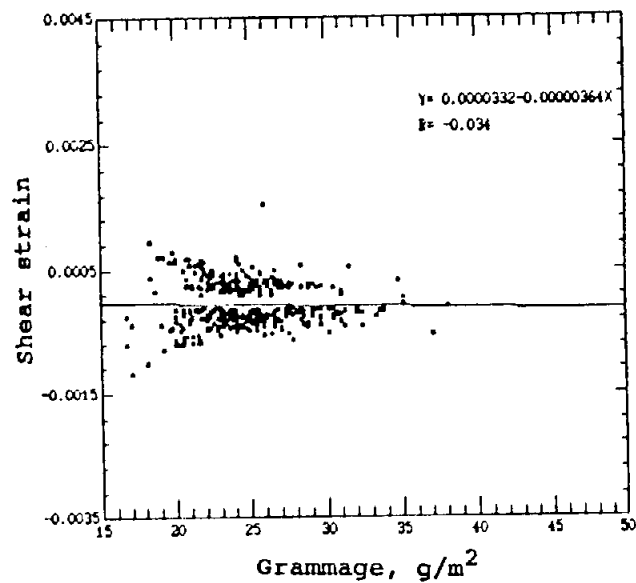


Fig. 21.3. MD specimen no. 3.

Fig. 21. Relationship between grammage and shear strain for MD specimens on 1 mm square basis.

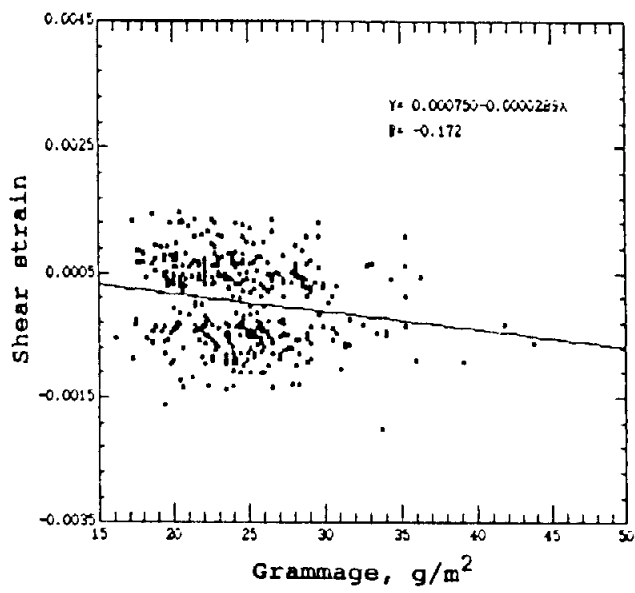


Fig. 22.1. CD specimen no. 1.

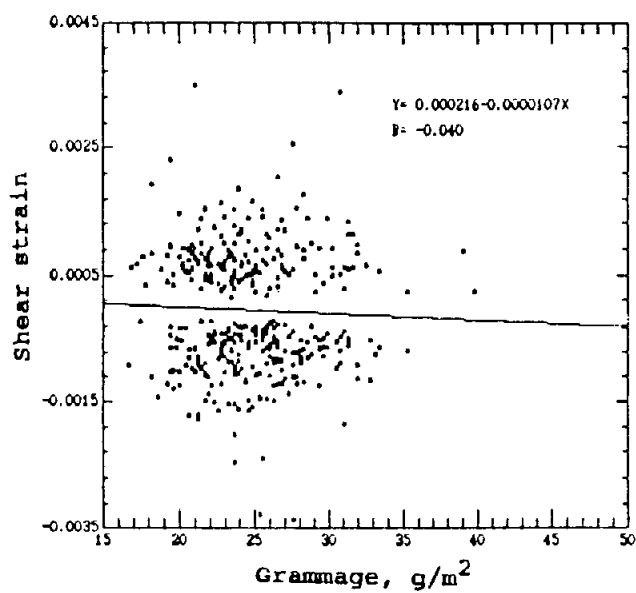


Fig. 22.2. CD specimen no. 2.

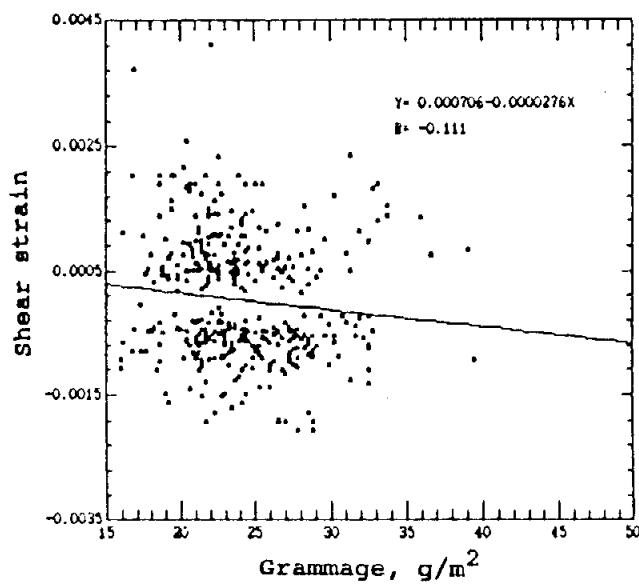


Fig. 22.3. CD specimen no. 3.

Fig. 22. Relationship between grammage and shear strain for CD specimens on 1 mm square basis.

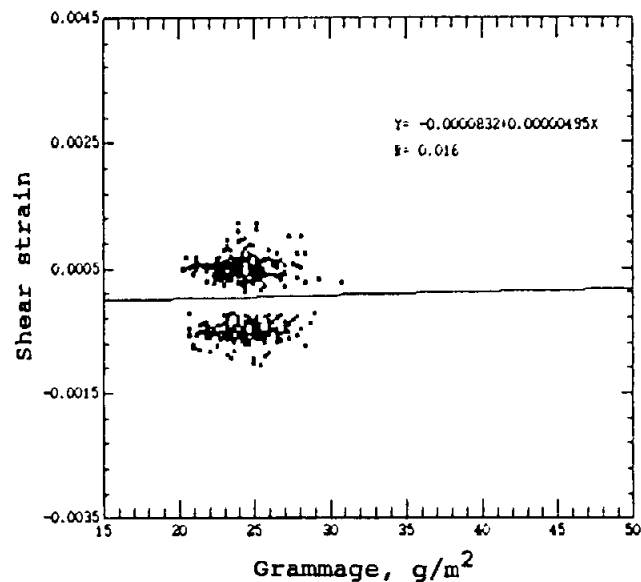
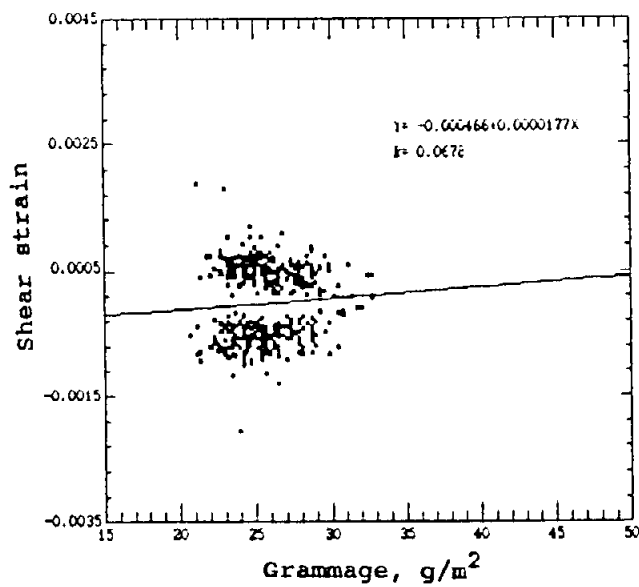


Fig. 23.1. HANDSHEET specimen no. 1. Fig. 23.2. HANDSHEET specimen no. 2.

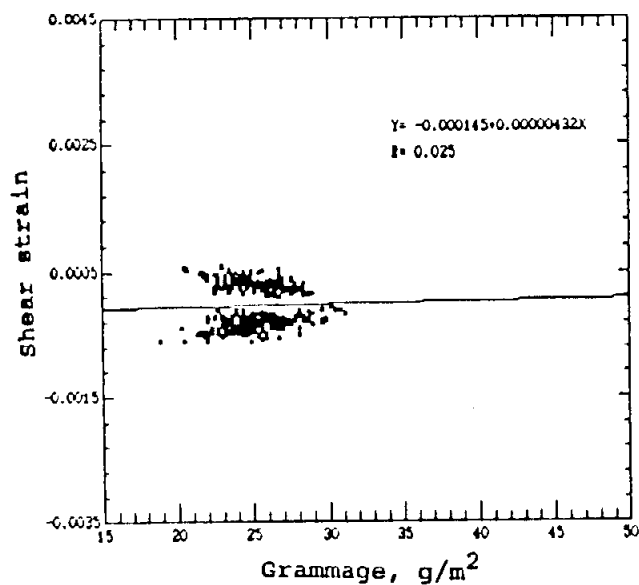


Fig. 23.3. HANDSHEET specimen no. 3.

Fig. 23. Relationship between grammage and shear strain for HANDSHEET specimens on 1 mm square basis.

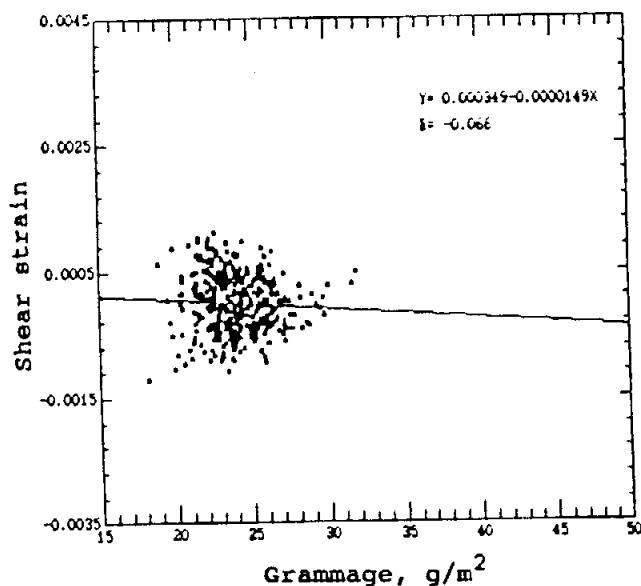


Fig. 24.1. Average from three specimens on 1 mm square basis.

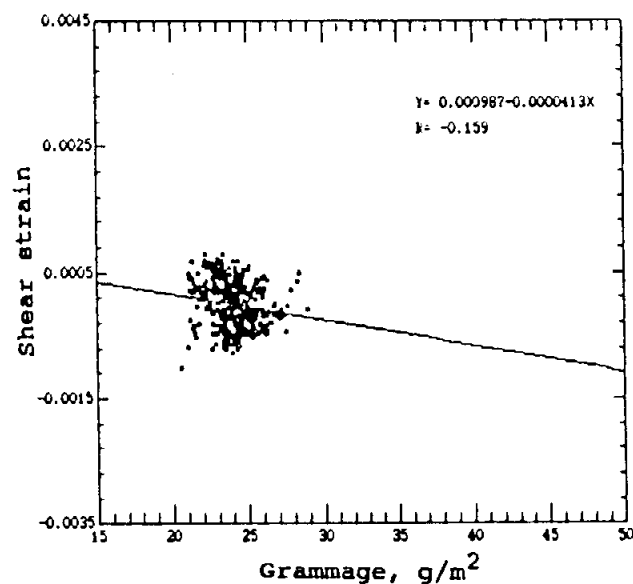


Fig. 24.2. Average from three specimens on 2 mm squares basis..

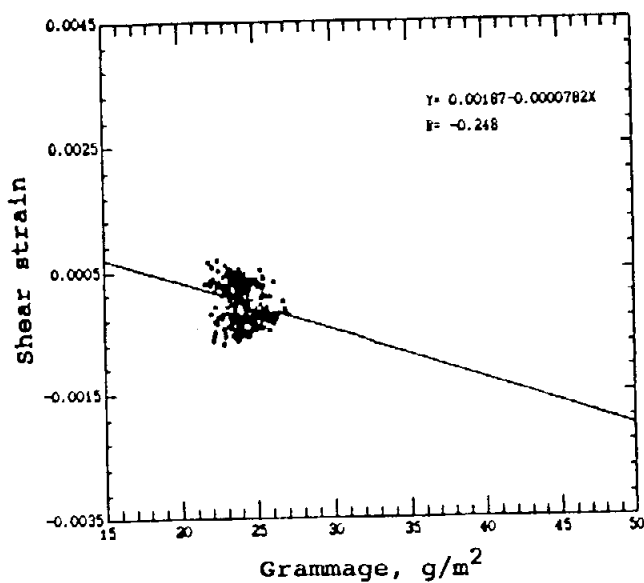


Fig. 24.3. Average from three specimens on 3 mm squares basis.

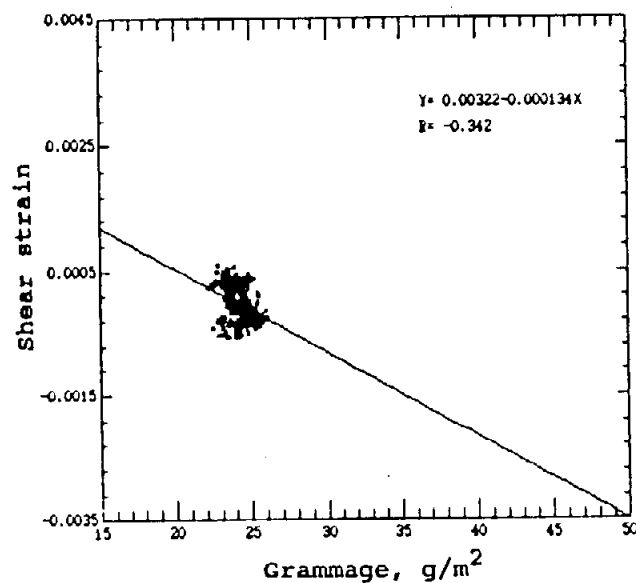


Fig. 24.4. Average from three specimens on 4 mm squares basis.

Fig. 24. Relationship between grammage and shear strain for MD specimens on 1, 2, 3 and 4 mm squares basis.

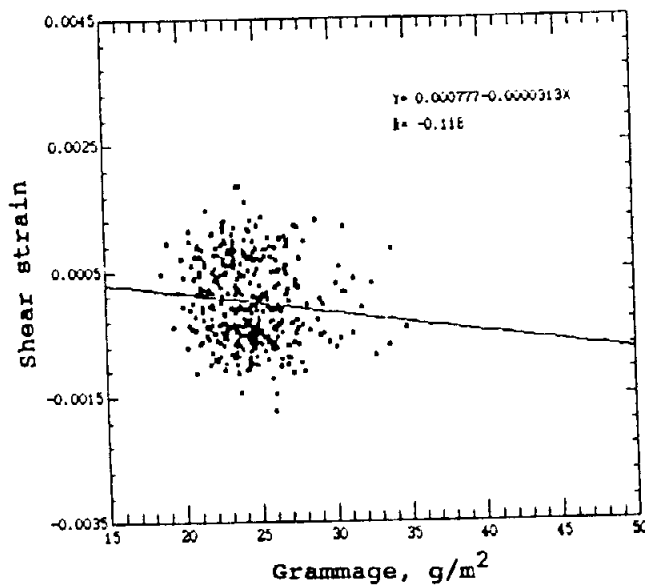


Fig. 25.1. Average from three specimens on 1 mm square basis.

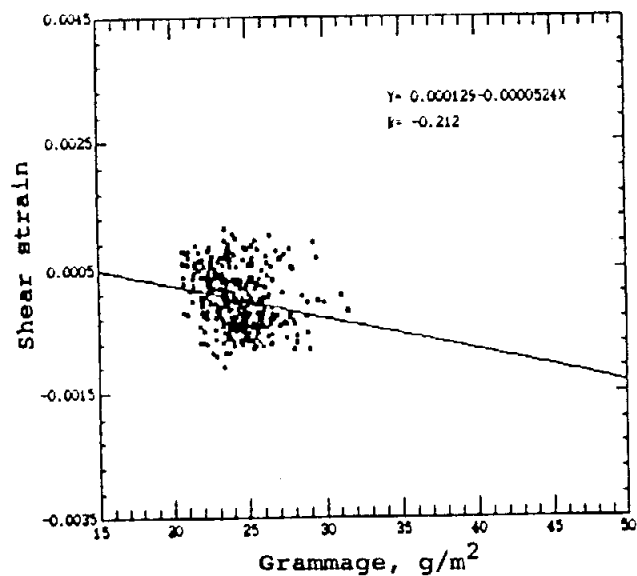


Fig. 25.2. Average from three specimens on 2 mm squares basis.

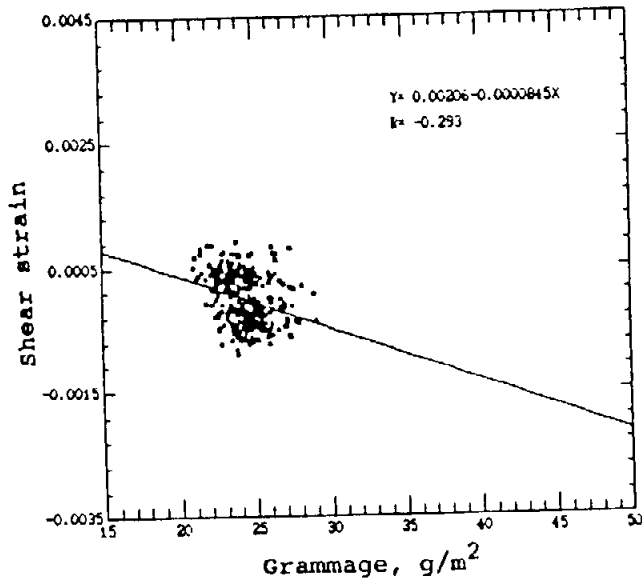


Fig. 25.3. Average from three specimens on 3 mm squares basis.

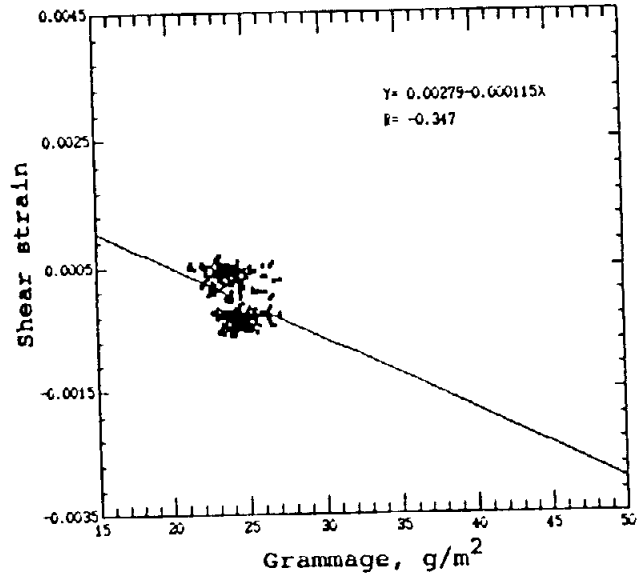


Fig. 25.4. Average from three specimens on 4 mm squares basis.

Fig. 25. Relationship between grammage and shear strain for CD specimens on 1, 2, 3 and 4 mm squares basis.

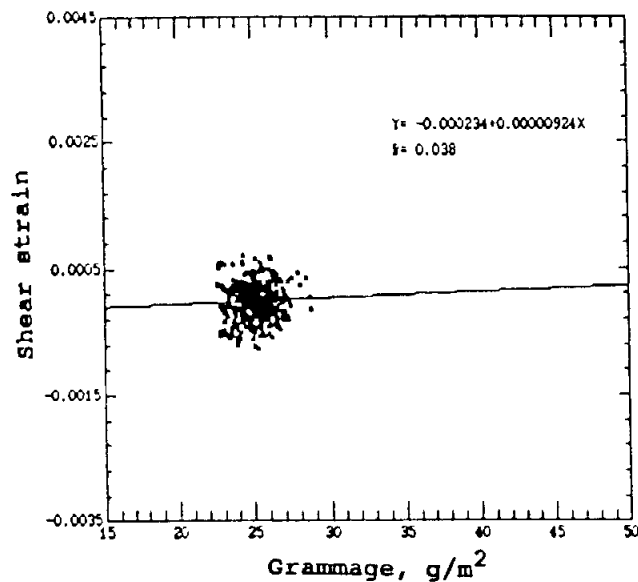


Fig. 26.1. Average from three specimens on 1 mm square basis.

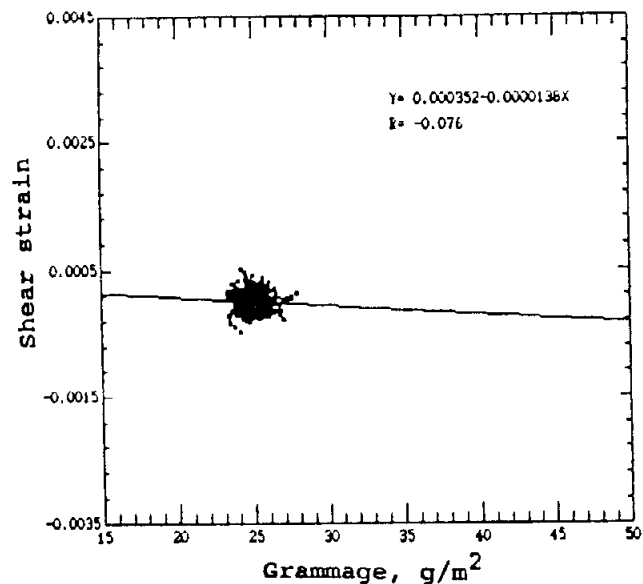


Fig. 26.2. Average from three specimens on 2 mm squares basis.

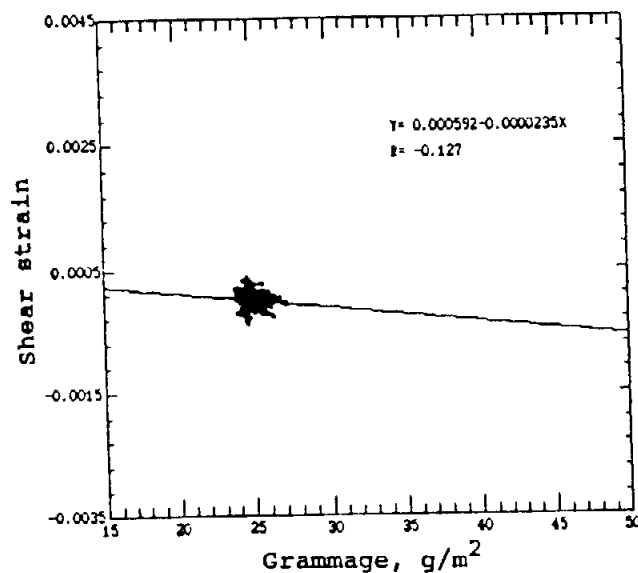


Fig. 26.3. Average from three specimens on 3 mm squares basis.

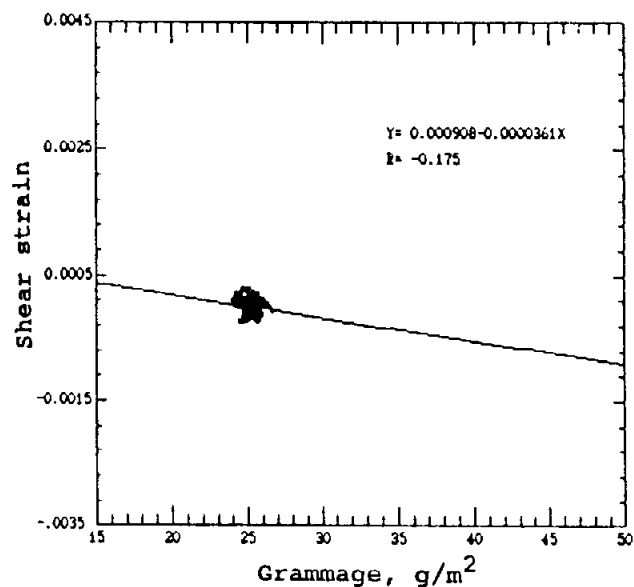
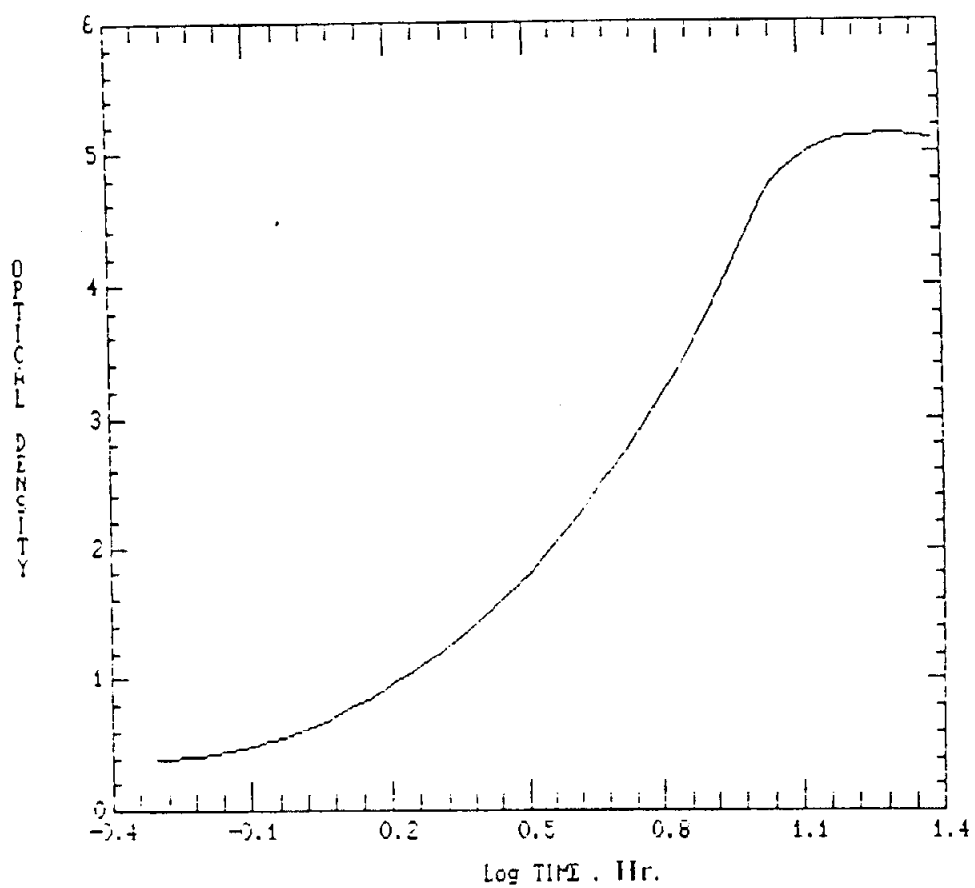


Fig. 26.4. Average from three specimens on 4 mm squares basis.

Fig. 26. Relationship between grammage and shear strain for HANDSHEET specimens on 1, 2, 3 and 4 mm squares basis.

APPENDICES

Appendix A. Sensitometric Curve of the X-Ray Industrex-R
Film.



Appendix B. Operating Conditions for the MacBeth TD-504
Transmission Densitometer and for the X-Y MC2000
Programmable Translation Stage.

1. MacBeth TD-504 Transmission Densitometer

- 1.1. Filter: Standard filter: white light
- 1.2. Aperture: Standard square aperture, 1x1mm
- 1.3. Calibration: Adjustment of zero and calibration on density reference of 2.79
- 1.4. Measurement: Computerized scanning procedure of the radiographs fitted to an x-y programmable translation stage

2. MC2000 Programmable Translation Stage

- 2.1. Movement: Intermittent stepwise basis of
1mm
- 2.2. Acceleration: 4 revs/sec./sec.
- 2.3. Velocity: 3 revs/sec.
- 2.4. Positional accuracy: ± 0.00005 in/in of
travel
- 2.5. Operation control: Computerized motion
control according to APL functions:
ATCONTROL, CONTROL, MD, MOD, MODHOR, MODIN,
MODOUT, MODVERT, OFF, ON, ONLINE, SUB, GO
and WAIT. These functions are described in
Appendix E.

Appendix C. Standard Radiographic Development Procedure.

Temperature: 22 °C

Safelight: 7.5 watt, GBX-2 Filter

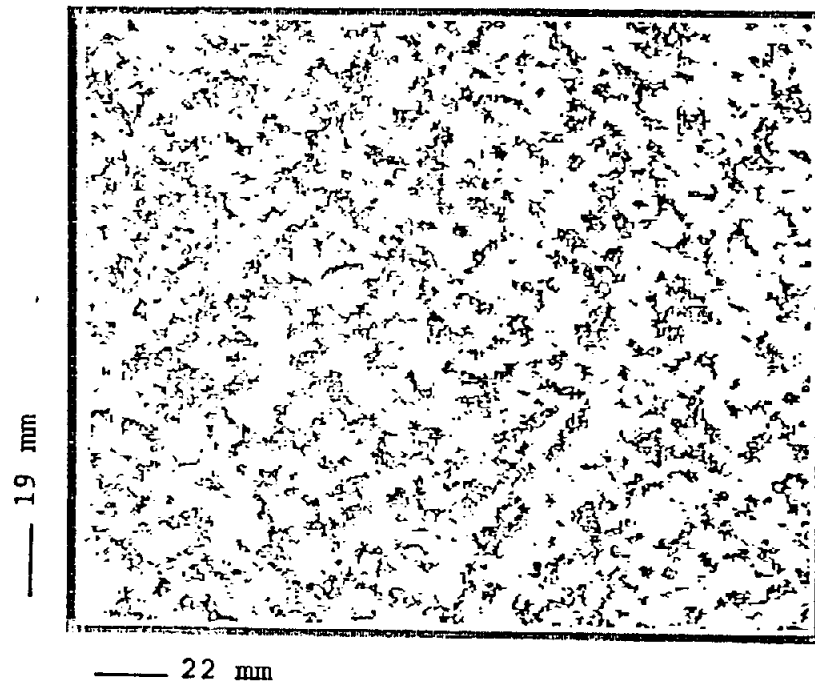
1. Development: - Developer: Kodax GBX
- Time: 5 minutes, no agitation
2. Stopping: - Stopper: 1.5% acetic acid
- Time: 30 seconds, continuous agitation
3. Fixing: - Fixer: Kodak GB
- Time: 10 minutes, intermittent agitation
4. Washing: - Temperature: 20 °C water
- Time: 30 minutes in rotating washer
5. Rinsing: - Detergent: Kodak Photo Flo
- Time: 30 seconds
6. Drying: - Air drying at room temperature

Appendix D. Preliminary Results of Floc Analysis and Optically
Determined Basis Weight Distribution of Machine
Made Paper and Handsheet.

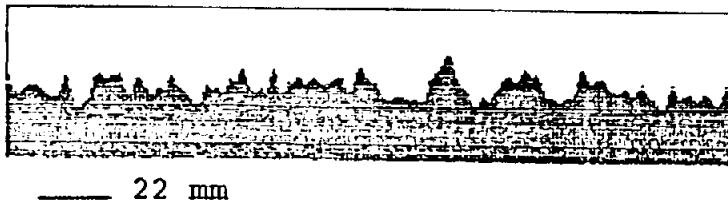
1. Machine Made Paper.

1.1. Quantity and floc size.

Total floc count= 348
Average size= 9.44 sq.mm



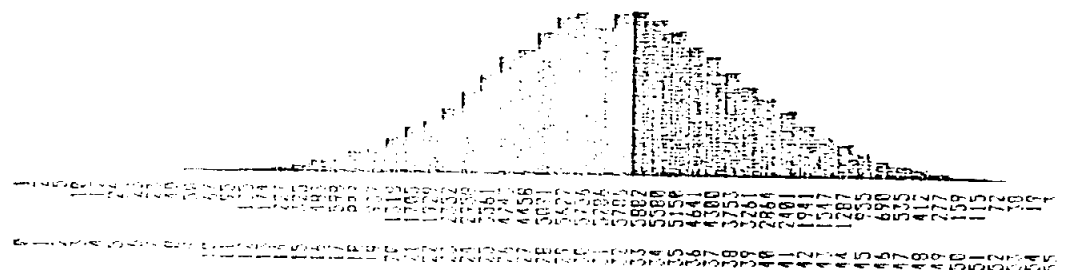
1.2. Optical Floc Image.



1.3. Optical Basis Weight Profile.

Number of data
points per class

Number of class



1.4. Optical Basis weight distribution.

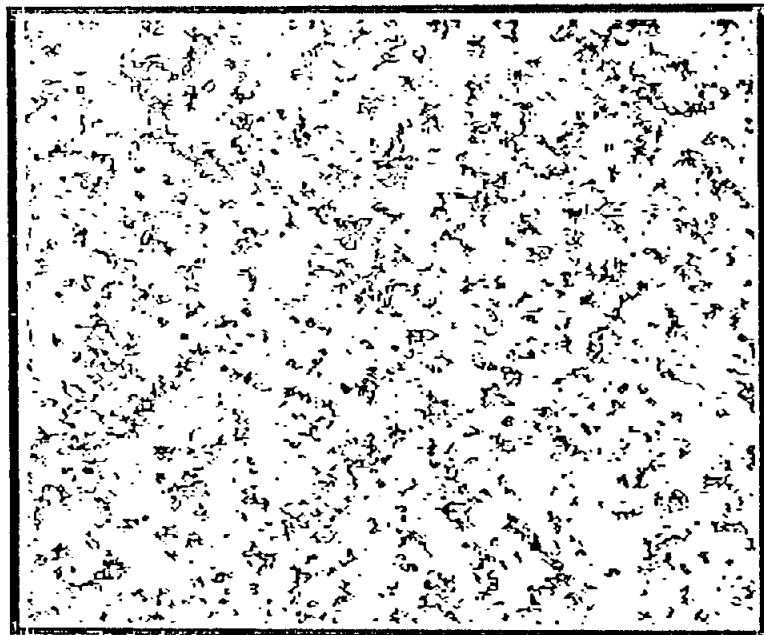
2. Handsheet.

2.1. Quantity and Floc size.

Area
 0.00
 0.01
 0.02
 0.03
 0.04
 0.05
 0.06
 0.07
 0.08
 0.09
 0.10
 0.11
 0.12
 0.13
 0.14
 0.15
 0.16
 0.17
 0.18
 0.19
 0.20
 0.21
 0.22
 0.23
 0.24
 0.25
 0.26
 0.27
 0.28
 0.29
 0.30
 0.31
 0.32
 0.33
 0.34
 0.35
 0.36
 0.37
 0.38
 0.39
 0.40
 0.41
 0.42
 0.43
 0.44
 0.45
 0.46
 0.47
 0.48
 0.49
 0.50
 0.51
 0.52
 0.53
 0.54
 0.55
 0.56
 0.57
 0.58
 0.59
 0.60
 0.61
 0.62
 0.63
 0.64
 0.65
 0.66
 0.67
 0.68
 0.69
 0.70
 0.71
 0.72
 0.73
 0.74
 0.75
 0.76
 0.77
 0.78
 0.79
 0.80
 0.81
 0.82
 0.83
 0.84
 0.85
 0.86
 0.87
 0.88
 0.89
 0.90
 0.91
 0.92
 0.93
 0.94
 0.95
 0.96
 0.97
 0.98
 0.99
 1.00

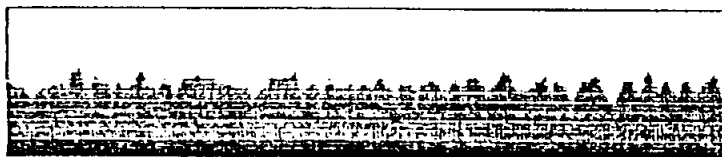
Total Floc Count= 565
 Average size= 3.84 sq.mm

19 mm



22 mm

2.2. Optical Floc Image.

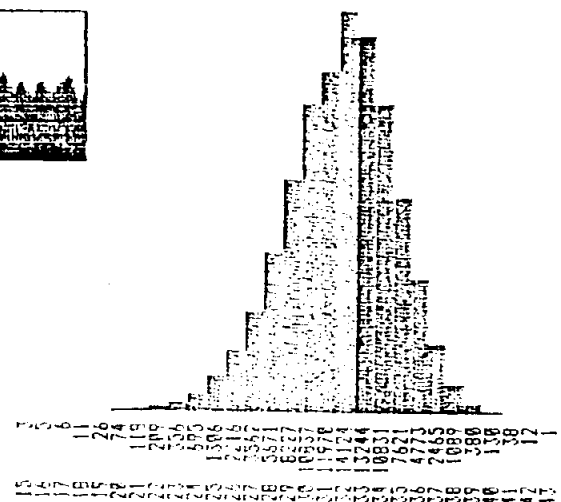


22 mm

2.3. Optical Basis Weight Profile.

Number of data points per class

Number of class



2.4. Optical Basis Weight Distribution.

Appendix E. Data Acquisition Software for Beta-Radiography
Technique


```

00] HELP[0]
01] ' ' ' ' ' 72p*'
02] '***** THIS SOFTWARE MAKES THE ACQUISITION OF OPTICAL DENSITIES *****'
03] '***** OF RADIOGRAPHS IN A SEMI-AUTOMATIC SCANNING PROCEDURE *****'
04] 72p*' ' '
05] ' THE MAIN FUNCTIONS ARE DESCRIBED...' ' ' '
06] 'SCAN: This function makes the acquisition of the densities (=Absorbance)'
07] ' of the radiographs obtained by the beta-radiography technique. It '
08] ' calls the function ATCONTROL responsible for the scanning procedu-'
09] ' re performed by the X-Y programable translation stage. It calls '
10] ' the function CONTROL for initial alignment of the radiograph.'
11] '
12] 'CALIBRATION: This function is called in the SCAN function. It makes the '
13] ' acquisition of data necessary to perform the calibration'
14] ' procedure. Here some terms definition are provide:'
15] '
16] ' OPTICAL DENSITY FOR ZERO GRAMMAGE: This is the optical '
17] ' density measured on the exposed part of the radiograph '
18] ' free of calibration strips and paper sample.'
19] '
20] 'PRESS ENTER TO CONTINUE:' ' PAUSE+M
21] ' OPTICAL DENSITY FOR FILM BACKGROUND: This is the optical'
22] ' density measured in an unexposed part of the film. '
23] '
24] ' OPTICAL DENSITY FOR CALIBRATION STRIPS: This is the opti-'
25] ' cal density measured on an exposed part of the film over '
26] ' the calibration strips.'
27] '
28] 'GRAMMAGE: This function convert the optical density to grammage.'
29] ' Here some variables definition are provide:'
30] '
31] ' MYW: This is a vector representing the grammage of the mylar'
32] ' strips used on the calibration procedure.'
33] '
34] ' MYOD: This is the optical densities of the mylar strips used'
35] ' on the calibration procedure.'
36] '
37] ' MYCOD: This is the corrected optical densities of the mylar'
38] ' strips used on the calibration procedure.'
39] '
40] ' MYOW: This is the optical grammages of the mylar strips used'
41] ' on the calibration procedure.'
42] '
43] 'PRESS ENTER TO CONTINUE:' ' PAUSE+M
44] ' MYMU: This is the absorption coefficient of the mylar strips'
45] ' used on the calibration procedure.'
46] '
47] ' PW: This is a scalar representing the average commercial'
48] ' grammage of the paper samples.'
49] '
50] ' AW: This is the optical densities for the paper sample.'
51] '
52] ' PCOD: This is the corrected optical densities for the paper'
53] ' sample.'
54] '
55] ' PMU: This is the absorption coefficient of the paper sample.'
56] '
57] ' GRAM: This is the calculated grammages of the paper sample.'
58] ' ' ' ' ' ' ' ' ' ' ' ' ' ' ' ' ' ' ' ' ' ' ' ' ' ' ' ' ' ' ' ' ' ' ' '
59] 'PRESS ENTER TO GO BACK TO MAIN MENU:' ' PAUSE+M
60] OPTIONS

```

```

SCAN[0]
00 SCAN; LENX; LENY; N; AW; I
10 MORE:CONTROL
20 CALIBRATION
30 'ENTER THE LENY and then LENX FOR THIS RADIOGRAPHY:'  $\diamond$  LENY+0  $\diamond$  LENX+0
40 LENY DFAPPEND 1951  $\diamond$  LENX DFAPPEND 1951
50  $N+(LENY \times LENX) \diamond AW+N+0 \diamond I+0$ 
60 LOOP1:I+I+1
70 'ENTER OPTICAL DENSITY FOR THIS LOCATION:'  $\diamond$  AW+I+0  $\diamond$   $\rightarrow(I=N)/JUMP \diamond$  ATCONTROL
80  $JUMP:\rightarrow(I=N)/LOOP1 \diamond AW \diamond$  'DO YOU WANT TO SAVE THIS DATA? (Y or N)'
90  $\rightarrow('N'=1+0) \diamond$  MORE  $\diamond$  AW DFAPPEND 1951  $\diamond$  DFUNTIE 1951  $\diamond$  OFF
100 'DO YOU WISH TO CONTINUE THE DATA ACQUISITION? (Y or N)'
110  $\rightarrow('Y'=1+0) \diamond$  MORE  $\diamond$  OFF
120 OPTIONS

```

```

CALIBRATION[0]
00 CALIBRATION; AO; AI; MYOD
10 DFLIB 1
20 'ENTER A FILE NAME FOR THIS RADIOGRAPHY:(Drive No. then File)'
30 'Grammage, Tension or Cyclic, H or L or HS, Machine Plane, Sample No.'
40 NAME+0  $\diamond$  NAME DFCREATE 1951
50 'ENTER OPTICAL DENSITY FOR ZERO GRAMMAGE:'  $\diamond$  AO+0
60 'ENTER OPTICAL DENSITY FOR FILM BACKGROUND:'  $\diamond$  AI+0
70 'ENTER OPTICAL DENSITIES FOR CALIBRATION STRIPS:(as a vector)'  $\diamond$  MYOD+0
80 AO DFAPPEND 1951  $\diamond$  AI DFAPPEND 1951  $\diamond$  MYOD DFAPPEND 1951

```

```

GRAMMAGE[0]
00 GRAMMAGE; NAME; AO; AI; MYOD; LENX; LENY; AW; MYCOD; MYMU; MYW; MYOW; PCOD; PMU; PW; GRAM
10 BEGIN:DFLIB 0  $\diamond$  MYW+ 8.4 12.3 16.9 26.3 32.1 50.22
20 'ENTER NAME OF THE FILE TO BE READ:'  $\diamond$  NAME+0  $\diamond$  NAME DFTIE 1951
30 AO+DFREAD 1951,1  $\diamond$  AI+DFREAD 1951,2  $\diamond$  MYOD+DFREAD 1951,3
40 LENY+DFREAD 1951,4  $\diamond$  LENX+DFREAD 1951,5  $\diamond$  AW+DFREAD 1951,6
50  $MYCOD+((\rightarrow(AO-AI))-(\rightarrow(MYOD-AI))) \diamond$  MYMU+0.0352
60 *Calculation of the calibration equation:
70  $MYOW+(MYCOD-MYMU) \diamond$  Eq+MYOW+MYW*. * 0 1
80 *Calculation of the correlation coefficient for this radiography:
90  $MYW+MYW-((+/MYW) \diamond$  MYW)  $\diamond$  MYCOD+MYCOD-((+/MYCOD) \diamond MYCOD)
100  $SOMXY+(MYW \times MYCOD) \diamond$  SOMXY+((+/SOMXY)  $\diamond$  SOMX+(MYW+2)  $\diamond$  SOMX+((+/SOMX)
110  $SOMY+(MYCOD+2) \diamond$  SOMY+((+/SOMY)  $\diamond$  r+SOMXY+((SOMX \times SOMY)+0.5)
120 'THE CORRELATION COEFFICIENT(r) FOR THIS RADIOGRAPHY IS:'  $\diamond$  r
130 *Grammage calculation for the paper sample:
140  $PCOD+((\rightarrow(AO-AI))-(\rightarrow(AW-AI))) \diamond$  PMU+0.0328
150  $PCOD+(PCOD-PMU) \diamond$  GRAM+((PCOD-Eq(1)) \diamond Eq(2))  $\diamond$  DFUNTIE 1951
160 '***** THE GRAMMAGE DISTRIBUTION OF THIS SAMPLE IS *****'  $\diamond$  GRAM  $\diamond$  ''
170 'THE AVERAGE FOR THIS SAMPLE IS:'  $\diamond$  AVERGRAM+((+/GRAM) \diamond AVERGRAM
180 'DO YOU WANT OF SAVE THIS DATA? (If not type N)'
190 OPTI+0  $\diamond$   $\rightarrow(OPTI='N')/JUMP \diamond$  DFLIB 1
200 'ENTER A NEW FILE NAME FOR THIS DATA: (Drive No. then File)'
210 'Grammage, Tension or Cyclic, H, L or S, Machine Plane, Sample No.'
220 NAME+0  $\diamond$  NAME DFCREATE 1951  $\diamond$  GRAM DFAPPEND 1951  $\diamond$  DFUNTIE 1951
230 JUMP:'DO YOU WANT TO CONTINUE? (Y or N)'
240  $\rightarrow('Y'=1+0) \diamond$  BEGIN
250 OPTIONS

```

```

      ▽FREADD[0]
01  FREAD;NAME;AO;AI;MYOD;LENX;LENY
11  BEGIN: 0 DFLIB 1
21  'ENTER NAME OF THE FILE TO BE READ:' 0 NAME+0 0 NAME OFTIE 1951
31  AO+DFREAD 1951,1 0 'THE OPTICAL DENSITY FOR ZERO GRAMMAGE IS:' 0 AO
41  AI+DFREAD 1951,2 0 'THE OPTICAL DENSITY FOR FILM BACKGROUND IS:' 0 AI
51  MYOD+DFREAD 1951,3 0 'THE OPTICAL DENSITY FOR CALIBRATION STRIPS ARE:'
61  MYOD 0 LENY+DFREAD 1951,4 0 LENX+DFREAD 1951,5
71  'THE LENY and LENX FOR THIS FILE ARE, RESPECTIVELY:' 0 LENY 0 LENX
81  'DO YOU WANT TO SEE THE DATA IN MATRIX FORM? (If not, type N)'
91  OPTI+0 0 →(OPTI='N')/JUMP
101 '***** THE OPTICAL DENSITY DISTRIBUTION FOR THIS SAMPLE IS *****'
111 NAME+DFREAD 1951,6 0 NAME+(LENX,LENY)0NAME 0 NAME 0 ''
121 'PRESS ENTER TO CONTINUE' 0 PAUSE+0 0 →JUMP1
131 JUMP:'***** THE OPTICAL DENSITY DISTRIBUTION FOR THIS SAMPLE IS *****'
141 NAME+DFREAD 1951,6 0 NAME 0 'PRESS ENTER TO CONTINUE:' 0 PAUSE+0
151 JUMP1:DFUNTIE 1951
161 'IS IT THE FILE THAT YOU WANT TO USE? (If not, and if you want to try'
171 'an other one, type the letter N)'
181 EXIT+0 0 →(EXIT='N')/BEGIN
191 OPTIONS

```

```

      ▽RENAME[0]
01  RENAME
11  MORE:
21  DFLIB 0 0 DFLIB 1
31  'ENTER THE NAME OF THE FILE TO BE RENAMED:(Drive no. then File)' 0 NAME+0
41  NAME OFTIE 1951
51  'ENTER A NEW NAME FOR THIS FILE:(Drive no. then File)' 0 NEWNAME+0
61  NEWNAME DFRENAME 1951 0 DFUNTIE 1951
71  'DO YOU WISH TO CONTINUE RENAMING? (Y or N)'
81  →('Y'=1+0)0MORE
91  OPTIONS

```

```

      ▽ERASE[0]
01  ERASE
11  MORE:
21  DFLIB 0 0 DFLIB 1
31  'ENTER THE NAME OF THE FILE TO BE ERASED:(Drive no. then File)' 0 NAME+0
41  NAME OFTIE 1951 0 NAME OFERASE 1951 0 DFUNTIE 1951
51  'DO YOU WISH TO CONTINUE ERASING? (Y or N)'
61  →('Y'=1+0)0MORE
71  OPTIONS

```

```

      ▽ASK[0]
01  Z+ASK N
11  0+N+,N
21  Z+(0N)+0

```

▽ATCONTROL[0]

```

01 ATCONTROL
11 ON
21 MD 0 C XY 0 XF+XF+XX 0 YF+YF+YY 0 →END
31 OUT:YF+0 0 MODOUT 0 ' ' 0 70p*' 0 ' ' 0 ' '
41 'STOP FOR CHECKING THE DENSITOMETER CALIBRATION, IF OK... PRESS ENTER'
51 ' ' 0 ' ' 0 70p*' 0 ' ' 0 ' ' 0 ' '
61 PAUSE+0 0 MODIN 0 SUB
71 MODVERT 0 MODHOR 0 →ED
81 END:50p*' 0 YFF+YF×2.54E-4 0 ' ' 0 ' ' 0 +(YFF=15.999968)/OUT
91 ('Y AXIS='),(45YFF),('MM')
101 ED:

```

▽BUFFER[0]

```

101 BUFFER;R
11 ATTHIS FUNCTION EMPTIES DATA IN BUFFER.
21 R+ 1 1 1 0 0 32000 DABIN ' ' 0 DERASE 'R'

```

▽CONTROL[0]

```

101 CONTROL;Q;RE;XA;YA;XFF;YFF
11 BE:' ' 0 ' ' 0 ON
21 50p*' 0 ' ' 0 ' 1) GO ONE STEP FORWARD'
31 ' 2) GO ONE STEP BACK' 0 ' 3) GO TO REFERENCE POINT'
41 ' 4) MODIFY X AND Y STEPS'
51 ' 5) IF YOU WANT TO MAKE THIS POSITION AS REFERENCE'
61 ' POINT, TYPE 5'
71 ' 6) TO EXIT, TYPE 6'
81 ' ' 0 ' TYPE THE NUMBER YOU WANT TO DO'
91 ' ' 0 50p*' 0 Q+0 0 RE+Q+9 0 +(RE=15)/ED 0 →RE
101 MD 0 C XY 0 OFF 0 XF+XF+XX 0 YF+YF+YY 0 →END
111 SUB 0 OFF 0 XF+XF+XX 0 YF+YF+YY 0 XX+-1×XX 0 YY+-1×YY 0 →END
121 XA+XX 0 XX+-1×XF 0 YA+YY 0 YY+-1×YF 0 MD 0 C XY 0 OFF 0 XX+XA 0 YY+YA 0 →14
131 MOD 0 →BE
141 XF+YF+0
151 END:XFF+XF×2.54E-4 0 YFF+YF×2.54E-4 0 ' ' 0 ' '
161 (' X AXIS = '),(45XFF),(' MM') 0 (' Y AXIS = '),(45YFF),(' MM') 0 →BE
171 ED:

```

▽MD[0]

```

01 MD;VEE;ACC;X2;Y2;X1;Y1
11 ACC+3AC 0 VEE+3VE 0 +(XX=0)/FX
21 X1+3XX 0 X2+3X1 0 +(Y=0)/(1+X1)/WE
31 E:+(YY=0)/FY 0 Y1+3YY 0 Y2+3Y1 0 +(Y=0)/(1+Y1)/WEE 0 →END
41 FX:Y1+3YY 0 Y2+3Y1 0 +(Y=0)/(1+Y1)/WEE 0 →FF
51 WE:X1+X1[1+(1(X2-1))] 0 X1+-1,X1 0 →E
61 WEE:Y1+Y1[1+(1(Y2-1))] 0 Y1+-1,Y1 0 →FF
71 WEEE:Y1+Y1[1+(1(Y2-1))] 0 Y1+-1,Y1
81 END:XY+('1A'),(ACC),(' U'),(VEE),(' D'),(X1)
91 XY+XY,(' 2A'),(ACC),(' U'),(VEE),(' D'),(Y1),(' G') 0 →0
101 FF:XY+(' 2A'),(ACC),(' U'),(VEE),(' D'),(Y1),(' G') 0 →0
111 FY:XY+('1A'),(ACC),(' U'),(VEE),(' D'),(X1),(' G')

```

```

      MOD[0]
03 MOD;RE;QQ
11 BE:' ' 0 ' '
12 50p*' 0 ' ' 0 ' MODIFICATION OF THE X AND Y STEPS'
3  ' 0 ' FROM LEFT TO RIGHT IS + IN X AXIS'
4  ' FROM TOP TO BOTTOM IS + IN Y AXIS'
53 ' X AND Y VALUE SHOULD HAVE IDENTICAL SIGN' 0 ' '
6 (' 1) X = '), (03XX) 0 (' 2) Y = '), (03YY)
7 (' 3) ACCELERATION = '), (03AC)
8 (' 4) VELOCITY = '), (03VE)
9 (' 5) IF IT IS ALRIGHT, TYPE 5'
10 ' ' 0 ' TYPE THE NUMBER YOU WANT TO MODIFY' 0 ' '
11 50p*' 0 QQ+0 0 RE+QQ+11 0 +(RE=16)/END 0 +RE
12 ' MODIFY X VALUE' 0 XX+0 0 +BE
13 ' MODIFY Y VALUE' 0 YY+0 0 +BE
14 ' MODIFY ACCELERATION' 0 AC+0 0 +BE
15 ' MODIFY VELOCITY' 0 VE+0 0 +BE
16 END:MD

```

```

      MODHOR[0]
03 MODHOR
11 OFF
2 XX+0 0 YY+3937
3 MD

```

```

      MODIN[0]
03 MODIN
1 YY+240157
2 ON

```

```

      MODOUT[0]
03 MODOUT
1 YY+177165
2 ON
3 MD 0 C XY

```

```

      MODVERT[0]
03 MODVERT
11 YY+0 0 XX+3937
12 ON
3 SUB 0 XF+XF+XX 0 YF+YF+YY 0 XX+11XX 0 YY+11YY
4 XFF+XFF*2.54E-4 0 ('X AXIS='), (43XFF), ('MM')
      OFF[0]
03 OFF
1 C ' F'

```

```

      ON[0]
03 ON
1 C ' E'

```

▽ONLINE[0]

```
0] RES←ONLINE AVD
1] 2 DARBIN AVD,DTCHL
[2] RES← 2 2 1 0 0 100 DARBIN AVD,DTCHL
```

▽SUB[0]

```
0] SUB
[1] XX←1×XX ◊ YY←1×YY ◊ MD ◊ C XY
```

▽GO[0]

```
0] GO
1] C 'G'
```

▽WAIT[0]

```
[0] WAIT DUR;M;SUP
1] M←0 ◊ SUP←50×DUR
2] LOOP:M←M+1
[3] +(M≤SUP)/LOOP
```

▯TAKEASTRIDJ

```

[00] TAKEASTE
[10] '' ◊ I+0 ◊ ASTRI+((LENX-STEPX),(LENY-STEPY))◊0
[20] LOOPE:I+I+1
[30] ASTRI(I;J)+(ASTRI(I;J)+ASTRI(I+1;J))/2
[40] +(I((LENY-STEPY))/LOOPE
[50] 'THE AXIAL STRAIN FIELD FOR CORRELATION IS:' ◊ 8 3 ◊ASTRI ◊ ''
[60] ASTR2+((LENX-STEPX)*(LENY-STEPY))◊ASTRI
[70] 'ENTER NAME OF FILE TO STORE THIS DATA:(Drive No. then File)'
[80] NAME+D ◊ NAME OFCREATE 1951 ◊ ASTR2 OFAPPEND 1951
[90] OFUNTIE 1951
[100] ▯

```

▯TAKELSTRIDJ

```

[00] TAKELSTE
[10] '' ◊ I+0 ◊ LSTR1+((LENX-STEPX),(LENY-STEPY))◊0
[20] LOOPE:I+I+1
[30] LSTR1(I;J)+(LSTR1(I;J)+LSTR1(I+1;J))/2
[40] +(I((LENX-STEPX))/LOOPE
[50] 'THE LAT. STRAIN FIELD FOR CORRELATION IS:' ◊ 8 3 ◊LSTR1 ◊ ''
[60] LSTR2+((LENX-STEPX)*(LENY-STEPY))◊LSTR1
[70] 'ENTER NAME OF FILE TO STORE THIS DATA:(Drive No. then File)'
[80] NAME+D ◊ NAME OFCREATE 1951 ◊ LSTR2 OFAPPEND 1951
[90] OFUNTIE 1951
[100] ▯

```

▯TAKESHSEDJ

```

[00] TAKESHSE
[10] '' ◊ SHS1+((LENX-STEPX)*(LENY-STEPY))◊SHS
[20] 'ENTER NAME OF FILE TO STORE THIS DATA:(Drive No. then File)'
[30] NAME+D ◊ NAME OFCREATE 1951 ◊ SHS1 OFAPPEND 1951
[40] OFUNTIE 1951
[50] ▯

```



```

      VSAP2[0]
[0]  SAP2
  1]  ATHIS PROGRAM AVERAGE OUT STEP BY STEP 4 DATA SET(2 BY 2MM) OF GRAMMAGE,
  2]  AAXIAL, LAT. AND SHEAR STRAINS OVER THE ENTIRE MATRIX OF DATA.
[3]  'ENTER THE VARIABLE NAME TO READ:' & NAME&
  4]  'ENTER THE LENX, then LENY FOR THIS VARIABLE:' & LENX& & LENY&
  5]  NAME+(LENX,LENY)&NAME & 1&0 & NAME1+((LENX-1),(LENY))&0
[6]  'NOW...,PROCESSING IN THE ROW DIRECTION...'
  7]  LOOPA:1+1+1
  8]  NAME1[1;]+NAME1[;]+NAME1[1+1;]
  9]  +(1((LENX-1))/LOOPA
[10]  'NOW...,PROCESSING IN THE COLUMN DIRECTION...'
  11]  1&0 & NAME2+((LENX-1),(LENY-1))&0
  12]  LOOPB:1+1+1
[13]  NAME2[;]+(NAME1[;]+NAME1[;1+1])÷4
  14]  +(1((LENY-1))/LOOPB
  15]  'YOUR DATA IN MATRIX FORM IS:' & &NAME2 & '' & NAME2
[16]  NAME3+((LENX-1)×(LENY-1))&NAME2
[17]  'PLEASE..., ASSIGN **NAME3** TO NEW VARIABLE NAME(VARIABLE NAME+NAME3)'

```

```

      VSAP3[0]
[0]  SAP3
  1]  ATHIS PROGRAM AVERAGE OUT STEP BY STEP 9 DATA SET(3 BY 3MM) OF GRAMMAGE
  2]  AAXIAL, LAT. AND SHEAR STRAINS OVER THE ENTIRE MATRIX OF DATA.
[3]  'ENTER THE VARIABLE NAME TO READ:' & NAME&
  4]  'ENTER THE LENX, THEN LENY FOR THIS VARIABLE:' & LENX& & LENY&
  5]  'NOW..., PROCESSING IN THE ROW DIRECTION...'
[6]  NAME+(LENX,LENY)&NAME & 1&0 & NAME1+((LENX-2),(LENY))&0
[7]  LOOPA:1+1+1
  8]  NAME1[1;]+NAME1[;]+NAME1[1+1;]+NAME1[1+2;]
  9]  +(1((LENX-2))/LOOPA
[10]  'NOW..., PROCESSING IN THE COLUMN DIRECTION...'
  11]  1&0 & NAME2+((LENX-2),(LENY-2))&0
  12]  LOOPB:1+1+1
[13]  NAME2[;]+(NAME1[;]+NAME1[;1+1]+NAME1[;1+2])÷9
  14]  +(1((LENY-2))/LOOPB
  15]  'YOUR DATA IN MATRIX FORM IS:' & &NAME2 & '' & NAME2
[16]  NAME3+((LENX-2)×(LENY-2))&NAME2
[17]  'PLEASE..., ASSIGN **NAME3** TO NEW VARIABLE NAME(VARIABLE NAME+NAME3)'

```

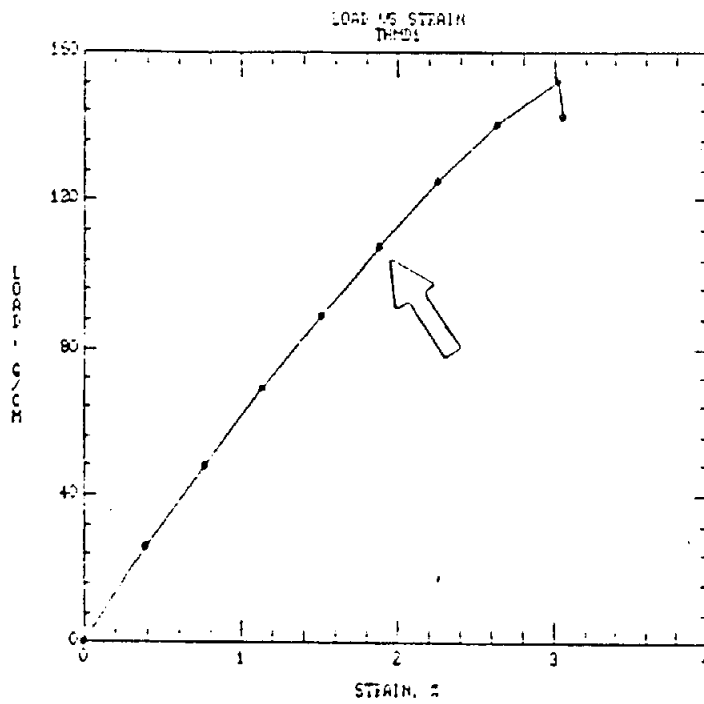
```

      VSAP4[0]
[0]  SAP4
  1]  ATHIS PROGRAM AVERAGE OUT STEP BY STEP 16 DATA SET(4 BY 4MM) OF GRAMMAGE
  2]  AAXIAL, LAT. AND SHEAR STRAINS OVER THE ENTIRE MATRIX OF DATA.
[3]  'ENTER THE VARIABLE NAME TO READ:' & NAME&
  4]  'ENTER THE LENX, THEN LENY FOR THIS VARIABLE:' & LENX& & LENY&
  5]  'NOW..., PROCESSING IN THE ROW DIRECTION...'
[6]  NAME+(LENX,LENY)&NAME & 1&0 & NAME1+((LENX-3),(LENY))&0
[7]  LOOPA:1+1+1
  8]  NAME1[1;]+NAME1[;]+NAME1[1+1;]+NAME1[1+2;]+NAME1[1+3;]
  9]  +(1((LENX-3))/LOOPA
[10]  'NOW..., PROCESSING IN THE COLUMN DIRECTION...'
  11]  1&0 & NAME2+((LENX-3),(LENY-3))&0
  12]  LOOPB:1+1+1
[13]  NAME2[;]+(NAME1[;]+NAME1[;1+1]+NAME1[;1+2]+NAME1[;1+3])÷16
  14]  +(1((LENY-3))/LOOPB
  15]  'YOUR DATA IN MATRIX FORM IS:' & &NAME2 & '' & NAME2
[16]  NAME3+((LENX-3)×(LENY-3))&NAME2
[17]  'PLEASE..., ASSIGN **NAME** TO NEW VARIABLE NAME(VARIABLE NAME+NAME3)'

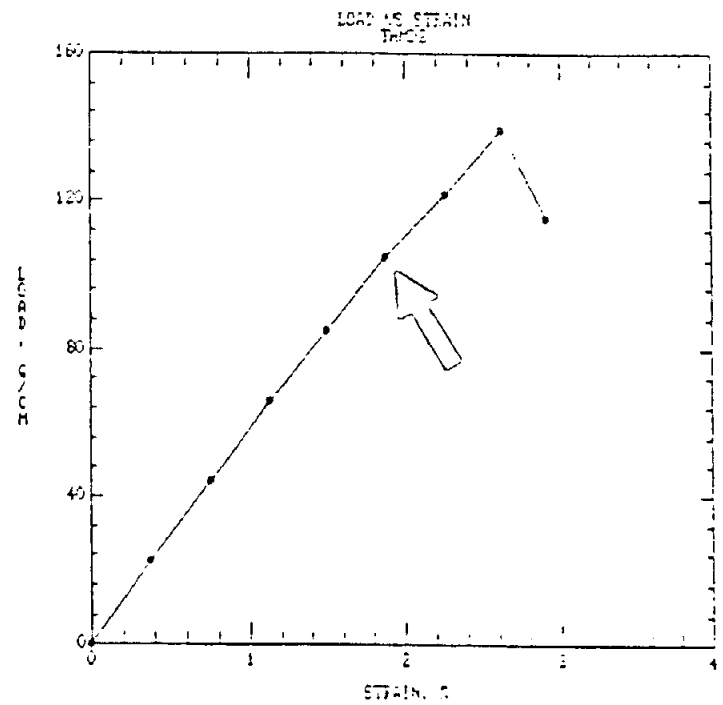
```

Appendix F. Load per unit of width - strain curves for
Machine made paper (MD and CD) and Handsheet

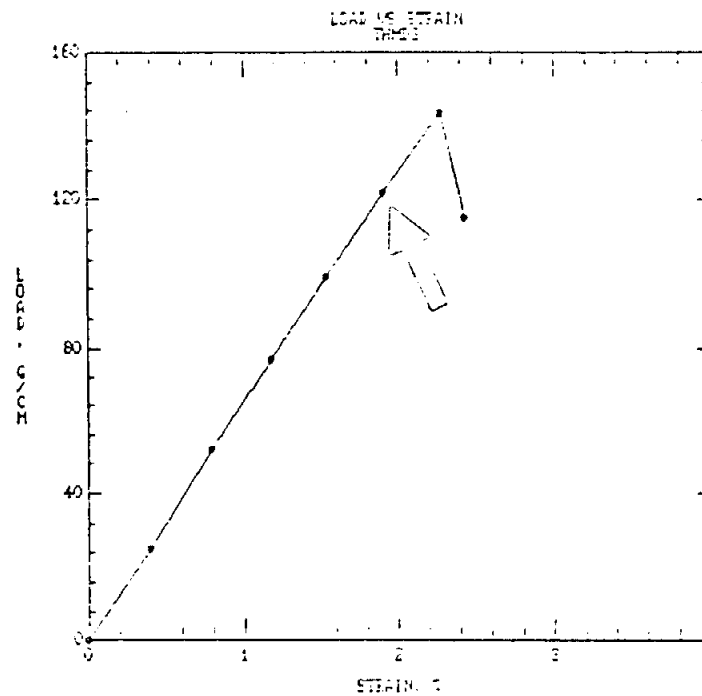
1. Machine made paper (MD specimens)



1.1 Specimen no. 1

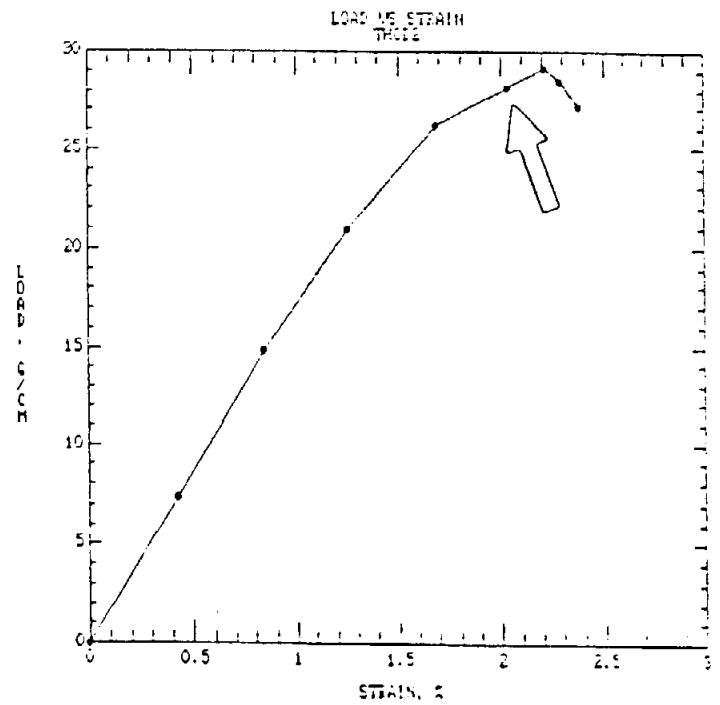
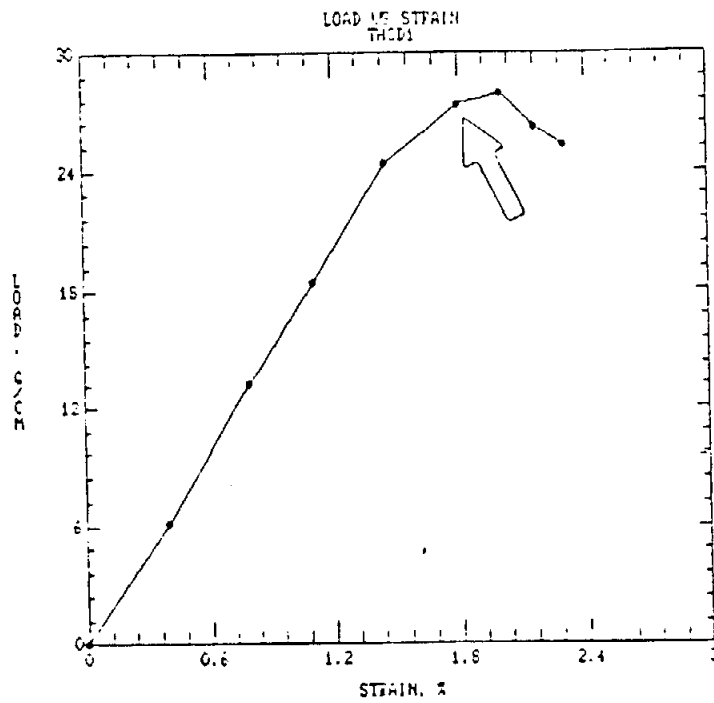


1.2. Specimen no. 2



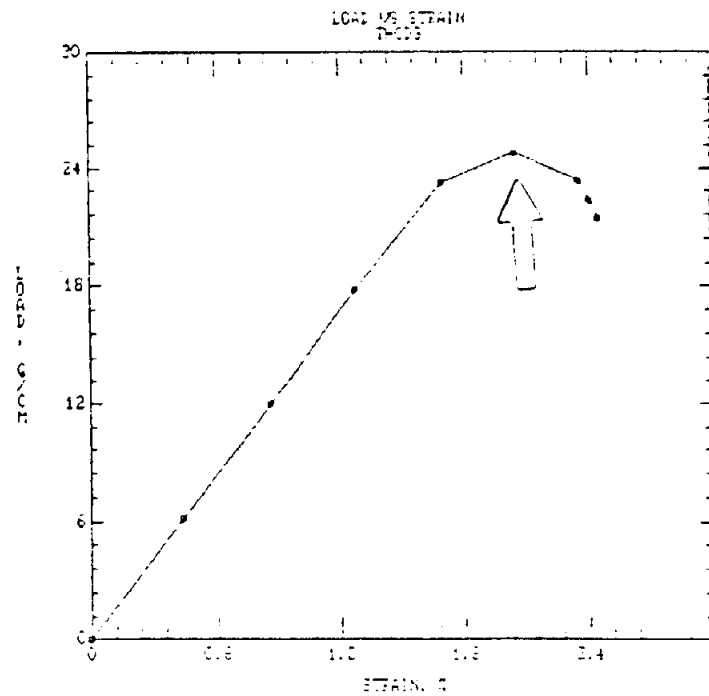
1.3. Specimen no. 3

2. Machine made paper (CD specimens)



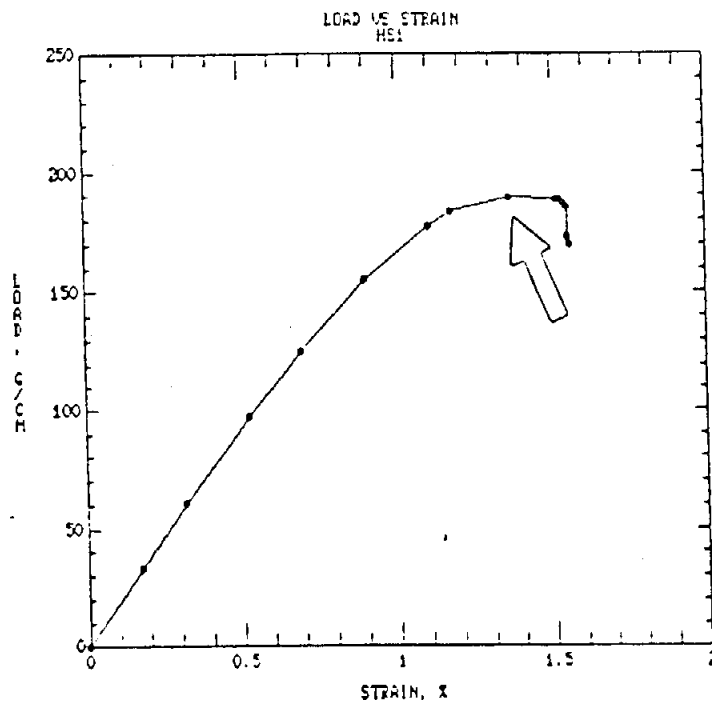
2.1. Specimen no. 1

2.2 Specimen no. 2

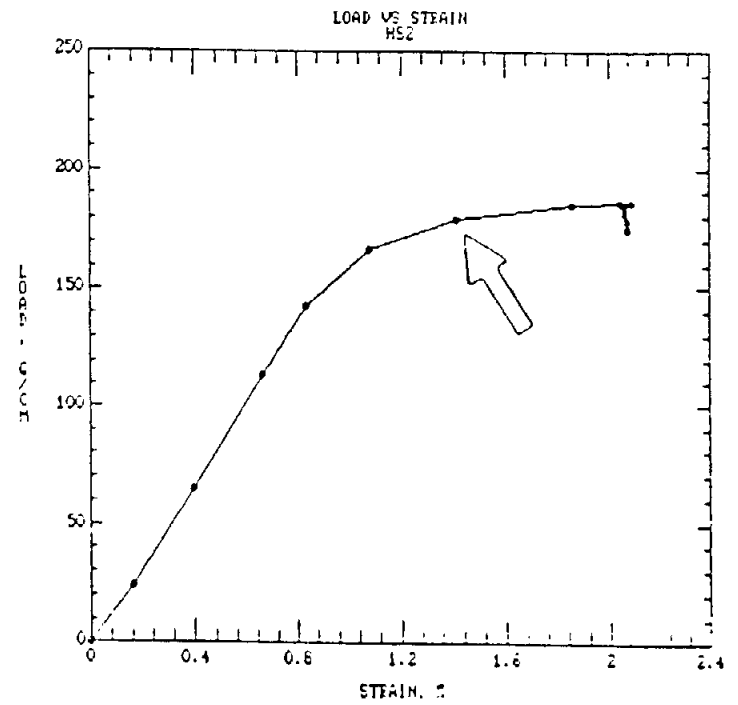


2.3. Specimen no. 3

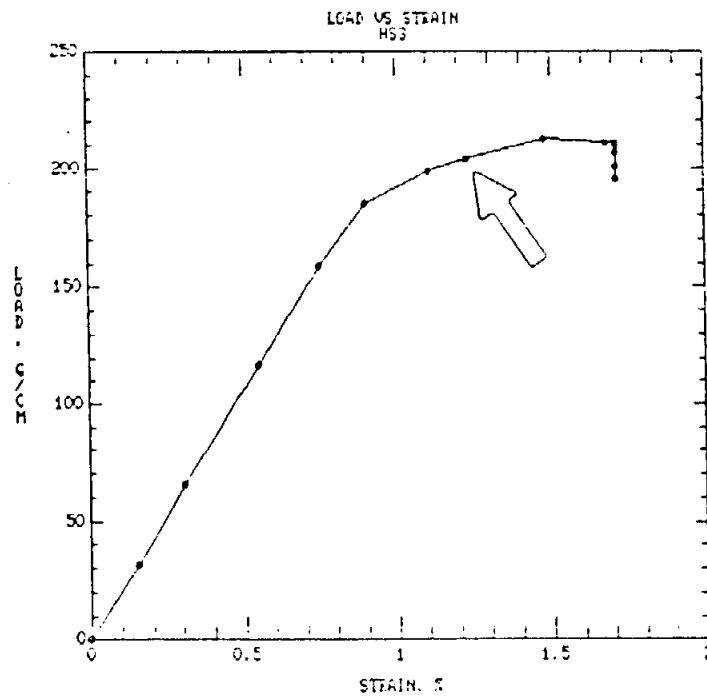
3. Handsheets



3.1. Specimen no.1

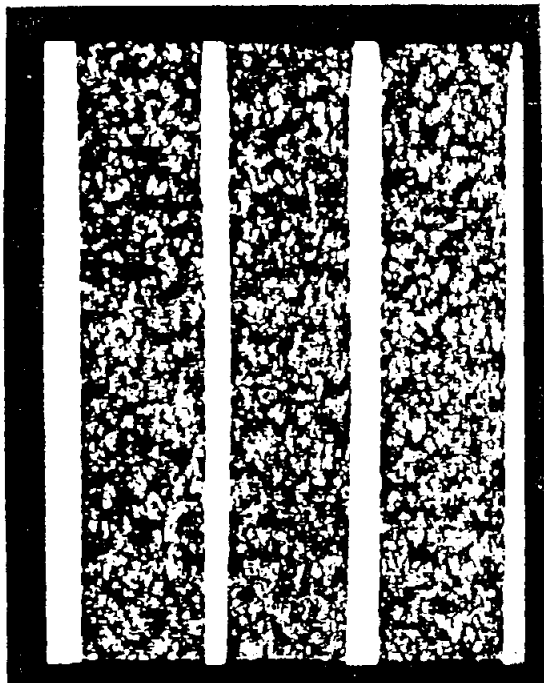


3.2. Specimen no. 2



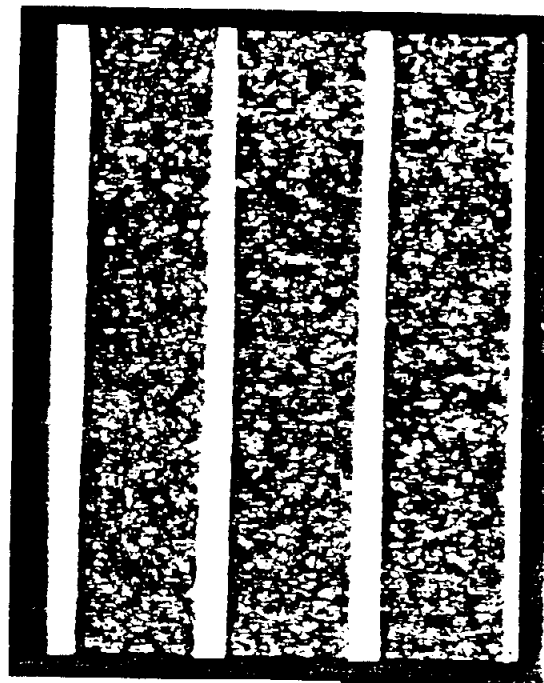
3.3. Specimen no. 3

Appendix G. Beta-radiograph of Machine Made Paper(MD and CD) and
Handsheets specimens.



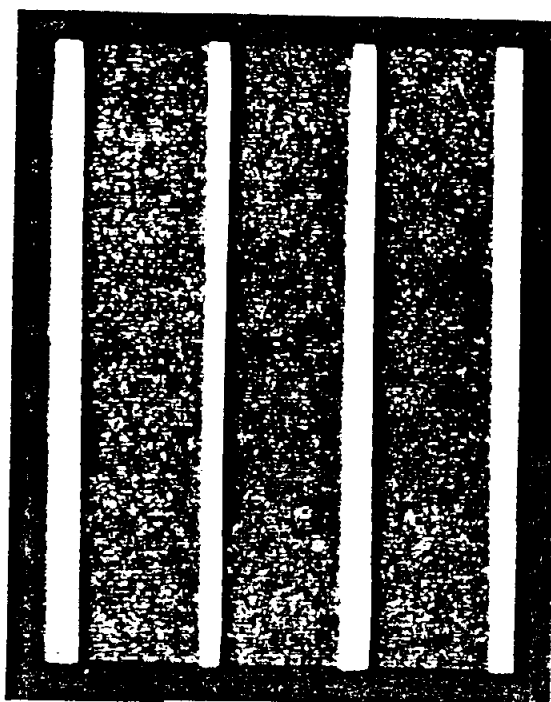
_____ 20 mm

1. Three MD specimens.



_____ 20 mm

2. Three CD specimens.



_____ 20 mm

3. Three Handsheet specimens.

VITA

NAME: Rubens Chaves de Oliveira

DATE AND PLACE OF BIRTH: August 23, 1951
Bom Jesus do Norte, ES, Brazil

EDUCATION:

Institution and Location	Dates	Degree
Federal University of Vicosa Vicosa, MG, Brazil	1973-1976	B.S.-Forest Engineer
Federal University of Vicosa Vicosa, MG, Brazil	1977-1979	M.S.-Pulp and Paper Technology

EMPLOYMENT:

Employer	Date	Position
Federal University of Vicosa Vicosa, MG, Brazil	since 1979	Professor